DYNAMIC ANALYSIS AND CONTROL OF MICROGRIDS

BY

MOHAMED ALI ALI HASSAN

A Dissertation Presented to the

FACULTY OF THE COLLEGE OF GRADUATE STUDIES

KING FAHD UNIVERSITY OF PETROLEUM & MINERALS

DHAHRAN, SAUDI ARABIA

In Partial Fulfillment of the
Requirements for the Degree of

DOCTOR OF PHILOSOPHY

In

ELECTRICAL ENGINEERING

JUNE, 2011

KING FAHD UNIVERSITY OF PETROLEUM & MINERALS

DHAHRAN 31261, SAUDI ARABIA

DEANSHIP OF GRADUATE STUDIES

This dissertation, written by ***MOHAMED ALI ALI HASSAN*** under the direction of his dissertation advisor and approved by his dissertation committee, has been presented to and accepted by the Dean of Graduate Studies, in partial fulfillment of the requirements for the degree of **DOCTOR OF PHILOSOPHY** in ***ELECTRICAL ENGINEERING***.

Dissertation Committee:

Prof. MOHAMMAD ABIDO *(Chairman)*

Prof. ABU-HAMED M. ABDUR-RAHIM *(Member)*

Prof. IBRAHIM EL-AMIN *(Member)*

Prof. ZAKARIYA AL-HAMOUZ *(Member)*

Dr. MAHMOUD KASSAS *(Member)*

Dr. ALI, A. AL-SHAIKHI
(Department Chairman)

Dr. SALAM ZUMMO
(Dean of Graduate Studies)

عمادة الدراسات العليا
DEANSHIP OF GRADUATE STUDIES

Date: 21/6/11

Dedicated to My Beloved Country "Egypt",

My Beloved Parents,

My Sincere Wife

and

My Sons (Ibrahim & Youssof)

ACKNOWLEDGEMENT

All praises due to ALLAH; we praise him, seek His help, and ask for His forgiveness. I am thankful to ALLAH who permitted me and supplied me with the courage, the guidance and the ability to complete this research work.

Also, I can't forget the ideal man of the world and most respectable personality for whom ALLAH created the whole universe, Prophet MOHAMMED (Peace Be Upon Him).

Acknowledgement is due to King Fahd University of Petroleum& Minerals for providing support for all these years to carry out this work.

I must thank my supervisor Prof. Mohammed A. Abido for his guidance, help, support and the enormous effort that he has spent for me. I am grateful to him for his constant encouragement, invaluable instructions, suggestions that helped me in accomplishing this work successfully. He kept his eye on the progress of this work continuously. Also, his programming experience was of great benefit for me. He has set many good examples for me to follow. He is always dealing with me as his young brother. I would like to express my deep appreciation to him. After ALLAH, this work couldn't be finished without him.

Many thanks are due to my committee members Dr. Abu-Hamed M. Abdur-Rahim, Dr. Ibrahim Mohamed El-Amin, Dr. Zakariya Al-Hamouz and Dr. Mahmoud Kassas for their excellent comments on my research that improved this dissertation a lot. I also thank many of my colleagues in KFUPM for helping and supporting my work over the years.

I owe my deepest gratitude to my family for their unflagging love and support throughout this dissertation. I would like to acknowledge the inspiration and support from my mother for her love, care and praying all the time for me. I am indebted to my father for his care and love. They are waiting this day more than me.

It would be inappropriate if I don't acknowledge the support from my wife Eman who took all the pain to give me time to finish this work. My wife has been an encourager, motivator, and counselor along every step of this thesis; in fact this thesis cannot be completed without her encouragement.

For everyone who had helped and supported me:

جزاكم الله خيراً !

TABLE OF CONTENTS

LIST OF TABLES

Table **Table Title** **Page**

LIST OF FIGURES

Figure **Figure Title** **Page**

THESIS ABSTRACT

Name	MOHAMED ALI ALI HASSAN
Title	DYNAMIC ANALYSIS AND CONTROL OF MICROGRIDS
Degree	Doctor of Philosophy
Major Field	Electrical Engineering
Date of Degree	June 2011

Dynamic analysis and control of the microgrids have received much attention recently. A microgrid is a distributed generation unit connected close to a cluster of loads. It can be operated in either a grid connected mode or an autonomous mode to achieve some operational requirements in each mode. The stability and the effectiveness of control in the inverter-based distributed generation interfacing have faced the challenge of the uncertain and dynamic nature of the distribution network. The droop characteristics are used to manage power sharing between distributed generators in the autonomous mode while the power controllers are used in grid-connected mode.

A new technique for stability enhancement of a microgrid operating in both autonomous and grid-connected modes is proposed in this thesis. Linear and nonlinear models of microgrids operating in different modes are developed. Optimal designs of LC filter, controller parameters, and damping resistance are carried out for the case of the grid-connected mode. On the other hand, controller parameters and power sharing coefficients are optimized for the case of the autonomous mode. The control problem has been formulated as an optimization problem where particle swarm optimization is employed to search for optimal settings of the optimized parameters in each mode. In addition, nonlinear time-domain based as well as eigenvalue based objective functions are proposed to minimize the error in the measured power and to enhance the damping

characteristics. The nonlinear time domain simulation has been carried out to assess the effectiveness of the proposed controllers under different disturbances and loading conditions. The obtained results demonstrate a high dynamic performance with efficient damping characteristics of the microgrid considered in this study. At the end, the stability of the microgrid has been investigated in the Real Time Digital Simulator (RTDS) environment. The obtained RTDS results are compared with those obtained from MATLAB simulation to assess the validity and accuracy of the proposed controller model. The obtained results of the RTDS illustrate that the optimal proposed controller not only ensures fast response, perfect tracking for its reference values with no significant overshoot and delay time but also improve the system stability.

خلاصة

درجةالدكتوراة في الفلسفة

الاسم:	**محمد على على حسن**
عنوان الرسالة:	**التحليل الدينامكى والتحكم فى الشبكات الكهربائية الصغيره**
التخصص:	**الهندسه الكهربائية**
تاريخ التخّرج:	**يونيو2011**

زاد الإهتمام فى الأعوام الأخيرة بإستخدام الشبكات الصغيرة نتيجه للإهتمام المتزايد بالعوامل البيئية وتأثير بناء المحطات الكهربائية فى مختلف البلدان أضف إلى ذلك الإتجاة السائد فى أنحاء العالم بإعاده هيكلة الشبكات الكهربائية وكذلك ظهور التكنولوجيا المتقدمة المستخدمة فى بناء هذه الشبكات. يؤدي إستخدام هذه الشبكات إلى زيادة مرونة النظام للتغيرات المختلفة التى قد تطرأ عليه بالأضافة إلى تحسين عملية تشغيل النظام وتقليل الطاقة المفقودة فى النظام.عادة ما تتصل هذه الشبكات الصغيرة مع الشبكة الرئيسية عن طريق إلكترونيات القدرة مما يؤدى لزيادة فاعلية النظام. وتعمل هذه الشبكات الصغيرة فى وجهين مختلفين. من الممكن أن تتصل هذه الشبكات مع الشبكة الرئيسية وفى هذه الحالة تقوم هذه الشبكات الصغيرة بإمداد الشبكة بالطاقة الكهربائية اللازمة لتحسين أداء الشبكة عامة. بينما من الممكن أن تقوم هذه الشبكات الصغيرة بتغذية بعض الأحمال المنفصلة عن الشبكة الرئيسية كأن تكون هذه الأحمال مثلا بعيدة عن الشبكة الرئيسية مما يصعب عليه تغذية هذه الأحمال بواسطة الشبكة. ولهذا فإن إختيار مضبط التحكم بعناية من الأشياء المهمة جدا فى تشغيل هذه الشبكات الصغيرة فى كلا الوجهين. ويقوم البحث على حساب قيمة مضبط التحكم الأمثل بالإضافة إلى حساب قيمة الفلتر الأمثل ومعاملات مشاركة القدرة والتى تؤدى إلى ضمان إتزان النظام خصوصا فى حالة تعرض النظام لأى تغيير طارىء كحدوث خطأ فى النظام أو زيادة طارئة فى الطاقة المدفوعة بواسطة الشبكات الصغيرة. وفى هذا سوف يتم إستخدام الطريقة المسماة "سرب الجسيمات الأمثل" لتصميم مضبط التحكم والفلتر ومعاملات مشاركة القدرة. بالإضافة إلى التأكد من صلاحية الدراسة النظرية وذلك عن طريق إستخدام جهاز"المحاكاة الرقمية فى الوقت الحقيقي" لمحاكاة النظام المستخدم فى الدراسة النظرية وذلك عندما تكون الشبكات الصغيرة إما متصلة مع الشبكة الرئيسية أو تعمل مع الاحمال منفصلة عن الشبكة الرئيسية.

CHAPTER 1

INTRODUCTION

1.1 BACKGROUND

Conventional power system consists of large power generation plants. These power plants are centrally located at adequate geographical places depending on the primary energy sources of these plants which may be either nuclear fuel, fossil fuel or hydro-powered. The amount of these generated powers is around several hundreds of MW's to few GW's. This power is transmitted to the large consumers through long transmission lines. Nowadays, the power system construction has been changed in the last two decades. The interest of local connection of the Renewable Energy Sources (RES) at the distribution level has been increased. The increased use of RES is attributed to many factors such as environmental, economical benefits, electricity restructuring and new technological developments in the distributed generation (DG) units. Internal combustion engines, gas turbines, microturbines, photovoltaic, fuel cells and wind power are different forms of DG. DG can be divided into two categories depending on the connection with the utility. The first category includes internal combustion engines and small hydro plants which presently use the rotating machinery. These types of DGs are directly connected to the grid. The other category which is the majority of RES includes microturbines, fuel

cells, photovoltaic systems and several kinds of wind generators. They are interfaced to the utility through power electronic converters [1]-[7]. They are using DC/AC Pulse Width Modulated (PWM) Voltage Source Inverter (VSI) systems to interface with the utility grid or to the customer load [2]. Compared with conventional generators, the use of inverters to interface RES makes the energy sources more flexible in operation and control. However, this interface introduces new issues such as the absence of the physical inertia, wide-band of dynamics, limited overload capability, susceptibility to parameters variation and switching harmonics generation. An inverter-based DG system will be subjected to considerable network disturbances and parameters variations when it is connected to weak microgrids. This is caused by the uncertain nature of the distribution system [8]. These disturbances remarkably challenge the stability and control effectiveness of an inverter-based generator [8]. The control, protection, dynamics, operational procedures and energy management strategies are the main issues discussed in the conventional power system. These issues are also important in the DG case but in some cases they are different from those in a conventional system. High penetration DG units, non-dispatchable nature of the DG units, fast dynamics and control response of the electronically-interfaced DG units are also very important in the system studies [9]. DG can either operate in the grid-connected mode or in an islanded mode within a microgrid [10]. In a grid-connected mode, DG unit is controlled to feed a certain power into the network at an established voltage [10]. It behaves as a controllable load or source by either absorbing or supplying power to the main grid, depending on the generation, load mix and market policies [11]. In the island mode, a cluster of DG units is formed to maintain the reliability of critical loads, mainly when the utility supply is not available.

The island mode is also called autonomous mode or standalone mode. Islanding is defined as a condition that a portion of the microgrid containing DG and load is isolated from the rest of the utility. The microgrid will provide adequate power to local sensitive loads and maintain service within the microgrid [12]. Both the stability problems under fault conditions and instability under small disturbances are affected by increasing the penetration of DG units in distribution networks. The ability of the system to withstand or recover from large perturbations is an important aspect of the stability analysis. In the last years, several stability problems associated with the DG units in distribution networks have been reported [8]-[9]. These problems have been mainly attributed to the control features of individual inverters.

In the conventional power system when the load changes, the frequency changes due to the kinetic energy of the rotating parts while the majority of the microsources do not contain rotating parts because they are interfaced with the utility using the power electronics. This means that the microsources have a lack of inertia in the system so there will be no frequency response when the load changes as in the conventional power system. The interfacing inverter is controlled to mimic the operation of a synchronous generator. In this way, the power sharing mechanism is designed to share the powers between different DGs in the microgrid [13]-[14].

1.1.1 Motivation for DG development

In the last two decades, many factors are pushing the utility forward towards a new electrical power system. These factors are summarized as follows:

- A large increase in demand which requires a high reliable system.
- New transmission lines constraints.

- Electricity market liberalization and regulatory environment.
- Increased CO_2 emission.
- Nuclear waste problem.
- Developments in DG technologies.
- Technological innovations in axillaries elements used.
- Advanced controls of power flows.

Actually, a DG is expected to become an important element in the future generation system. DG systems are not new phenomena since they are using the alternating current to supply the loads, all energy requirements are supplied at or near their point of use. The concept of DG has reappeared in the early 1990s [15]. Actually, DG has multiple attractive advantages. Some of these advantages are related to the sources and the others are related to the consumers. The advantages related to the sources can be summarized as follows:

- Decreasing the cost of generation depending on the preferred fuel source.
- Generation of the system's backup or in the event of an emergency.
- Decreasing the electrical losses.
- Improving the power system quality.
- Reducing the planning and the installation time.
- System reliability will be achieved and the system will be more flexible.
- An environmentally clean and low noise source of power is also achieved.
- Newer distributed generators can run on fuels generated from bio-gasification.
- Decreasing the transmission and the distribution costs.

From the end-user perspective, DG is also attractive for several reasons:

- Power reliability and power quality of the DGs will be much higher than the central generating stations case.
- The prices of the Electricity will be reduced if more DGs are available.
- Some DG technologies provide cogeneration possibilities.
- Larger efficiency by using the heat produced for heating, warming water for industrial processes.

1.1.2 DG definitions

Different definitions for DG are presented in the literatures [16]-[24]. The different definitions are based on DGs connection, basic characteristics and voltage levels. The early DG's definition, given by the working group of CIGRE, depends on the maximum capacity of generation [17]. This maximum capacity is between 50 MW and 100 MW. These units are usually connected to the distribution network. They are neither centrally planned nor dispatched. DG is also defined as the generation of electricity by facilities that are sufficiently smaller than central generating plants so as to allow interconnection at nearly any point in a power system [18]. The definition given by International Energy Agency is opposite to the previous definitions. There is no reference to the generation capacity level. The DG is seen as unit producing power on a customer's site. It is also located within local distribution utilities. It supplies power directly to the local distribution network. DG definitions are summarized in [19]. DG is defined as a small source of electric power generation or storage in [20]. Typically it is ranging from less than few KWs to tens of MWs that is not a part of a large central power system and

located close to the load. DG may be defined as relatively small generation units of 30 MW or less [21]. DGs are sited at or near customer sites to meet specific customer needs, and/or support economic operation of the distribution grid. An overview of the different definitions proposed in the literature is finally given in [22], where DG is defined in terms of connection and location rather than in terms of generation capacity [23].

1.1.3 DG applications

The DG applications have been summarized in [9] as follows:

- Emergency, stand-by generators and battery systems.
- Cogeneration and renewable energy systems (e.g., solar, wind, small hydro-electric and biomass facilities).
- DG installed to serve remote or isolated loads.
- Installed Uninterruptible Power Supply (UPS) systems.
- DGs are located close to loads so they can provide operators by their requests.
- DGs give more electric price signals.

1.1.4 Movement from DG to Microgrids

As given before in the last section, the microgrid is defined as a small-scale power supply network that is designed to provide power for a small community. The emerging potential of generation units and associated loads are viewed as a subsystem, or a "microgrid" in a systematic approach [25]-[26]. The concept of the microgrid has been discussed in [27]. The operation of a microgrid is considered as an aggregate of generation and ideal

conventional loads [28]. The commercial distributed generation incentives are probably insufficient to provide ancillary services to the local network [4].

1.1.5 DG and Microgrids interconnections with the Grid

DG systems can be interfaced to the power system via three ways; synchronous generators, induction generators and power electronics. Synchronous machines must run at a synchronous speed when they are connecting with the utility. They are used with most reciprocating engines and high power turbines such as gas, steam, and hydro. Induction generators are typically used in wind turbines and some low-head hydro applications. The power electronics are used to convert the electric power from the energy source to fixed frequency ac power. So the flexibility and adaptability of the system will be increased. They provide the grid by the ancillary services or benefits such as backup power, power quality improvement and demand management functions [1]-[2]. Power converters technology has been increased in the last decays. They can be used with Distributed Energy Resources (DER) to facilitate the integration of DG in the utility.

1.1.6 DG connections modes

Microgrids can operate in both autonomous and grid-connected modes. Security, quality, reactive power support and power flow management are the main issues in the grid-connected mode. During this mode, the microgrid is used to support the load by its requirements and contractual obligations. The capability of microgrid should be achieved to regulate the active and reactive output powers and to ensure high power quality levels. The amount of injected real power can be determined by the utility and the DG owner. It depends on the connected load and the market situation. It behaves as a controllable load

or source. It should not actively regulate the voltage at the point of common coupling (PCC). The microgrid should be disconnected when an abnormal condition occurs in the grid or when it is used to feed separated loads. Thereby it shifts to island mode of operation. In this case, the microgrid is faced with the important issues such as voltage and frequency management, balance between supply and demand, power quality, microsource issues and communication among microgrid components. In the autonomous mode, the inverter is controlled to feed the load with the pre-defined voltage and frequency values according to a specific control strategy. In this mode, the DG has the responsibility of maintaining the frequency and the voltage of the microgrid system as well as supports the loads by the required active and reactive powers.

1.2 PROBLEM DESCRIPTION

Large penetration of DG units recently in distribution networks challenges the control and stability of DGs. The main function of a DG unit in the grid-connected mode is to supply the agreed fundamental frequency active power while in the autonomous operation mode the inverter-based DG has to support their loads by the required powers while maintaining the voltage and frequency within their allowed limits. Stability studies in the autonomous and grid-connected modes are required to ensure a safe operation with good performance. The control of the inverter-based DG should be designed to overcome different problems in the two modes.

In the autonomous mode, the inverter-based DG faces the following problems;

1. When more than one DG is used to support their loads in the autonomous mode, a proper load sharing between these DG units is required.

2. The control features of each inverter-based DG have been affected by the stability problems associated with the droop-based control.
3. Disturbances due to load changes might be challenged in autonomous mode.
4. Different modes are created due to power sharing, load conditions and controller parameters of the system control.
5. The closed-loop inner controllers should track voltage and current references perfectly, accurately and quickly
6. An outer power controller should set the reference for the inductor currents from the given fundamental real and reactive power commands
7. Controller should be used to obtain a zero steady-state error and compensate for the inverter switching nonlinearities and inductor non-idealities

In the grid connected mode, it faces the following problems;

1. The capability of inverter to inject the required fundamental frequency real and reactive powers.
2. Reduce or attenuate the switching frequency ripple in the output voltage.
3. Avoid the resonance between the filter and coupling or grid inductance.
4. The basic inverter control should be designed to achieve the fundamental frequency real and reactive power control.

In the autonomous mode, the stability can be affected by controller parameters as well as power sharing coefficients. In the grid-connected mode, controller parameters and filter parameters are the key factors of microgrid stability. Generally, careful selection of the controller, filter, and power sharing parameters maintains power quality within the regulated range and enhance the system performance against load changes and

disturbances. So the stability of microgrid systems requires deeper studies to understand the behavior of the system after different disturbances. Determining the optimal parameters that affect the stability in both modes is the main issue of this thesis.

1.3 OBJECTIVES

This research aims at broadly developing a new scope to obtain the optimal parameters that contribute to dynamic analysis of an inverter-based microgrid. These optimal parameters will be able to guarantee stable and high power quality injection under the disturbances and uncertainties. Numbers of takes are building to achieve the main target which is obtaining the system stability.

In brief, the following issues have been handled in this thesis:

1. Analyzing the small signal stability characteristics is necessary to understand the stability behavior of the microgrid system. The impact of critical system parameters on the stability is also studied using eigenvalues analysis.
2. Eigenvalue based objective functions are proposed to enhance the damping characteristics.
3. Nonlinear time-domain based as well as eigenvalue based objective functions are proposed to minimize the error in the measured power and to enhance the damping characteristics respectively.
4. Also, the nonlinear time domain simulation has been carried out to assess the effectiveness of the proposed controllers under different disturbances and loading conditions.

5. The control problem has been formulated as an optimization problem where particle swarm optimization is employed to search for optimal settings of the optimized parameters in each mode.
6. Two different objective functions are proposed to enhance the system stability.
7. A new scope is used to obtain the optimal parameters that contribute to dynamic analysis of an inverter-based microgrid.
8. Different disturbances will be applied to demonstrate the effectiveness of the proposed design approach.
9. Real Time Digital Simulation (RTDS) environment is also used to verify the effectiveness of the proposed control strategies.

1.4 DISSERTATION OUTLINE AND SUMMARY OF CONTRIBUTIONS

The dynamic nature of the distribution network challenges the stability and control effectiveness of the microgrids in both autonomous and grid-connected modes. An extensive literature survey has been presented in chapter two to clarify the importance of the stability and control problems in the autonomous and grid-connected operation modes. The motivation of this work is to get the optimal parameters affecting the system stability. Linear and nonlinear models for both operation modes will be developed and presented in chapters 3 and 4 respectively. The modeling of the autonomous and grid-connected modes is established to study the stability of the microgrid in both modes. This modeling is also used to control the voltage source inverter (VSI) of the inverter-based DG to feed the grid by required injected power in the grid connection mode and to support loads by their required active and reactive powers in the autonomous mode.

Linear and nonlinear models of a microgrid include VSI, power, current and voltage controllers, filter, lines and loads in the autonomous mode while include VSI, phase locked loop (PLL), power and current controllers, filter components, coupling inductor and utility in the grid-connected mode. Chapter 5 presents the problem formulation, problem constraints and optimization problem. Overview, advantages, steps and implementation of PSO are also introduced in this chapter. The design of different controllers, filter, and power sharing coefficients is formulated as an optimization problem. Two different objective functions to enhance the system stability are proposed. PSO technique is employed to search for the optimal settings of the optimized parameters.

Simulation results and discussion of the autonomous mode microgrid are reported in chapter 6. Simulation results and discussion of the grid-connected microgrid mode are illustrated in chapter 7. Different disturbances are applied to demonstrate the effectiveness of the proposed design approach. In the grid-connected mode, the step change is used to verify the system capability to track its reference power. In the autonomous mode, step change and fault disturbances are used to verify the system stability. Chapter 8 presents an introduction in RTDS while the RTDS simulation results of the grid-connected microgrid mode are given in Chapter 9. Chapter 10 presents the conclusions drawn from this research work and some directions suggested for the possible future work.

The main contributions can be summarized as follows;

- In the autonomous microgrid mode:

1. The nonlinear model of a microgrid, network and load is proposed to minimize the error in the measured power.
2. A small-signal state-space model of a microgrid is also developed to enhance the damping characteristics.
3. The optimal power sharing coefficients of the power controller are obtained using PSO to achieve the centralized power sharing between DGs in the autonomous microgrid system.
4. The optimal proportional integral (PI) gains of the voltage controller are obtained using PSO to control the output voltage within given reference voltage.
5. The PI gains of the current controller are optimized to control the filter inductor current and to set the reference output voltage of the inverter.
6. The stability of the autonomous microgrid operation is investigated in the linear model using eigenvalues analysis.
7. The stability of the autonomous microgrid operation is investigated in the nonlinear model by introducing different disturbances such as fault scenario.
8. Different cost functions are applied to check the effectiveness of the proposed controllers under various disturbances.

- In the grid-connected microgrid mode:
    1. The nonlinear model of a microgrid and utility is developed.
    2. A small-signal state-space model of a microgrid is also developed.

3. Time domain simulation is carried out under various operating conditions such as real power step change.
4. Optimal controller design of the nonlinear model is obtained.
5. Optimal filter design of the nonlinear model is obtained to attenuate switching frequency ripple.
6. Optimal damping resistance design is obtained to avoid the resonance that may arise with coupling or grid inductance.
7. The stability of the microgrid operation is verified in both linear and nonlinear models.
8. The step change test is used to verify the system capability to follow its reference value.
9. The nonlinear model is implemented using RTDS to verify the proposed controller.
10. The performance of this controller is verified by simulation using RTDS.

CHAPTER 2

LITERATURE REVIEW

2.1 INTRODUCTION

Microgrids are small electrical distribution systems that connect multiple customers to multiple distributed sources of generation and storage interfacing through power electronic inverters. The capability of the microgrid system to increase the system reliability and to maintain the stability of the distribution network makes it a potential field of research. Microgrid is the future of the electrical distribution network. This chapter presents a detailed literature survey on the microgrid. It includes brief survey on the interfacing, control and management of microgrids. Also, the behavior of the microgrid dynamics under different disturbances during grid-connected and autonomous modes is also addressed.

2.2 MICROGRIDS INTERFACING

Most of the microsources must be power electronic based to provide the required flexibility and to ensure controlled operation as a single aggregated system [1]-[2]. Power

electronic technology plays great role in converting the DC voltage or variable frequency AC voltage into the desired voltage magnitude and frequency for a grid connection. It also serves as a conditioning system to address the difference between the DG units and the system requirements. It is being widely used to interface between DG and utility due to two main reasons [29]:

1. The development of fast semiconductor switches capable of switching quickly and handling high powers.
2. The development of digital controllers that can implement advanced and complex control algorithms.

The most common power electronics interfaces for Distributed Energy (DE) applications are described in [30]. Also, possible power electronics topologies that will lead to low cost and reliable power electronics interfaces are outlined. New trends in power-electronic technology for the integration of renewable energy sources and energy-storage systems are presented in [1]. The current technology and future trends of variable-speed wind turbines are also described. Power-conditioning systems used in grid-connected photovoltaic (PV) generation plants are presented in [2]. The development of modern power electronic technology is also presented to enable a successful integration with the utility. Controlling and interfacing DG with the utility using power electronic has been addressed in microgrids [3]-[5]. The general structures of the systems interfacing and the characteristics of some dispersed generation units such as wind power, fuel cells and PV generators are also presented. Various power electronics topologies for different DE systems are introduced to find a generalized topology that can be used for different DE applications with very small or almost no modification [30]. The benefits of using power

electronics interfaces for system integration and optimization issues associated with DE systems are examined [6]. The power electronic interfaces needed for microsources of the Consortium for Electric Reliability Technology Solutions (CERTS) microgrid is presented in [31]. The details of an energy storage module, a variable-speed synchronous generator based microsource when operating in the CERTS microgrid and an electronic interface for microsources are described. Control the operation of storage module based on dynamics of the prime mover is also reported.

2.3 CONTROL OF MICROGRIDS

Control of microgrids in both modes has been investigated recently [32]-[45]. In the grid-connected mode, the control of the inverter is required to make the microgrid capable of regulating the active and reactive output currents, ensuring high power quality levels, and achieving relative immunity to grid perturbations. In the autonomous mode, the inverter is controlled to feed the load with the pre-defined voltage and frequency values according to a specific control strategy.

The island operation issues of the microgrids are enumerated and discussed [32]. The comparison between strategies based on their applicability to different control requirements is presented. The operation of an island-mode microgrid is adopted to study the feasibility of the control strategies [33]. The need of storage devices and load shedding strategies is also evaluated. Control techniques of the DG plants using feedback of locally measurable variables are introduced [34]. The potential-function based method for secondary and tertiary control of islanded and grid-connected microgrid modes is introduced [35]. It is defined for each controllable unit of the microgrid such as the minimum of the potential function corresponds to the control goal. It is applied for the

secondary voltage control of two microgrids with single and multiple feeders. The studies are conducted in the time-domain using the PSCAD/EMTDC software environment. The microgrid concept and its properties are presented in [36]. Strategies towards their efficient and fault-tolerant control with RES, intelligent loads and storage units are developed. These strategies are based on fully local control and they do not require any communication between the DER units. Control, islanding detection, load shedding and re-closure algorithms of the grid-connected DG are proposed [37]. A control strategy to implement intentional islanding operation of microgrids is described. Two interface controls are used, one for grid-connected operation and the other for intentional-islanding operation. An islanding detection algorithm is designed to switch between the two controls. The control techniques required for microgrid operation is discussed [38]. A simple control strategy of microgrid model is implemented using MATLAB. The modeling and control strategy are kept elementary. The power quality control issues, pre-set conditions of islanded mode and operation of autonomous microgrid mode are discussed. In the autonomous mode, the non-critical loads are automatically eliminated while the critical loads are continuously supplied. Different control systems are investigated in order to accommodate DG in the distribution network level and to improve the performance of DG units without violating network constraints [39]. They are also used to provide appropriate frameworks to participate effectively in the power system and market operation.

Different controls of DG have been reviewed [40]. They include DG control, network control and paradigms control. DG control is responsible for producing and injecting power to the network. Network control is able to improve the DG performance without

causing the network operational problems. Control paradigms such as microgrid, cell, and virtual power plant provide frameworks of participating, controlling and management DER in the system. Simple control schemes for a three-phase VSI intended for grid-connected operation have been presented [41]. The controllers are selected to provide stable and fast response to the system. Control schemes of the inverter-based DG are employed using linear models. The decoupled power controller concept for tracking load demand of an inverter-interfaced DG system is introduced [42]. The controller design is based on the reference frame theory. An adaptable and flexible hierarchy control strategy of interconnected inverter-based mini-grids based on the conventional power control structure is presented [43]. It is able to handle both conventional and modern DG sources. The operational hierarchy control structures of interconnected power systems are analyzed. The ability of the control functions to support future sources and power system architectures are examined. These hierarchical control levels are the primary control at unit level, the secondary control at local level and the tertiary control at supervisory level. The proposed strategy is modular, flexible and reliable. A new control method based on the microgrid line frequency variation is introduced [44]. The stability and robustness of the DG control operation under transients and dynamic conditions are checked when different energy sources are integrated within the microgrid system. The power system is framed as a game between players to facilitate the definition of individual objectives [45]. The control decision process of individual sources and loads in small-scale and dc power systems is presented. The game theoretic methodology enhances the reliability and robustness of the system by avoiding the need for central or supervisory control. It is also a way to integrate and combine supply and demand side management into a single

approach. A simple nine bus dc power system is used to demonstrate the proposed method for various scenarios.

2.4 MICROGRID ENERGY MANAGEMENT

DGs are controlled to manage the power between the DGs inside the microgrid [46]-[60]. A control scheme of microgrids with passive local loads is presented [46]. A microgrid with its local loads is simulated in the MATLAB/SIMULINK and the ATP Draw software environment. Several line-interactive UPS systems are parallel connected in either grid-connected or islanded microgrid [47]. The control technique is based on the droop method to avoid critical communications among UPS units. A small-signal analysis is presented in order to analyze the system stability. Design rules the main control parameters are given. Future energy production, consumption and storage techniques are smartly applied to achieve a more energy efficient electricity supply chain [48]. Three-step control methodology is proposed to manage the cooperation between these technologies. The global objectives of this approach are to achieve the peak shaving or forming a virtual power plant without harming the comfort of residents. Also a better matching between demand and supply are achieved using good predictions, in advance planning and real time control of domestic appliances. Linear time-invariant robust servomechanism controller for islanded operation of a DG unit and its local load is proposed [49]. A new optimal controller design procedure is introduced. The proposed controller utilizes an internal oscillator for frequency control and a robust servomechanism controller to regulate the island voltage. Despite uncertainty of the load parameters, the proposed controller guarantees robust stability and pre-specified performance criteria, e.g., fast transient response and zero steady-state error. The

theoretical aspects of the proposed robust servomechanism controller including the existence conditions, controller design, and robust stability analysis of the closed-loop system are studied.

The well-known droop control is used to share the fundamental real and reactive powers with other microgrid sources. In the droop control, the inverter emulates the behavior of a synchronous machine. The power angle δ depends mainly on real power P, while the voltage depends mainly on reactive power Q. So the angle δ is controlled by regulating P, while the output inverter voltage is controlled through Q. Controlling the frequency dynamically controls the power angle and, thus, the real power flow. Therefore, by adjusting P and Q independently, frequency and voltage amplitude of the microgrid can be determined [50]-[52]. A voltage-power droop/frequency-reactive power boost (VPD/FQB) control scheme is presented [52]. The controller allows paralleled multiple Voltage Source Converters (VSC) to operate in a VSC fed microgrid. Each current controlled VSC uses its controller to set the reference currents to regulate the voltage and frequency of a common microgrid bus. The proposed control scheme is also operated in grid-connected mode. The real and reactive power management strategies of multiple electronically interfaced DG units are addressed [53]. Power management and control strategies of DGs are based on locally measured signals without communications. These strategies are based on voltage-droop characteristic, voltage regulation, and load reactive power compensation. The real power of each DG unit is controlled based on a frequency-droop characteristic and a complimentary frequency restoration strategy. A systematic approach is also presented to develop a small-signal dynamic model of a multiple-DG microgrid. It includes real and reactive power management strategies. The microgrid

eigen structure is used to investigate the microgrid dynamic behavior, to select control parameters of DG units and to incorporate power management strategies in the DG controllers. The design sensitivity to the parameters and the operating point changes is investigated. Also, it is used to optimize performance of the microgrid system. An Energy Management System (EMS) for a stand-alone droop-controlled microgrid is presented [54]. EMS is used to adjust the output power of the generators to minimize fuel consumption and also to ensure stable operation. Using qualitative analysis and small-signal techniques, the relationship between frequency-droop gains and stability margins are also identified. A novel frequency-voltage frame transformation to improve the system stability is proposed [55]. A control algorithm is proposed to guarantee the operation of the microgrid within the predetermined voltage and frequency variation limits. An adaptive reactive power droop method is also proposed. The maximum reactive power limit of a DG unit is automatically updated based on its current rating and actual real power output to improve the system stability. An adaptive decentralized droop controller of paralleled inverter-based DG units to preserve the power sharing stability is presented [14]. The proposed power sharing strategy is based on the static droop characteristics combined with an adaptive transient droop function. The transient droop gains are adaptively scheduled via small-signal analysis of the power sharing mechanism to define the immigration of the power modes at different loading conditions. The adaptive nature of the proposed controller is used to ensure active damping of power oscillations at different operating conditions and to yield stable and robust performance of the paralleled inverter system.

Power sharing principles among multiple DGs under various system conditions such as load variation during grid-connected operation, load variation during islanded operation, and disconnection from the main grid are investigated [56]. Unit output power control and feeder flow control (FFC) are introduced and analyzed to control the active power of DGs. An algorithm of modifying the droop constant of the FFC-mode DGs is proposed to ensure proper power sharing among DGs because the FFC control mode is limited by the existing droop controller. The principles and the proposed algorithm are verified using PSCAD simulation. The impact of droops and primary reserve scheduling on the microgrid stability is evaluated using the bifurcation theory [57]. The methodology is based on finding the worst primary reserve share. After rescheduling the droops of selected generating units, the worst sharing is found. A measure of the distance to instability in a given direction is found in a multi-parameter space endowed with coordinates corresponding to the droop coefficients. The proposed approach is analyzed in a 69-bus and 11-generation unit isolated microgrid. The distances and normal vectors provide valuable insight on the correct scheduling from the stability point of view. The stability of three inverter ring connected microgrids has been examined in [58]. The mathematical model using justifiable assumptions is simply formed. The stability of the microgrid is analyzed with each inverter transformed into an equivalent network. The impedances of the interconnections are included in each equivalent inverter network. The effect of the droop control laws is separately examined. The interconnection cables are predominantly assumed inductive then the droop laws are decoupled. The model for a large and complex microgrid is written as a product of models of each inverter with its droop control laws. An improved voltage and current control loop based on the

decoupling of the cross-coupling terms in a synchronous reference frame is presented in [59]. The effects of the decoupling of the cross-coupling terms when PI synchronous regulators are used in droop characteristic converter are analyzed. The PI synchronous regulators are implemented for both voltage and current control. The performance of angle and frequency droops in VSC interfaced DGs are compared in [60]. The output voltage angle of the DGs through droop is controlled to provide a proper load sharing among the DGs. Both the angle and frequency droop controllers are designed through eigenvalues analysis. The performance of these two controllers is then performed through PSCAD simulations.

2.5 MICROGRID STABILITY

Stability of microgrid in both modes has recently attracted more attention of researchers [61]-[71]. The safe and stable operation of an autonomous power system interconnecting an AC source with various types of power electronic loads has been investigated [61]. The system stability under large-perturbations by means of parameter space mapping, energy functions, and time domain simulations is studied. The voltage stability of the island microgrid is studied. A systematic approach is also used to develop a small-signal dynamic model of a multiple-DG microgrid [62], [66]-[68]. It includes real and reactive power management strategies. The microgrid eigen structure is used to investigate the microgrid dynamic behavior, to select control parameters of DG units, and to incorporate power management strategies in the DG controllers. The model is also used to investigate sensitivity of the design to changes of parameters and operating point and to optimize performance of the microgrid system. A MATLAB/SIMULINK model of microgrid simulated is presented [62]. A small signal state-space model is derived for the microgrid

system to determine the eigenvalues of the system. A detailed analysis is carried out to investigate the effect of constant power load on the stability of an autonomous microgrid. A sensitivity analysis is carried out to determine whether it is possible to move Right Hand Side (RHP) poles to Left Hand Side (LHP) by changing the current and voltage controller gain values. The stability analysis for multiple converters is introduced [63]. Linear state space model of an autonomous microgrid is formed. The generalized method to define the stability is given [64]. Parallel-connected inverters are controlled by decentralized active power/voltage frequency and reactive power/voltage magnitude droop control laws. The systems have stability problems for large values of active power/voltage frequency droop control gain. The stability of the microgrid is examined by simplifying the differential algebraic equations of the system. The problem of appropriate load sharing in an autonomous microgrid is investigated [65]. Frequency-domain modeling, eigenvalue analysis, and time-domain simulations are used to demonstrate the conflict between high gain angle droop control and its negative impact on overall stability. A supplementary droop control loop is proposed to stabilize the system. It is formulated as a parameter optimization problem and solved using an evolutionary technique. Small-signal models for microgrids consisting of DGs connected in a chain topology are developed [66]. Small-signal dynamic behavior of number of DG chain microgrid is carried out using eigenvalues analysis. Sufficient conditions are developed to guarantee their small signal stability. A small-signal dynamic model of a microgrid system is presented in a rotating dq0 frame [67]. The DG units of the microgrid comprise of a synchronous generator and an electronically interfaced DG unit. The control strategies for various microgrid operation modes are also presented. Frequency

restoration is carried out by the governor of the synchronous machine. Microgrid dynamics are investigated and the controllers of the electronically interfaced DG unit during grid-connected and islanded modes of operation are designed. The microgrid stability is obtained using the sensitivity analysis through changing the controller parameters and power coefficient parameters. A dynamic model of single shaft Microturbine Generation (MTG) system is developed in MATLAB/ SIMULINK using SimPowerSystems toolbox [68]. It is suitable for grid connecting/islanding operation. The bidirectional power flow between grid and MTG system is allowed in the presented model. The control strategies for both operation modes of a DG system are also given. A synchronous condenser and a microturbine with an inverter interface are implemented in parallel to regulate the local voltage [69]. To utilize distributed power sources effectively in the laboratory, dynamic microgrid is proposed [70]. The modeling and analysis of autonomous operation of inverter-based microgrids is developed [71]. The small-signal state-space model of an individual inverter is constructed. The model includes the controllers, output filter and coupling inductor on a synchronous reference frame. The eigenvalues are used to indicate the frequency and damping of oscillatory components in the transient response. The method depends on changing the controller parameters until achieving the stability of the autonomous microgrid. A sensitivity analysis is also used to study the effect of these parameters in achieving microgrid stability. The method depends on trial and error therefore it takes long time to obtain the controller parameters which achieve the microgrid stability. The microgrid stability has been affected by different factors in both modes. For example, in the autonomous mode, the stability has been affected by controller parameters as well as power sharing coefficients. But in the grid-

connected mode, the selected controller parameters, the filter inductance and filter capacitance are very important to achieve the system stability. Most selection of controller parameters is based on a trial and error approach incorporating knowledge of the overall system characteristics. Furthermore, trial and error approaches cannot reliably predict all microgrid operational scenarios that can result in poor power quality or angle/voltage instability [72]. So the controller and filter parameters should be selected carefully in order to maintain power quality within the regulated range and support the system against any load changes or any disturbances. Although using LC filter mitigates the switching ripple injected in the grid by the three-phase inverters, the stability problem could arise in the current control loop [73]-[75]. The stability of the microgrids operating in either mode is quite essential and it is affected by different parameters. In the autonomous mode, the stability can be affected by controller parameters as well as power sharing coefficients. In the grid-connected mode, controller parameters and filter parameters are the key factors of microgrid stability. Generally, careful selection of the controller, filter, and power sharing parameters maintains power quality within the regulated range and enhance the system performance against load changes and disturbances. Different approaches to select the controller parameters and control strategies, where trial and error approach used, have been reported in the literature [54], [71]. This approach is time consuming and no guarantee that the adopted settings are the optimal ones. In addition, it does not provide a systematic procedure to solve the controller design problem. Recently, computational intelligence algorithms such as Genetic Algorithm (GA) and PSO have been applied to different power system problems with impressive success [76]. However, some deficiencies in GA performance such as the

premature convergence have been recorded [76]. On the other hand, PSO has been widely implemented and stamped as one of the promising optimization techniques due its simplicity, computational efficiency, and robustness. Generally, PSO has been motivated by the behavior of organisms, such as fish schooling and bird flocking. It combines social psychology principles in socio-cognition human agents and evolutionary computations. Unlike the other heuristic techniques, PSO has a flexible and well-balanced mechanism to enhance the global and local exploration abilities [77]. PSO has been also employed to obtain the controller parameters and power sharing coefficients in both modes [72]-[78]. However, the LC filter design and coupling inductance have not been taken into consideration in the presented approach. It is worth mentioning that the microgrid stability is strongly affected also by the filter parameters [64]. In [72], PSO algorithm has been applied directly to a power-electronic-switch-level microgrid simulation model instead of small-signal models. Additionally, the method presented in [72]-[78] needs external software to simulate the system and calculate the objective function.

CHAPTER 3

MICROGRID MODELING IN AUTONOMOUS MODE

During the autonomous operation mode, DGs are responsible for supplying the active and reactive powers required and maintaining the voltage and frequency within their allowable limits. In addition, it is necessary to ensure a proper load sharing among the generation units to avoid over-loading of any individual unit. This section provides the mathematical model of the autonomous microgrid consisting of VSI controller connected to the loads through LC filter and coupling inductance.

3.1 NONLINEAR MODEL OF THE AUTONOMOUS MICROGRID

3.1.1 VSI Model

Power, current, and voltage controllers used to control the microgrid inverter in the autonomous mode are shown in Fig. 3.1 [71]. Firstly, the active and reactive powers are calculated using the measured output current and voltage of the VSI.

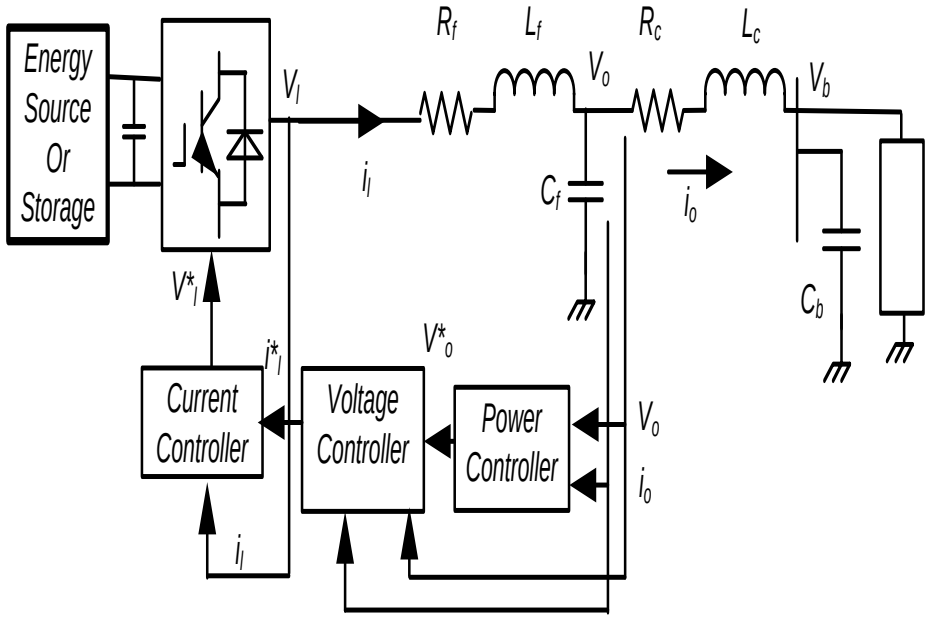

Fig. 3.1 Microgrid in autonomous mode

An external power control loop sets the magnitude and frequency (and hence phase) for the fundamental component of the inverter output voltage according to the droop characteristics set for the real and reactive powers. Then, the voltage and current controllers are designed to reject high frequency disturbances and provide sufficient damping for the *LC* filter [14]. Individual components of the microgrid are modeled as follows;

(a) Power Controller Model

In a conventional power system, synchronous generators share any increase in the load by decreasing the frequency according to their governor droop characteristics. In the autonomous mode, the inverter emulates the behavior of a synchronous machine. Therefore, the angle δ can be controlled by regulating *P*, while the output voltage is

controllable through Q. Controlling the power angle and, thus, the real power flow is achieved by control of frequency [13]. For stable operation, the real and reactive power output of the inverters should be properly controlled. The measured output voltage and current are used firstly to calculate the instantaneous active P_m and reactive power Q_m as follows;

$$P_m = v_{od} i_{od} + v_{oq} i_{oq},$$

$$Q_m = v_{od} i_{oq} - v_{oq} i_{od} \tag{3.1}$$

where:

v_{od} is the d- component of the output voltage on individual reference frame (V),

v_{oq} is the q- component of the output voltage on individual reference frame (V),

i_{od} is the d- component of the output current on individual reference frame (A) and

i_{oq} is the q- component of the output current on individual reference frame (A).

Secondly, the real and reactive powers P_c and Q_c corresponding to the fundamental components are obtained after passing these powers through low pass filter. The block diagram of power controller is shown in Fig. 3.2.

$$P_c = \frac{\omega_c}{\omega_c + s} P_m,$$

$$Q_c = \frac{\omega_c}{\omega_c + s} Q_m \tag{3.2}$$

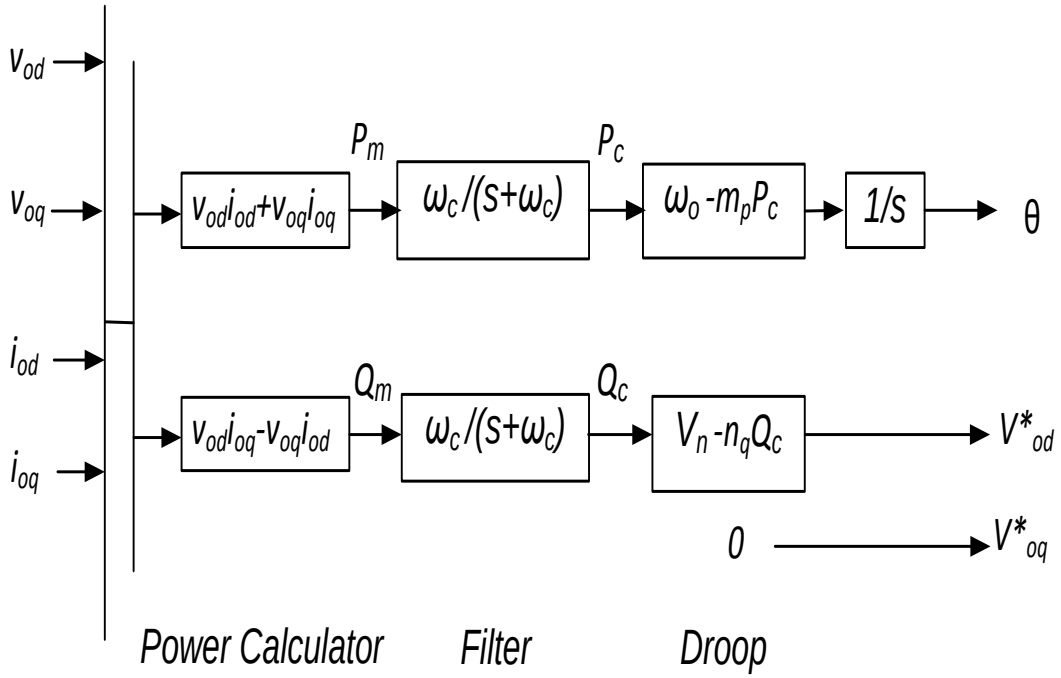

Fig. 3.2 The block diagram of power controller

Finally, the frequency ω and the output *d*-axis voltage magnitude reference v^*_{od} are determined as:

$$\omega = \omega_n - m_p P_c \quad , \quad \dot{\theta} = \omega \tag{3.3}$$

$$v^*_{od} = V_n - n_q Q_c \ , \ v^*_{oq} = 0 \tag{3.4}$$

where;

m_p is the real power droop gain of the power controller,

n_q is the reactive power droop gain of the power controller,

V_n is the nominal output voltage reference of the inverter (V),

θ is the phase angle reference of the inverter output voltage (rad),

v^*_{oq} is the q-component of the output voltage reference on individual reference frame (V),

v^*_{od} is the d-component of the output voltage reference on individual reference frame (V), and ω_n is the nominal frequency of the inverter (rad/sec).

The different droop characteristics show that any number of inverters can share the total real and reactive power as shown in Fig. 3.3. The reference frame of one of the inverters is taken as the common frame. The angle δ shown in Fig. 3.4 represents the angle between an individual inverter reference frame and the common reference frame. This angle is used to translate the variables from an individual inverter reference frame onto the common frame.

$$\delta = \int \omega - \omega_{com} \tag{3.5}$$

where ω_{com} is the frequency of the common reference frame.

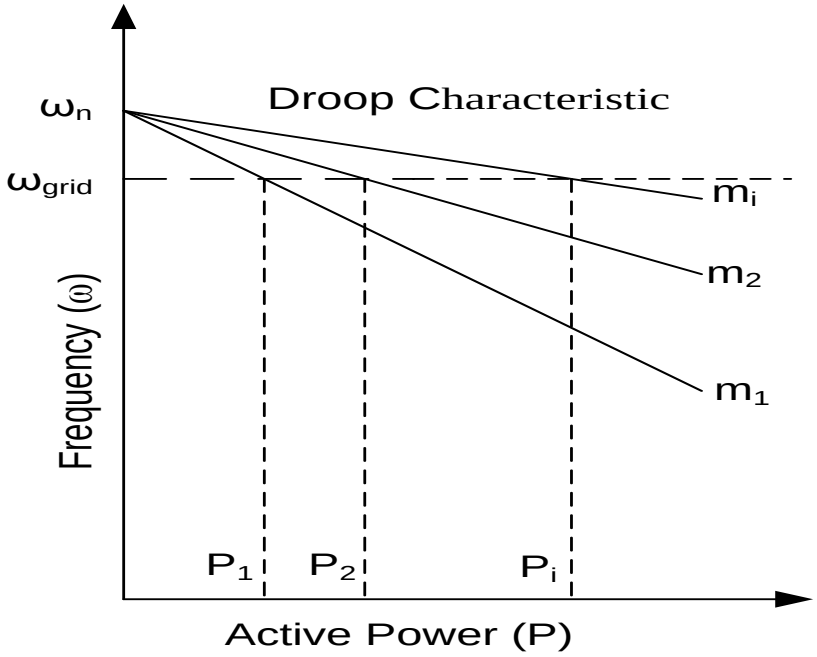

(a)

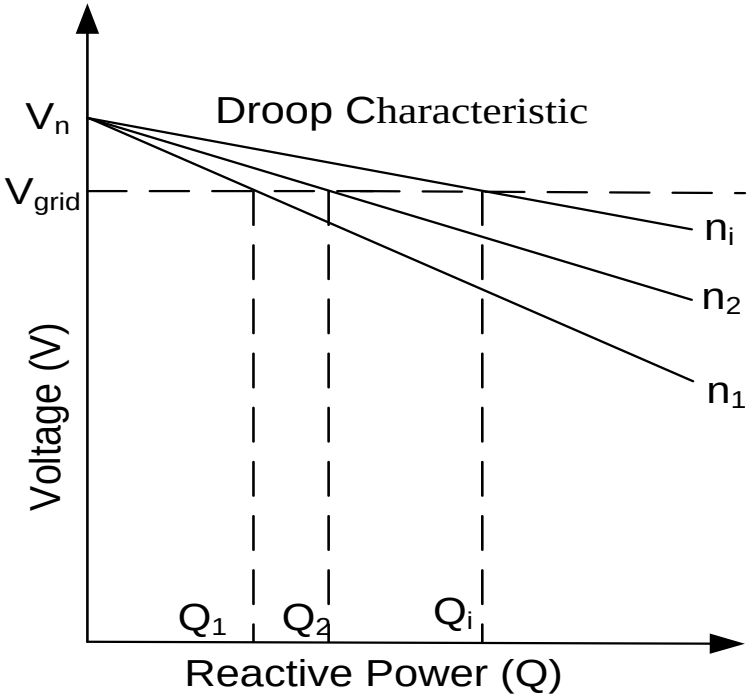

(b)

Fig. 3.3 Droop characteristics

(a) Frequency against active power

(b) Voltage against reactive power

where;

V_{grid} is the nominal grid voltage (V),

P_i is the output active power of each inverter (W) and

Q_i is the output reactive power of each inverter (VAR).

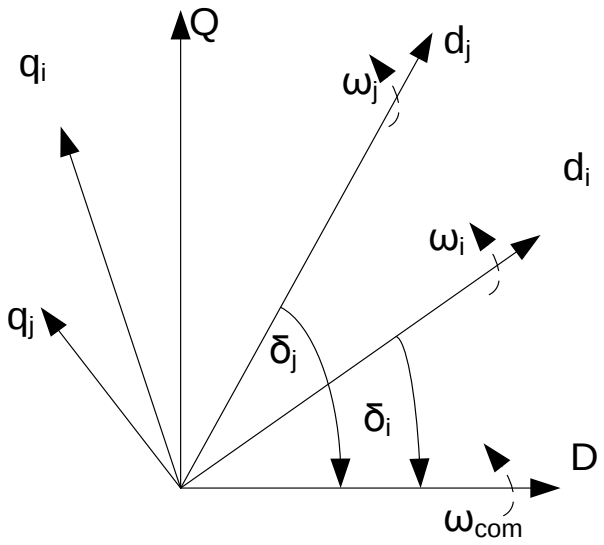

Fig. 3.4 Reference frame transformation

where;

δ_i is the angle between the inverter (i) and the common reference frames (rad) and

ω_i is the frequency of each inverter (rad/sec).

(b) Voltage Controller Model

The *PI* voltage controller is shown in Fig. 3.5. The corresponding state equations are given as:

$$\begin{aligned}\dot{\phi}_d &= v^*_{od} - v_{od} \\ \dot{\phi}_q &= v^*_{oq} - v_{oq}\end{aligned} \tag{3.6}$$

where;

φ_d is the d-axis state variable of the voltage controller and

φ_q is the q-axis state variable of the voltage controller;

Along with the algebraic equations:

$$\begin{aligned}i^*_{ld} &= Fi_{od} - \omega_n C_f v_{oq} + K_{pv}(v^*_{od} - v_{od}) + K_{iv}\phi_d \\ i^*_{lq} &= Fi_{oq} + \omega_n C_f v_{od} + K_{pv}(v^*_{oq} - v_{oq}) + K_{iv}\phi_q\end{aligned} \tag{3.7}$$

where;

F is the feed forward voltage controller gain,

K_{pv} and K_{iv} are the PI voltage controller parameters,

C_f is the capacitance of the filter capacitor,

i^*_{ld} is the reference (d-axis) inductor current and

i^*_{lq} is the reference (q-axis) inductor current.

(c) Current Controller Model

The *PI* current controller structure is shown in Fig. 3.6. The corresponding state space model is:

$$\begin{aligned}\dot{\gamma}_d &= i^*_{ld} - i_{ld} \\ \dot{\gamma}_q &= i^*_{lq} - i_{lq}\end{aligned} \tag{3.8}$$

where;

γ_d is the d-axis state variable of the current controller,

γ_q is the q-axis state variable of the current controller,

i_{ld} is the d- component of the inductor current on individual reference frame (A) and

i_{lq} is the q- component of the inductor current on individual reference frame (A).

$$\begin{aligned} v_{ld}^{*} &= -\omega_n L_f i_{lq} + K_{pc}(i_{ld}^{*} - i_{ld}) + K_{ic}\gamma_d \\ v_{lq}^{*} &= \omega_n L_f i_{ld} + K_{pc}(i_{lq}^{*} - i_{lq}) + K_{ic}\gamma_q \end{aligned} \tag{3.9}$$

where;

K_{pc} and K_{ic} are the *PI* current controller parameters,

L_f is the inductance of the filter inductance,

v^*_{ld} is the d- component of the reference voltage on individual reference frame (V) and

v^*_{lq} is the q- component of the reference voltage on individual reference frame (V).

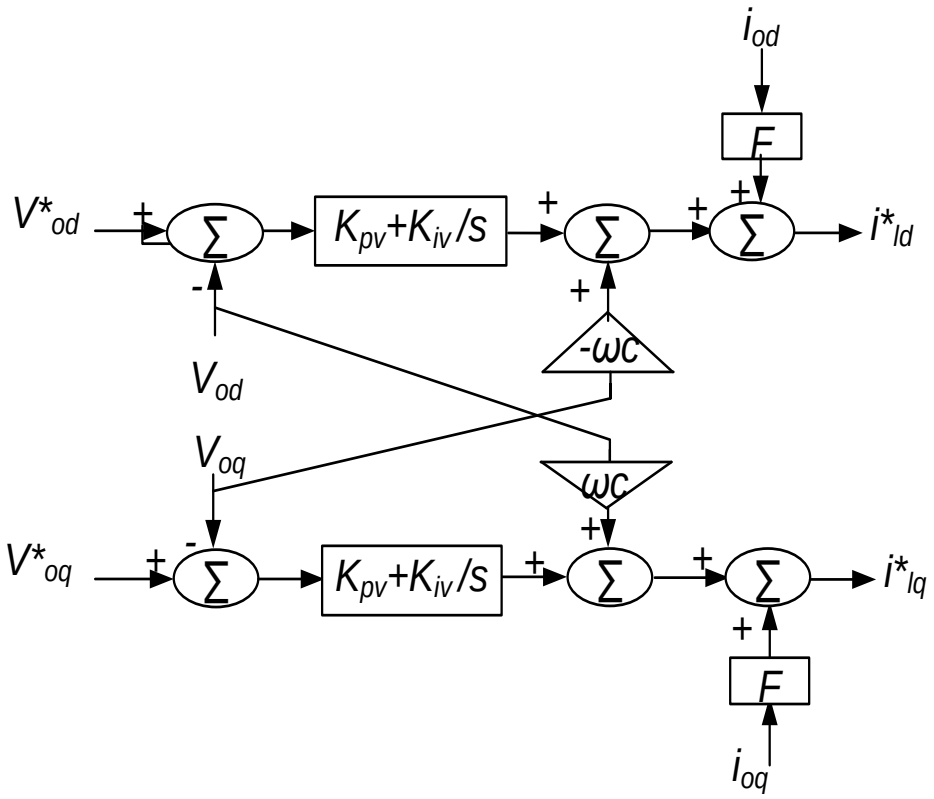

Fig. 3.5 Voltage controller in autonomous mode

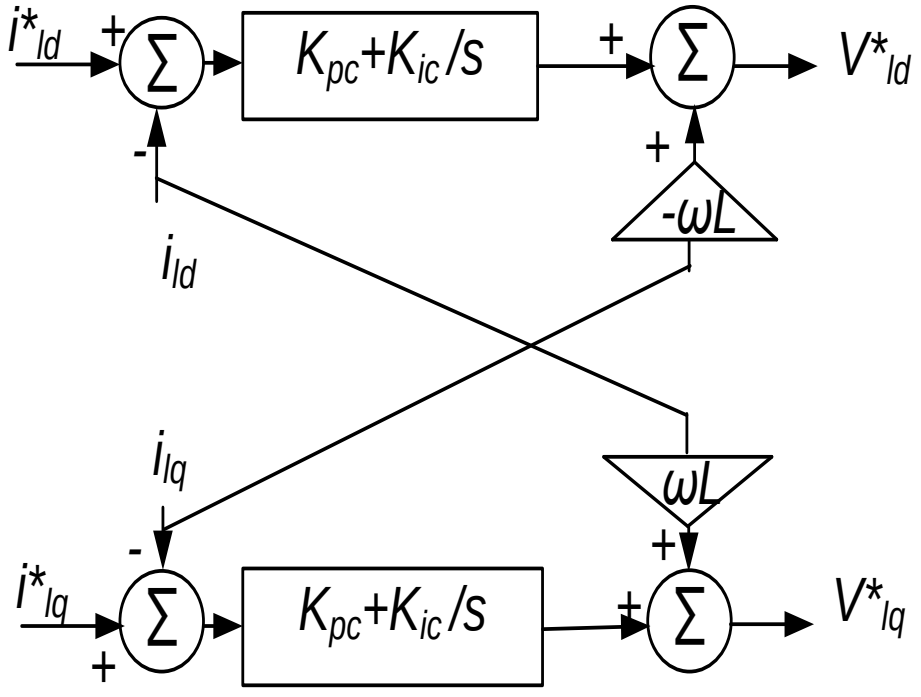

Fig. 3.6 Current controller in autonomous mode

(d) LC Filter and Coupling Inductance Model

The *LC* filter and the coupling inductance model are described with the following state equations assuming that inverter produces the demanded voltage $v_l = v^*_l$.

$$\dot{i}_{ld} = -\frac{R_f}{L_f} i_{ld} + \omega i_{lq} + \frac{1}{L_f}(v_{ld} - v_{od}) \tag{3.10}$$

$$\dot{i}_{lq} = -\frac{R_f}{L_f} i_{lq} - \omega i_{ld} + \frac{1}{L_f}(v_{lq} - v_{oq}) \tag{3.11}$$

$$\dot{v}_{od} = \omega v_{oq} + \frac{1}{C_f}(i_{ld} - i_{od}) \tag{3.12}$$

$$\dot{v}_{oq} = -\omega v_{od} + \frac{1}{C_f}(i_{lq} - i_{oq}) \tag{3.13}$$

$$\dot{i}_{od} = -\frac{R_c}{L_c} i_{od} + \omega i_{oq} + \frac{1}{L_c}(v_{od} - v_{bd}) \tag{3.14}$$

$$\dot{i}_{oq} = -\frac{R_c}{L_c} i_{oq} - \omega i_{od} + \frac{1}{L_c}(v_{oq} - v_{bq}) \tag{3.15}$$

where;

L_c is the coupling inductance (H),

R_c is the coupling resistance (Ω),

v_{ld} is the d- component of the inverter bridge voltage on individual reference frame (V),

v_{lq} is the q- component of the inverter bridge voltage on individual reference frame (V),

v_{od} is the (d-axis) output voltage (V),

v_{bd} is the (d-axis) load voltage (V),

v_{bq} is the (q-axis) load voltage (V) and

v_{oq} is the (q-axis) output voltage (V).

(e) Complete Inverter Model

To build the whole model of the system, the output variables of each inverter should be converted to the common reference frame using the following transformation:

$$f_{DQ} = T_i f_{dq} \tag{3.16}$$

$$T_i = \begin{bmatrix} \cos(\delta_i) & -\sin(\delta_i) \\ \sin(\delta_i) & \cos(\delta_i) \end{bmatrix} \tag{3.17}$$

The bus voltage which is the input signal to the inverter model should be expressed also on the common reference frame using reverse transformation.

3.1.2 Line Model

The state equations of line current of i^{th} line connected between nodes j and k are expressed on a common reference frame as follows:

$$\dot{i}_{lineDi} = -\frac{r_{linei}}{L_{linei}} i_{lineDi} + \omega i_{lineQi} + \frac{1}{L_{linei}}(v_{bDj} - v_{bDk}) \tag{3.18}$$

$$\dot{i}_{lineQi} = -\frac{r_{linei}}{L_{linei}} i_{lineQi} - \omega i_{lineQi} + \frac{1}{L_{linei}}(v_{bQj} - v_{bQk}) \tag{3.19}$$

3.1.3 Load Model

The state equations of the RL load connected at i^{th} node are given as follows:

$$\dot{i}_{loadDi} = -\frac{R_{loadi}}{L_{loadi}} i_{loadDi} + \omega i_{loadQi} + \frac{1}{L_{loadi}} v_{bDi} \tag{3.20}$$

$$\dot{i}_{loadQi} = -\frac{R_{loadi}}{L_{loadi}} i_{loadQi} - \omega i_{loadDi} + \frac{1}{L_{loadi}} v_{bQi} \tag{3.21}$$

The load voltages are also given as follows:

$$\dot{v}_{bDi} = \omega v_{bQi} + \frac{1}{C_f}(i_{oDi} - i_{loadDi} \pm i_{lineDi,j}) \tag{3.22}$$

$$\dot{v}_{bQi} = -\omega v_{bDi} + \frac{1}{C_f}(i_{oQi} - i_{loadQi} \pm i_{lineQi,j}) \tag{3.23}$$

The sign in the (3.22) and (3.23) depends on the current direction in the line.

3.2 LINEAR MODEL OF THE AUTONOMOUS MICORGRID

Small signal analysis is used to analyze the dynamic performance and to design the control system [66]-[67]. The linear model of the autonomous microgrid mode is obtained by linearizing the nonlinear model equations given above.

3.2.1 Small Signal Model of the Inverter-based DG

The small-signal model of the inverter-based DG includes the small signal model of the power, current and voltage controllers as well as the LC filter and the coupling

inductance model. By linearizing the equations (3.1)-(3.23) described in nonlinear model, the state-space model of a single inverter unit is obtained as follows;

(a) Small Signal Model of the Power Controller

The state space model of the power controller is given as;

$$\Delta\dot{\delta} = \Delta\omega - \Delta\omega_{com} \tag{3.24}$$

where $\Delta\omega_{com}$ is the deviation in the frequency of the common reference inverter.

Since $\omega = \omega_n - m_p P_c$ then $\Delta\omega = -m_p \Delta P$ so

$$\Delta\dot{\delta} = -m_p \Delta P_c - \Delta\omega_{com} \tag{3.25}$$

From (3.2), the other states ($\Delta\dot{P}$ and $\Delta\dot{Q}$) are obtained from $\dot{P_c} = \omega_c(P_m - P_c)$ and $\dot{Q_c} = \omega_c(Q_m - Q_c)$ as follows;

$$\Delta\dot{P_c} = \omega_c(\Delta P_m - \Delta P_c)$$

and $$\Delta\dot{Q_c} = \omega_c(\Delta Q_m - \Delta Q_c)$$

where ΔP_m and ΔQ_m are obtained by linearizing the equation (3.1) as follows;

$$\Delta P_m = V_{od}\Delta i_{od} + V_{oq}\Delta i_{oq} + I_{od}\Delta v_{od} + I_{oq}\Delta v_{oq}$$

and $$\Delta Q_m = -V_{oq}\Delta i_{od} + V_{od}\Delta i_{oq} + I_{oq}\Delta v_{od} - I_{od}\Delta v_{oq}$$

So $$\Delta\dot{P_c} = \omega_c(V_{od}\Delta i_{od} + V_{oq}\Delta i_{oq} + I_{od}\Delta v_{od} + I_{oq}\Delta v_{oq} - \Delta P_c) \tag{3.26}$$

And $$\Delta\dot{Q_c} = \omega_c(-V_{oq}\Delta i_{od} + V_{od}\Delta i_{oq} + I_{oq}\Delta v_{od} - I_{od}\Delta v_{oq} - \Delta Q_c) \tag{3.27}$$

(b) Small-Signal Model of the Voltage Controller

The corresponding state equations are given in (3.28), along with the algebraic equations given in (3.6) and (3.7).

$$\Delta\dot{\phi}_d = \Delta v^*_{od} - \Delta v_{od} \tag{3.28}$$

Since $v^*_{od} = V_n - n_q Q_c$ then $\Delta v^*_{od} = -n_q \Delta Q_c$

then $$\Delta\dot{\phi}_d = -n_q \Delta Q_c - \Delta v_{od} \tag{3.29}$$

Since $$\Delta\dot{\phi}_q = \Delta v^*_{oq} - \Delta v_{oq} \tag{3.30}$$

But $v^*_{oq} = 0$ then $\Delta v^*_{oq} = 0$

So $$\Delta\dot{\phi}_q = -\Delta v_{oq} \tag{3.31}$$

(c) Small-Signal Model of the Current Controller

The corresponding state equations are given in (3.32), along with the algebraic equations given in (3.8) and (3.9).

$$\Delta\dot{\gamma}_d = \Delta i^*_{ld} - \Delta i_{ld} \tag{3.32}$$

where $\Delta i^*_{ld} = F\Delta i_{od} - \omega_n C_f \Delta v_{oq} + K_{pv}(\Delta v^*_{od} - \Delta v_{od}) + K_{iv}\Delta\phi_d$ and $\Delta v^*_{od} = -n_q \Delta Q_c$

$$\Delta\dot{\gamma}_d = F\Delta i_{od} - \omega_n C_f \Delta v_{oq} + K_{pv}(n_q \Delta Q_c - \Delta v_{od}) + K_{iv}\Delta\phi_d - \Delta i_{ld} \tag{3.33}$$

$$\Delta\dot{\gamma}_q = \Delta i^*_{lq} - \Delta i_{lq} \tag{3.34}$$

where $\Delta i^*_{lq} = F\Delta i_{oq} + \omega_n C_f \Delta v_{od} + K_{pv}(\Delta v^*_{oq} - \Delta v_{oq}) + K_{iv}\Delta\phi_q$ and $\Delta v^*_{oq} = 0$

$$\Delta\dot{\gamma}_q = F\Delta i_{oq} + \omega_n C_f \Delta v_{od} - K_{pv}\Delta v_{oq} + K_{iv}\Delta\phi_q - \Delta i_{lq} \qquad (3.35)$$

(d) Signal Model of the Output LC Filter and Coupling Inductance

The corresponding state equations are given in (3.36) and (3.38), along with the algebraic equations given in (3.10) and (3.11).

$$\Delta\dot{i}_{ld} = -\frac{R_f}{L_f}\Delta i_{ld} + \omega\Delta i_{lq} + \frac{1}{L_f}(\Delta v_{ld} - \Delta v_{od}) \qquad (3.36)$$

Since $v_{ld}^* = -\omega_n L_f i_{lq} + K_{pc}(i_{ld}^* - i_{ld}) + K_{ic}\gamma_d$ and $v_{ld} = v_{ld}^*$

then $\Delta v_{ld} = -\omega_n L_f \Delta i_{lq} + K_{pc}(\Delta i_{ld}^* - \Delta i_{ld}) + K_{ic}\Delta\gamma_d$

where $\Delta i_{ld}^* = F\Delta i_{od} - \omega_n C_f \Delta v_{oq} + K_{pv}(\Delta v_{od}^* - \Delta v_{od}) + K_{iv}\Delta\phi_d$ and $\Delta v_{od}^* = -n_q\Delta Q_c$

then

$$\begin{aligned}\Delta\dot{i}_{ld} = &-m_p I_{lq}\Delta P_c - \frac{n_q K_{pv} K_{pc}}{L_f}\Delta Q_c + \frac{K_{iv}K_{pc}}{L_f}\Delta\phi_d + \frac{K_{ic}}{L_f}\Delta\gamma_d \\ &-\frac{(r_f + K_{pc})}{L_f}\Delta i_{ld} + (\omega_o - \omega_n)\Delta i_{lq} - \frac{(1 + K_{pv}K_{pc})}{L_f}\Delta v_{od} \\ &-\frac{\omega_n C_f K_{pc}}{L_f}\Delta v_{oq} + \frac{K_{pc}F}{L_f}\Delta i_{od}\end{aligned} \qquad (3.37)$$

$$\Delta\dot{i}_{lq} = -\frac{R_f}{L_f}\Delta i_{lq} - \omega\Delta i_{ld} + \frac{1}{L_f}(\Delta v_{lq} - \Delta v_{oq}) \qquad (3.38)$$

Since $v_{lq}^* = \omega_n L_f i_{ld} + K_{pc}(i_{lq}^* - i_{lq}) + K_{ic}\gamma_q$ and $v_{lq} = v_{lq}^*$

$$\Delta v_{lq} = \omega_n L_f \Delta i_{ld} + K_{pc}(\Delta i_{lq}^* - \Delta i_{lq}) + K_{ic}\Delta\gamma_q$$

where $\Delta i_{lq}^* = F\Delta i_{oq} + \omega_n C_f \Delta v_{od} + K_{pv}(\Delta v_{oq}^* - \Delta v_{oq}) + K_{iv}\Delta\phi_q$ and $\Delta v_{oq}^* = 0$

$$\Delta \dot{i}_{lq} = m_p I_{ld} \Delta P_c + \frac{K_{iv}}{L_f} \Delta \phi_q + \frac{K_{ic}}{L_f} \Delta \gamma_q - \frac{(r_f + K_{pc})}{L_f} \Delta i_{lq} - (\omega_o - \omega_n) \Delta i_{ld} - \frac{(1 + K_{pv} K_{pc})}{L_f} \Delta v_{oq} - \frac{\omega_n C_f K_{pc}}{L_f} \Delta v_{od} + \frac{K_{pc} F}{L_f} \Delta i_{oq} \quad (3.39)$$

(e) Complete Small-Signal Model of an Individual Inverter

By combining the state-space models of the power controller, voltage controller, current controller, output *LC* filter and coupling inductor, given by equations (3.25), (3.26), (3.27), (3.31), (3.33), (3.35), (3.37) and (3.39), the complete state-space small-signal model of the inverter, given in (3.40) and (3.41) is obtained. There are totally 13 states, 3 inputs and 2 outputs in each individual inverter model except the inverter whose reference frame is the common reference frame, which has 3 outputs.

$$\Delta \dot{x}_{DG} = A_{DG} \Delta x_{DG} + B_{DG} \Delta v_o \quad (3.40)$$

$$\Delta x_{DG} = \begin{bmatrix} \Delta\delta & \Delta P_c & \Delta Q_c & \Delta \phi_{dq} & \Delta \gamma_{dq} & \Delta i_{ldq} & \Delta v_{odq} & \Delta i_{odq} \end{bmatrix}^T_{13\times 13} \quad (3.41)$$

where δ is the angle between the inverter reference frame and a common reference frame; ϕ_{dq} and γ_{dq} are the states of the voltage and current controllers (the integrator states), respectively; v_o is the supply voltage at the PCC transferred to a common reference frame; and A_{DG} and B_{DG} are the state and input matrices. The state matrix A_{DG} is given by;

$$A_{DG}=\begin{bmatrix}
0 & -m_p & 0 & 0 & 0 & 0 & 0 & 0 & 0 & 0 & 0 & 0 & 0\\
0 & -\omega_c & 0 & 0 & 0 & 0 & 0 & 0 & 0 & \omega_c I_{od} & \omega_c I_{oq} & \omega_c V_{od} & \omega_c V_{oq}\\
0 & 0 & -\omega_c & 0 & 0 & 0 & 0 & 0 & 0 & \omega_c I_{oq} & -\omega_c I_{od} & -\omega_c V_{oq} & \omega_c V_{od}\\
0 & 0 & -n_q & 0 & 0 & 0 & 0 & 0 & 0 & -1 & 0 & 0 & 0\\
0 & 0 & 0 & 0 & 0 & 0 & 0 & 0 & 0 & 0 & -1 & 0 & 0\\
0 & 0 & -n_q K_{pv} & K_{iv} & 0 & 0 & 0 & -1 & 0 & K_{pv} & -\omega_n C_f & F & 0\\
0 & 0 & 0 & 0 & K_{iv} & 0 & 0 & 0 & -1 & \omega_n C_f & K_{pv} & 0 & F\\
0 & -m_p I_{lq} & -\frac{n_q K_{pv} K_{iv}}{L_f} & \frac{K_{iv}}{L_f} & 0 & \frac{K_{ic}}{L_f} & 0 & -\frac{(r_f+K_{pc})}{L_f} & \omega_o-\omega_n & -\frac{(1+K_{pc}K_{iv})}{L_f} & -\frac{\omega_n C_f K_{pc}}{L_f} & \frac{FK_{pc}}{L_f} & 0\\
0 & m_p I_{ld} & 0 & 0 & \frac{K_{iv}}{L_f} & 0 & \frac{K_{ic}}{L_f} & \omega_n-\omega_o & -\frac{(r_f+K_{pc})}{L_f} & \frac{\omega_n C_f K_{pc}}{L_f} & -\frac{(1+K_{pc}K_{iv})}{L_f} & 0 & \frac{FK_{pc}}{L_f}\\
0 & -m_p V_{oq} & 0 & 0 & 0 & 0 & 0 & \frac{1}{C_f} & 0 & 0 & \omega_o & -\frac{1}{C_f} & 0\\
0 & m_p V_{od} & 0 & 0 & 0 & 0 & 0 & 0 & \frac{1}{C_f} & -\omega_o & 0 & 0 & -\frac{1}{C_f}\\
\frac{V_{bD}\sin\delta_o - V_{bQ}\cos\delta_o}{L_f} & -m_p I_{oq} & 0 & 0 & 0 & 0 & 0 & 0 & 0 & \frac{1}{L_c} & 0 & -\frac{r_c}{L_c} & \omega_o\\
\frac{V_{bD}\cos\delta_o + V_{bQ}\sin\delta_o}{L_f} & m_p I_{od} & 0 & 0 & 0 & 0 & 0 & 0 & 0 & 0 & \frac{1}{L_c} & -\omega_o & -\frac{r_c}{L_c}
\end{bmatrix}_{13\times 13}$$

(3.42)

3.2.2 Small Signal Model of the Lines

A number of inverter-based DGs `*s*' can be connected with `*p*' number of load points through '*n*' number of lines. On a common reference frame, the state equations of line current of i^{th} line, which is connected between nodes j and k, are given in (3.43) and (3.44).

$$\Delta \dot{i}_{lineDi} = -m_p I_{lineQi}\Delta P_c - \frac{r_{linei}}{L_{linei}}\Delta i_{lineDi} + \omega_o \Delta i_{lineQi} + \frac{1}{L_{linei}}(\Delta v_{bDj} - \Delta v_{bDk}) \quad (3.43)$$

$$\Delta \dot{i}_{lineQi} = m_p I_{lineDi}\Delta P_c - \frac{r_{linei}}{L_{linei}}\Delta i_{lineQi} - \omega_o \Delta i_{lineDi} + \frac{1}{L_{linei}}(\Delta v_{bQj} - \Delta v_{bQk}) \quad (3.44)$$

The last two equations can be written in the following form;

$$\begin{bmatrix} \Delta \dot{i}_{lineDi} \\ \Delta \dot{i}_{lineQi} \end{bmatrix} = \begin{bmatrix} -\frac{r_{linei}}{L_{linei}} & \omega_o \\ -\omega_o & -\frac{r_{linei}}{L_{linei}} \end{bmatrix} \begin{bmatrix} \Delta i_{lineDi} \\ \Delta i_{lineQi} \end{bmatrix} + \begin{bmatrix} -m_p I_{lineQio} \\ -m_p I_{lineDio} \end{bmatrix} \Delta P_c + \frac{1}{L_{linei}} \begin{bmatrix} (\Delta v_{bDj} - \Delta v_{bDk}) \\ (\Delta v_{bQj} - \Delta v_{bQk}) \end{bmatrix} \tag{3.45}$$

3.2.3 Small Signal Model of the Load

Although, many types of load can exist in microgrids, a general *RL* load is considered in this work. The state equation of the *RL* load connected at i^{th} node is given in (3.46) and (3.47).

$$\Delta \dot{i}_{loadDi} = -m_p I_{loadQi} \Delta P_c - \frac{R_{loadi}}{L_{loadi}} \Delta i_{loadDi} + \omega_o \Delta i_{loadQi} + \frac{1}{L_{loadi}} (\Delta v_{bDi}) \tag{3.46}$$

$$\Delta \dot{i}_{loadQi} = m_p I_{loadDi} \Delta P_c - \frac{R_{loadi}}{L_{loadi}} \Delta i_{loadQi} - \omega_o \Delta i_{loadDi} + \frac{1}{L_{loadi}} (\Delta v_{bQi}) \tag{3.47}$$

Then these equations can be written in the following form;

$$\begin{bmatrix} \Delta \dot{i}_{loadDi} \\ \Delta \dot{i}_{loadQi} \end{bmatrix} = \begin{bmatrix} -\frac{r_{loadi}}{L_{loadi}} & \omega_o \\ -\omega_o & -\frac{r_{linei}}{L_{loadi}} \end{bmatrix} \begin{bmatrix} \Delta i_{loadDi} \\ \Delta i_{loadQi} \end{bmatrix} + \begin{bmatrix} -m_p I_{oadQio} \\ -m_p I_{loadDio} \end{bmatrix} \Delta P_c + \frac{1}{L_{loadi}} \begin{bmatrix} (\Delta v_{bDi}) \\ (\Delta v_{bQi}) \end{bmatrix} \tag{3.48}$$

$$\Delta \dot{v}_{bDi} = -m_p V_{bQi} \Delta P_c + \frac{1}{C_b} (\Delta i_{oDi} - \Delta i_{loadDi} \pm \Delta i_{lineDi,j}) + \omega_o \Delta v_{bQi} \tag{3.49}$$

$$\Delta \dot{v}_{bDi} = m_p V_{bDi} \Delta P_c + \frac{1}{C_b} (\Delta i_{oQi} - \Delta i_{loadQi} \pm \Delta i_{lineQi,j}) - \omega_o \Delta v_{bDi} \tag{3.50}$$

Rewrite equations (3.49) and (3.50) in the following form;

$$\begin{bmatrix} \dot{\Delta v}_{bDi} \\ \dot{\Delta v}_{bQi} \end{bmatrix} = \begin{bmatrix} -m_p V_{bQi} \\ m_p V_{bDi} \end{bmatrix} \Delta P + \begin{bmatrix} \frac{1}{C_b} & \frac{1}{C_b} \\ \frac{1}{C_b} & \frac{1}{C_b} \end{bmatrix} \begin{bmatrix} \Delta i_{oDi} \\ \Delta i_{oQi} \end{bmatrix} - \begin{bmatrix} \frac{1}{C_b} & \frac{1}{C_b} \\ \frac{1}{C_b} & \frac{1}{C_b} \end{bmatrix} \begin{bmatrix} \Delta i_{loadDi} \\ \Delta i_{loadQi} \end{bmatrix}$$
$$\pm \begin{bmatrix} \frac{1}{C_b} & \frac{1}{C_b} \\ \frac{1}{C_b} & \frac{1}{C_b} \end{bmatrix} \begin{bmatrix} \Delta i_{lineDi,j} \\ \Delta i_{lineQi,j} \end{bmatrix} + \begin{bmatrix} 0 & \omega_o \\ -\omega_o & 0 \end{bmatrix} \begin{bmatrix} \Delta v_{bQi} \\ \Delta v_{bDi} \end{bmatrix} + \quad (3.51)$$

3.2.4 Small-Signal Model of the whole Autonomous Microgrid

The whole system model consists of the models of inverter-based DGs, lines and loads. Since each inverter has its own reference frame and the system should have the common reference frame, the whole system model requires that the output variables of each DG need to be converted to the common reference frame. The output variables of the inverter model are the output currents represented as a vector i_{odq}. Using the transformation technique introduced in (3.1) and (3.2), the small-signal output current on the common reference frame, i.e. i_{oDQ}, can be obtained as follows;

$$\left[\Delta i_{oDQ}\right] = \left[T_s\right]\left[\Delta i_{odq}\right] + \left[T_c\right]\left[\delta\right] \quad (3.52)$$

where

$$T_s = \begin{bmatrix} \cos(\delta_o) & \sin(\delta_o) \\ -\sin(\delta_o) & \cos(\delta_o) \end{bmatrix}$$

and

$$T_c = \begin{bmatrix} -I_{od}\sin(\delta_o) - I_{oq}\cos(\delta_o) \\ I_{od}\cos(\delta_o) - I_{oq}\sin(\delta_o) \end{bmatrix}$$

Similarly, the input signal to the inverter model is the bus voltage which is expressed on the common reference frame. The bus voltage is converted to the individual inverter reference frame using the reverse transformation, given by (3.53),

$$\left[\Delta v_{bdq}\right]=\left[T_s^{-1}\right]\left[\Delta v_{bDQ}\right]+\left[T_v^{-1}\right]\left[\delta\right] \tag{3.53}$$

where $$T_v^{-1}=\begin{bmatrix}-V_{bD}\sin(\delta_o)+V_{bQ}\cos(\delta_o)\\ -V_{bD}\cos(\delta_o)-V_{bQ}\sin(\delta_o)\end{bmatrix}$$

The complete state-space small-signal model of the overall system including the inverter, lines and loads are written in the following equation;

$$\Delta\dot{x}_{overall\_system}=A_{overall\_system}\Delta x_{overall\_system} \tag{3.54}$$

Where

$$\Delta x_{overall\_system}=\begin{bmatrix}\Delta\delta & \Delta P_c & \Delta Q_c & \Delta\phi_{dq} & \Delta\gamma_{dq} & \Delta i_{ldq} & \Delta v_{odq} & \Delta i_{odq} & \Delta i_{lineDQ} & \Delta i_{loadDQ} & \Delta v_{bDQ}\end{bmatrix}^T \tag{3.55}$$

$A_{overall\_system}$ is the matrix of the overall system.

CHAPTER 4

MICROGRID MODELING IN GRID-CONNECTED MODE

In this chapter, an inverter-based grid-connected microgrid shown in Fig. 4.1 is presented. It includes power and current controllers, PLL, LC filter, and coupling inductance. VSI control circuit of the grid-connected mode is shown in Fig. 4.2. The power controller is used to calculate the inductor reference current which represents the output reference powers. The PI current controller is aimed to minimize the error in the inductor current with respect to its reference value. Since the PI controller is operating effectively on the pseudo-stationary voltages and currents, the current control is performed in a rotational reference frame [73]. A PLL is used to provide the reference angle for the rotating frame. The measured voltage at PCC will be transformed to the *dq* values using the transformation matrix as follows:

$$\begin{pmatrix} v_{od} \\ v_{oq} \\ v_{oo} \end{pmatrix} = \sqrt{\frac{2}{3}} \begin{pmatrix} \cos\theta & \cos\left(\theta - \frac{2\pi}{3}\right) & \cos\left(\theta + \frac{2\pi}{3}\right) \\ -\sin\theta & -\sin\left(\theta - \frac{2\pi}{3}\right) & -\sin\left(\theta + \frac{2\pi}{3}\right) \\ \frac{1}{\sqrt{2}} & \frac{1}{\sqrt{2}} & \frac{1}{\sqrt{2}} \end{pmatrix} \begin{pmatrix} v_{oa} \\ v_{ob} \\ v_{oc} \end{pmatrix} \quad (4.1)$$

The rotational frame angle θ is used to transfer the voltages and currents from the *abc* to *dq* and vice versa. The state space model of different microgrid components can be written as follows;

$$\dot{x} = Ax + R(x,u) \quad (4.2)$$

4.1 PHASE-LOCKED LOOP (PLL) MODEL

The PLL form adopted in this study, shown in Fig. 4.3, is based on aligning the angel of the *dq* transformation such that the voltage at the connection point has no q-axis component [73]. A PI regulator acts on the alignment error to set the rotation frequency. Then this frequency is used to obtain the transformation angle θ as:

$$\omega = K_P^{PLL} v_{oq} + K_I^{PLL} \int v_{oq} dt \quad (4.3)$$

$$\theta = \int \omega dt \quad (4.4)$$

where K_P^{PLL} and K_c^{PLL} are the PI controller of the PLL.

The PLL states is described as follows $x_{PLL} = \begin{bmatrix} \theta & \Phi_{PLL} \end{bmatrix}$ where $\Phi_{PLL} = \int v_{oq} dt$ so the equations (4.3) and (4.4) of the PLL model is written as follows;

$$\dot{x}_{PLL} = \begin{bmatrix} 0 & K_I^{PLL} \\ 0 & 0 \end{bmatrix} \begin{bmatrix} 0 \\ \phi_{PLL} \end{bmatrix} + \begin{bmatrix} K_P^{PLL} v_{oq} \\ v_{oq} \end{bmatrix} \tag{4.5}$$

In short; $\dot{x}_{PLL} = A_{PLL} x_{PLL} + R_{PLL}(x,u)$

where the PLL output is $y_{PLL} = \begin{bmatrix} \theta & v_{od} & v_{oq} \end{bmatrix}$.

4.2 POWER CONTROLLER MODEL

The power controller shown in Fig. 4.4 is used to calculate the reference currents in *dq* forms with the aid of reference active and reactive powers. The output reference currents i^*_{od} and i^*_{oq} are calculated using the reference powers and the output *dq*-voltages v_{od} and v_{oq} as follows;

$$i^*_{od} = \frac{v_{od} P^* - v_{oq} Q^*}{{v_{od}}^2 + {v_{oq}}^2} \tag{4.6}$$

$$i^*_{oq} = \frac{v_{oq} P^* + v_{od} Q^*}{{v_{od}}^2 + {v_{oq}}^2} \tag{4.7}$$

where P^* and Q^* are the injected (reference) active and reactive power.

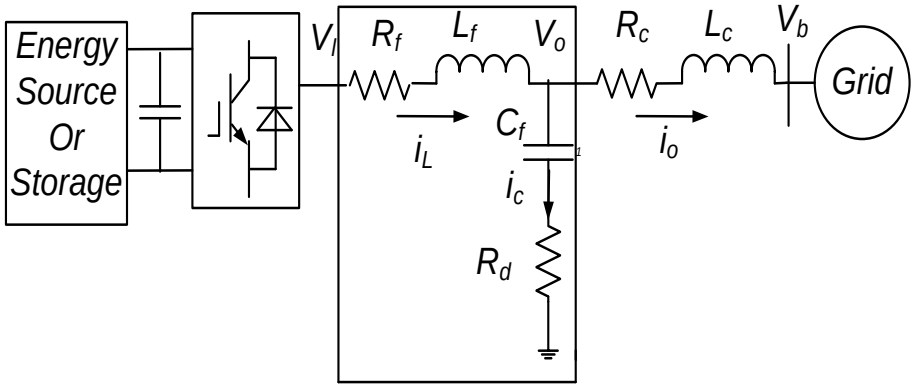

Fig. 4.1 Grid-connected mode of microgrid

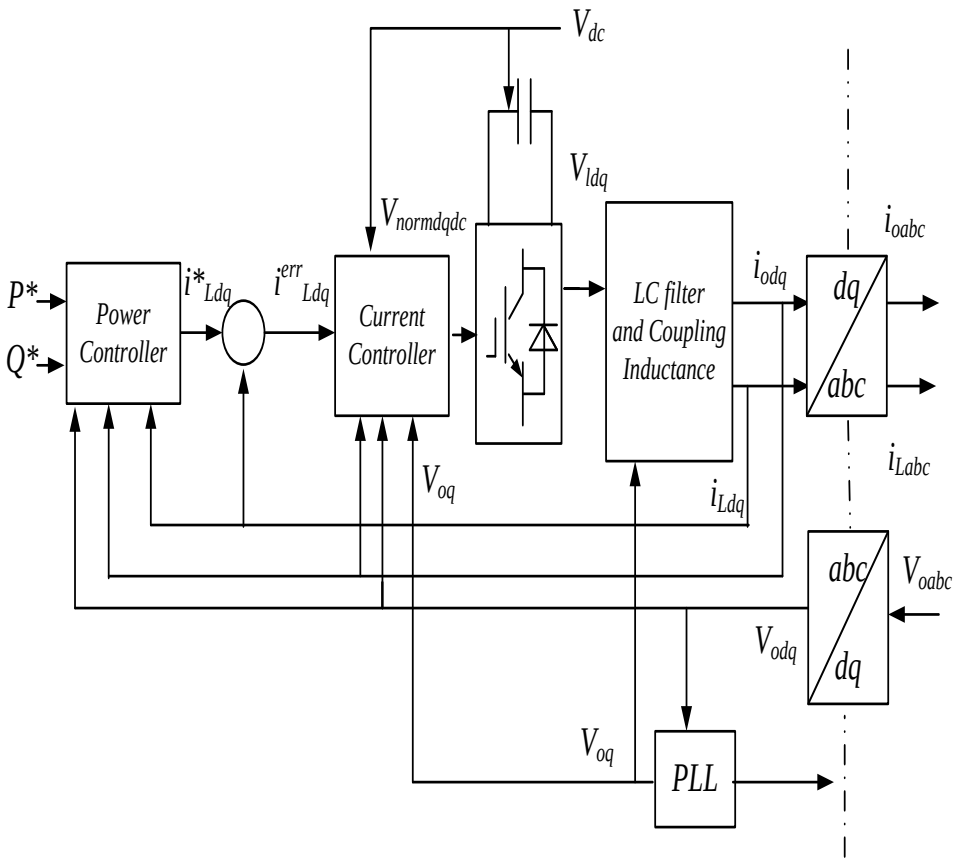

Fig. 4.2 VSI Control circuit in grid-connected mode

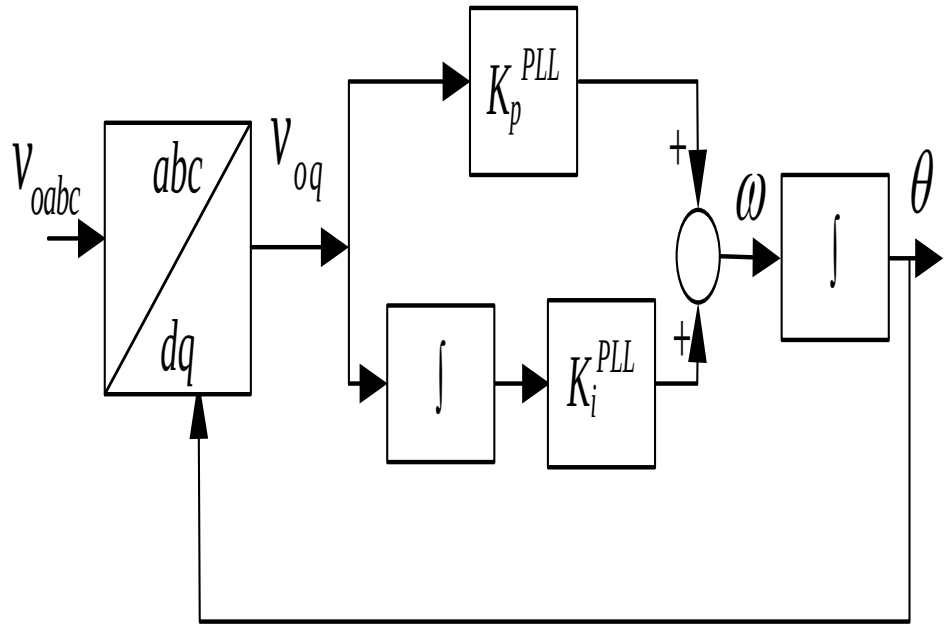

Fig. 4.3 PLL model

The reference coupling inductance currents i^{Σ}_{d} and i^{Σ}_{q} are expressed as follows;

$$i_d^{\Sigma} = i_{od}^{*} + i_{od} = i_{od}^{*} + (i_{Ld} - i_{od}) \tag{4.8}$$

$$i_q^{\Sigma} = i_{oq}^{*} + i_{oq} = i_{oq}^{*} + (i_{Lq} - i_{oq}) \tag{4.9}$$

A low-pass filter is used to remove the harmonics and noises which may be resulted from the distortion of the voltage of PCC [73]. The current controller references i^{*}_{Ld} and i^{*}_{Lq} after filtering are given as:

$$i_{Ld}^{*} = \frac{\omega_c^2}{s^2 + \sqrt{2}s\,\omega_c + \omega_c^2} i_d^{\Sigma} \tag{4.10}$$

$$i_{Lq}^{*} = \frac{\omega_c^2}{s^2 + \sqrt{2}s\,\omega_c + \omega_c^2} i_q^{\Sigma} \tag{4.11}$$

where ω_c is the cut-off frequency of the low-pass filter. These two equations can be rewritten as follows;

$$\frac{di_{Ld}^{*}}{dt} = \omega_c^2 \int \left(i_d^{\Sigma} - i_{Ld}^{*} \right) dt - \sqrt{2}\omega_c i_{Ld}^{*} \tag{4.12}$$

$$\frac{di_{Lq}^{*}}{dt} = \omega_c^2 \int \left(i_q^{\Sigma} - i_{Lq}^{*} \right) dt - \sqrt{2}\omega_c i_{Lq}^{*} \tag{4.13}$$

Equations (4.12) and (4.13) can be rewritten as follows;

$$\frac{di_{Ld}^{*}}{dt} = q_{3d} - \sqrt{2}\omega_c i_{Ld}^{*} \tag{4.14}$$

$$\frac{di_{Lq}^{*}}{dt} = q_{3q} - \sqrt{2}\omega_c i_{Lq}^{*} \tag{4.15}$$

where $q_{3d} = \int \left(i_d^{\Sigma} - i_{Ld}^{*} \right) dt$ and $q_{3q} = \int \left(i_q^{\Sigma} - i_{Lq}^{*} \right) dt$. The state space model of the power controller will be as follows;

$$\dot{x}_{P\_controller} = \begin{bmatrix} -\sqrt{2}\omega_c & 0 & \omega_c^2 & 0 \\ 0 & -\sqrt{2}\omega_c & 0 & \omega_c^2 \\ -1 & 0 & 0 & 0 \\ 0 & -1 & 0 & 0 \end{bmatrix} \begin{bmatrix} i_{Ld}^{*} \\ i_{Lq}^{*} \\ q_{3d} \\ q_{3q} \end{bmatrix} + \begin{bmatrix} 0 \\ 0 \\ \dfrac{v_{od} P^{*} - v_{oq} Q^{*}}{v_{od}^{\,2} + v_{oq}^{\,2}} + i_{Ld} - i_{od} \\ \dfrac{v_{oq} P^{*} + v_{od} Q^{*}}{v_{od}^{\,2} + v_{oq}^{\,2}} + i_{Lq} - i_{oq} \end{bmatrix} \tag{4.16}$$

In short;

$$\dot{x}_{P\_controller} = A_{P\_controller} x_{P\_controller} + R_{P\_controller}(x, u)$$

where $x_{p\_controller} = \begin{bmatrix} i_{Ld}^{*} & i_{Lq}^{*} & q_{3d} & q_{3q} \end{bmatrix}^T$ is the state vector,

$u_{p\_controller} = \begin{bmatrix} P^{*} & Q^{*} & v_{od} & v_{oq} & i_{Ld} & i_{Lq} & i_{od} & i_{oq} \end{bmatrix}^T$ is the input vector and;

$y_{p\_controller} = \begin{bmatrix} i_{Ld}^{*} & i_{Lq}^{*} \end{bmatrix}^T$ is the output vector.

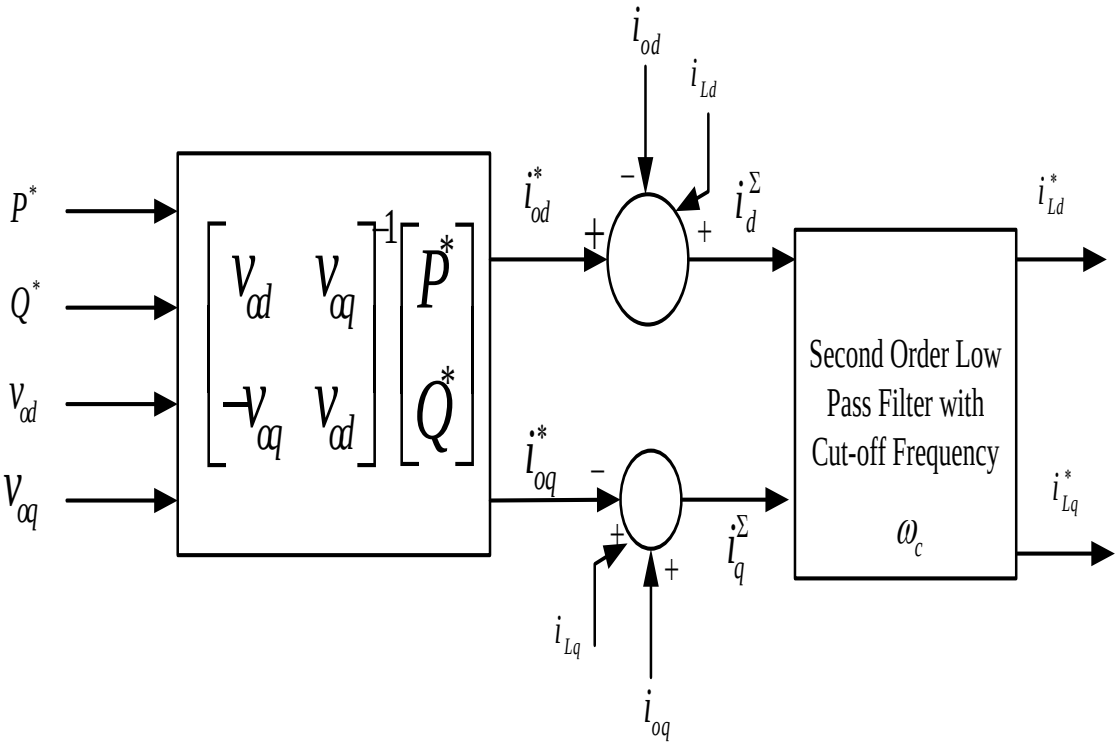

Fig. 4.4 Power controller (calculator)

4.3 CURRENT CONTROLLER MODEL

In grid connection mode, the current controller is used to improve the power system quality [73]. The PI current controller used in this study is shown in Fig. 4.5. The voltage signal required by the inverter is written as:

$$v_{ld}^* = v_{od} - \omega L_f i_{Ld} + K_P^d i_{Ld}^{err} + K_I^d \int i_{Ld}^{err} dt \tag{4.17}$$

$$v_{lq}^* = v_{oq} + \omega L_f i_{Lq} + K_P^q i_{Lq}^{err} + K_I^q \int i_{Lq}^{err} dt \tag{4.18}$$

where;

$K_P{}^{\mathrm{d}}$ and K_I^d are the d-axis PI controller of the current controller,

$K_P{}^{\mathrm{q}}$ and K_I^q are the q-axis PI controller of the current controller,

L_f is the inductance of the filter inductor (H),

v^*_{ld} is the d-axis reference voltage (V),

v^*_{lq} is the q-axis reference voltage (V),

v_{od} is the d-axis output voltage (V),

v_{oq} is the q-axis output voltage (V),

i_{Ld} is the d- component of the inductor current (A),

i_{Lq} is the q- component of the inductor current (A),

i^{err}_{Ld} is the d-axis difference between the reference and measured currents (A) and

i^{err}_{Lq} is the q-axis difference between the reference and measured currents (A).

So the state space model of the current controller is given as follows:

$$\dot{x}_{C\_controller} = \begin{bmatrix} 0 & 0 \\ 0 & 0 \end{bmatrix} \begin{bmatrix} q^{err}_{ld} \\ q^{err}_{lq} \end{bmatrix} + \begin{bmatrix} 1 & 0 & 0 & 0 & 0 & 0 \\ 0 & 1 & 0 & 0 & 0 & 0 \end{bmatrix} \begin{bmatrix} i^{err}_{Ld} \\ i^{err}_{Lq} \\ i_{Ld} \\ i_{Lq} \\ v_{od} \\ v_{oq} \end{bmatrix} \tag{4.19}$$

In short;

$$\dot{x}_{C\_controller} = A_{C\_controller} x_{C\_controller} + B_{C\_controller} u_{C\_controller}$$

where $q_{ld}^{err} = \int i_{Ld}^{err} dt$, $q_{lq}^{err} = \int i_{Lq}^{err} dt$; $x_{C\_controller} = \begin{bmatrix} q_{ld}^{err} & q_{lq}^{err} \end{bmatrix}^T$ is the state vector and; $u_{C\_controller} = \begin{bmatrix} i_{Ld}^{err} & i_{Lq}^{err} & i_{Ld} & i_{Lq} & v_{od} & v_{oq} \end{bmatrix}^T$ is the input vector. The output equation can be written as follows:

$$y_{C\_controller} = \frac{1}{V_{DC}} \left(\begin{bmatrix} K_I^d & 0 \\ 0 & K_I^q \end{bmatrix} \begin{bmatrix} q_{ld}^{err} \\ q_{lq}^{err} \end{bmatrix} + \begin{bmatrix} K_P^d & 0 & 0 & 1 & 0 & 0 \\ 0 & K_P^q & 0 & 0 & 1 & 0 \end{bmatrix} \begin{bmatrix} i_{Ld}^{err} \\ i_{Lq}^{err} \\ i_{Ld} \\ i_{Lq} \\ v_{od} \\ v_{oq} \end{bmatrix} + \begin{bmatrix} -\omega L i_{Lq} \\ \omega L i_{Ld} \end{bmatrix} \right) \quad (4.20)$$

4.4 INVERTER MODEL

In this study, the voltage gain model of the VSI in state-space variables shown in Fig. 4.6 is adopted. Therefore, inverter is represented by $\dot{x}_{inverter} = [0]$ and $y_{inverter} = \begin{bmatrix} v_{ld} & v_{lq} \end{bmatrix}$ is the output vector of the inverter.

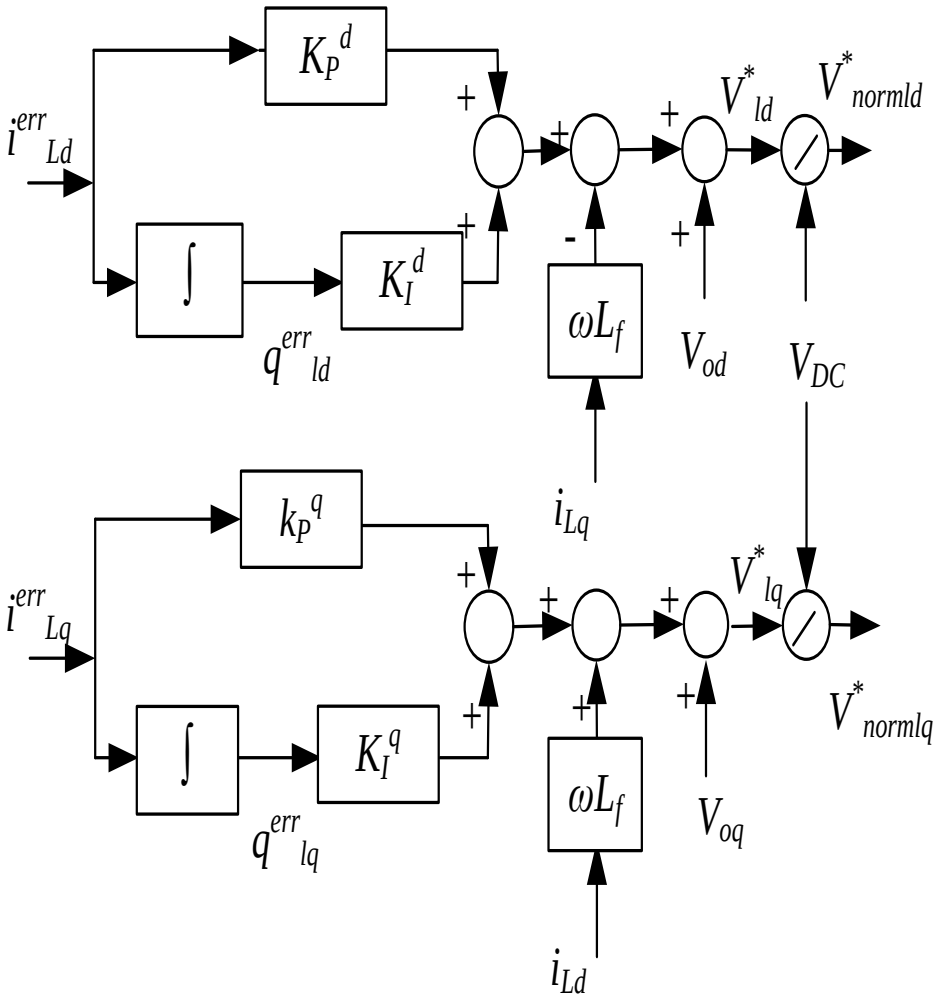

Fig. 4.5 Current controller in grid-connected mode

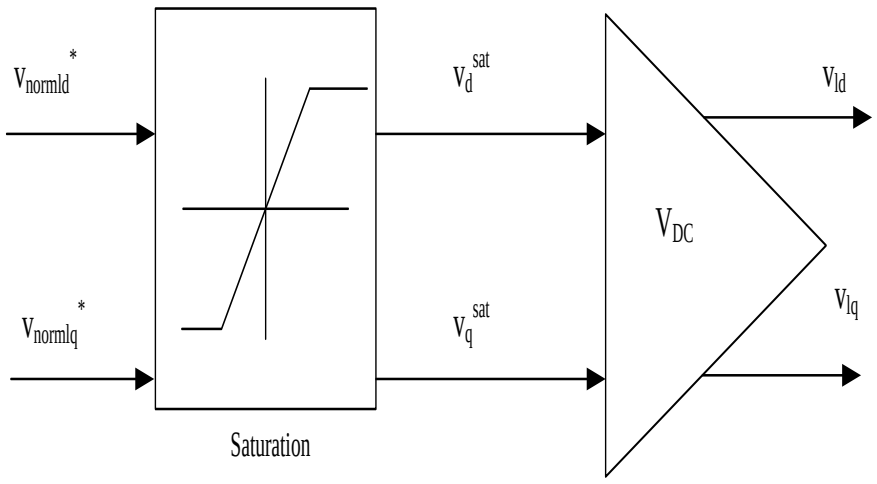

Fig. 4.6 Inverter model

4.5 LC FILTER AND COUPLING INDUCTANCE MODEL

A passive low-pass filter is used to attenuate switching frequency ripple. The filter has important dynamic effects on the system stability [74]-[75]. To avoid the resonance that may arise with coupling or grid inductance, a passive damping circuit is added to the filter such as damping resistors [75]. Assuming that the inverter input and output voltage are equal i.e. $v_l=v^*_l$, the small signal model of the output LC filter and coupling inductance can be represented as;

$$v_{la} = i_{La}R_f + L_f \frac{di_{La}}{dt} + v_{Ca} + i_{Ca}R_d \tag{4.21}$$

$$v_{ba} = -i_{oa}R_c - L_c \frac{di_{oa}}{dt} + v_{Ca} + i_{Ca}R_d \tag{4.22}$$

$$C_f \frac{dv_{Ca}}{dt} = i_{La} - i_{oa} \tag{4.23}$$

where;

v_{la} is the phase-a output voltage of the inverter (V),

v_{ba} is the phase-a grid voltage of the inverter (V),

R_d is the resistance of the damping resistor (Ω),

i_{La} is the phase-a output current of the inverter (A),

i_{oa} is the phase-a current of the coupling inductor (A),

v_{Ca} is the phase-a voltage at the capacitor (V) and

i_{Ca} is the phase-a current of the capacitor (A).

In the *dq* frame, equations (4.21)-(4.23) can be rewritten as;

$$\frac{di_{Ld}}{dt} = -\frac{R_f}{L_f} i_{Ld} - \frac{1}{L_f}\left(v_{cd} - v_{ld}\right) + \omega i_{Lq} - R_d i_{Cd} \tag{4.24}$$

$$\frac{di_{Lq}}{dt} = -\frac{R_f}{L_f} i_{Lq} - \frac{1}{L_f}\left(v_{cd} - v_{ld}\right) - \omega i_{Ld} - R_d i_{Cq} \tag{4.25}$$

$$\frac{di_{od}}{dt} = -\frac{R_f}{L_f} i_{od} + \frac{1}{L_c}\left(v_{cd} - v_{bd}\right) + \omega i_{oq} - R_d i_{Cd} \tag{4.26}$$

$$\frac{di_{oq}}{dt} = -\frac{R_f}{L_f} i_{oq} + \frac{1}{L_c}\left(v_{cq} - v_{bd}\right) - \omega i_{od} - R_d i_{Cq} \tag{4.27}$$

$$\frac{dv_{Cd}}{dt} = \frac{1}{C_f}\left(i_{Ld} - i_{od}\right) + \omega v_{Cq} \tag{4.28}$$

$$\frac{dv_{Cq}}{dt} = \frac{1}{C_f}\left(i_{Lq} - i_{oq}\right) - \omega v_{Cd} \tag{4.29}$$

where;

i_{Ld} is the d- component of the inductor current (A),

i_{Lq} is the q- component of the inductor current (A),

i_{od} is the d- component of the coupling inductor current (A),

i_{oq} is the q- component of the coupling inductor current (A),

i_{cd} is the d- component of the capacitor current (A),

i_{cq} is the q- component of the capacitor current (A),

v_{ld} is the d- component of the inverter voltage (V),

v_{lq} is the q- component of the inverter voltage (V),

v_{bq} is the q- component of the grid voltage (V),

v_{bd} is the d- component of the grid voltage (V),

v_{cd} is the d- component of the capacitor voltage (V) and

v_{cq} is the q- component of the capacitor voltage (V).

The state space model of the LC filter and coupling inductance can be given as:

$$x_{filter} = \begin{bmatrix} -\frac{R_f}{L_f} & 0 & -\frac{1}{L_f} & 0 & 0 & 0 \\ 0 & -\frac{R_f}{L_f} & 0 & -\frac{1}{L_f} & 0 & 0 \\ \frac{1}{C_f} & 0 & 0 & 0 & -\frac{1}{C_f} & 0 \\ 0 & \frac{1}{C_f} & 0 & 0 & 0 & -\frac{1}{C_f} \\ 0 & 0 & \frac{1}{L_c} & 0 & -\frac{R_c}{L_c} & 0 \\ 0 & 0 & 0 & \frac{1}{L_c} & 0 & -\frac{R_c}{L_c} \end{bmatrix} \begin{bmatrix} i_{Ld} \\ i_{Lq} \\ v_{cd} \\ v_{cq} \\ i_{od} \\ i_{oq} \end{bmatrix} + \begin{bmatrix} \frac{1}{L_f} & 0 & 0 & 0 & 0 \\ 0 & \frac{1}{L_f} & 0 & 0 & 0 \\ 0 & 0 & 0 & 0 & 0 \\ 0 & 0 & 0 & 0 & 0 \\ 0 & 0 & 0 & -\frac{1}{L_c} & 0 \\ 0 & 0 & 0 & 0 & -\frac{1}{L_c} \end{bmatrix} \begin{bmatrix} v_{ld} \\ v_{lq} \\ v_{od} \\ v_{oq} \\ \omega \end{bmatrix} + \begin{bmatrix} \omega i_{Lq} \\ -\omega_{Ld} \\ \omega v_{cq} \\ -\omega v_{cd} \\ \omega i_{oq} \\ -\omega i_{od} \end{bmatrix} \quad (4.30)$$

In short, $\dot{x}_{filter} = A_{filter} x_{filter} + B_{filter} u_{filter} + R_{filter}(x,u)$

where $x_{filter} = \begin{bmatrix} i_{Ld} & i_{Lq} & v_{cd} & v_{cq} & i_{od} & i_{oq} \end{bmatrix}^T$ is the state vector,

$u_{filter} = \begin{bmatrix} v_{ld} & v_{lq} & v_{od} & v_{oq} & \omega \end{bmatrix}^T$ is the input vector,

$R_{filter}(x,u) = \begin{bmatrix} \omega i_{Lq} & -\omega i_{Ld} & \omega v_{cq} & -\omega v_{cd} & \omega i_{oq} & -\omega i_{od} \end{bmatrix}^T$ and,

$y_{filter} = \begin{bmatrix} i_{Ld} & i_{Lq} & i_{od} & i_{oq} & \omega \end{bmatrix}^T$ is the output vector.

4.6 COMPLETE MODEL

Aggregating the models of all microgrid components, the input vector (u_{cci}) is given by:

$$u_{cci} = \begin{bmatrix} V_{DC} & V_{oa} & V_{ob} & V_{oc} & P^* & Q^* \end{bmatrix}^T \tag{4.31}$$

The state variables are given by:

$$x_{cci} = \begin{bmatrix} \theta & \phi_{PLL} & i_{Ld}^* & i_{Lq}^* & q_{3d} & q_{3q} & q_{Ld}^{err} & q_{Lq}^{err} & i_{Ld} & i_{Lq} & v_{cd} & v_{cq} & i_{od} & i_{oq} \end{bmatrix}_{14\times 14}^T \tag{4.32}$$

The state matrix of the whole system A_{CCI} can be given as:

$$A_{CCI} = \begin{bmatrix} \left[A_{PLL}\right]_{2\times 2} & 0 & 0 & 0 \\ 0 & \left[A_{p\_controller}\right]_{4\times 4} & 0 & 0 \\ 0 & 0 & \left[A_{c\_controller}\right]_{2\times 2} & 0 \\ 0 & 0 & 0 & \left[A_{filter}\right]_{6\times 6} \end{bmatrix} \tag{4.33}$$

where

$$A_{CCI} = \begin{bmatrix} 0 & k_I^{PLL} & 0 & 0 & 0 & 0 & 0 & 0 & 0 & 0 & 0 & 0 & 0 & 0 \\ 0 & 0 & 0 & 0 & 0 & 0 & 0 & 0 & 0 & 0 & 0 & 0 & 0 & 0 \\ 0 & 0 & -\sqrt{2}\omega_c & 0 & \omega_c^2 & 0 & 0 & 0 & 0 & 0 & 0 & 0 & 0 & 0 \\ 0 & 0 & 0 & -\sqrt{2}\omega_c & 0 & \omega_c^2 & 0 & 0 & 0 & 0 & 0 & 0 & 0 & 0 \\ 0 & 0 & -1 & 0 & 0 & 0 & 0 & 0 & 0 & 0 & 0 & 0 & 0 & 0 \\ 0 & 0 & 0 & -1 & 0 & 0 & 0 & 0 & 0 & 0 & 0 & 0 & 0 & 0 \\ 0 & 0 & 0 & 0 & 0 & 0 & 0 & 0 & 0 & 0 & 0 & 0 & 0 & 0 \\ 0 & 0 & 0 & 0 & 0 & 0 & 0 & 0 & 0 & 0 & 0 & 0 & 0 & 0 \\ 0 & 0 & 0 & 0 & 0 & 0 & 0 & 0 & -\frac{R_f}{L_f} & 0 & -\frac{1}{L_f} & 0 & 0 & 0 \\ 0 & 0 & 0 & 0 & 0 & 0 & 0 & 0 & 0 & -\frac{R_f}{L_f} & 0 & -\frac{1}{L_f} & 0 & 0 \\ 0 & 0 & 0 & 0 & 0 & 0 & 0 & 0 & \frac{1}{C_f} & 0 & 0 & 0 & -\frac{1}{C_f} & 0 \\ 0 & 0 & 0 & 0 & 0 & 0 & 0 & 0 & 0 & \frac{1}{C_f} & 0 & 0 & 0 & -\frac{1}{C_f} \\ 0 & 0 & 0 & 0 & 0 & 0 & 0 & 0 & 0 & 0 & \frac{1}{L_c} & 0 & \frac{-R_c}{L_c} & 0 \\ 0 & 0 & 0 & 0 & 0 & 0 & 0 & 0 & 0 & 0 & 0 & \frac{1}{L_c} & 0 & \frac{-R_c}{L_c} \end{bmatrix}_{14\times 14}$$

CHAPTER 5

PROBLEM FORMULATION

For microgrid stability enhancement, the settings of controller parameters, filter components, and power sharing coefficients must be optimized. The design problem is formulated as follows;

5.1 OBJECTIVE FUNCTIONS

In grid-connected mode, the optimized parameters are K_p^d, K_i^d, K_p^q, K_i^q, L_f, C_f and R_d, while in autonomous mode, the optimized parameters are K_{pv}, K_{iv}, K_{pc}, K_{ic}, m_p, and n_{q}. Eigenvalue based as well as nonlinear time domain simulation based objective functions are proposed to improve the system stability. The linear time domain simulation based objective function given in (5.1) and the nonlinear time domain simulation based objective function given in (5.2) are used.

$$J_{linear\_model} = \max\left(\mathrm{Re}al\left(\lambda_i\right)\right) \tag{5.1}$$

$$J_{nonlinear\_model} = (P_{measured} - \mathrm{P}_{reference})^2 \tag{5.2}$$

Here, Real (λ_i) is the real part of the i^{th} mode eigenvalue. In the optimization process, it is aimed to minimize J_{linear_model} in order to shift the poorly damped eigenvalues to the left in *s*-plane. It is also aimed to minimize $J_{nonlinear\_model}$ in order to inject the required active and reactive powers from microgrid.

5.2 PROBLEM CONSTRAINTS

Controller parameters, filter capacitor, filter inductor, damping resistor and power sharing parameters are restricted by their lower and upper limits as follows:

$$K_p^{d\min} \le K_p^d \le K_p^{d\max} \tag{5.3}$$

$$K_i^{d\min} \le K_i^d \le K_i^{d\max} \tag{5.4}$$

$$K_p^{q\min} \le K_p^q \le K_p^{q\max} \tag{5.5}$$

$$K_i^{q\min} \le K_i^q \le K_i^{q\max} \tag{5.6}$$

$$L_f^{\min} \le L_f \le L_f^{\max} \tag{5.7}$$

$$C_f^{\min} \le C_f \le C_f^{\max} \tag{5.8}$$

$$R_d^{\min} \le R_d \le R_d^{\max} \tag{5.9}$$

$$K_{pv}^{\min} \le K_{pv} \le K_{pv}^{\max} \tag{5.10}$$

$$K_{iv}^{\min} \le K_{iv} \le K_{iv}^{\max} \tag{5.11}$$

$$K_{pc}^{\min} \le K_{pc} \le K_{pc}^{\max} \tag{5.12}$$

$$K_{ic}^{\min} \le K_{ic} \le K_{ic}^{\max} \tag{5.13}$$

$$m_{p}^{\min} \le m_{p} \le m_{p}^{\max} \tag{5.14}$$

$$n_{q}^{\min} \le n_{q} \le n_{q}^{\max} \tag{5.15}$$

It is worth mentioning that constraints (5.3) - (5.9) are applied in grid-connected mode while in autonomous mode, constraints (5.10) - (5.15) are applied only.

5.3 OPTIMIZATION PROBLEM

The overall optimization problem can be formulated as:

$$Minimize(J_{linear\_model}) \text{ or } Minimize(J_{nonlinear\_model}) \tag{5.16}$$

Subject to

Constraints given in (5.3) - (5.15)

In this study, PSO is proposed to solve this optimization problem to obtain the optimal parameters which used to achieve the system stability after getting disturbance in the grid-connected and autonomous modes.

5.4 PARTICLE SWARM OPTIMIZATION

5.4.1 Overview

PSO is a population based stochastic optimization technique developed by Eberhart and Kennedy [79], inspired by social behavior of bird flocking or fish schooling. The

particles motion has been affected by the inertia, the personal best and the group best. The inertia is the particles tendency to move in the direction of the original movement. The personal best is the best estimate of objective function for that particle. The group best position is the best solution represented by the swarm in any given time step. An interaction of these components generates a direction of movement corresponding to each particle for the next time step. The advantages of PSO over other traditional optimization techniques summarized in [63] as follows:

- PSO is a population-based search algorithm so it is less susceptible to getting trapped on local minima.
- It uses payoff (objective function) information to guide the search in the problem space.
- It is more flexible and robust than conventional methods because it uses probabilistic transition rules.
- It can overcome the premature convergence problem and enhances the search capability.
- The solution quality of the proposed approach does not rely on the initial population.
- The algorithm ensures the convergence to the optimal solution starting anywhere in the search space.

5.4.2 PSO Algorithm

In a PSO algorithm, the population has *n* particles that represent candidate solutions. Each particle is an *m*–dimensional real-valued vector, where *m* is the number of

optimized parameters. Therefore, each optimized parameter represents a dimension of the problem space. The PSO technique is described in the following steps [77];

Step 1) ***(Initialization)***:

- Set the time counter
- generate randomly *n* particles and generate randomly initial velocities for these particles:
- For each particle, evaluate the objective function then search for the best value of this objective function and put this value as a global best function J_{best} and global best particle x_{best}.
- Set the initial value of the inertia weight which is a control parameter used to control the impact of the previous velocity on the current velocity.

Step 2) ***(Time updating)***: Update the time counter.

Step 3) ***(Weight updating)***: Update the inertia weight using $w(t)= \alpha w(t-1)$ where α is a decrement constant smaller than but close to 1;

Step 4) ***(Velocity updating)***: update the velocity using the following equation:

$$v_{n+1}^{i} = wv_{n}^{i} + c_1 r_1 (p_{best} - x_{n}^{i}) + c_2 r_2 (g_{best} - x_{n}^{i}) \tag{5.17}$$

where c_1 and c_2 are positive constants,

r_1 and r_2 are uniformly distributed random numbers in [0,1].

Then check if the velocity violated its limit, set it at its proper limit. It is worth mentioning that the second term represents the cognitive part of PSO where the particle

changes its velocity based on its own thinking and memory. The third term represents the social part of PSO where the particle changes its velocity based on the social-psychological adaptation of knowledge.

Step 5) ***(Position updating)***: Based on the updated velocities, each particle changes its position according to the following equation:

$$x_{n+1}^{i} = x_{n}^{i} + v_{n+1}^{i} \tag{5.18}$$

Step 6) ***(Individual best updating)***: Each particle is evaluated according to the updated position.

If the cost function of this particle at this moment is less than the global best J_j^*, then update individual best as a global best and go to step 7; else go to step 7.

Step 7) ***(Global best updating)***: Search for the minimum value among the global best J_j^*, where min is the index of the particle with minimum objective function value, i.e.,

If $J_{\min} > J^{**}$ then update global best as $X^{**}=X_{min}$ and $J^{**}=J_{min}$ and go to step 8; else go to step 8.

Step 8) ***(Stopping criteria***): the stopping conditions are:

- The number of iterations since the last change of the best solution is greater than a pre-specified number;
- The number of iterations reaches the maximum allowable.

If one of the stopping criteria is satisfied, then stop, or else go to step 2.

5.4.3 PSO Implementation

The proposed PSO–based approach was implemented using the MATLAB code. Practically, our experience shows that the most effective parameters on PSO performance are the initial inertia weight and the maximum allowable velocity. It is worth mentioning that these parameters should be selected carefully for efficient performance of PSO. In the study, the following PSO data have been assumed as given;

- Population size (Pop_Size) =20;
- Acceleration constants: c_1, c_2 = 2;
- Generation or iteration (No_Gen) =100;
- Inertia weight factor =1;
- Decrement constant (α) = 0.98;
- Initial PSO parameter settings:

1. K_{pv_min}*=-0.5;*K_{pv_max}*=1.5;*
2. K_{iv_min}*=-1;*K_{iv_max}*=10;*
3. K_{pc_min}*=-10.5;*K_{pc_max}*=50.5;*
4. K_{ic_min}*=-16;*K_{ic_max}*=36;*
5. m_{p_min} *= -9.4e-5 ;*m_{p_max} *= 9.4e-4;*
6. n_{q_min} *= -1.3e-3 ;* n_{q_max} *= 1.3e-2;*

The computational flow chart of the proposed PSO based optimal design approach is shown in Fig. 5.1.

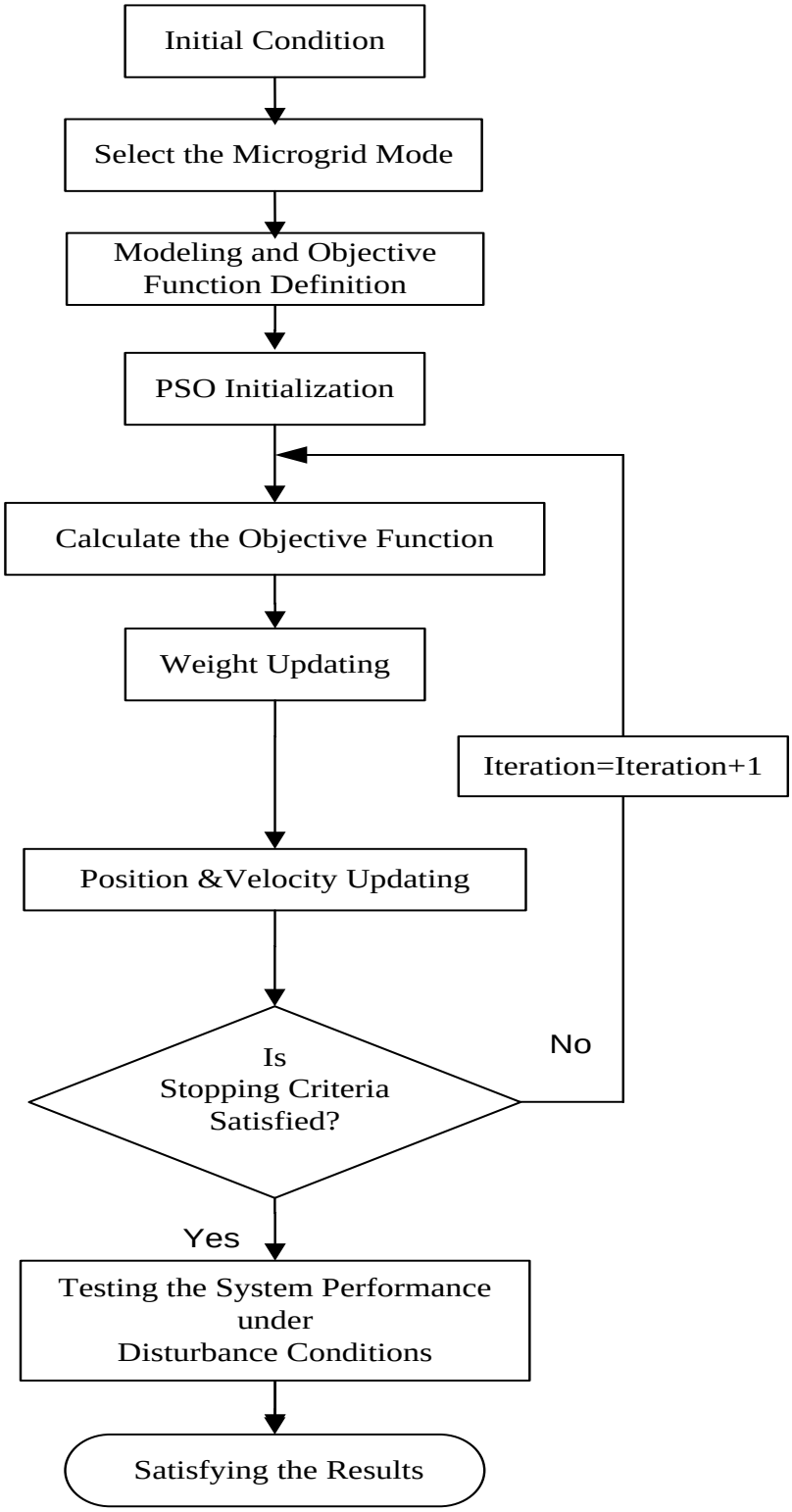

Fig. 5.1 Computational flow chart of the proposed PSO based optimal design approach

CHAPTER 6

RESULTS AND DISCUSSIONS OF AUTONOMOUS MODE

An important aspect of the stability analysis is related to the ability of the system to withstand or recover from large perturbations. The main objective of this chapter is to investigate the stability problems under fault conditions as well as changes in loads and power flows that occur regularly during normal power system operation. In this chapter, system stability has been investigated under different changes of different parameters as well as optimized parameters. Firstly, the impact of loading and system parameters such as controller parameters, filter inductance, filter capacitance and cut-off frequency on the system stability is investigated in linear and nonlinear models. This step is important to determine the parameters which affect the system stability. Then these should be selected in the optimization problem. Secondly, the system stability has been assessed using the

optimal controller parameters and optimal power coefficients. At the end, different cost functions have been used to obtain the optimal parameters.

In this study, three inverter-based DGs connected with two loads through filter and lines have been tested as an example of autonomous microgrid system. Simulation studies have been carried out in the MATLAB code. First, initial steady-state conditions of the system are obtained using a general power flow program. Second, linear model has been used to check the eigenvalues of the system. Finally, nonlinear time domain simulations have been carried out at two different disturbances to examine the effectiveness of the optimal settings of proposed controllers and power sharing coefficients. The first one is a step change in real power and the second is a fault disturbance at load 1.

6.1 SYSTEM DESCRIPTION

The complete layout of the three inverter-based DGs connected in autonomous microgrid is shown in Fig. 6.1. The autonomous microgrid contains three inverter-based DG units of equal ratings was simulated. Each DG unit is represented by a dc voltage source, a *VSI*, a series *LC* filter and coupling inductance L_c. Two load banks have been connected. One of these loads is located at bus-1 and the other is located at bus-3. The inverters are controlled to share the real and reactive powers over the lines 1 and 2. System parameters are given in Table 6.1. DG1 and DG2 are located relatively close to each other compared to DG3. A resistive load of 5.8 kW (25Ω per phase) at bus-1 and 7.3 kW (20Ω per phase) at bus-3 are considered as an initial operating point. A complete model of the test system was obtained using the procedure outlined in chapter three.

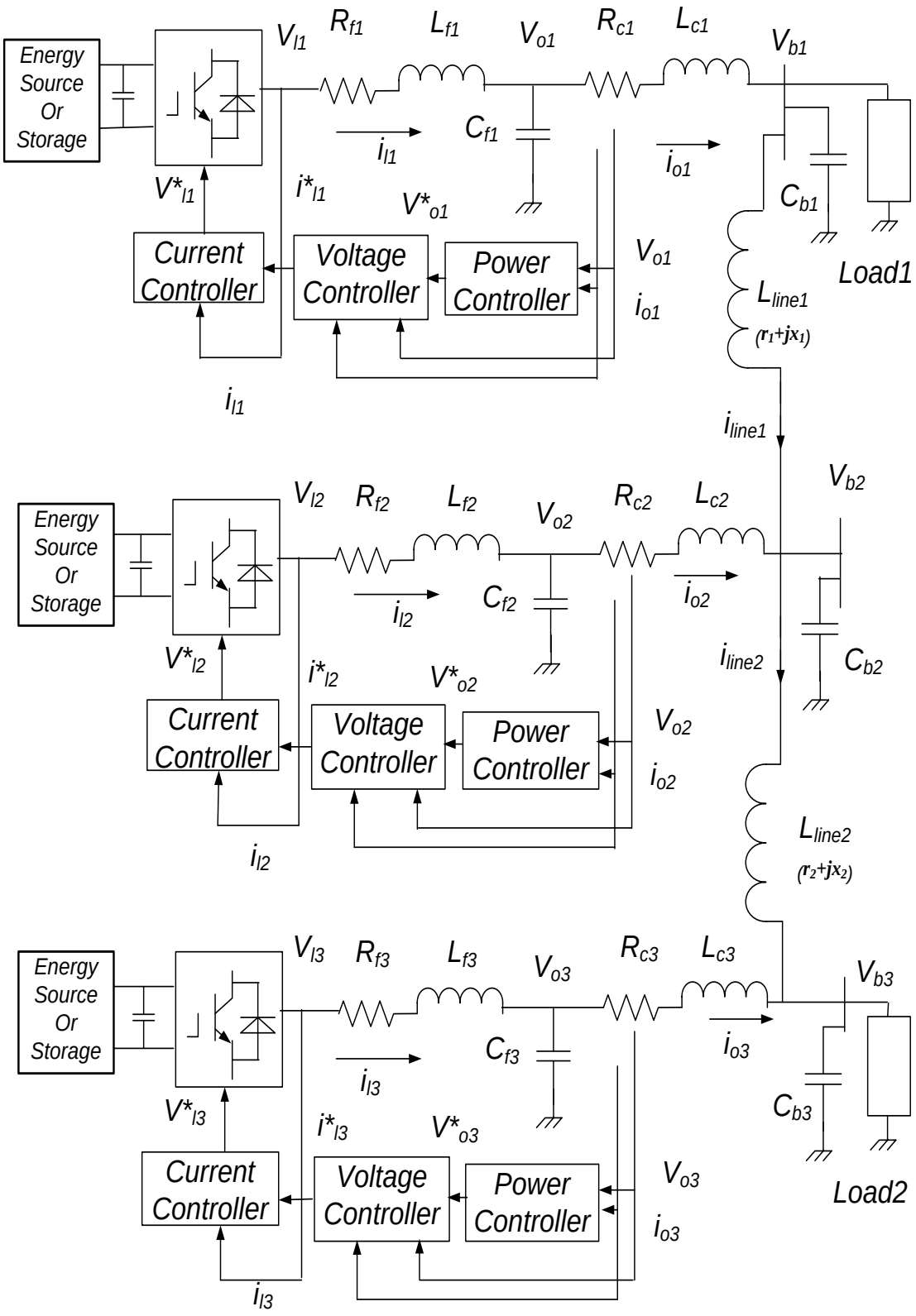

Fig. 6.1 Circuit diagram of three inverter-based microgrids

Table 6.1 System parameters of the autonomous microgrid

Parameter	*Value*	*Parameter*	*Value*
f_s	*8 kHz*	V_n	*381V*
L_f	*1.35mH*	L_c	*0.35mH*
C_f	*50e-6F*	C_b	*50e-6F*
r_f	*0.1Ω*	r_c	*0.03Ω*
ω_n	*314.16 rad/sec*	ω_c	*31.416 rad/sec*
r_1+jx_1	(0.23+j0.1) *Ω*	r_2+jx_2	(0.35+j0.58) *Ω*
m_p	*9.4e-5*	n_q	*1.3e-3*
K_{pv}	*0.05*	K_{iv}	*390*
K_{pc}	*10.5*	K_{ic}	*16000*
F	0.75		

6.2 LINEAR MODEL

Eigenvalue based objective function is proposed to enhance the damping characteristics. Applying the linearization steps described in chapter three, the complete state-space small-signal model of the overall system considered in Fig. 6.1 including the inverter, lines and loads can be written in the following equation;

$$\Delta \dot{x}_{overall\_system} = A_{overall\_system} \Delta x_{overall\_system} \tag{6.1}$$

where

$$\Delta x_{overall\_system} = \begin{bmatrix} \Delta\delta & \Delta P_c & \Delta Q_c & \Delta\phi_{dq} & \Delta\gamma_{dq} & \Delta i_{ldq} & \Delta v_{odq} & \Delta i_{odq} & \Delta i_{lineDQ} & \Delta i_{loadDQ} & \Delta v_{bDQ} \end{bmatrix}_{53}^{T} \tag{6.2}$$

$A_{overall\_system}$ is the matrix of the overall system given as follows;

$$A_{overall\_system} = \begin{bmatrix} [A_{inv1}]_{13\times13} & [0]_{13\times13} & [0]_{13\times13} & [B_{inv1}]_{13\times4} & [0]_{13\times4} & [0]_{13\times6} \\ [AB_{inv12}]_{13\times13} & [A_{inv2}]_{13\times13} & [0]_{13\times13} & [0]_{13\times4} & [B_{inv2}]_{13\times4} & [0]_{13\times6} \\ [AB_{inv13}]_{13\times13} & [0]_{13\times13} & [A_{inv3}]_{13\times13} & [0]_{13\times4} & [0]_{13\times4} & [B_{inv3}]_{13\times6} \\ [B_{net1}]_{4\times13} & [0]_{4\times13} & [0]_{4\times13} & [B_{net2}]_{4\times4} & [0]_{4\times4} & [B_{net3}]_{4\times6} \\ [B_{load1}]_{4\times13} & [0]_{4\times13} & [0]_{4\times13} & [0]_{4\times4} & [B_{load2}]_{4\times4} & [B_{load3}]_{4\times6} \\ [AB_{vb1}]_{6\times13} & [AB_{vb2}]_{6\times13} & [AB_{vb2}]_{6\times13} & [B_{vbline}]_{6\times4} & [B_{vbload2}]_{6\times4} & [B_{vbload3}]_{6\times6} \end{bmatrix}_{53\times53} \quad (6.3)$$

where; A_{invi} represents the matrix of each inverter as given by (3.42) and B_{invi} represents the matching between states i_{odq} and v_{bdq}

$$B_{invi} = \begin{bmatrix} 0 & 0 \\ 0 & 0 \\ 0 & 0 \\ 0 & 0 \\ 0 & 0 \\ 0 & 0 \\ 0 & 0 \\ 0 & 0 \\ 0 & 0 \\ 0 & 0 \\ 0 & 0 \\ -\frac{\cos\delta_o(i)}{L_c} & -\frac{\sin\delta_o(i)}{L_c} \\ \frac{\sin\delta_o(i)}{L_c} & -\frac{\cos\delta_o(i)}{L_c} \end{bmatrix}_{13\times2} \quad (6.4)$$

where i is the inverter number (1,2,3). AB_{invi}= [0] except $AB_{invi}(1,2) = -m_{p1}$. It represents the derivatives related to the states of ΔP_c. B_{neti} represents the matching between A_{matrix} and i_{lines};

$$B_{net1}=\begin{bmatrix} 0 & 0 & -m_p I_{lineQo}(1) & 0 & 0 & 0 & 0 & 0 & 0 & 0 & 0 & 0 & 0 \\ 0 & 0 & m_p I_{lineDo}(1) & 0 & 0 & 0 & 0 & 0 & 0 & 0 & 0 & 0 & 0 \\ 0 & 0 & -m_p I_{lineQo}(2) & 0 & 0 & 0 & 0 & 0 & 0 & 0 & 0 & 0 & 0 \\ 0 & 0 & m_p I_{lineDo}(2) & 0 & 0 & 0 & 0 & 0 & 0 & 0 & 0 & 0 & 0 \end{bmatrix}_{4\times 13}$$

$$B_{net2}=\begin{bmatrix} -\frac{r_{line}(1)}{L_{line}(1)} & \omega_o & 0 & 0 \\ -\omega_o & -\frac{r_{line}(1)}{L_{line}(1)} & 0 & 0 \\ 0 & 0 & -\frac{r_{line}(2)}{L_{line}(2)} & -\omega_o \\ 0 & 0 & -\omega_o & -\frac{r_{line}(2)}{L_{line}(2)} \end{bmatrix}_{4\times 4}$$

$$B_{net3}=\begin{bmatrix} \frac{1}{L_{line}(1)} & 0 & -\frac{1}{L_{line}(1)} & 0 & 0 & 0 \\ 0 & \frac{1}{L_{line}(1)} & 0 & -\frac{1}{L_{line}(1)} & 0 & 0 \\ 0 & 0 & \frac{1}{L_{line}(2)} & 0 & -\frac{1}{L_{line}(2)} & 0 \\ 0 & 0 & 0 & \frac{1}{L_{line}(2)} & 0 & -\frac{1}{L_{line}(2)} \end{bmatrix}_{4\times 6} \tag{6.5}$$

B_{loadi} represents the factors of the states of loads;

$$B_{load1}=\begin{bmatrix} 0 & 0 & -m_p I_{loadQo}(1) & 0 & 0 & 0 & 0 & 0 & 0 & 0 & 0 & 0 & 0 \\ 0 & 0 & m_p I_{loadDo}(1) & 0 & 0 & 0 & 0 & 0 & 0 & 0 & 0 & 0 & 0 \\ 0 & 0 & -m_p I_{loadQo}(2) & 0 & 0 & 0 & 0 & 0 & 0 & 0 & 0 & 0 & 0 \\ 0 & 0 & m_p I_{loadDo}(2) & 0 & 0 & 0 & 0 & 0 & 0 & 0 & 0 & 0 & 0 \end{bmatrix}_{4\times 13}$$

$$B_{load2}=\begin{bmatrix} -\frac{R_{load}(1)}{L_{load}(1)} & \omega_o & 0 & 0 \\ -\omega_o & -\frac{R_{load}(1)}{L_{load}(1)} & 0 & 0 \\ 0 & 0 & -\frac{R_{load}(2)}{L_{load}(2)} & \omega_o \\ 0 & 0 & -\omega_o & -\frac{R_{load}(2)}{L_{load}(2)} \end{bmatrix}_{4\times 4}$$

$$B_{load3}=\begin{bmatrix} \frac{1}{L_{load}(1)} & 0 & -\frac{1}{L_{load}(1)} & 0 & 0 & 0 \\ 0 & \frac{1}{L_{load}(1)} & 0 & 0 & 0 & 0 \\ 0 & 0 & 0 & 0 & \frac{1}{L_{load}(2)} & 0 \\ 0 & 0 & 0 & 0 & 0 & -\frac{1}{L_{load}(2)} \end{bmatrix}_{4\times 6} \tag{6.6}$$

B_{vbline} represents the matching between v_{bus} and i_{line};

$$B_{vbline}=\begin{bmatrix} -\frac{1}{C_b} & 0 & 0 & 0 \\ 0 & -\frac{1}{C_b} & 0 & 0 \\ \frac{1}{C_b} & 0 & -\frac{1}{C_b} & 0 \\ 0 & \frac{1}{C_b} & 0 & -\frac{1}{C_b} \\ 0 & 0 & \frac{1}{C_b} & 0 \\ 0 & 0 & 0 & \frac{1}{C_b} \end{bmatrix}_{6\times 4} \tag{6.7}$$

B_{vbload} represents the matching between v_{bus} and i_{loads};

$$B_{vbload2}=\begin{bmatrix} -\frac{1}{C_b} & 0 & 0 & 0 \\ 0 & -\frac{1}{C_b} & 0 & 0 \\ 0 & 0 & 0 & 0 \\ 0 & 0 & 0 & 0 \\ 0 & 0 & -\frac{1}{C_b} & 0 \\ 0 & 0 & 0 & -\frac{1}{C_b} \end{bmatrix}_{6\times 4} \quad B_{vbload3}=\begin{bmatrix} 0 & \omega_o & 0 & 0 & 0 & 0 \\ -\omega_o & 0 & 0 & 0 & 0 & 0 \\ 0 & 0 & 0 & \omega_o & 0 & 0 \\ 0 & 0 & -\omega_o & 0 & 0 & 0 \\ 0 & 0 & 0 & 0 & 0 & \omega_o \\ 0 & 0 & 0 & 0 & -\omega_o & 0 \end{bmatrix}_{6\times 6}$$

(6.8)

AB_{vb1} represents the matching between A_{matrix} and i_{loads};

$$AB_{vb1}=\begin{bmatrix} -(I_{od}(1)\sin\delta_o(1)+I_{oq}(1)\cos\delta_o(1)) & -m_pV_{bQo}(4) & 0&0&0&0&0&0&0&0 & \frac{\cos\delta_o(1)}{C_b} & \frac{-\sin\delta_o(1)}{C_b} \\ (I_{od}(1)\cos\delta_o(1)-I_{oq}(1)\sin\delta_o(1)) & m_pV_{bDo}(4) & 0&0&0&0&0&0&0&0 & \frac{-\sin\delta_o(1)}{C_b} & \frac{\cos\delta_o(1)}{C_b} \\ 0 & -m_pV_{bQo}(5) & 0&0&0&0&0&0&0&0 & 0 & 0 \\ 0 & m_pV_{bDo}(5) & 0&0&0&0&0&0&0&0 & 0 & 0 \\ 0 & -m_pV_{bQo}(6) & 0&0&0&0&0&0&0&0 & 0 & 0 \\ 0 & m_pV_{bDo}(6) & 0&0&0&0&0&0&0&0 & 0 & 0 \end{bmatrix}_{6\times 13} \quad (6.9)$$

$$AB_{vb2}=\begin{bmatrix} -(I_{od}(2)\sin\delta_o(2)+I_{oq}(2)\cos\delta_o(2)) & 0&0&0&0&0&0&0&0&0 & 0 & 0 \\ (I_{od}(2)\cos\delta_o(2)-I_{oq}(2)\sin\delta_o(2)) & 0&0&0&0&0&0&0&0&0 & 0 & 0 \\ 0 & 0&0&0&0&0&0&0&0&0 & \frac{\cos\delta_o(2)}{C_b} & \frac{-\sin\delta_o(2)}{C_b} \\ 0 & 0&0&0&0&0&0&0&0&0 & \frac{-\sin\delta_o(2)}{C_b} & \frac{\cos\delta_o(2)}{C_b} \\ 0 & 0&0&0&0&0&0&0&0&0 & 0 & 0 \\ 0 & 0&0&0&0&0&0&0&0&0 & 0 & 0 \end{bmatrix}_{6\times 13}$$

(6.10)

$$AB_{vb3} = \begin{bmatrix} -(I_{od}(3)\sin\delta_o(3) + I_{oq}(3)\cos\delta_o(3)) & 0 & 0 & 0 & 0 & 0 & 0 & 0 & 0 & 0 & 0 & 0 & 0 \\ (I_{od}(3)\cos\delta_o(3) - I_{oq}(3)\sin\delta_o(3)) & 0 & 0 & 0 & 0 & 0 & 0 & 0 & 0 & 0 & 0 & 0 & 0 \\ 0 & 0 & 0 & 0 & 0 & 0 & 0 & 0 & 0 & 0 & 0 & 0 & 0 \\ 0 & 0 & 0 & 0 & 0 & 0 & 0 & 0 & 0 & 0 & 0 & 0 & 0 \\ 0 & 0 & 0 & 0 & 0 & 0 & 0 & 0 & 0 & 0 & 0 & \frac{\cos\delta_o(3)}{C_b} & \frac{-\sin\delta_o(3)}{C_b} \\ 0 & 0 & 0 & 0 & 0 & 0 & 0 & 0 & 0 & 0 & 0 & \frac{-\sin\delta_o(3)}{C_b} & \frac{\cos\delta_o(3)}{C_b} \end{bmatrix}_{6\times 13}$$

(6.11)

The impact of different parameters given in Table 6.1 on the system stability has been investigated. Fig 6.2 shows that the system is not stable as a pair of eigenvalues is on the RHS of *s*-plane. Based on literature survey [8]-[9], [71], the microgrid stability is affected by the controller parameters. So before applying the optimization technique, the system stability has been assessed under changing the controller parameters of the system given in Fig. 6.1. The eigenvalues of the system under these changes are shown in Fig 6.3. Comparing the eigenvalues before and after optimization given in Fig 6.3 and Fig. 6.2, it can be concluded that some poles located in RHS move towards LHS. This means that the controller parameters affect the eigenvalues of the system performance and then the system stability.

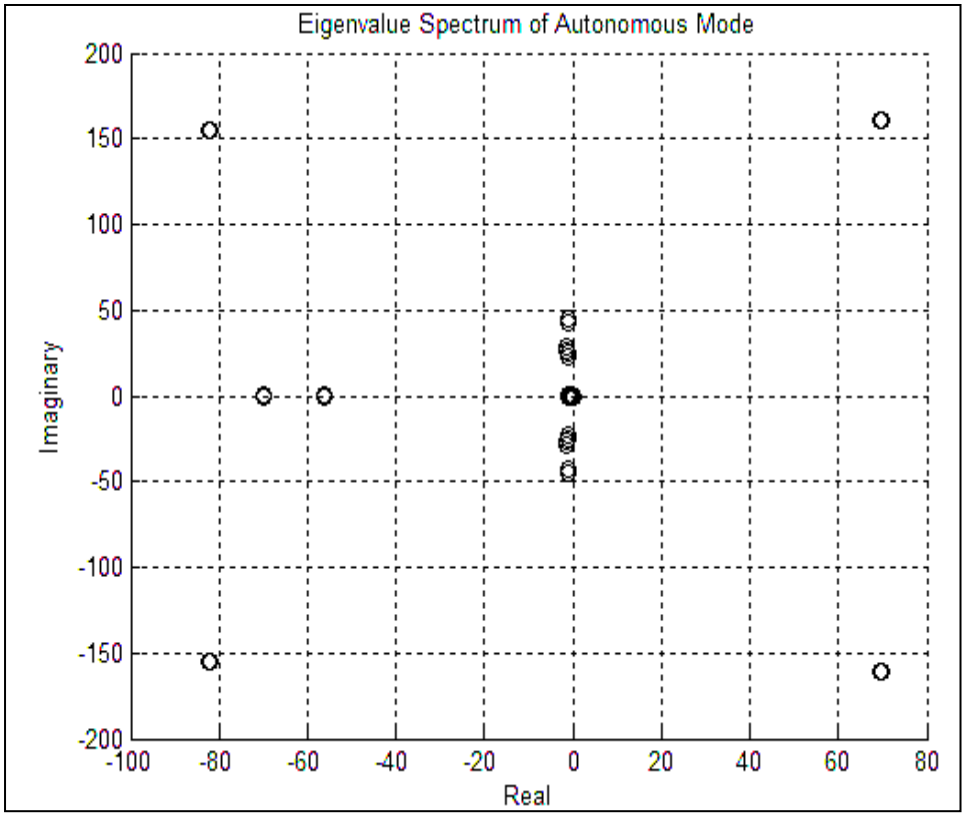

Fig. 6.2 The eigenvalues spectrum of the system with the parameters given in the Table1

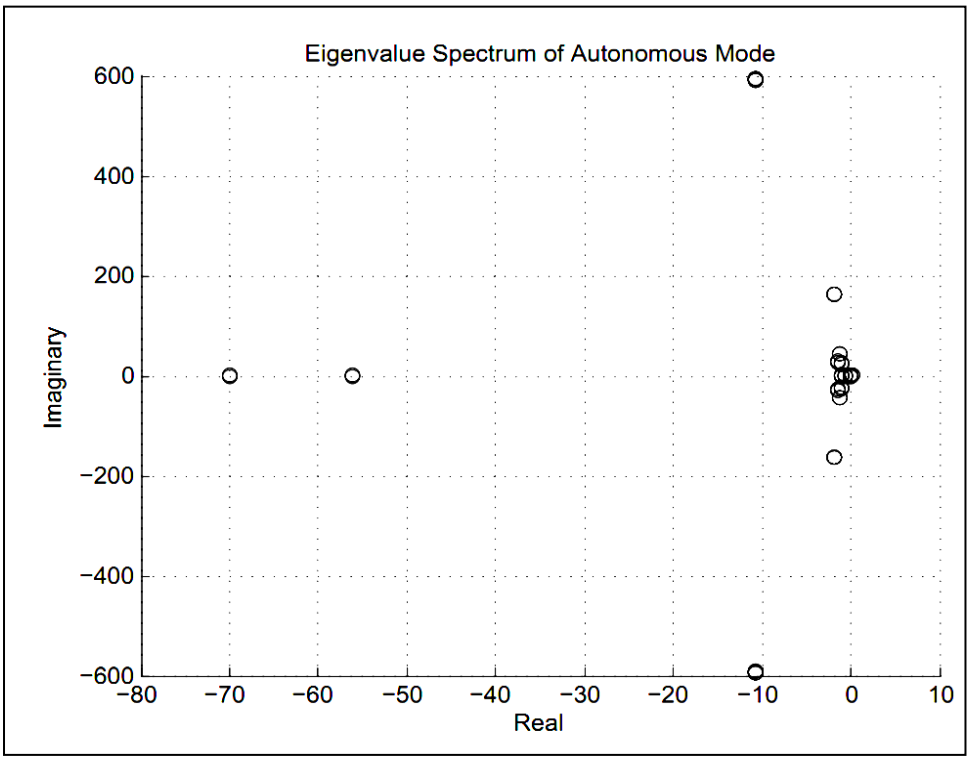

Fig. 6.3 The eigenvalue spectrum of the system under changing the controller parameters

6.2.1 Controller and Power Sharing Design Based on Linear Model

PSO is employed to search for optimal settings of the optimized controller parameters of the PI current and voltage controllers as well as power sharing coefficients. The values of the optimal parameters are provided in table 6.2.

Table 6.2 Optimal parameters in the autonomous microgrid mode

	DG1	DG2	DG3
K_{pv}	0.531129	0.614458	0.459892
K_{iv}	1.5556	1.91122	0.840236
K_{pc}	39.0829	23.8478	31.4614
K_{ic}	11.3107	20.1044	22.6824
m_p	7.37e-005	9.4e-005	0.000507392
n_q	0.0013	0.0013	0.00275689

Then the impact of optimal parameters given in Table 6.2 on system stability has been investigated. Fig.6.4 shows that all poles with the proposed settings are located in the LHS. This means that the system becomes now a stable. Fig. 6.4 also illustrates the effectiveness of using the optimization technique powerfully in achieving the stability of the system.

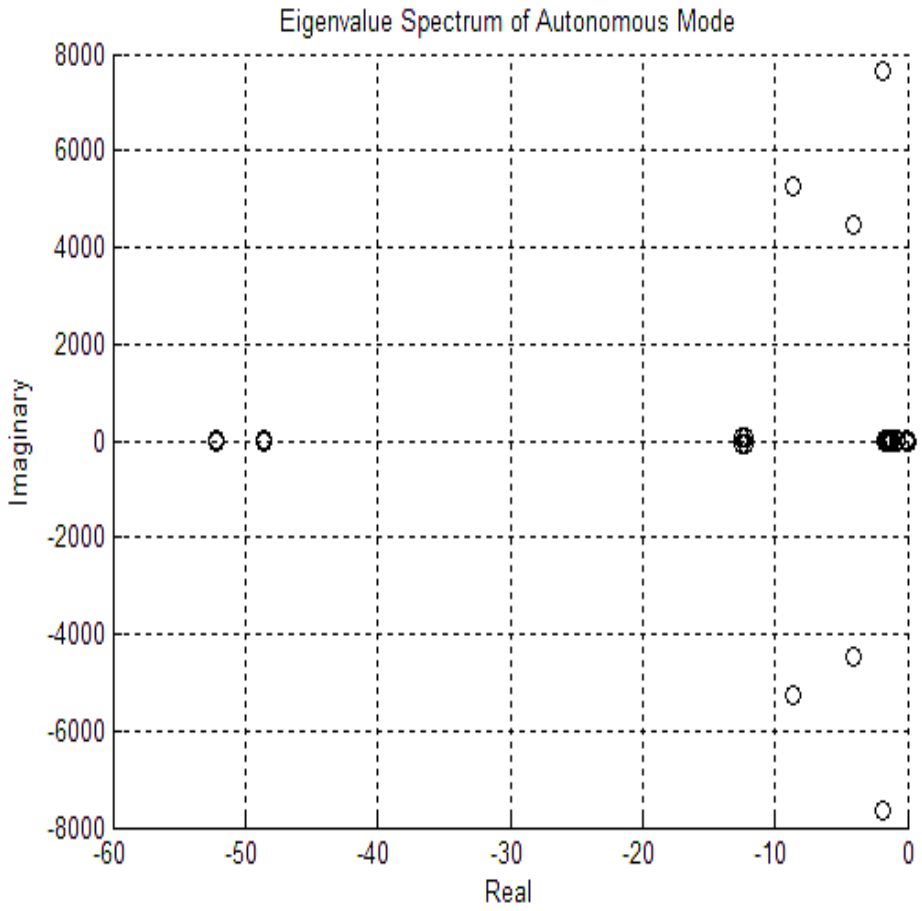

Fig. 6.4 The eigenvalue spectrum of the system using the optimization values

6.3 NONLINEAR MODEL

Nonlinear time-domain based objective function is proposed to minimize the error in the calculated active power as well as the error in the calculated reactive power. Firstly, the impact of system parameters given in Table 6.1 on system stability has been tested. The performance of the microgrid with the given controller parameters under different disturbances has been examined. Secondly, PSO has been applied to obtain the optimized controller parameters and the optimized power sharing coefficients which enhance the autonomous microgrid stability. The performance of the microgrid with the proposed

controllers and optimal settings under different disturbances has been investigated through the nonlinear time domain simulations.

6.3.1 Impact of the System Parameters given in Table 6.1 on the System Stability

Nonlinear time domain simulations have been carried out to assess the controller effectiveness of the system given in Table 6.1. The system stability has been assessed under the fault and step response using the controller parameters of the system given in Fig. 6.1.

(a) Step Response

The system stability has been examined under step response for parameters given in Table 6.1. The impact of the proportional and integral parameters of the voltage and current controller parameters K_{pv}, $K_{iv,}$ K_{pc} and K_{ic} on the system stability under step response has been tested. Figs. 6.5 - 6.12 represent the responses of the active power, reactive powers, d-axis and q-axis of inductor current, output current, and output voltage. The results illustrate that the system response is unstable for the given parameters.

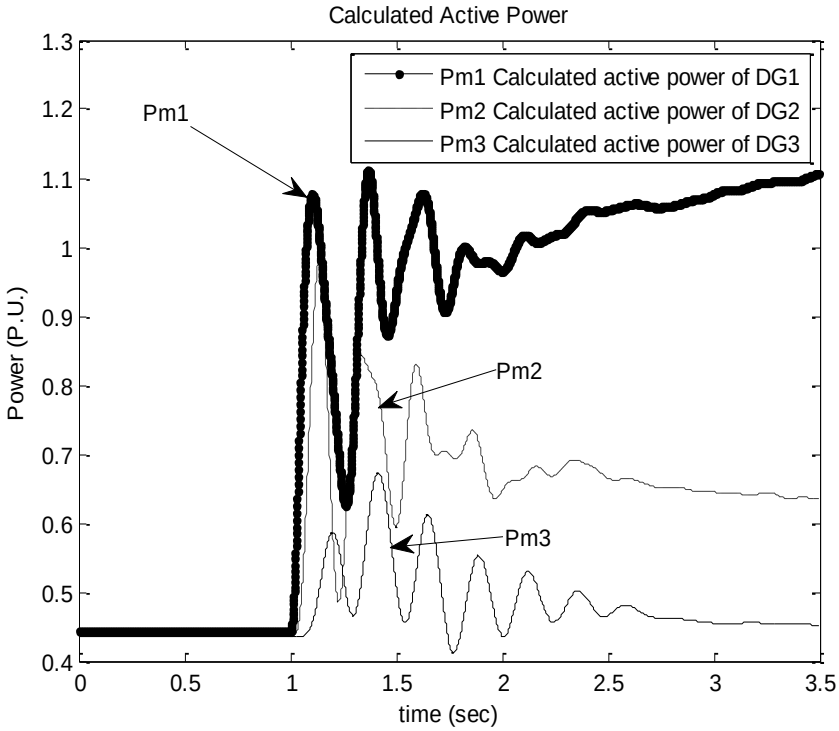

Fig. 6.5 Output active power response of the three DGs when step response occurs at *load1*

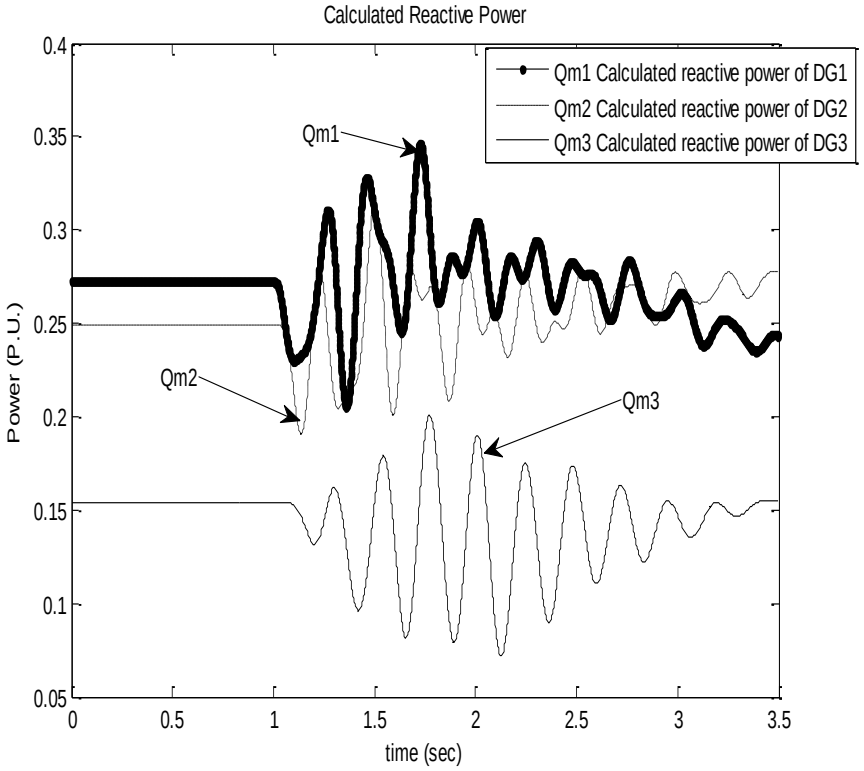

Fig. 6.6 Output reactive power response of the three DGs when step response occurs at *load1*

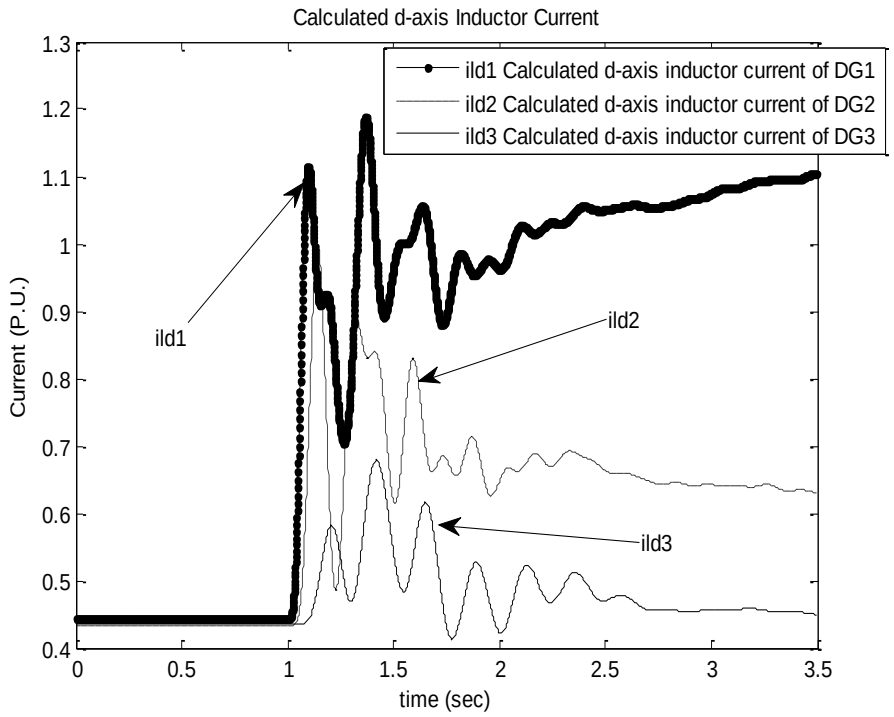

Fig. 6.7 D-axis inductor current response of the three DGs when step response occurs at *load1*

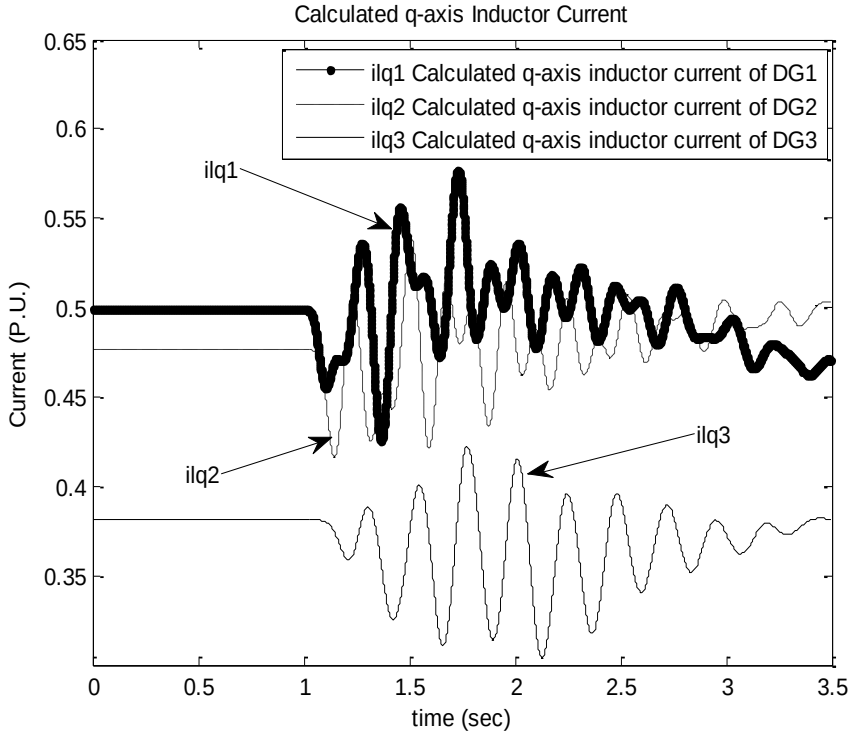

Fig. 6.8 Q-axis inductor current response of the three DGs when step response occurs at *load1*

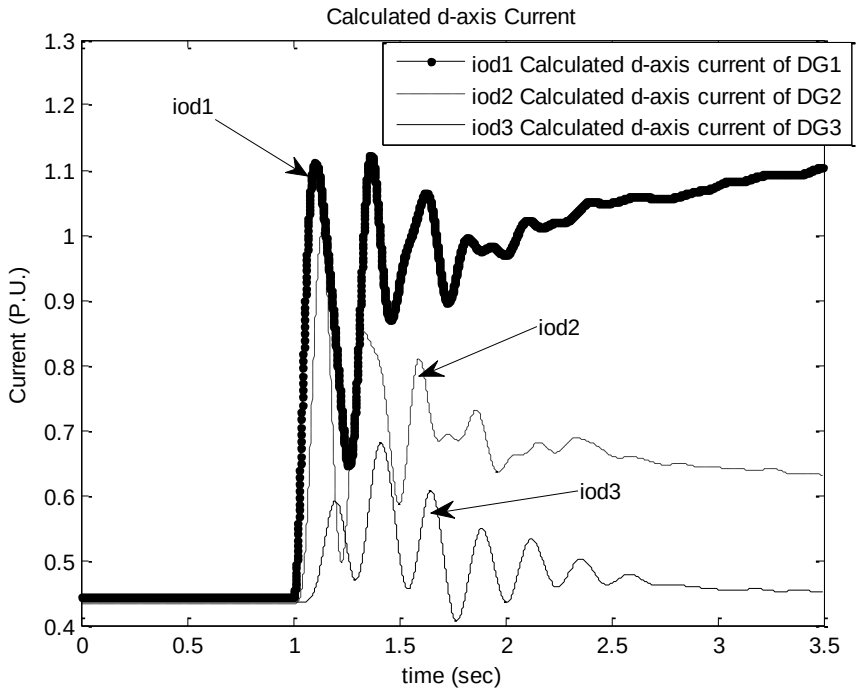

Fig. 6.9 D-axis output current response of the three DGs when step response occurs at *load1*

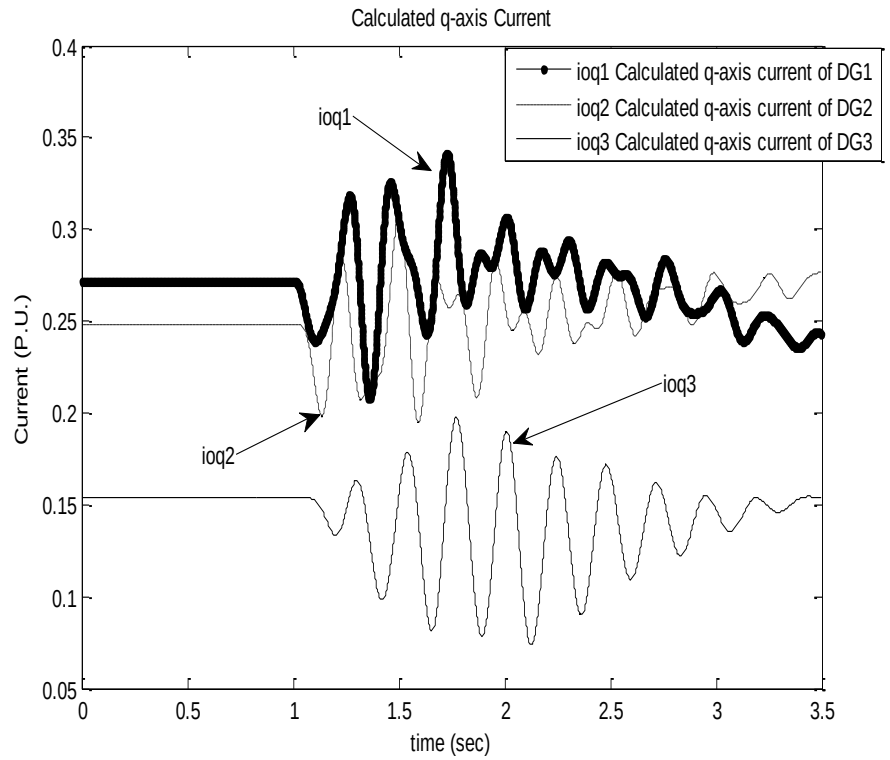

Fig. 6.10 Q-axis output current response of the three DGs when step response occurs at *load1*

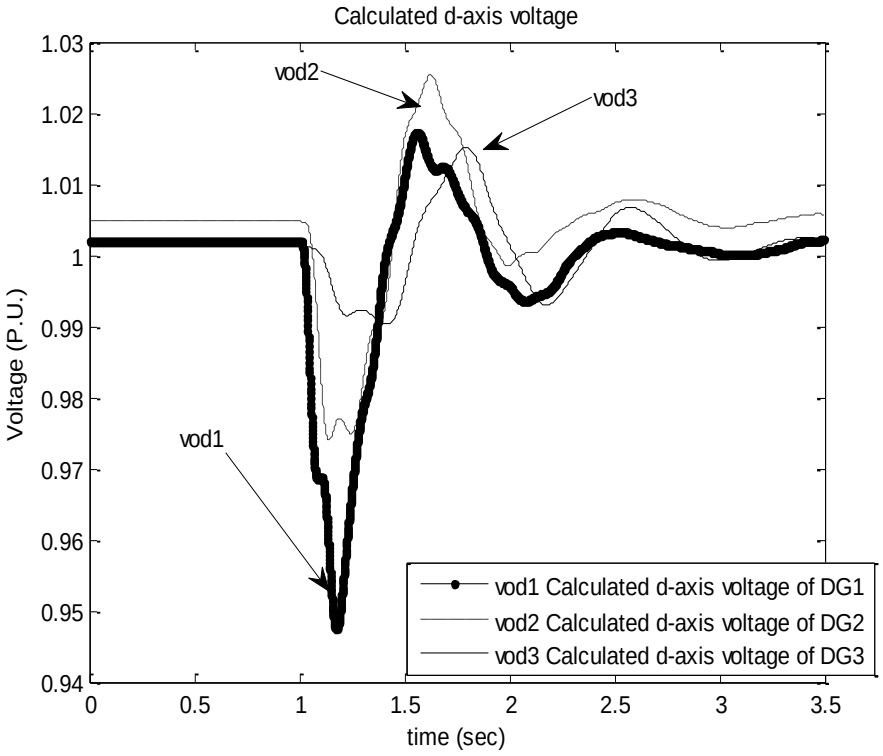

Fig. 6.11 D-axis output voltage response of the three DGs when step response occurs at *load1*

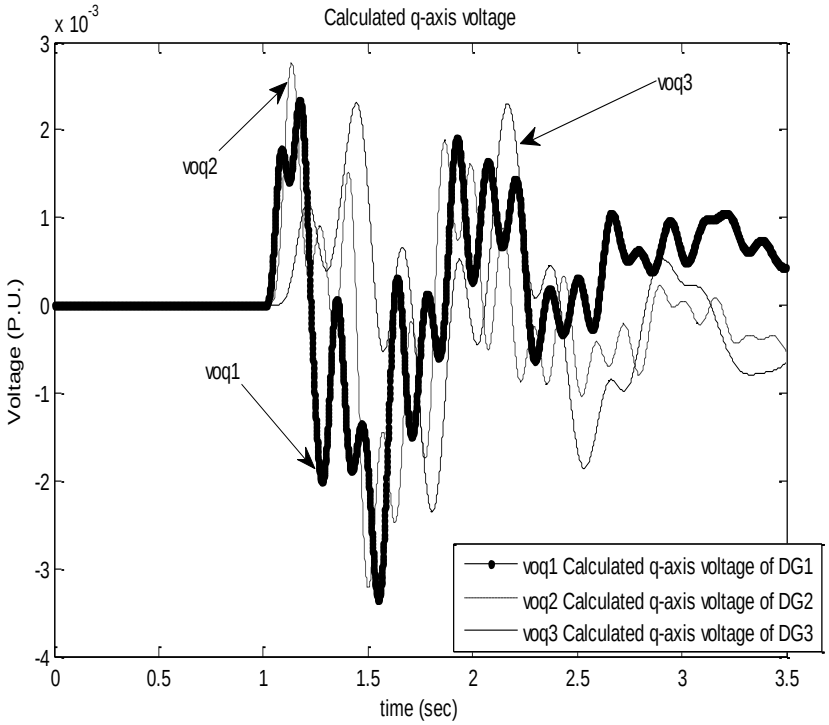

Fig. 6.12 Q-axis output voltage response of the three DGs when step response occurs at *load1*

(b) Fault Response

In this section, three phase fault has been applied at the load1 of the system given in Fig. 6.1. The system stability has been assessed under the fault response when the given controller parameters have been used. The impact of the controller parameters on the system stability is investigated to assess the effectiveness of the controller parameters. The fault response of the system with parameters given in the Table 6.1 is shown in Figs. 6.13 – 6.20. It is concluded that the system is unstable after getting fault at load1.

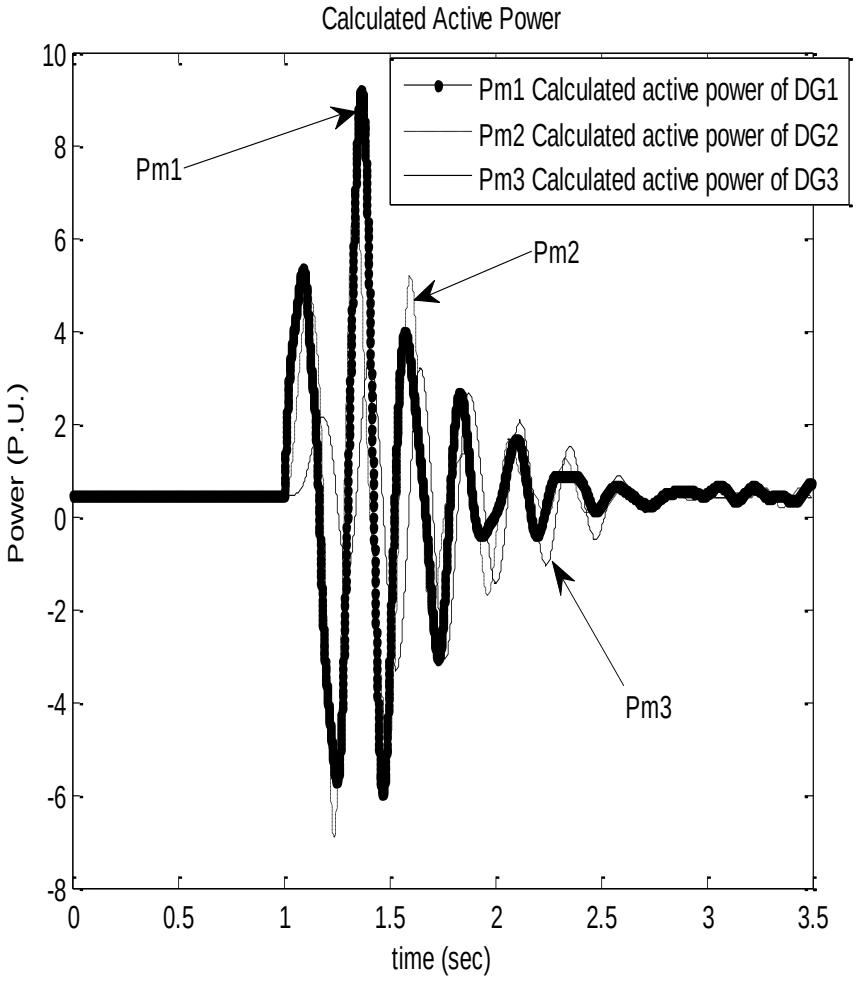

Fig. 6.13 Output active power response of the three DGs when the fault occurs at *load1* with parameters given in the Table 6.1

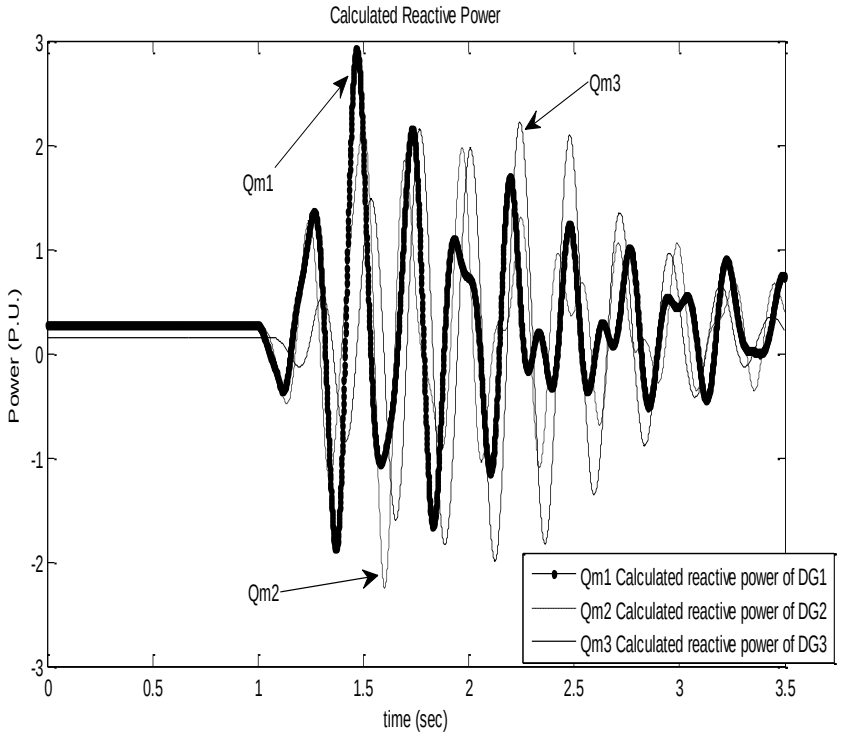

Fig. 6.14 Output reactive power response of the three DGs when the fault occurs at *load1*

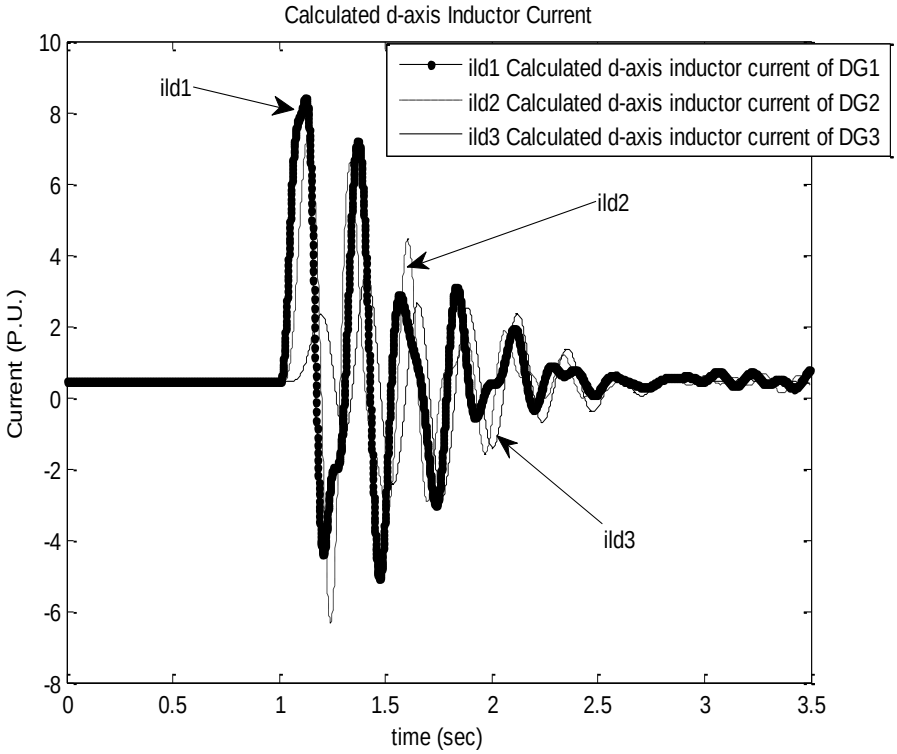

Fig. 6.15 D-axis inductor current response of the three DGs when the fault occurs at *load1*

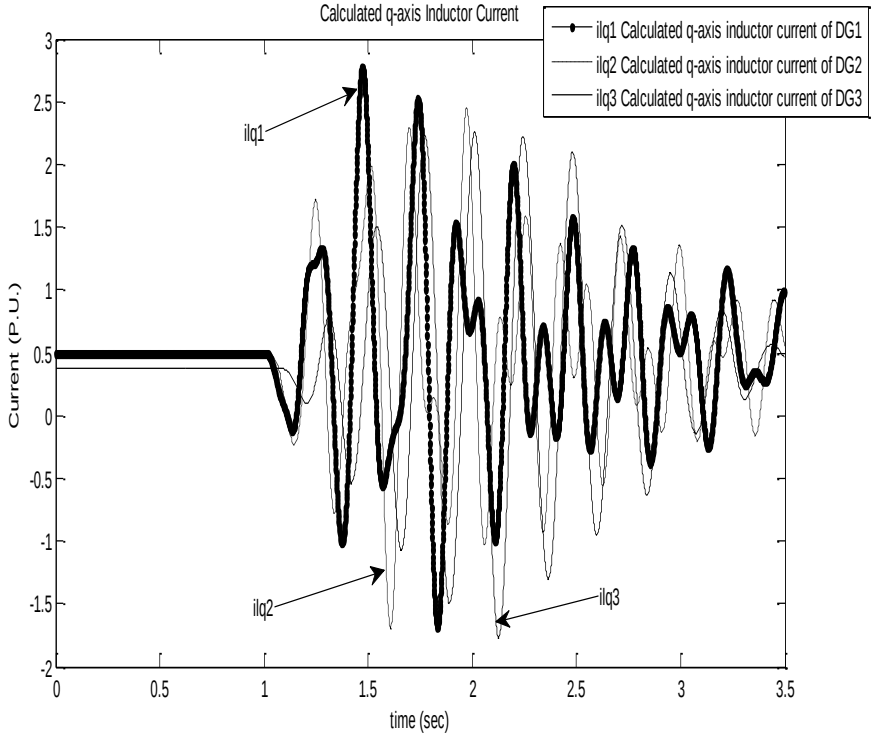

Fig. 6.16 Q-axis inductor current response of the three DGs when the fault occurs at *load1*

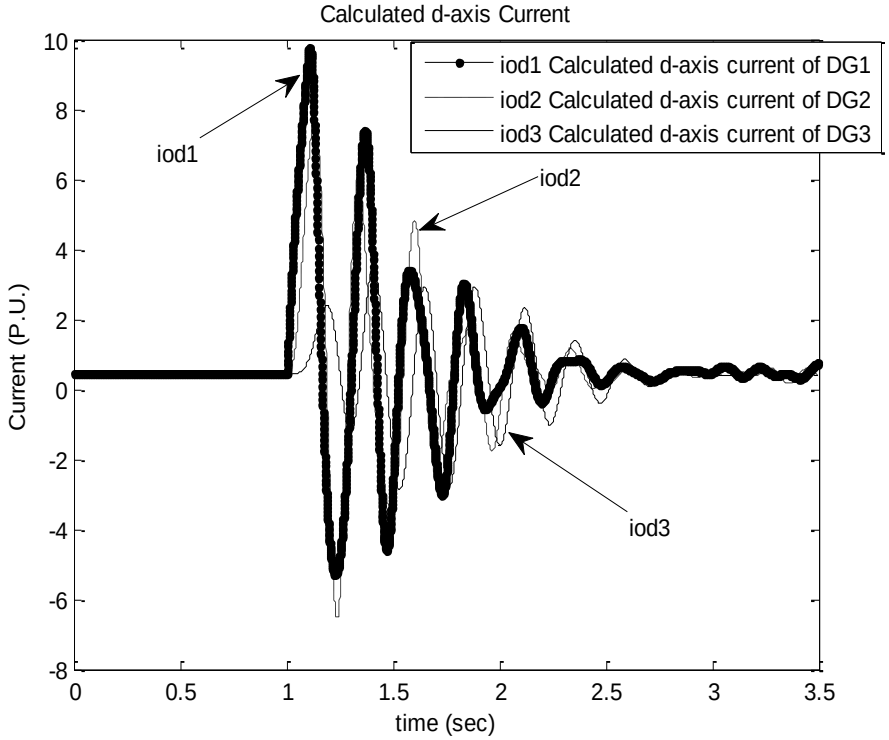

Fig. 6.17 D-axis output current response of the three DGs when the fault occurs at *load1*

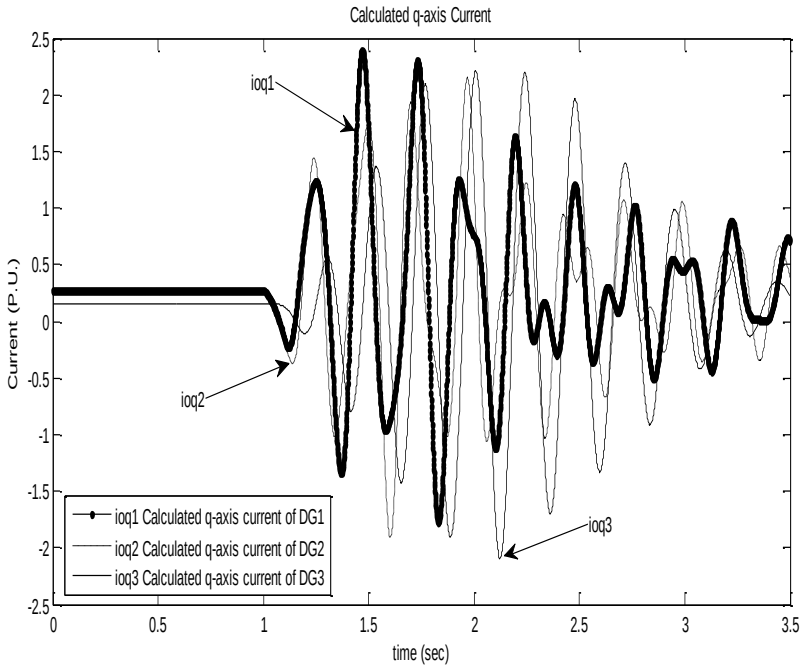

Fig. 6.18 Q-axis output current response of the three DGs when the fault occurs at *load1*

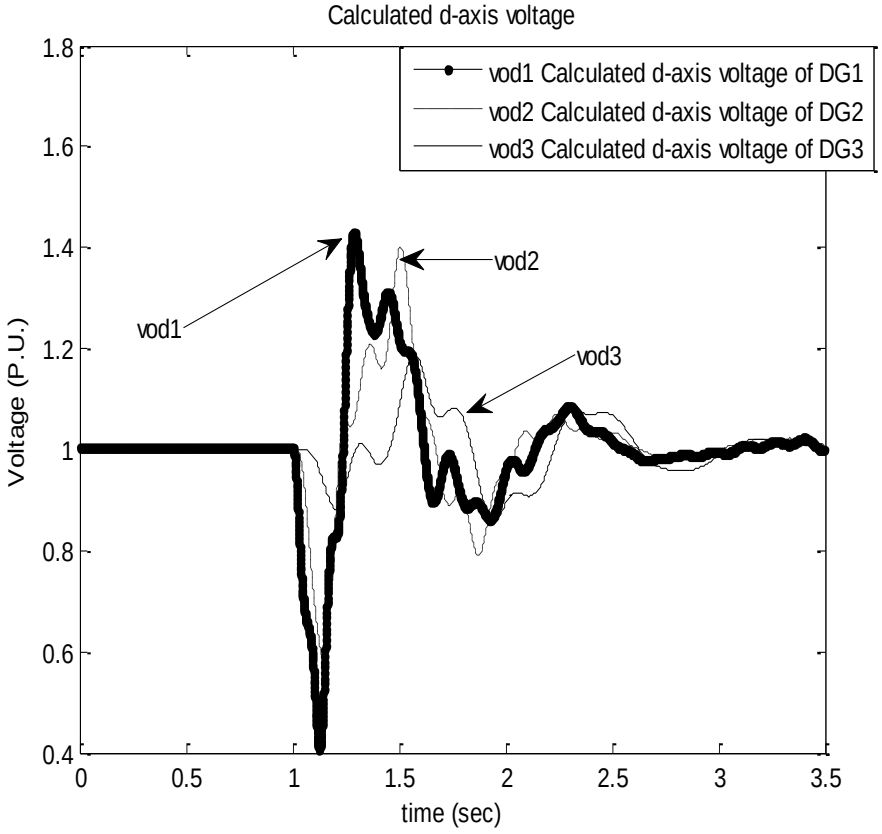

Fig. 6.19 Output d-axis voltage response of the three DGs when the fault occurs at *load1*

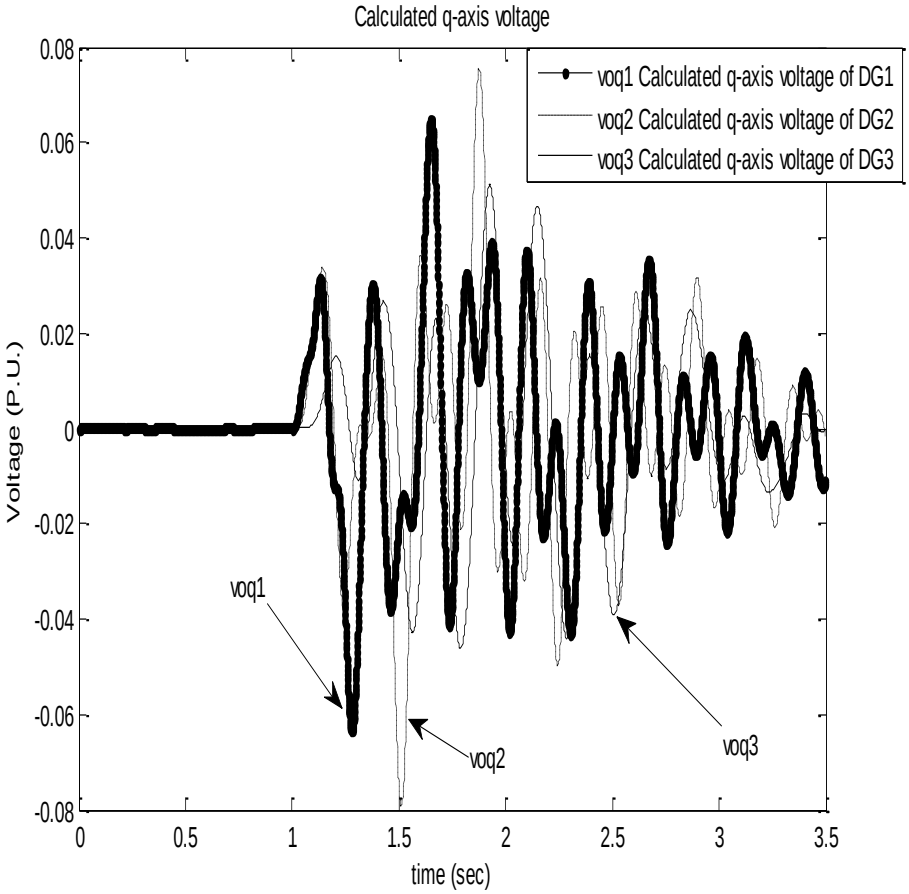

Fig. 6.20 Output q-axis voltage response of the three DGs when the fault occurs at *load1*

6.3.2 Controller and Power Sharing Design Based on Nonlinear Model

Considering the objective function given in (5.2), the proposed approach employs PSO to solve the optimization problem and search for the optimal controller parameters and optimal power sharing parameters. The effectiveness of these optimal parameters on the system stability is investigated when the optimized controller parameters and optimal power sharing parameters have been used. The difference between calculated and reference active power as well as reactive power has been used as cost function to assess the system stability.

(a) Step Response using the Optimal Parameters

First, the impact of the optimized controller parameters and optimal power sharing on the system stability is assessed when the step change of 3.8KW real power has been applied at load1. Figs. 6.21 - 6.28 show that the system response is stable under this disturbance when the optimized controller parameters have been used. The responses show that the damping characteristics are greatly enhanced and the system performance in terms of overshoots and settling time is improved significantly. The output active power response of the three DGs is given in Fig. 6.21. Fig. 6.22 shows the output reactive power response of the three DGs. DQ inductor and output current responses of the three DGs are presented in Fig. 6.23, 6.24, 6.25 and 6.26. Fig. 6.27 and Fig. 6.28 depict the output d-axis and q-axis voltage responses of all the three inverters for a step load change. Comparing the results given in Figs. 6.21 - 6.28 with the results given in Figs. 6.5 - 6.12, the system become stable after getting step disturbance when the optimal parameters have been used while the system become unstable when the system parameters of Table 6.1 have been used.

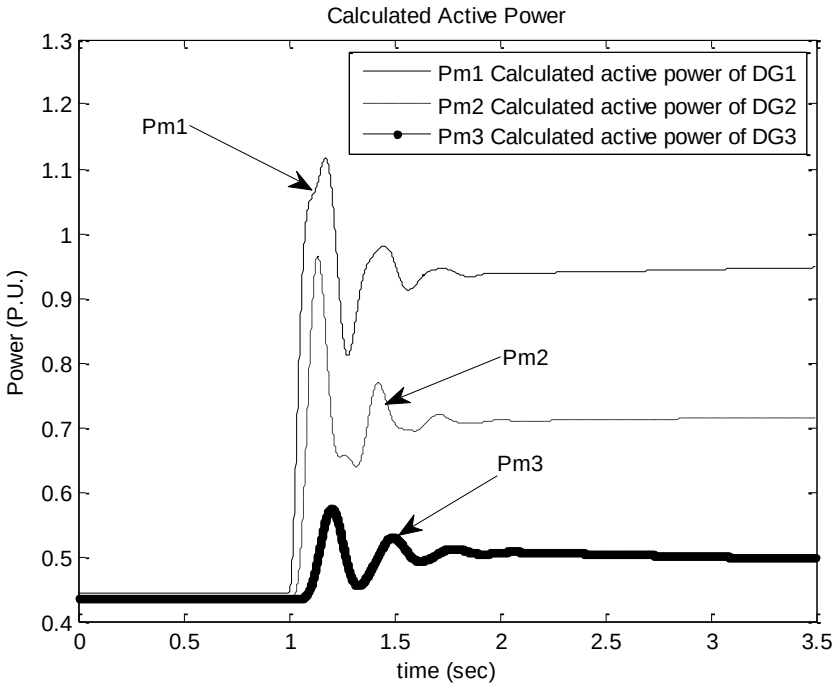

Fig. 6.21 Output active power response of the three DGs when step response occurs at *load1*

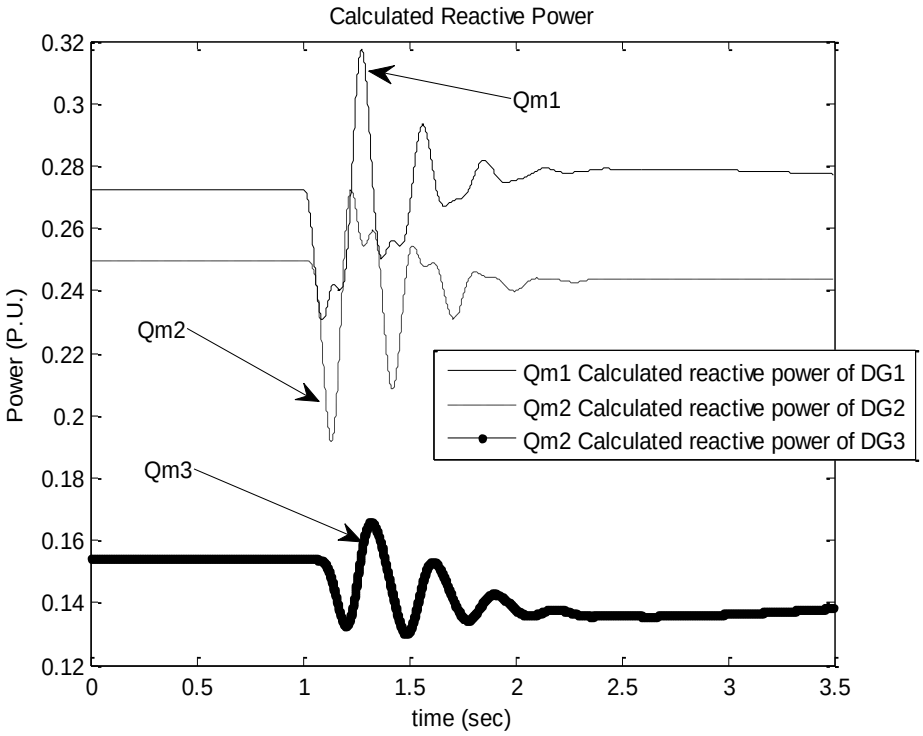

Fig. 6.22 Output reactive power response of the three DGs when step response occurs at *load1*

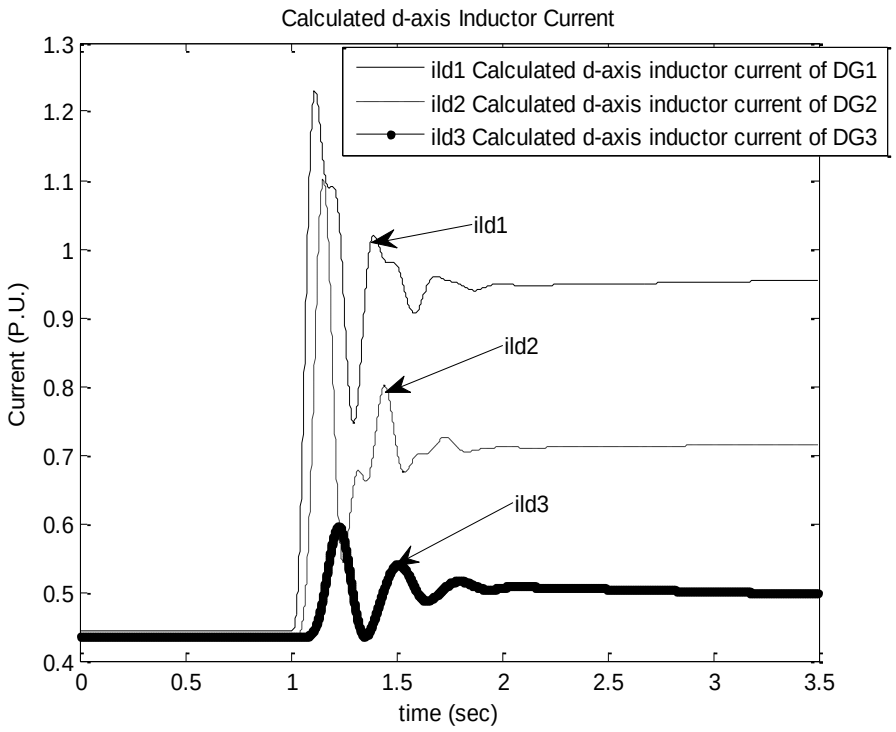

Fig. 6.23 D-axis inductor current response of the three DGs when step response occurs at *load1*

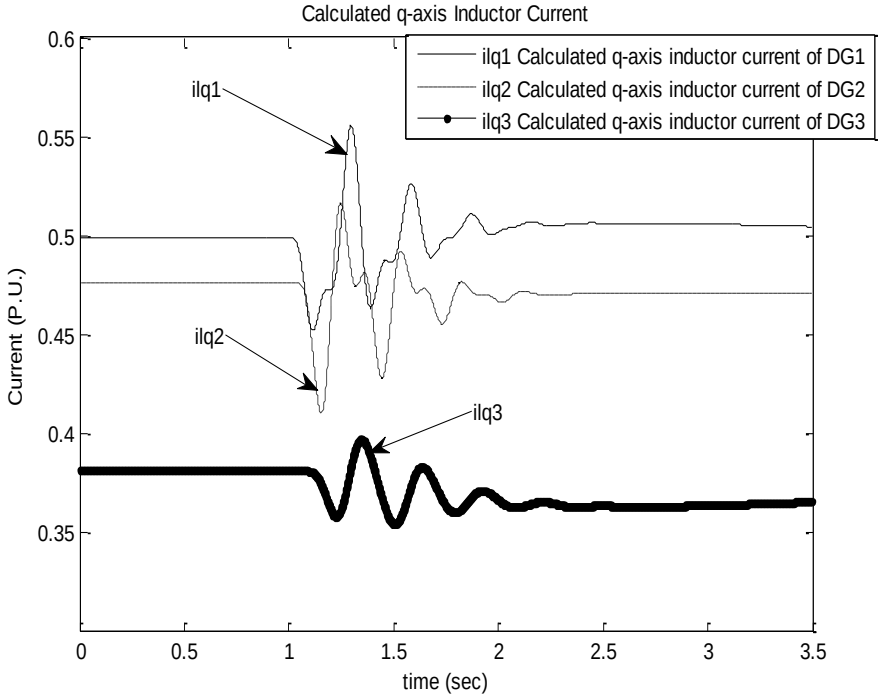

Fig. 6.24 Q-axis inductor current response of the three DGs when step response occurs at *load1*

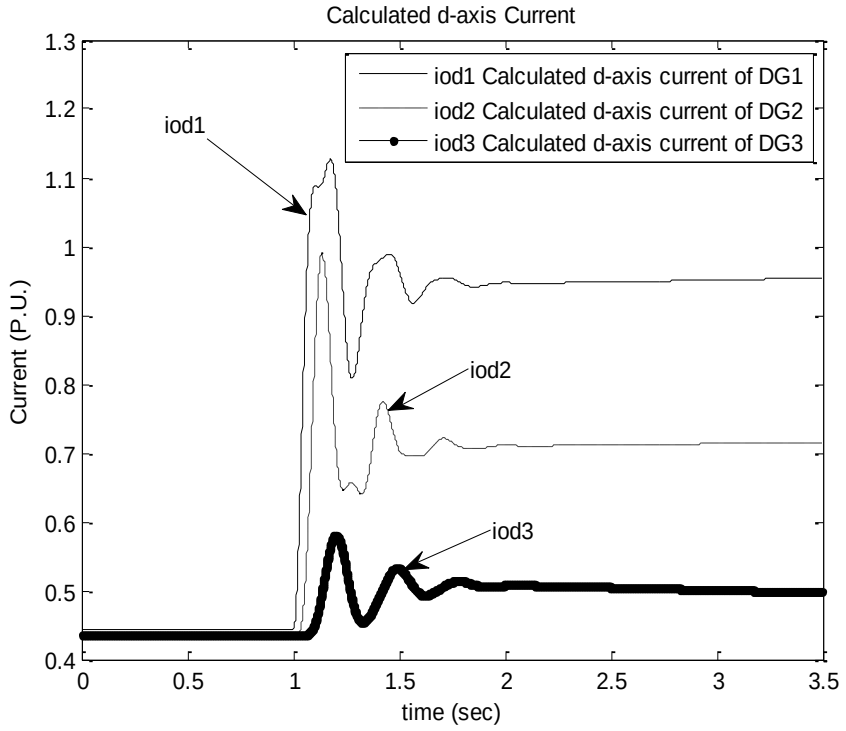

Fig. 6.25 D-axis output current response of the three DGs when step response occurs at *load1*

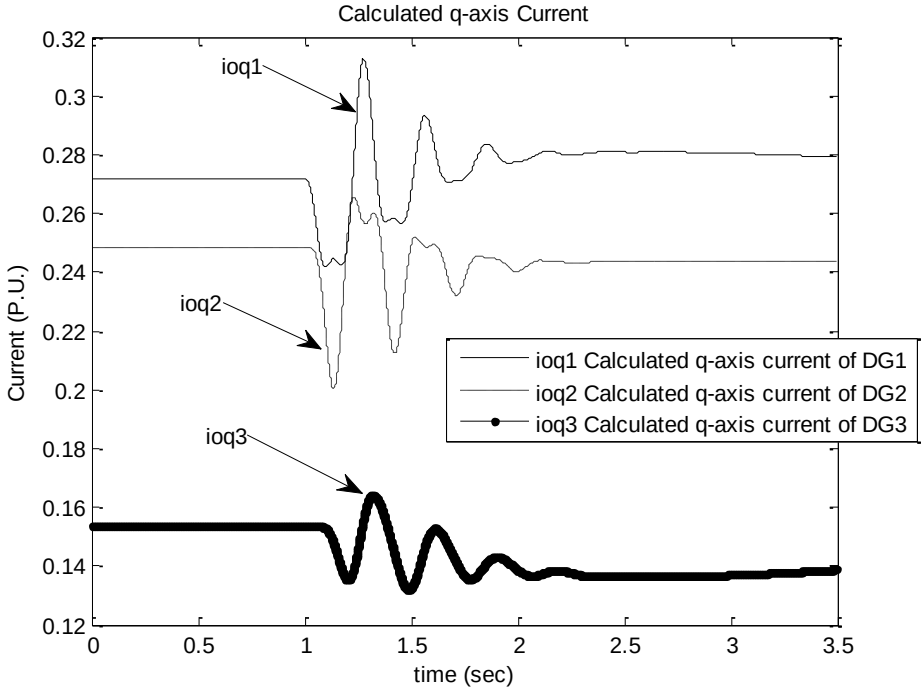

Fig. 6.26 Q-axis output current response of the three DGs when step response occurs at *load1*

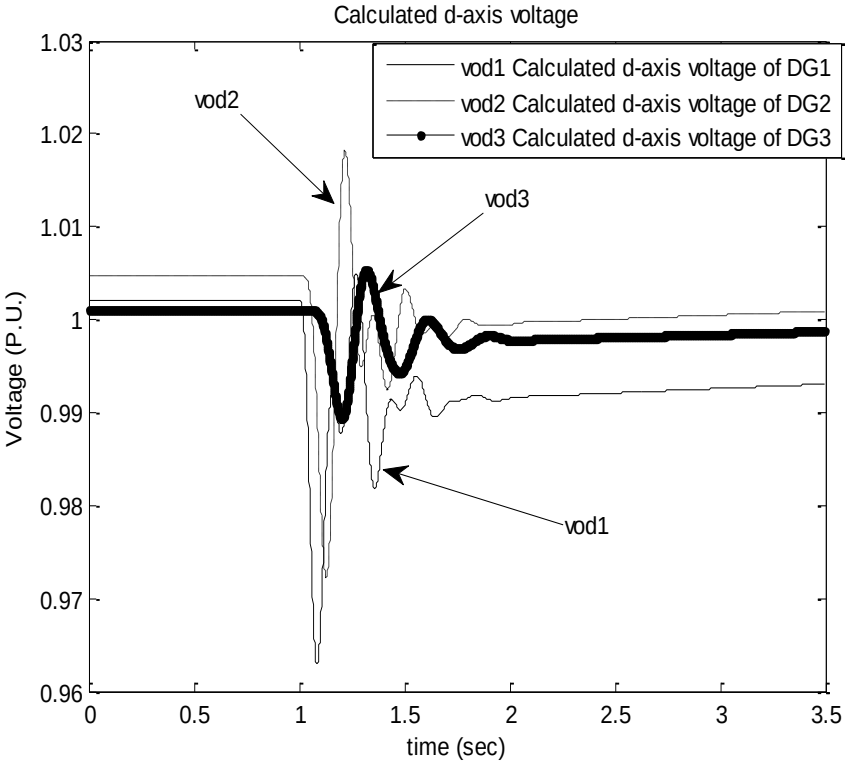

Fig. 6.27 D-axis output voltage response of the three DGs when step response occurs at *load1*

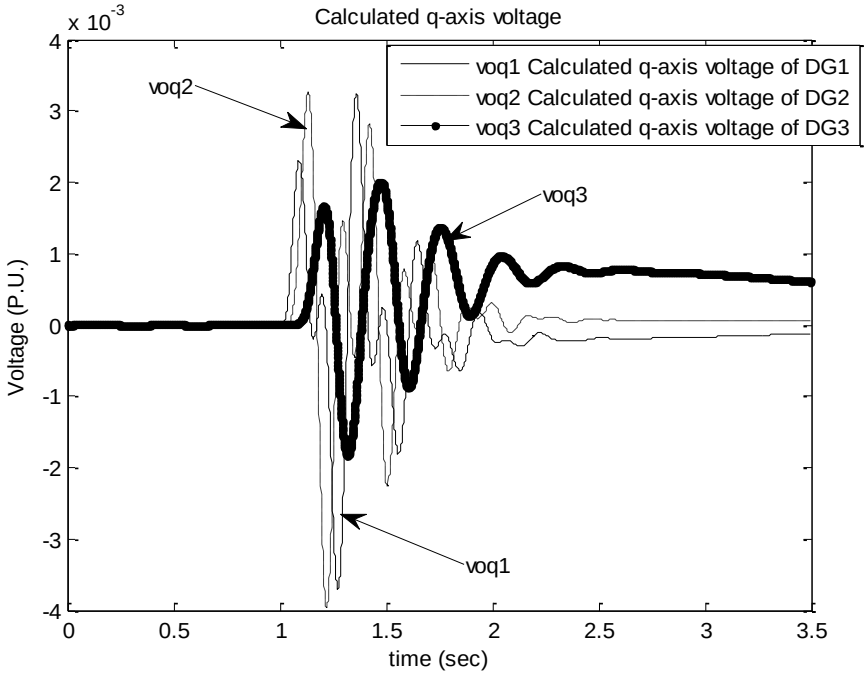

Fig. 6.28 Q-axis output voltage response of the three DGs when step response occurs at *load1*

Now, the cost function has been changed. Error in the calculated reactive power is used to be a cost function instead of error in calculated active power. Figs. 6.29 - 6.36 show the step response of the active, reactive, output and inductor currents and dq output voltages. The resuslts illustrate that changing the cost function doesn't affect the operation of the optimization technique and getting the system satbility.

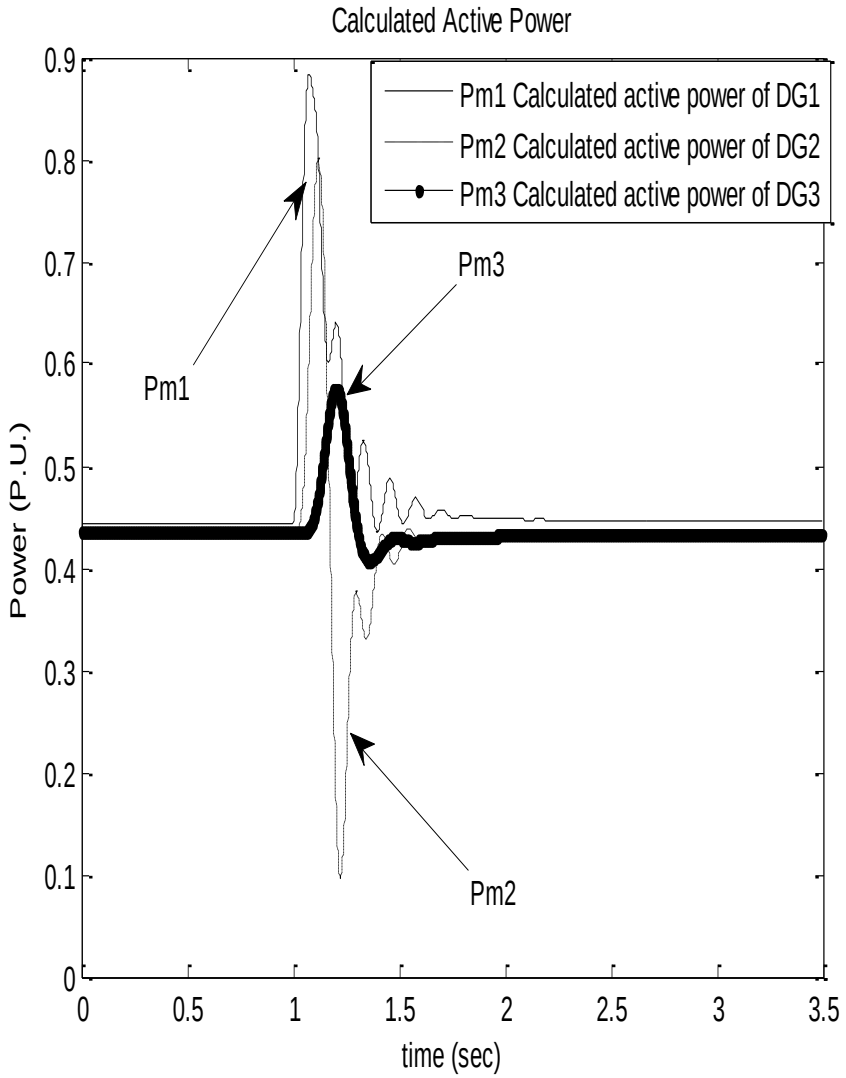

Fig. 6.29 Output active power response of the three DGs when the step response occurs at *load1*

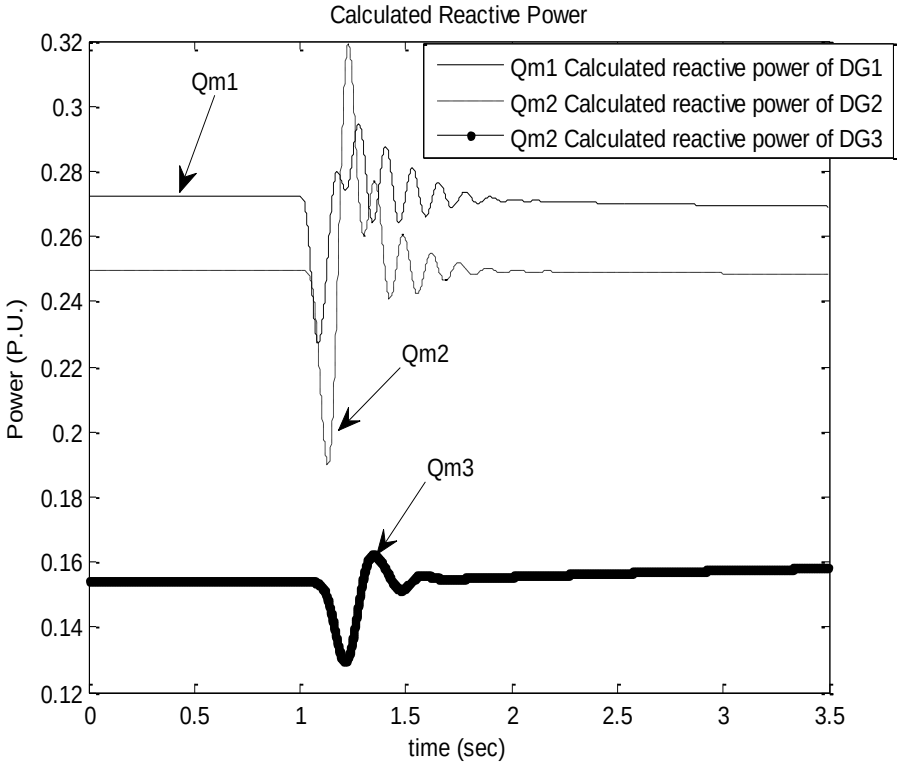

Fig. 6.30 Output reactive power response of the three DGs when the step response occurs at *load1*

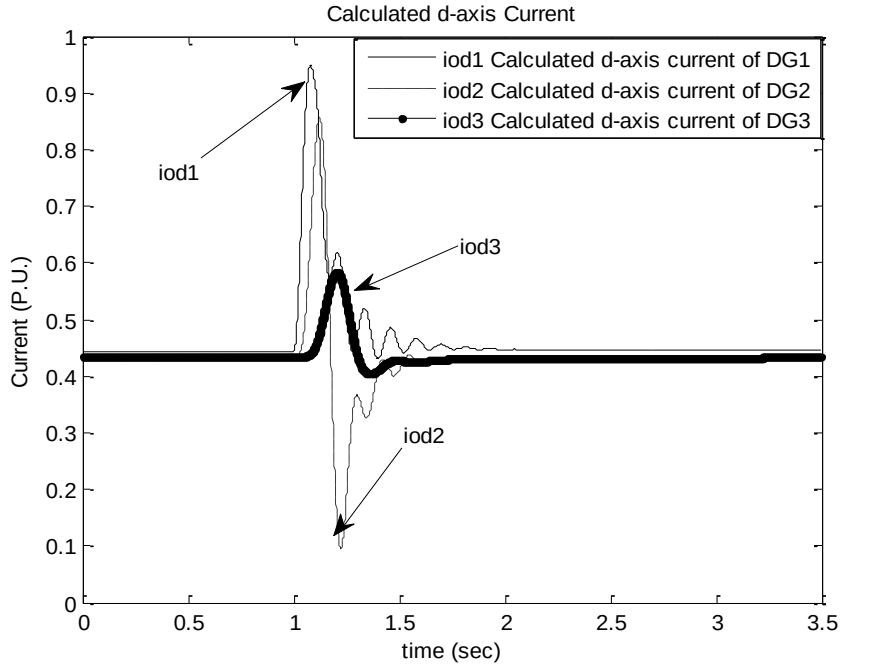

Fig. 6.31 D-axis output current response of the three DGs when the step response occurs at *load1*

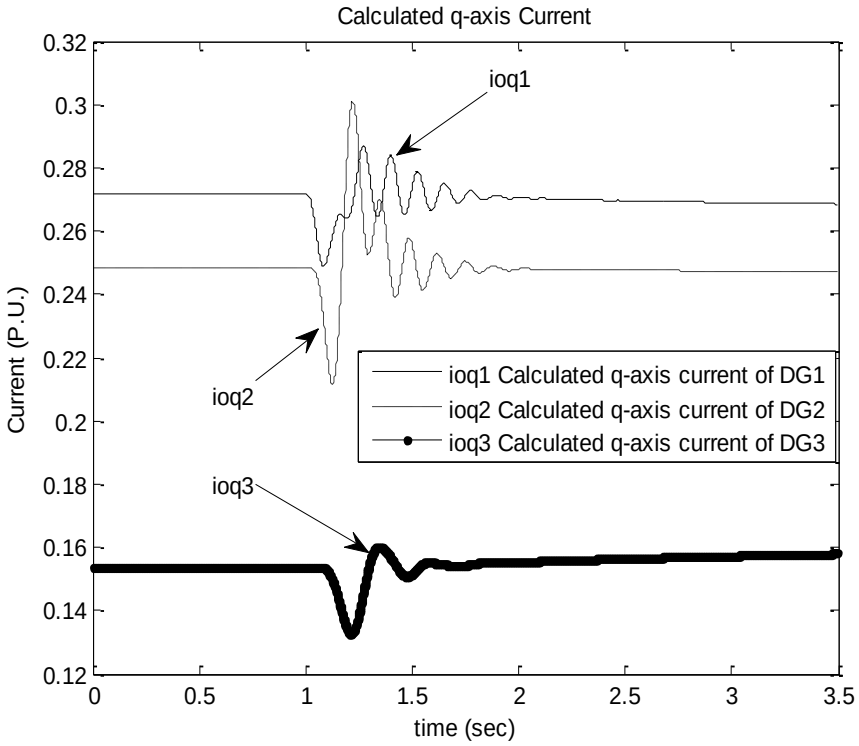

Fig. 6.32 Q-axis output current response of the three DGs when the step response occurs at *load1*

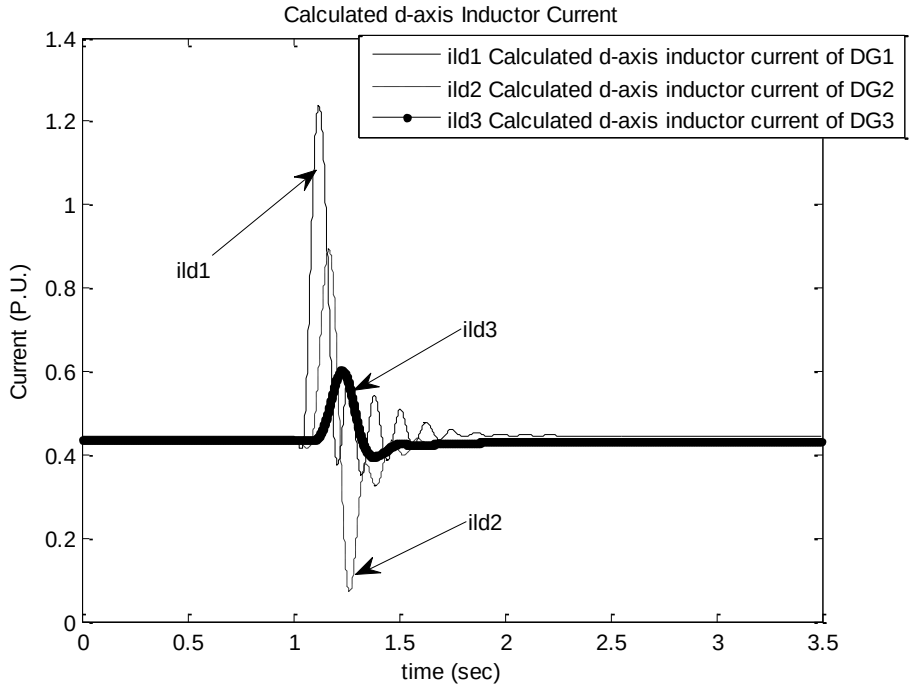

Fig. 6.33 D-axis inductor current response of the three DGs when the step response occurs at *load1*

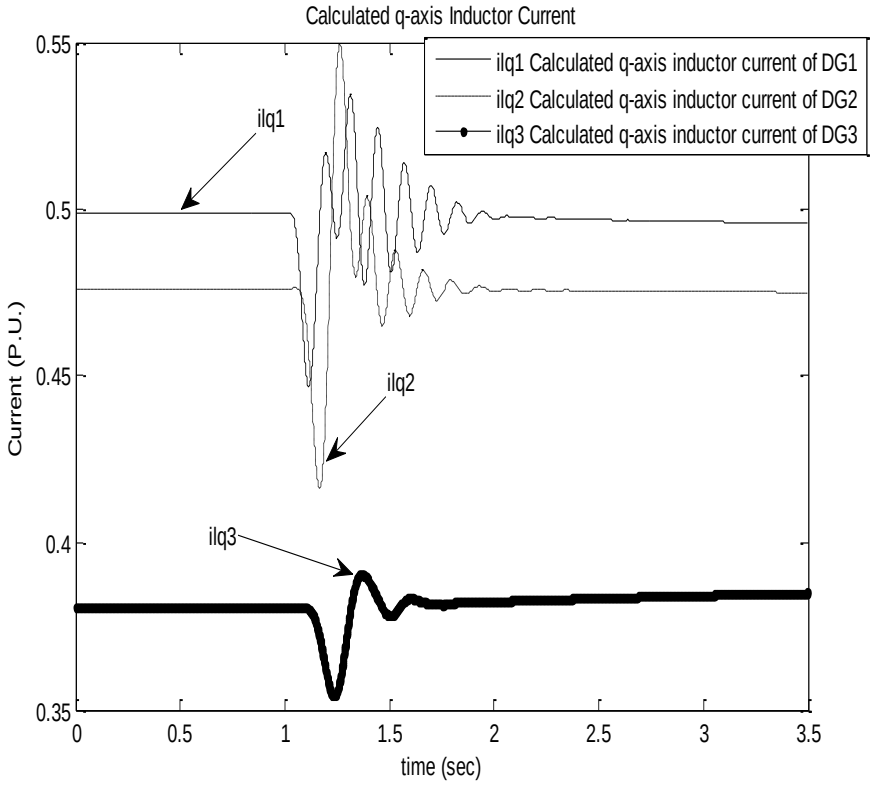

Fig. 6.34 Q-axis inductor current response of the three DGs when the step response occurs at *load1*

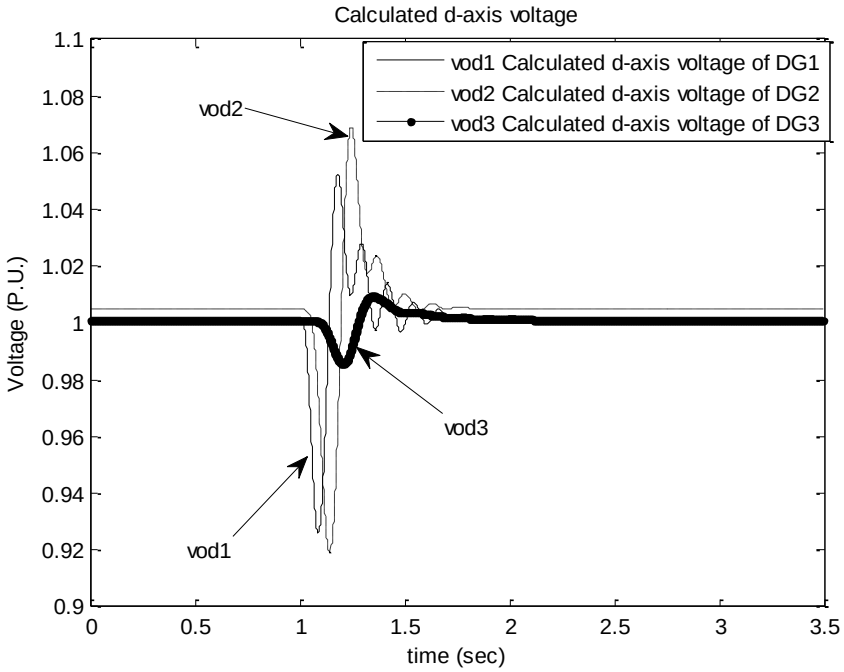

Fig. 6.35 D-axis output voltage response of the three DGs when the step response occurs at *load1*

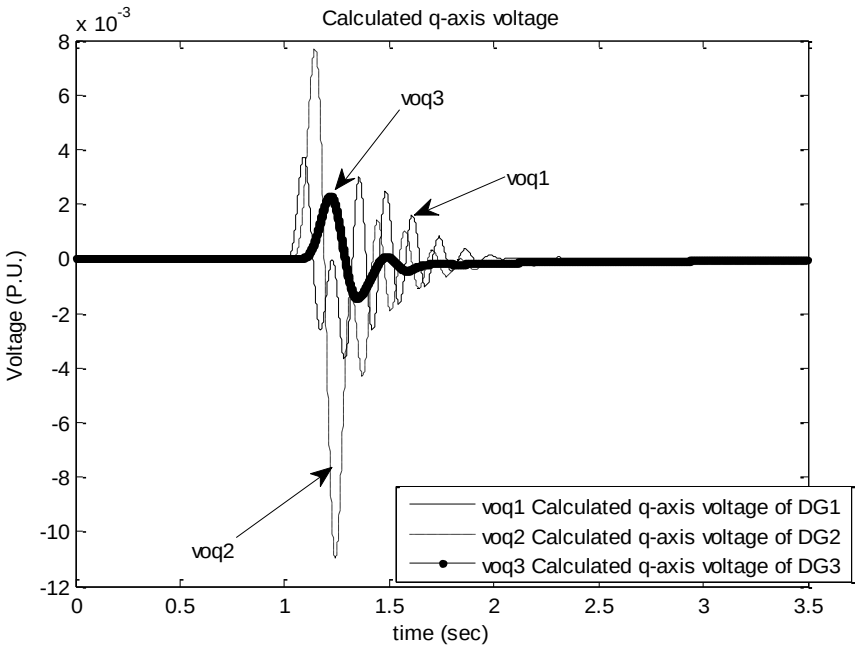

Fig. 6.36 Q-axis output voltage response of the three DGs when the step response occurs at *load1*

(b) Fault Response using the Optimal Parameters

A three phase fault has been carried out at the load1 of the system given in Fig. 6.1. The system stability has been assessed under the fault response when the optimal controller parameters have been used. Figs. 6.37 - 6.44 illustrate the system response under fault disturbance at load1. It can be seen that the system has satisfactory damping characteristics. Figs. 6.37 and 6.38 show the damped response of the active and reactive powers. Figs 6.39 - 6.42 investigate the dq output and inductor currents when the fault occurs at the load bus 1. The dq output voltage response is depicted in Figs. 6.43and 6.44. Comparing the results given in Figs. 6.37 - 6.44 with the results given in Figs. 6.13 - 6.20, the system become stable after getting step disturbance when the optimal parameters have been used while the system become unstable when the system parameters of Table 6.1 have been used.

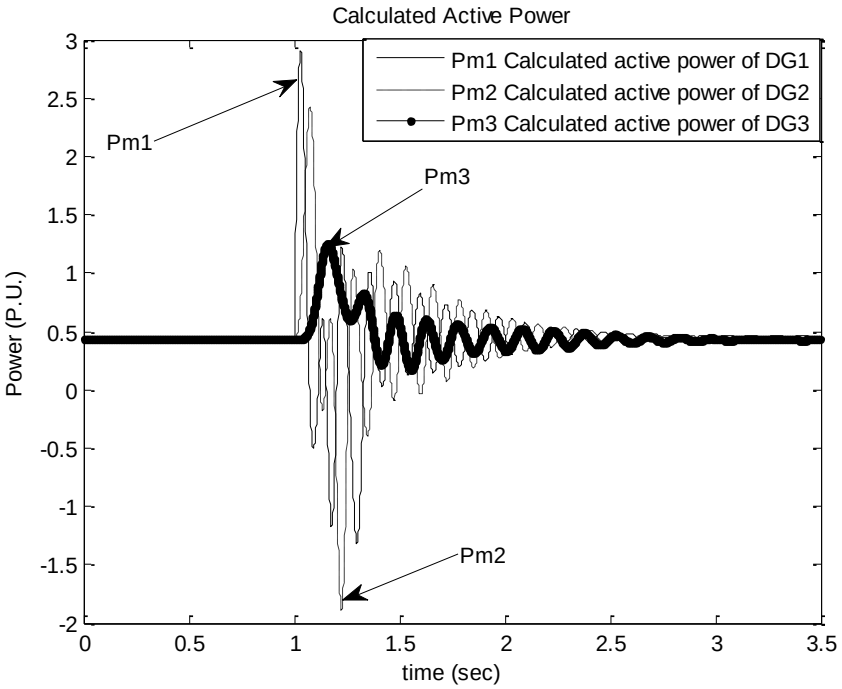

Fig. 6.37 Output active power response of the three DGs when the fault occurs at *load1*

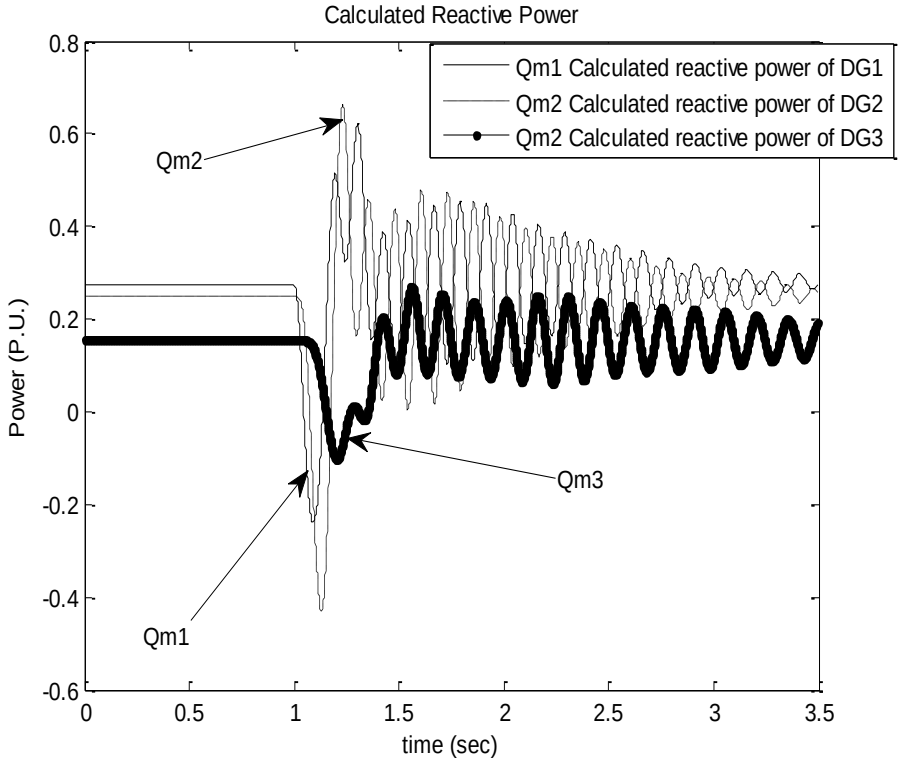

Fig. 6.38 Output reactive power response of the three DGs when the fault occurs at *load1*

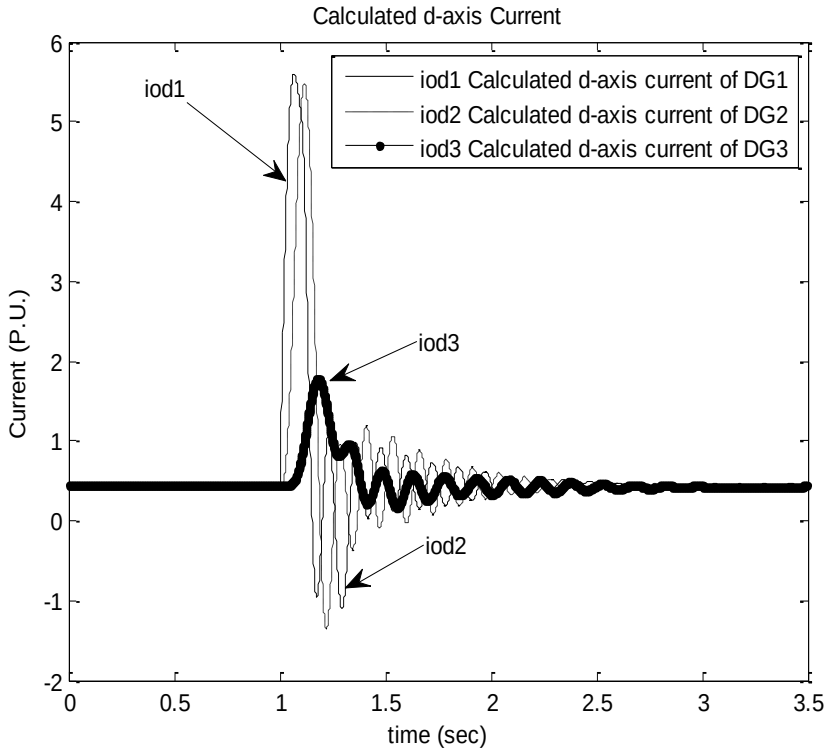

Fig. 6.39 D-axis output current response of the three DGs when the fault occurs at *load1*

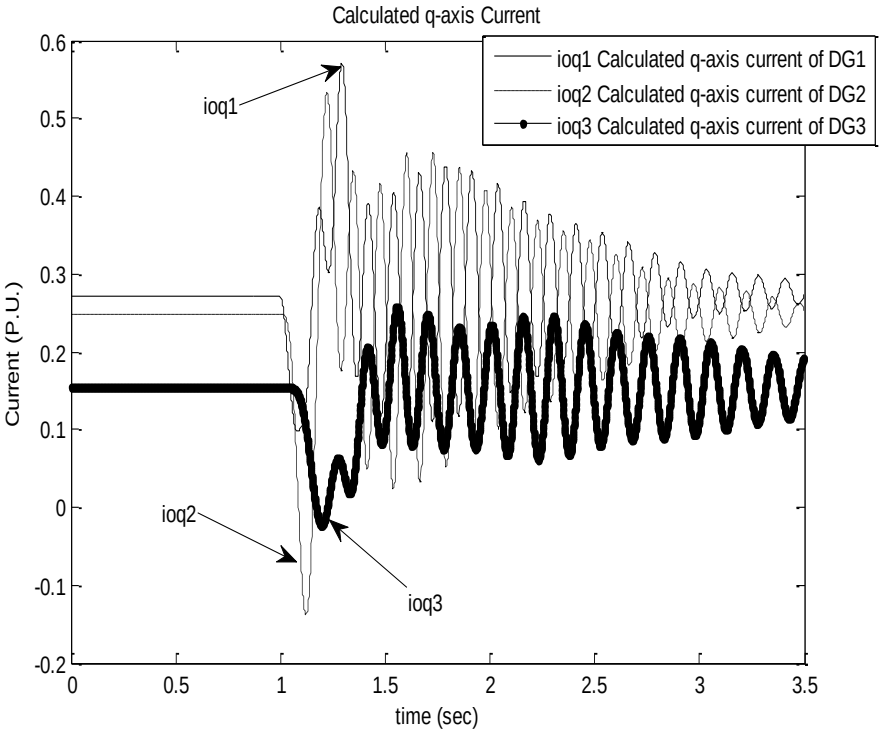

Fig. 6.40 Q-axis output current response of the three DGs when the fault occurs at *load1*

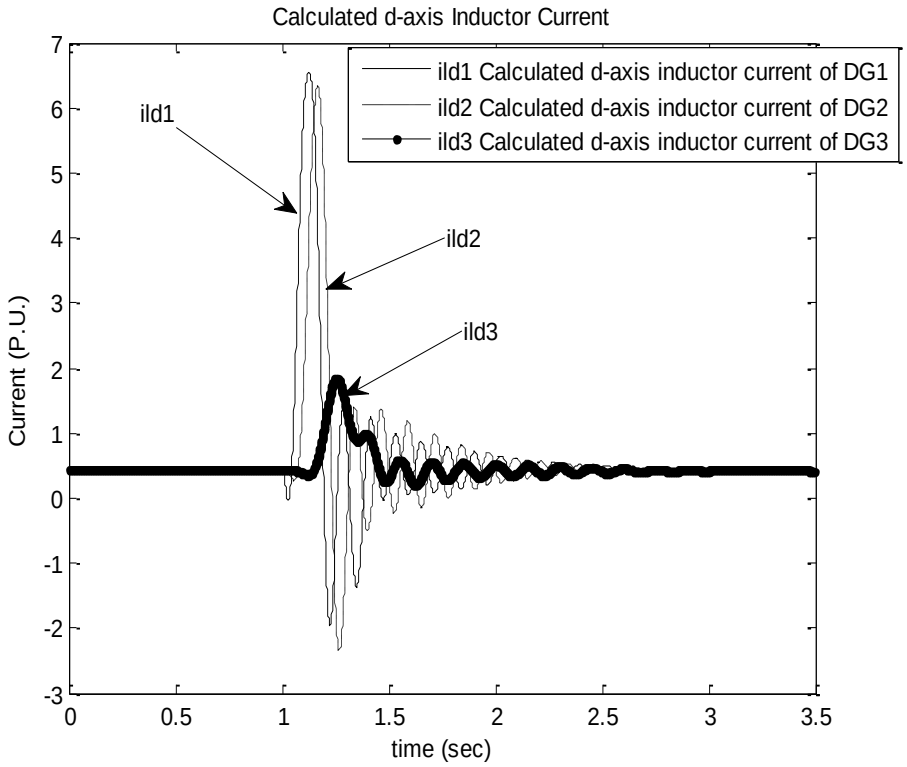

Fig. 6.41 D-axis inductor current response of the three DGs when the fault occurs at *load1*

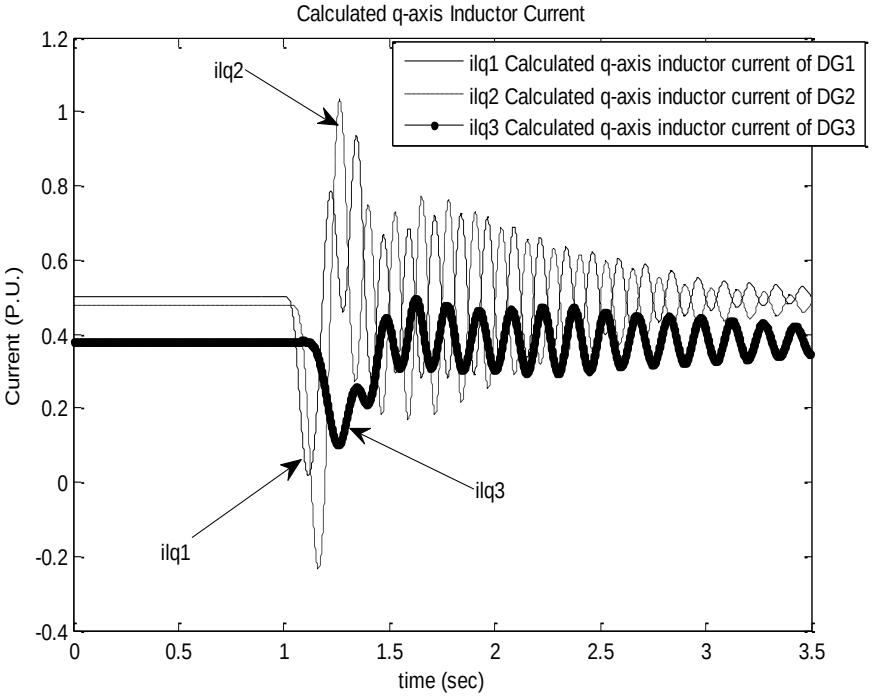

Fig. 6.42 Q-axis inductor current response of the three DGs when the fault occurs at

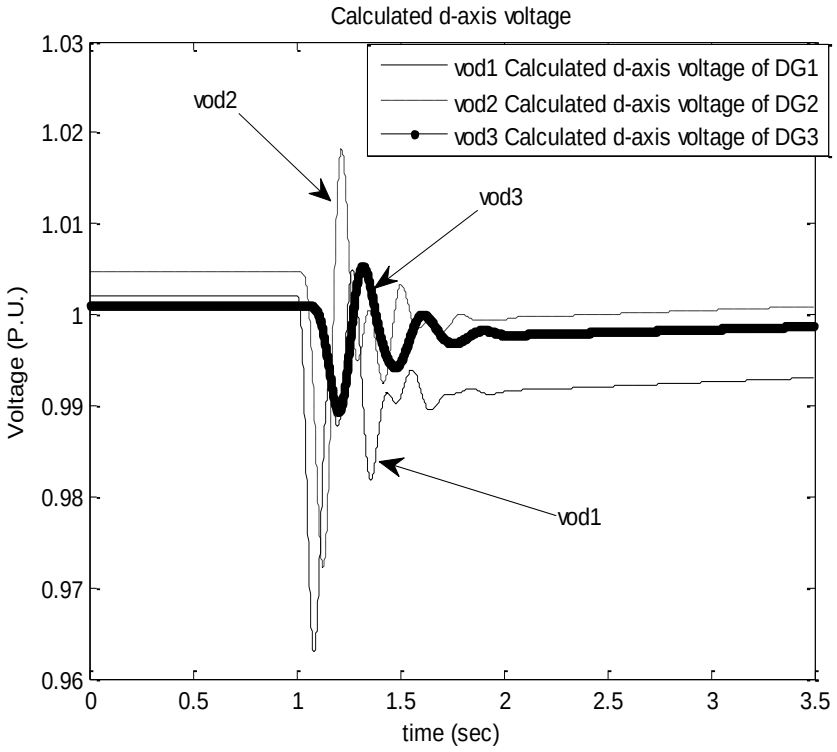

Fig. 6.43 D-axis output voltage response of the three DGs when the fault occurs at *load1*

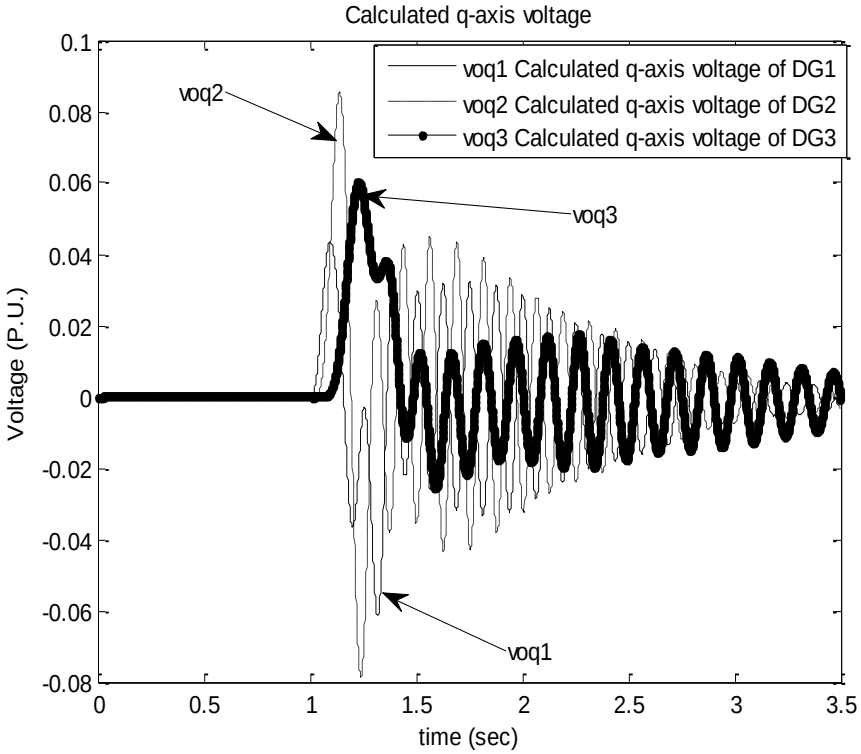

Fig. 6.44 Q-axis output voltage response of the three DGs when the fault occurs at *load1*
load1

Instead of using the objective function given in (5.2), the difference between calculated and reference reactive powers is considered as a cost function to assess the system stability. Figs. 6.45-6.52 illustrate that the system is stable after getting fault. After getting fault disturbance at load1, using the optimal controller parameters and optimal power sharing parameters, the system is going to stable mode. The damped response of the active power, the reactive power d-axis and q-axis output voltage of each inverter are given in Figs. 6.45, 6.46 6.47 and 6.48. The system stability assessment can be achieved by selecting different cost function. It can be seen from the previous results that the system has satisfactory damping characteristics. The responses show that the damping characteristics are greatly enhanced and the system performance in terms of overshoots and settling time is improved significantly.

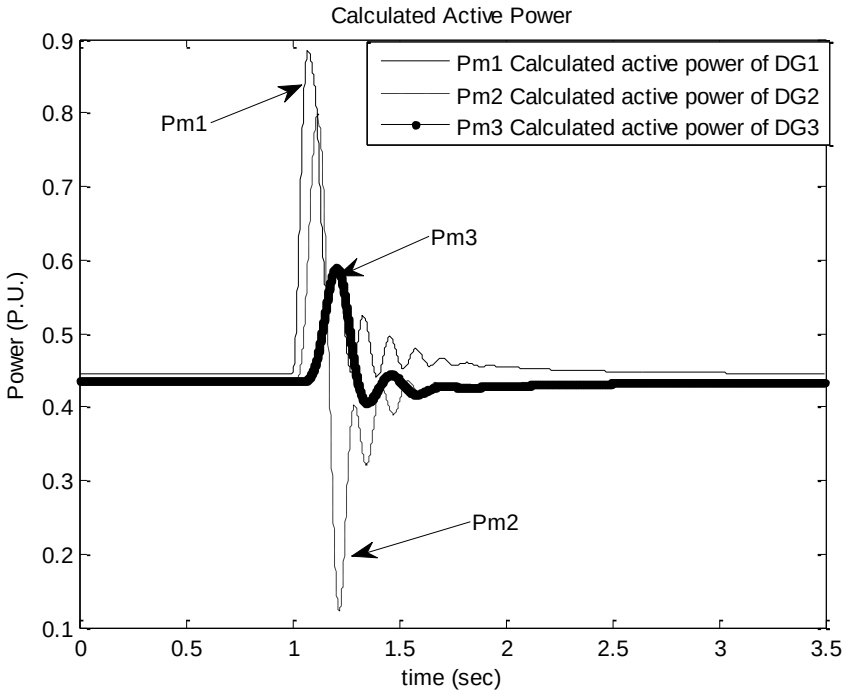

Fig. 6.45 Output active power response of the three DGs when the fault occurs at *load1*

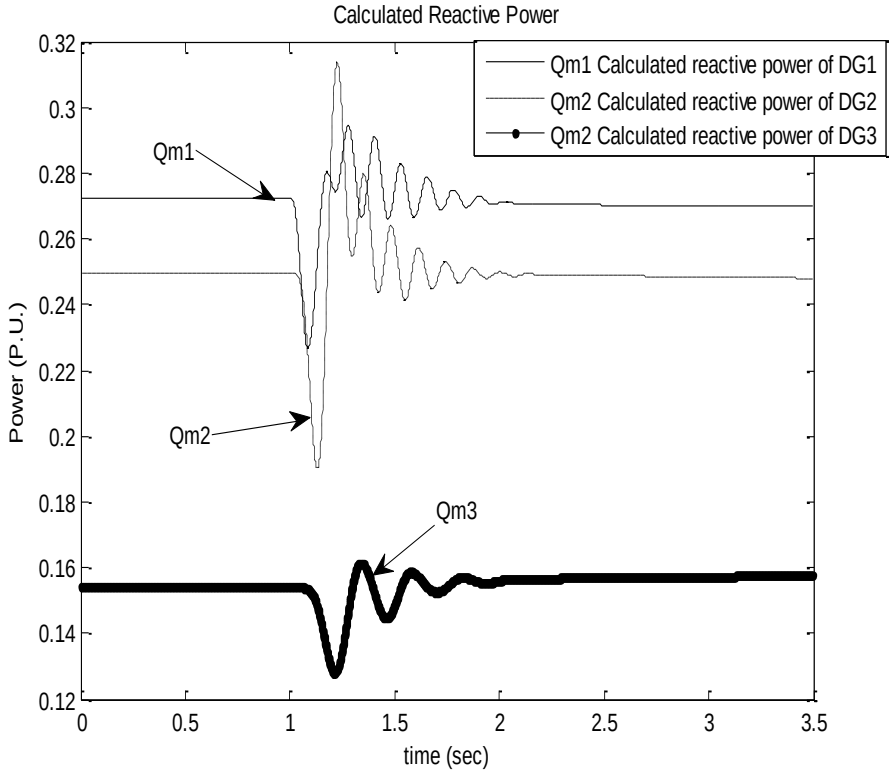

Fig. 6.46 Output reactive power response of the three DGs when the fault occurs at *load1*

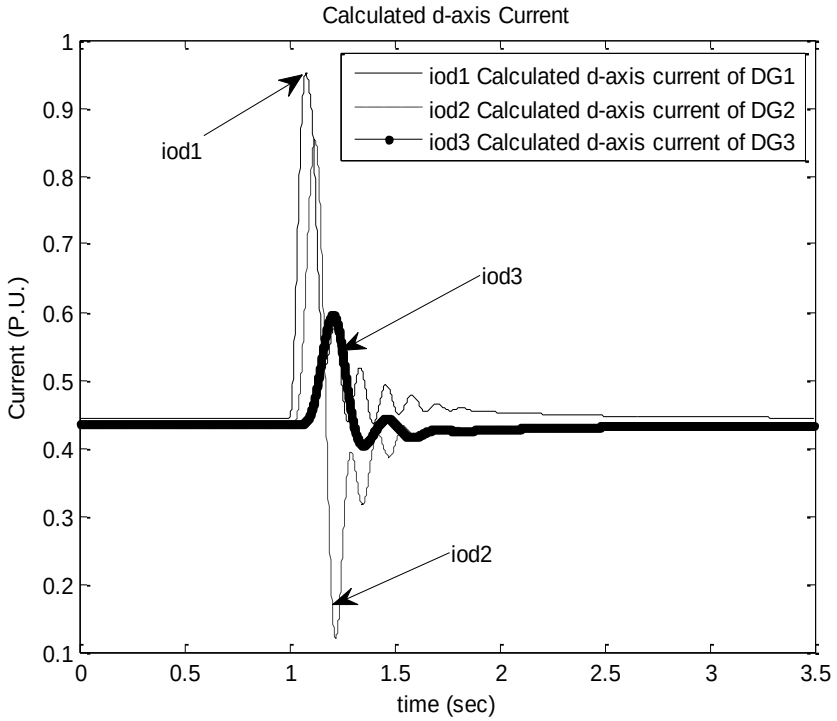

Fig. 6.47 D-axis output current response of the three DGs when the fault occurs at *load1*

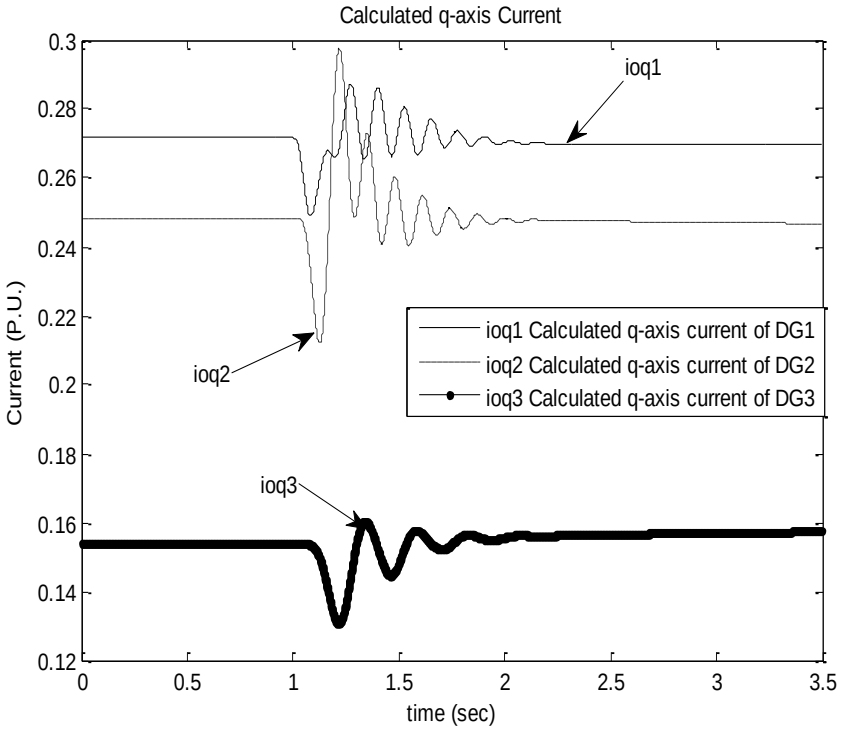

Fig. 6.48 Q-axis output current response of the three DGs when the fault occurs at *load1*

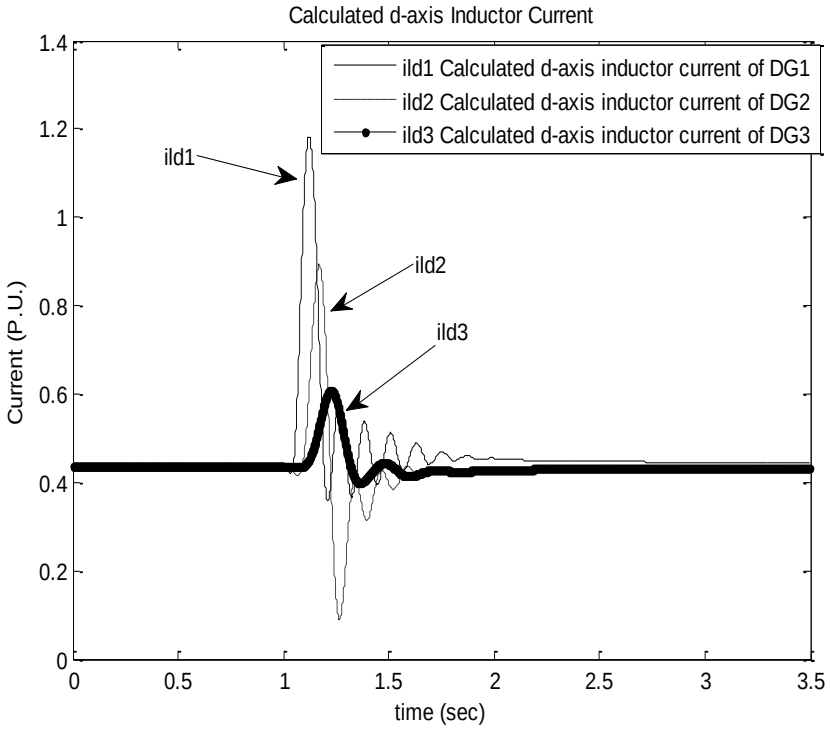

Fig. 6.49 D-axis inductor current response of the three DGs when the fault occurs at *load1*

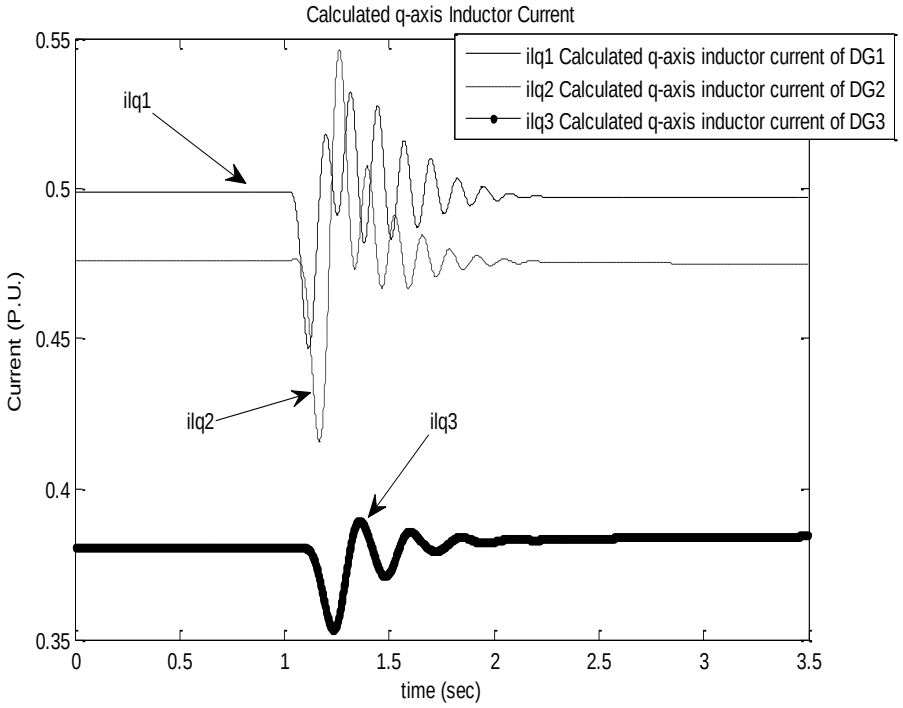

Fig. 6.50 Q-axis inductor current response of the three DGs when the fault occurs at *load1*

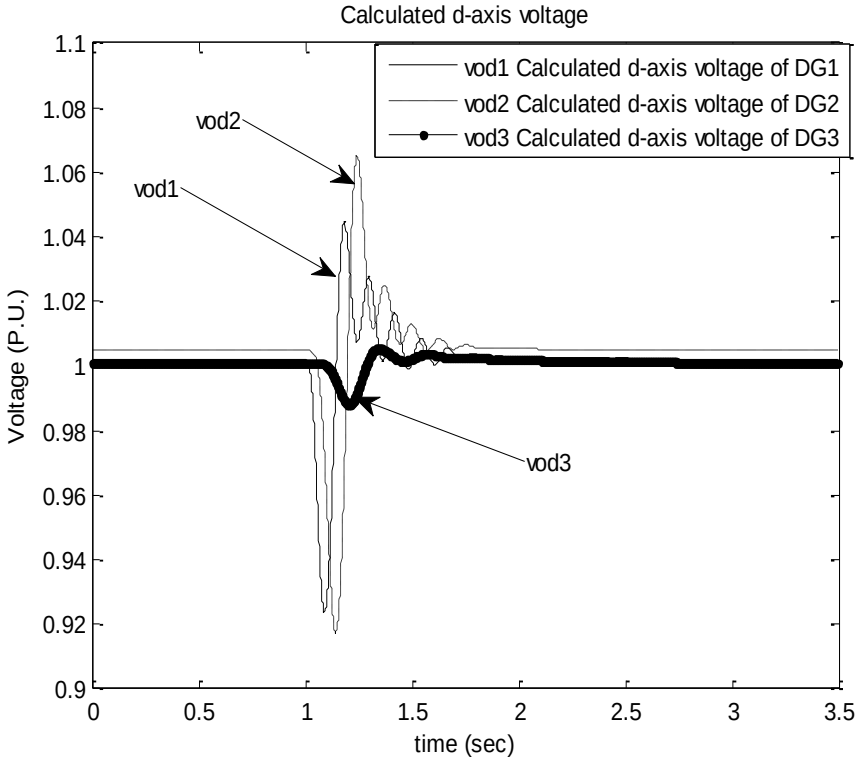

Fig. 6.51 D-axis output voltage response of the three DGs when the fault occurs at *load1*

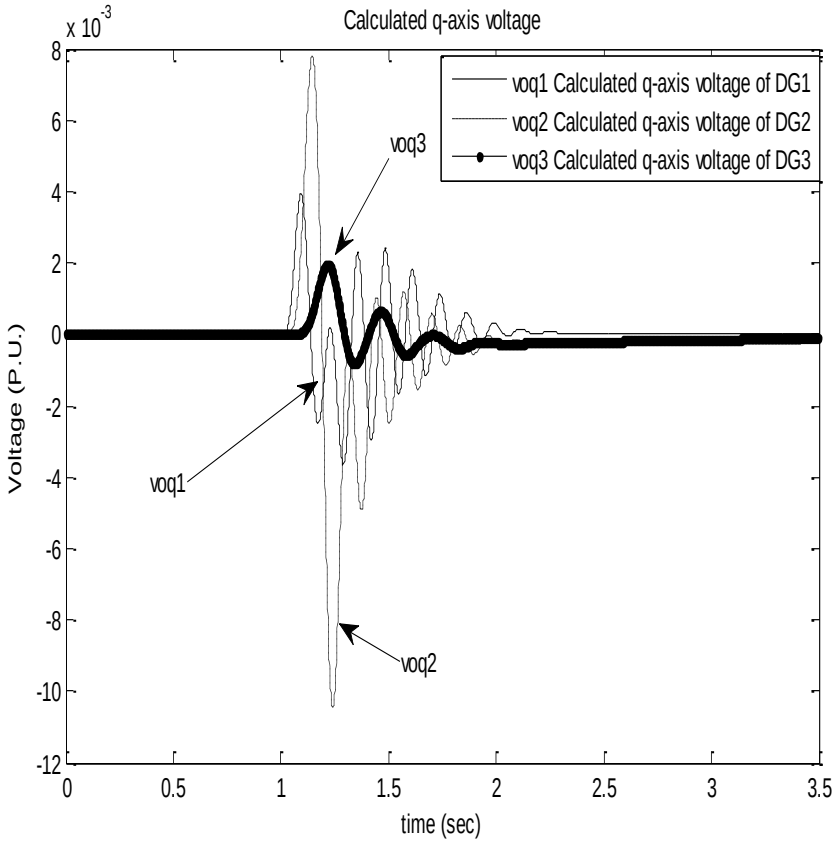

Fig. 6.52 Q-axis output voltage response of the three DGs when the fault occurs at *load1*

(c) Effectiveness and Robustness of the Proposed Controller

Several runs and different disturbances have been done to demonstrate and assess the effectiveness and the robustness of the proposed controller. First, several runs have been carried out with different initial populations. The convergence of objective function of the autonomous mode is shown in Fig. 6.53. It can be seen that the objective function reaches the same value in all runs. This confirms the robustness of the proposed design approach with respect to its initial guess and its capability to avoid trapping in local minima.

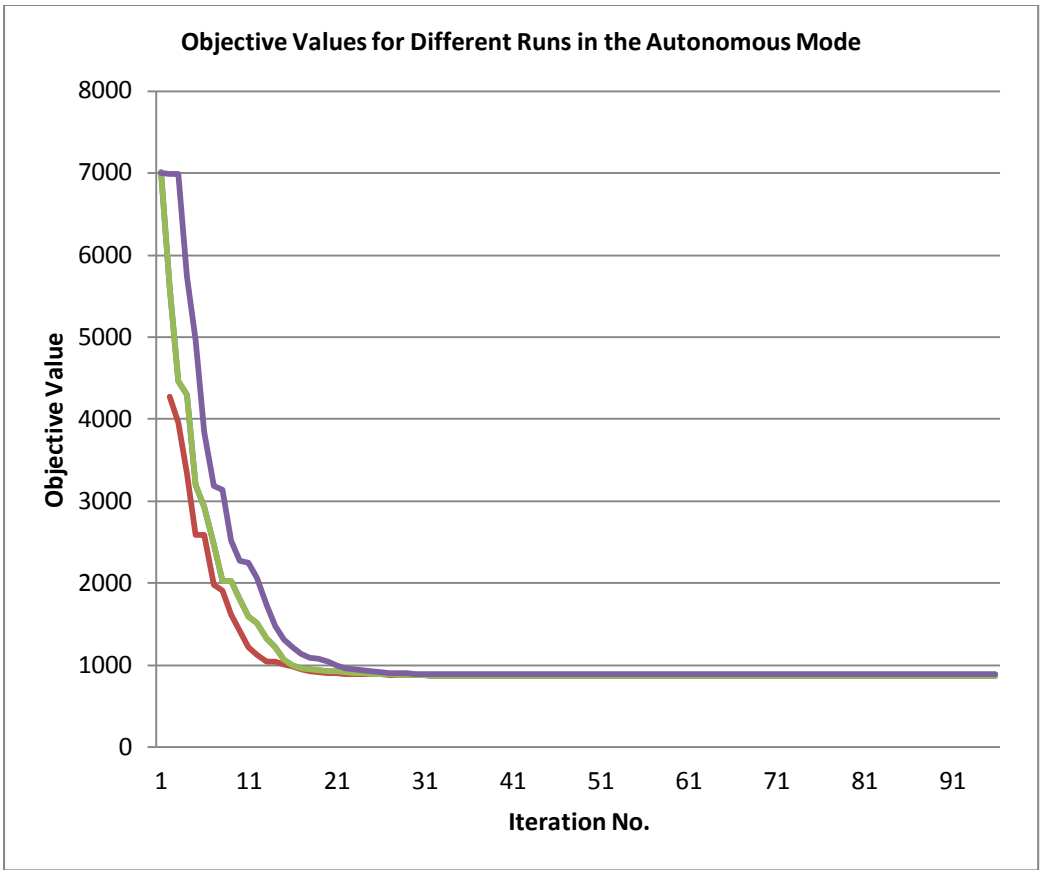

Fig. 6. 53 Objective function convergence in the autonomous mode

Second, the three phase fault location has been changed from load1 to load2. The optimized parameters obtained when the fault occurred at load1 are used when the fault location has been changed to investigate the robustness of the system for this fault. Figs. 6.54 - 6.61 illustrate that the system is robustness after changing the fault location using the optimal parameters obtained before. It can be seen from the results that the system has satisfactory damping characteristics. The responses show that the damping characteristics are greatly enhanced and the system performance in terms of overshoots and settling time is improved significantly.

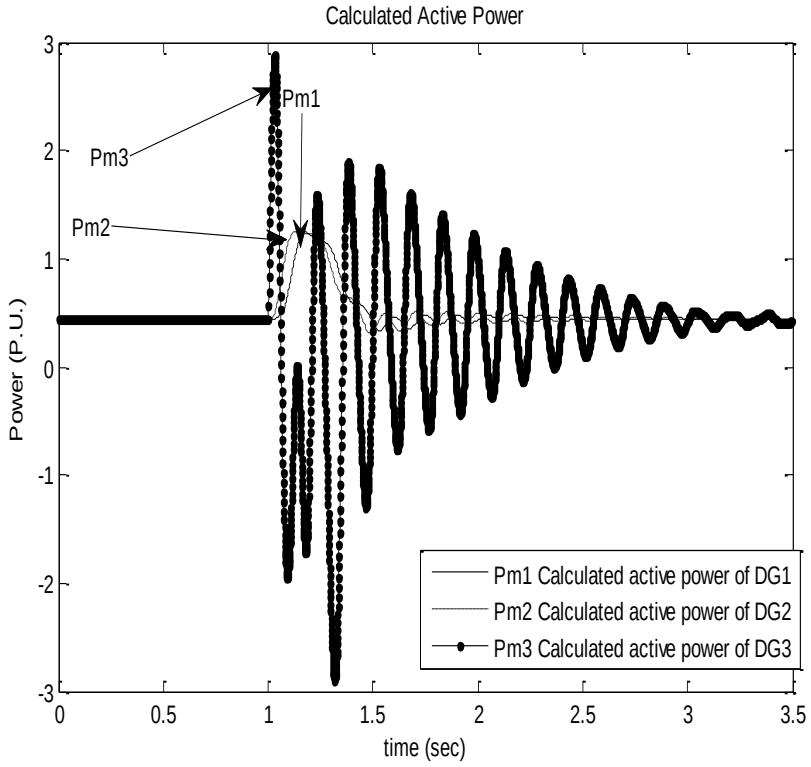

Fig. 6.54 Output active power response of the three DGs when the fault occurs at *load2*

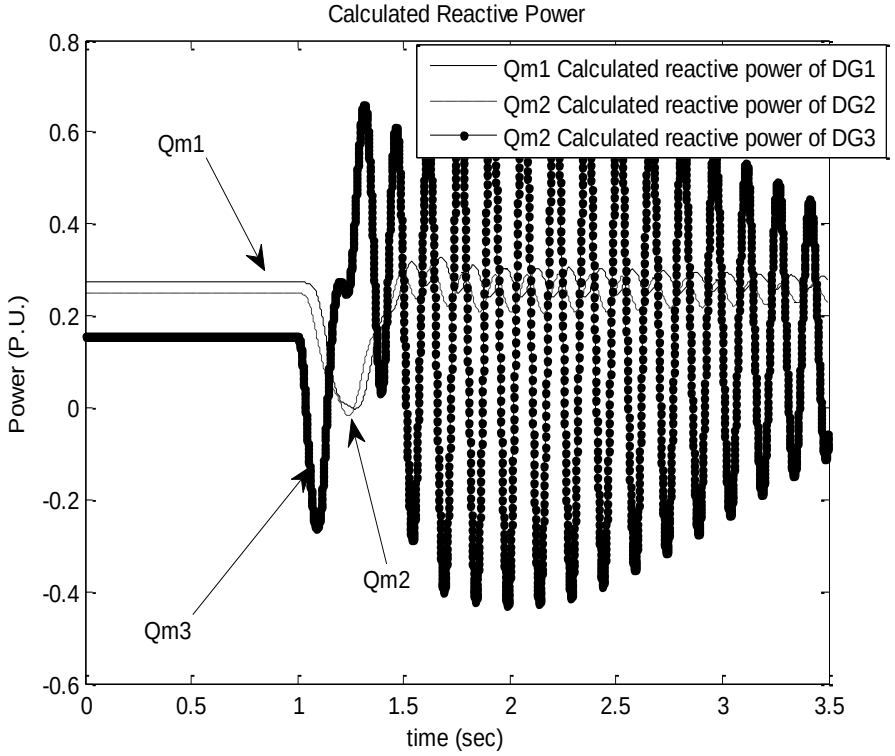

Fig. 6.55 Output reactive power response of the three DGs when the fault occurs at *load2*

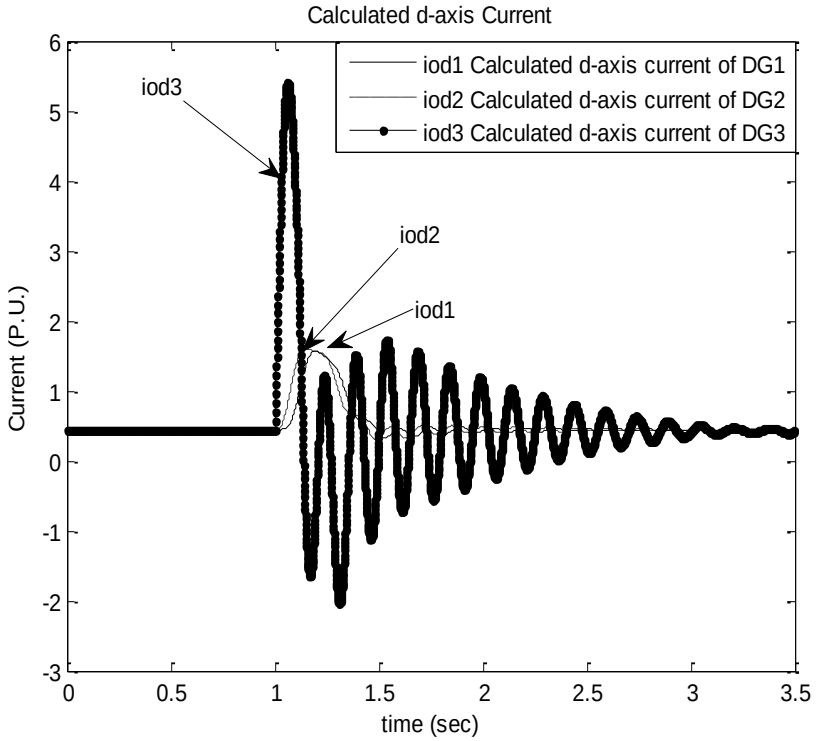

Fig. 6.56 D-axis output current response of the three DGs when the fault occurs at *load2*

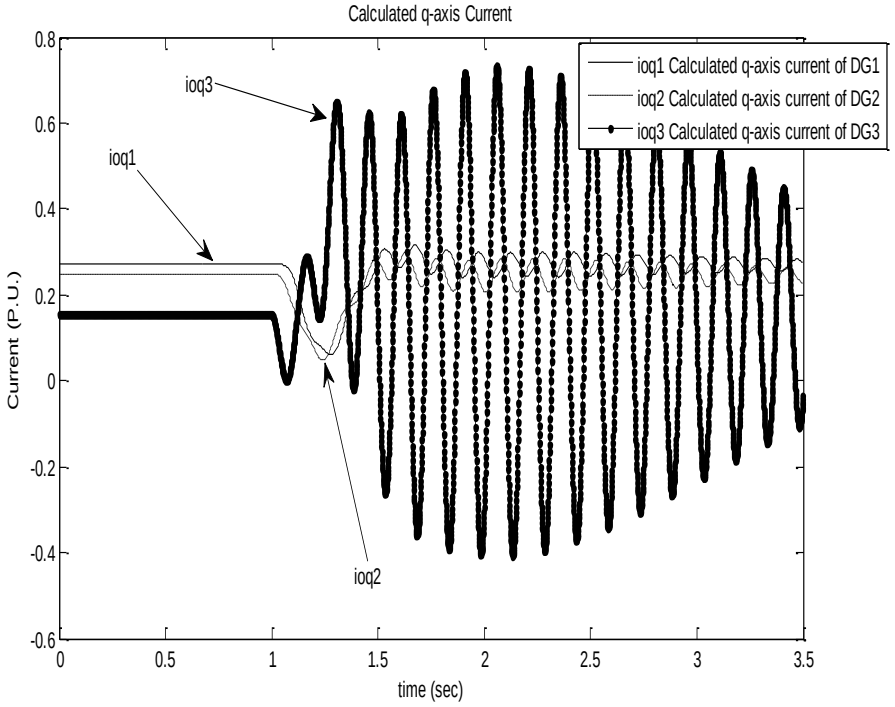

Fig. 6.57 Q-axis output current response of the three DGs when the fault occurs at *load2*

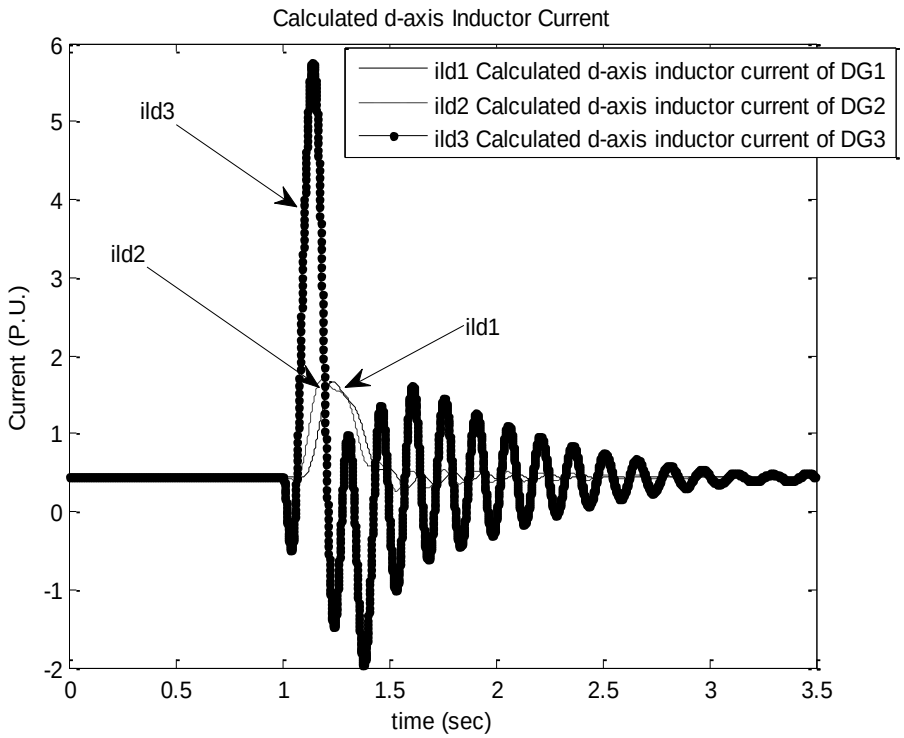

Fig. 6.58 D-axis inductor current response of the three DGs when the fault occurs at *load2*

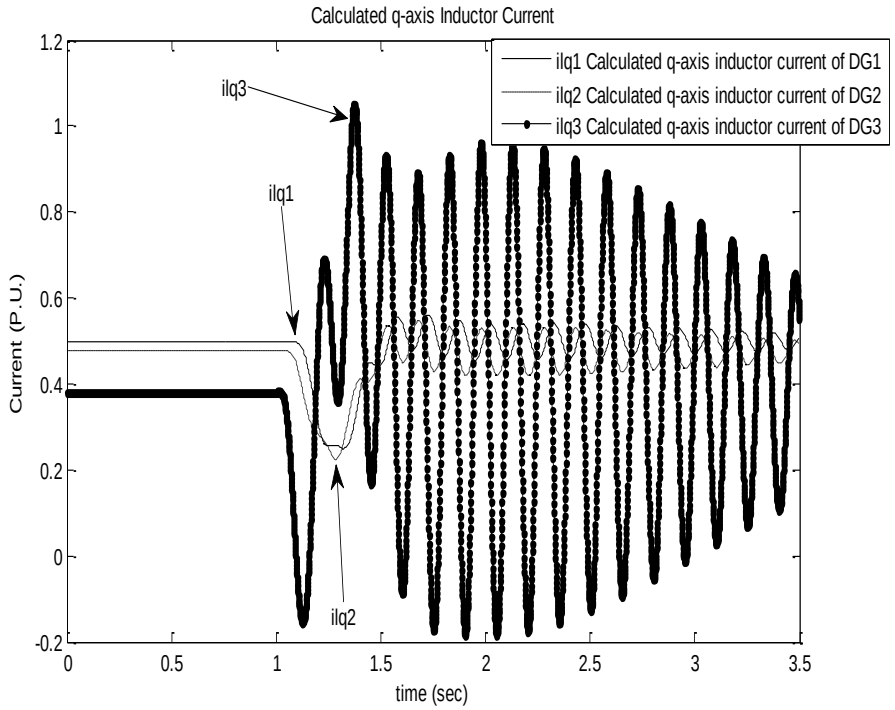

Fig. 6.59 Q-axis inductor current response of the three DGs when the fault occurs at *load2*

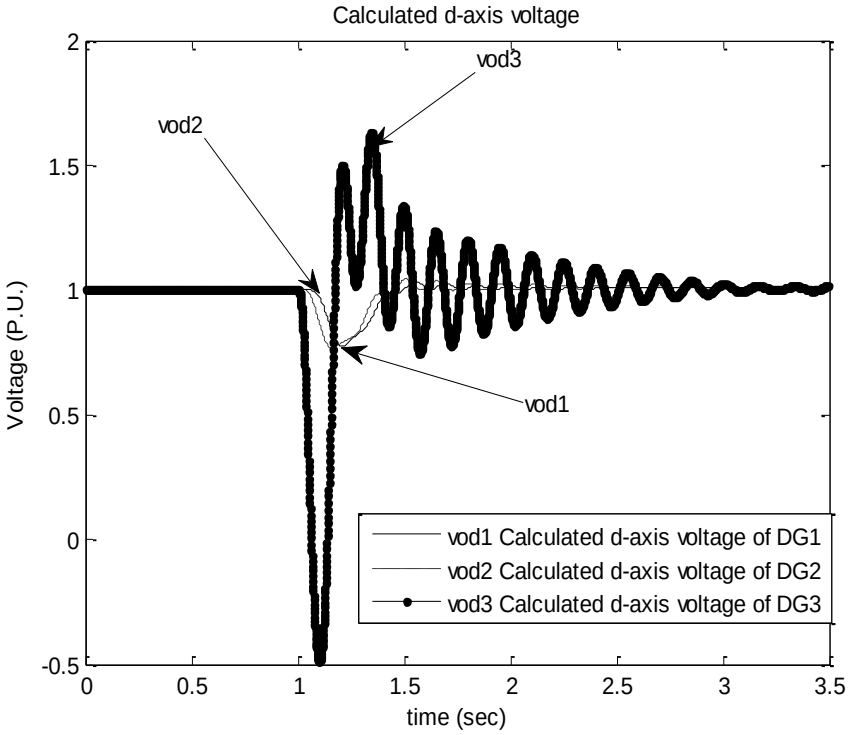

Fig. 6.60 D-axis output voltage response of the three DGs when the fault occurs at *load2*

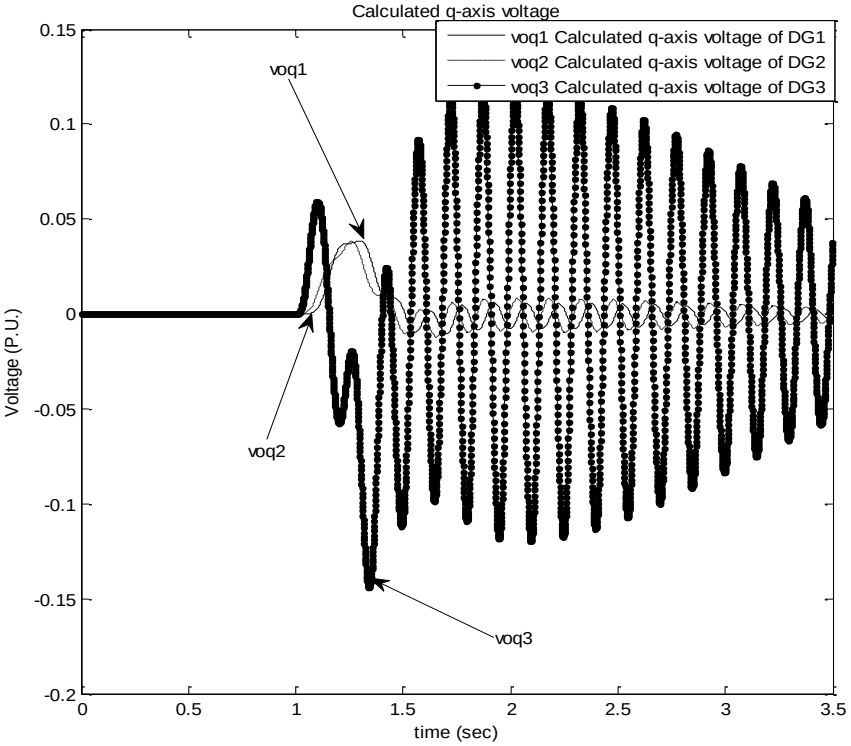

Fig. 6.61 Q-axis output voltage response of the three DGs when the fault occurs at *load2*

Finally, the optimal controller capability has been checked out when the first DG has been lost. The optimal parameters obtained in both step and fault cases have been used to investigate the controller capability. Figs. 6.62 -6.69 show the system response when the first DG has been lost using the optimal parameters obtained in the step case while Figs. 6.70 -6.77 show that the system response when the first DG has been lost using the optimal parameters obtained in the fault case. The optimized values obtained are used to assess the system stability. The results show the system is going to stable mode after getting loss DG disturbance.

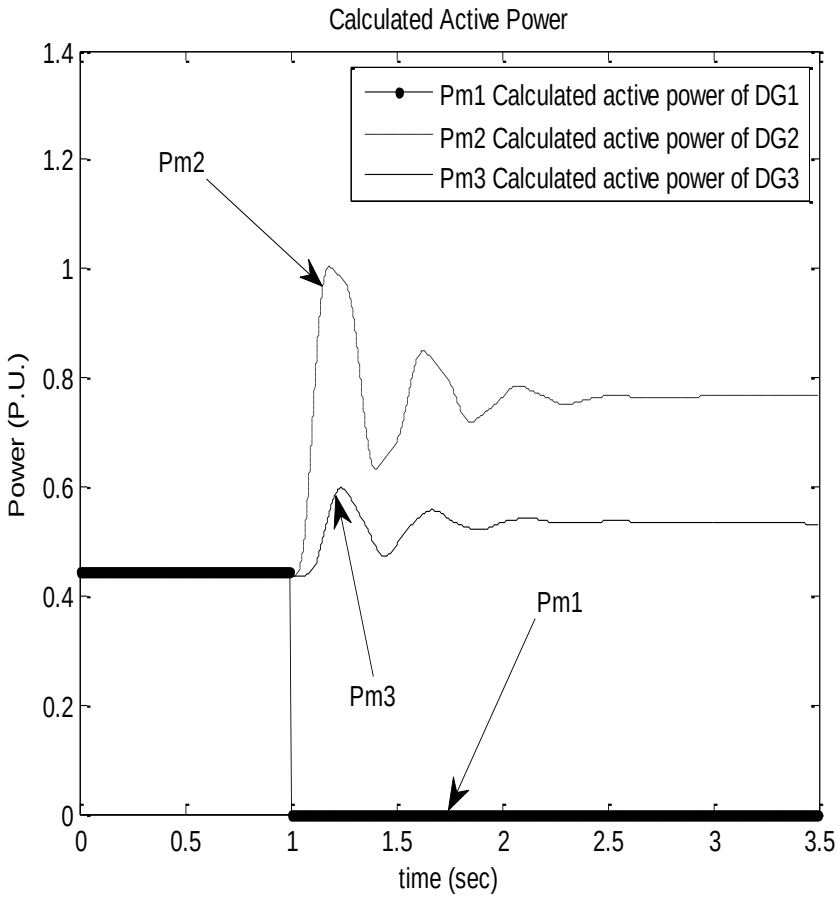

Fig. 6.62 Output active power response of the three DGs when the DG1 has been lost

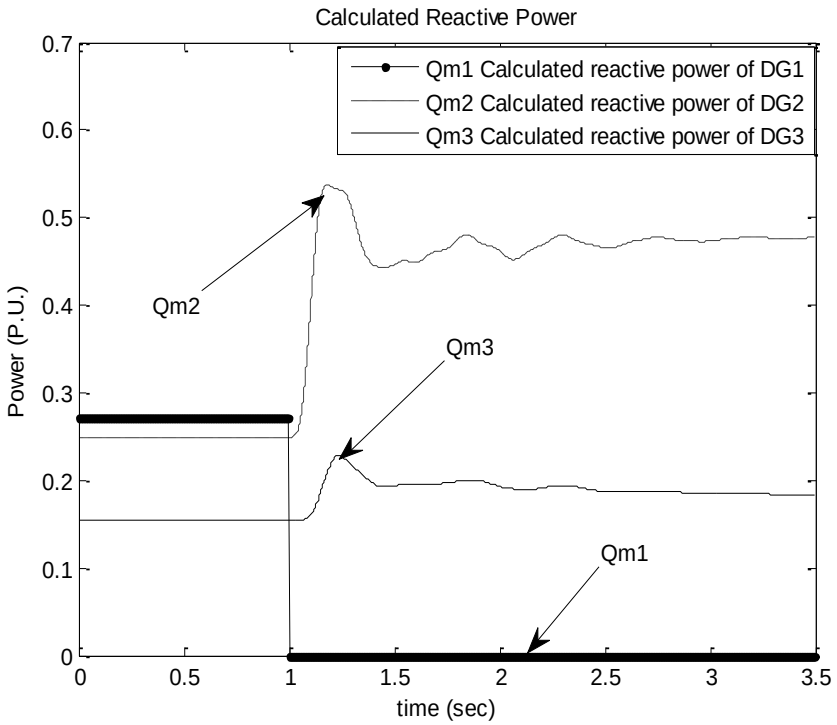

Fig. 6.63 Output reactive power response of the three DGs when the DG1 has been lost

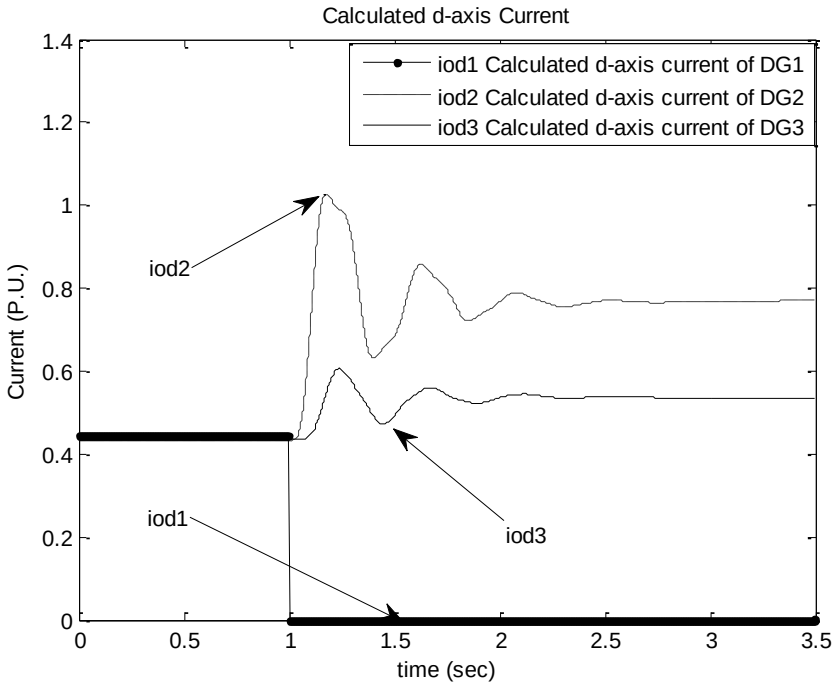

Fig. 6.64 D-axis output current response of the three DGs when the DG1 has been lost

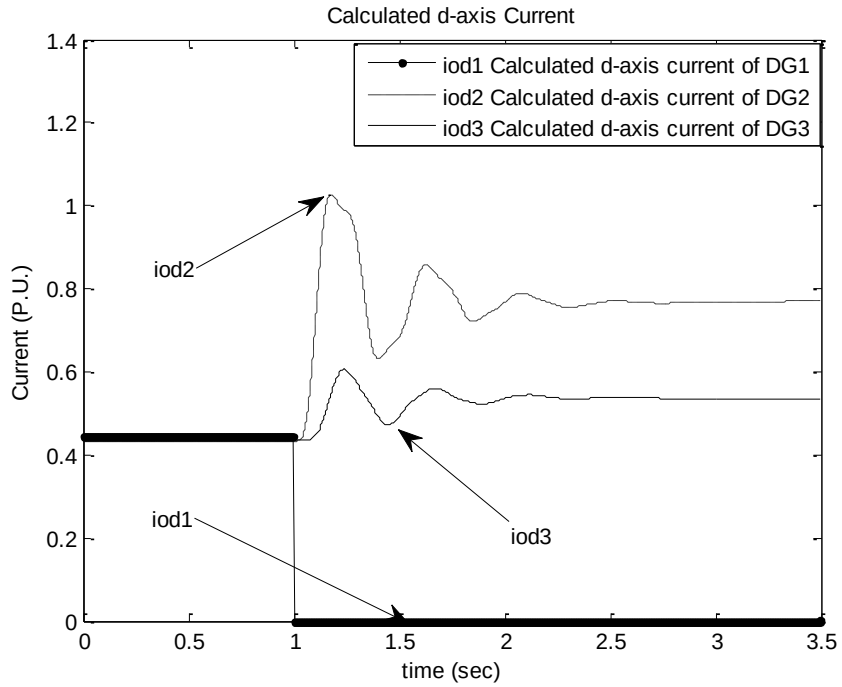

Fig. 6.65 Q-axis output current response of the three DGs when the DG1 has been lost

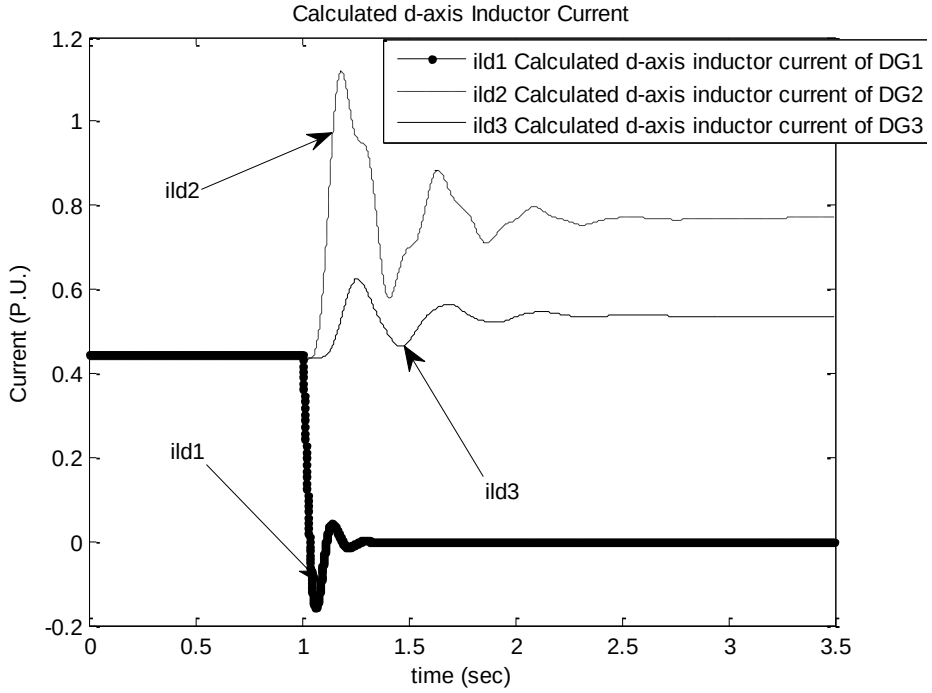

Fig. 6.66 D-axis inductor current response of the three DGs when the DG1 has been lost

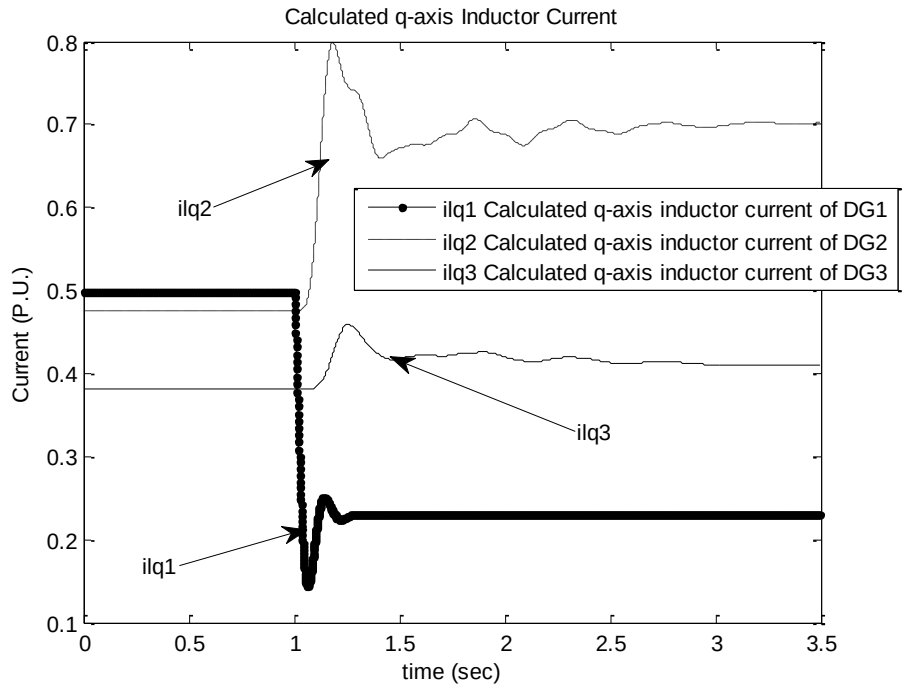

Fig. 6.67 Q-axis inductor current response of the three DGs when the DG1 has been lost

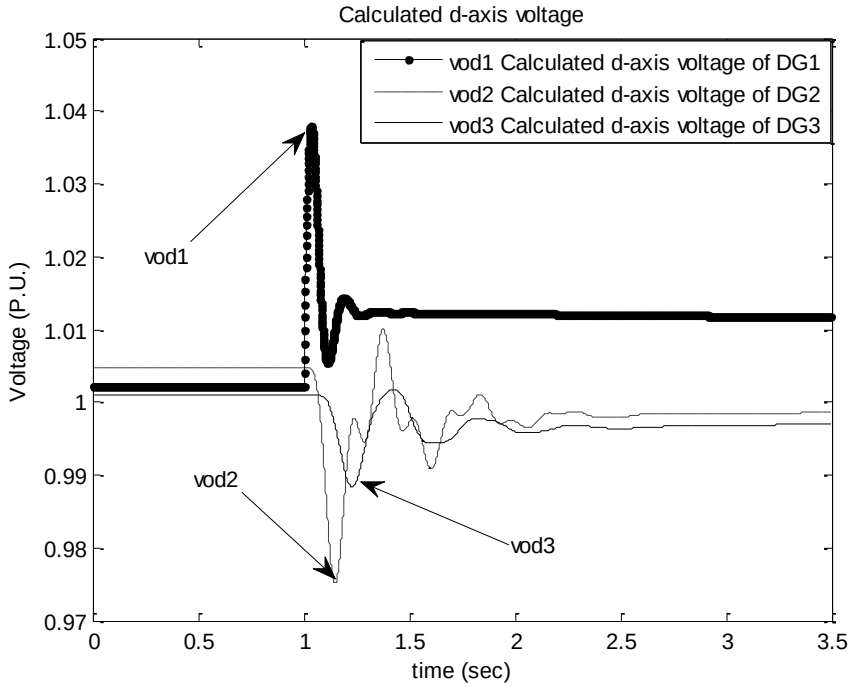

Fig. 6.68 D-axis output voltage response of the three DGs when the DG1 has been lost

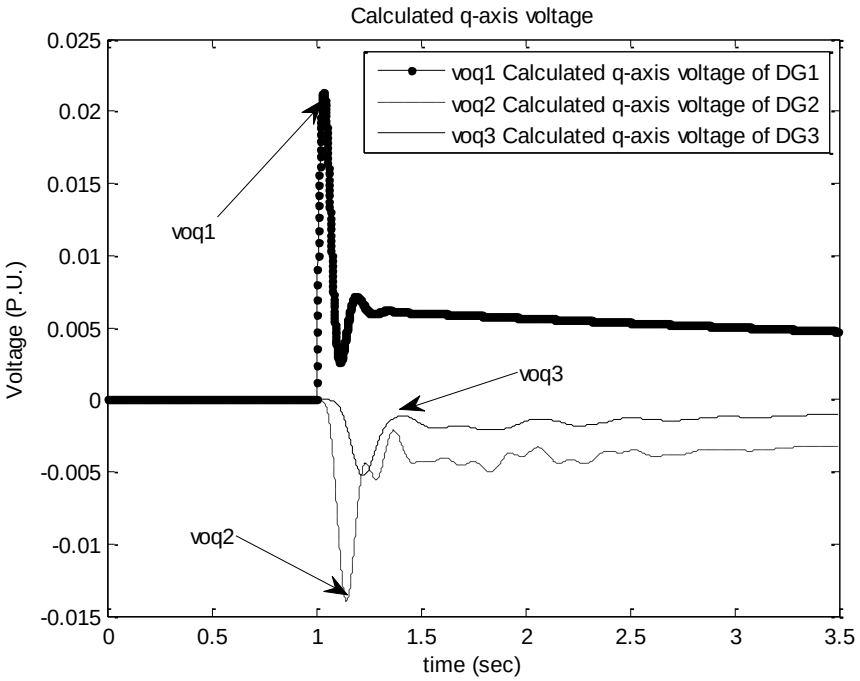

Fig. 6.69 Q-axis output voltage response of the three DGs when the DG1 has been lost

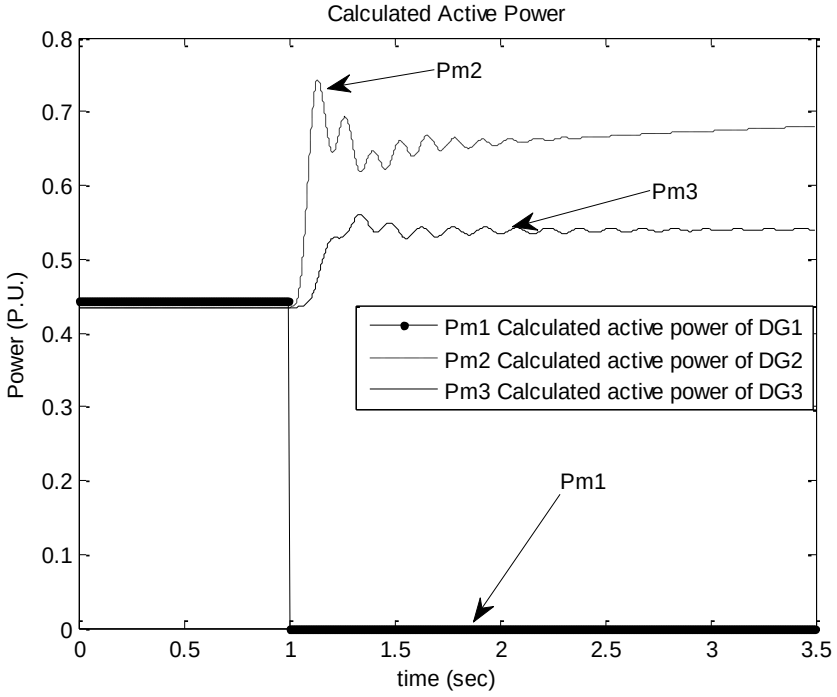

Fig. 6.70 Output active power response of the three DGs when the DG1 has been lost

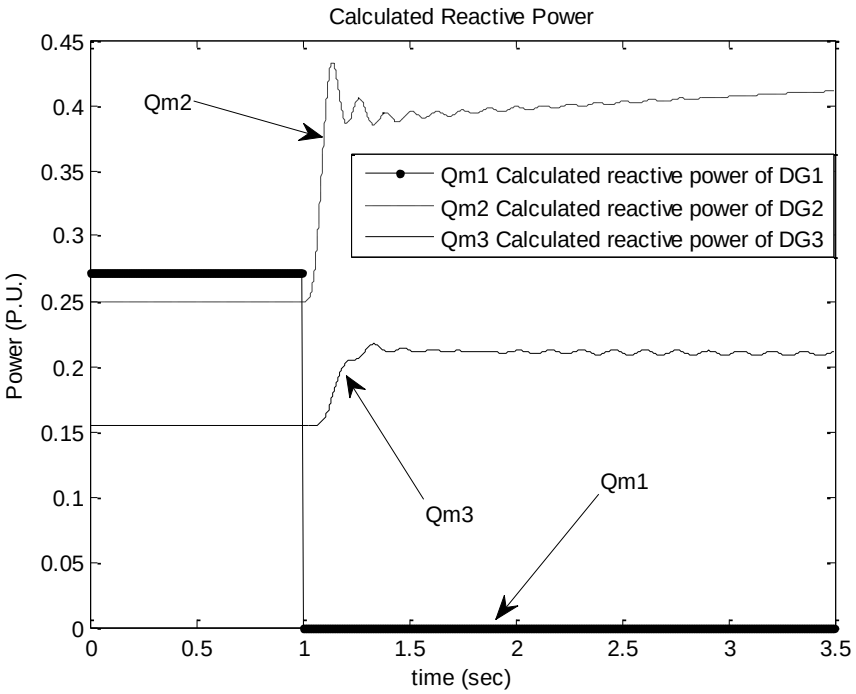

Fig. 6.71 Output reactive power response of the three DGs when the DG1 has been lost

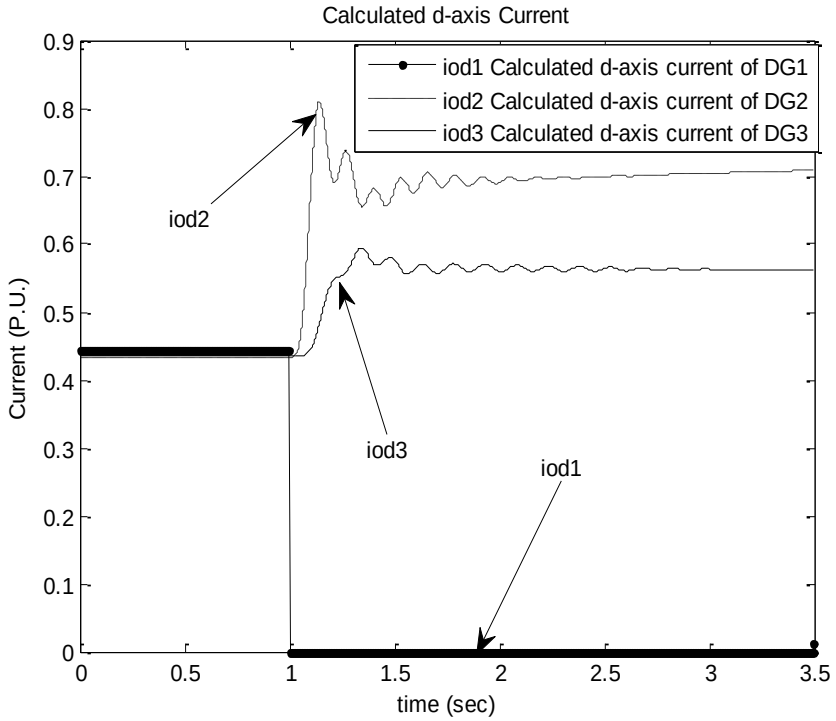

Fig. 6.72 D-axis output current response of the three DGs when the DG1 has been lost

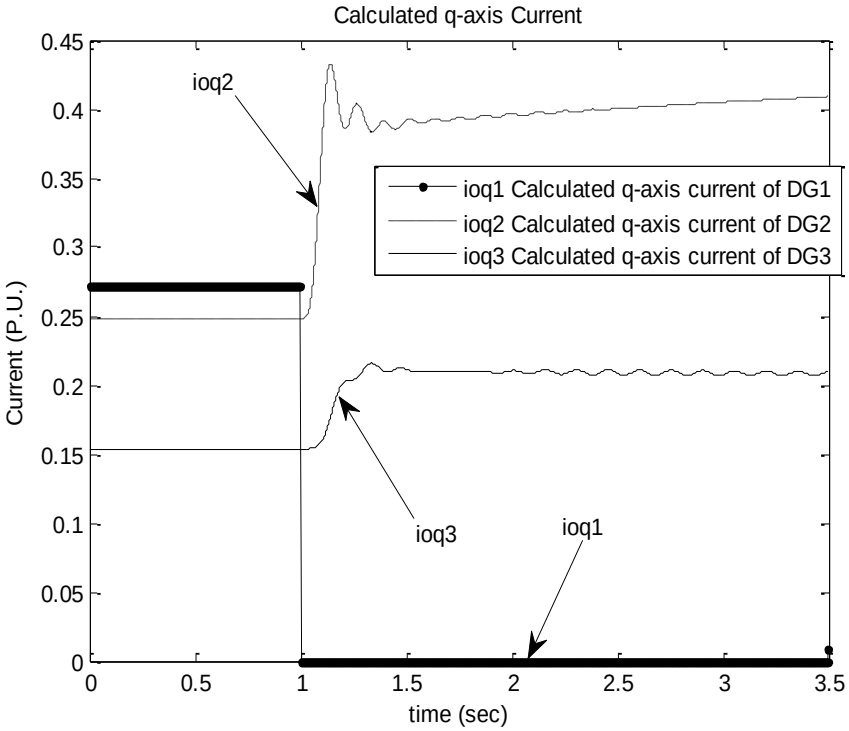

Fig. 6.73 Q-axis output current response of the three DGs when the DG1 has been lost

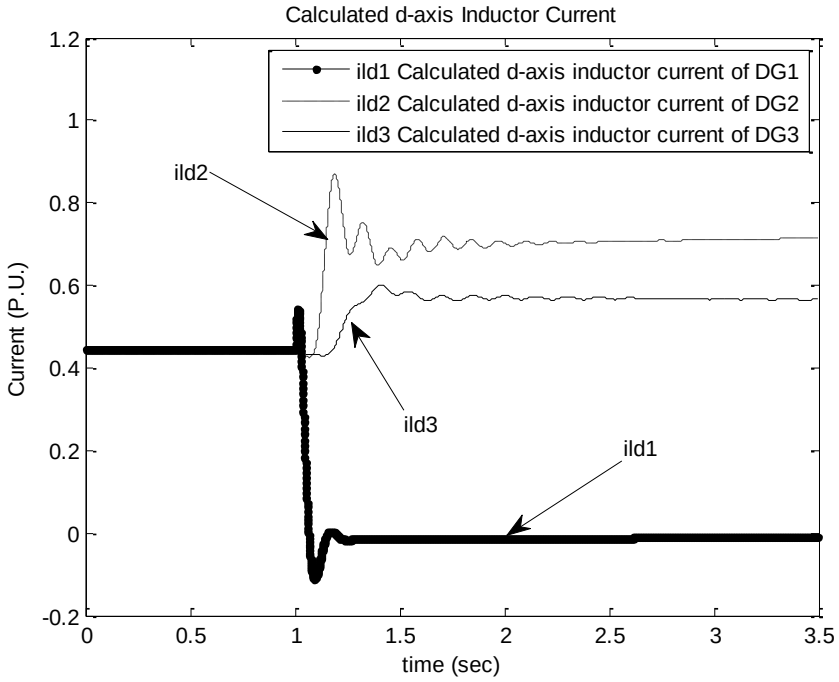

Fig. 6.74 D-axis inductor current response of the three DGs when the DG1 has been lost

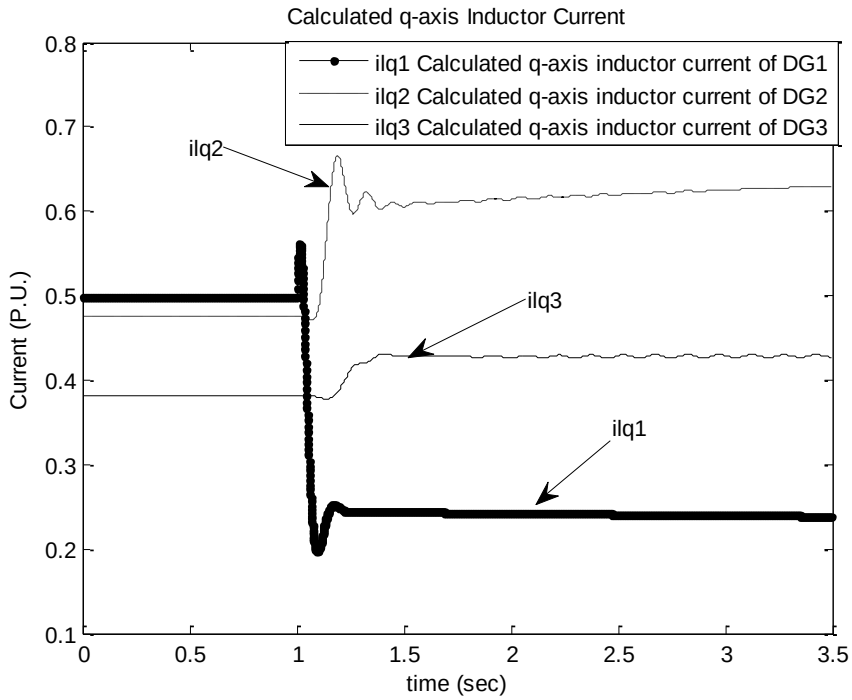

Fig. 6.75 Q-axis inductor current response of the three DGs when the DG1 has been lost

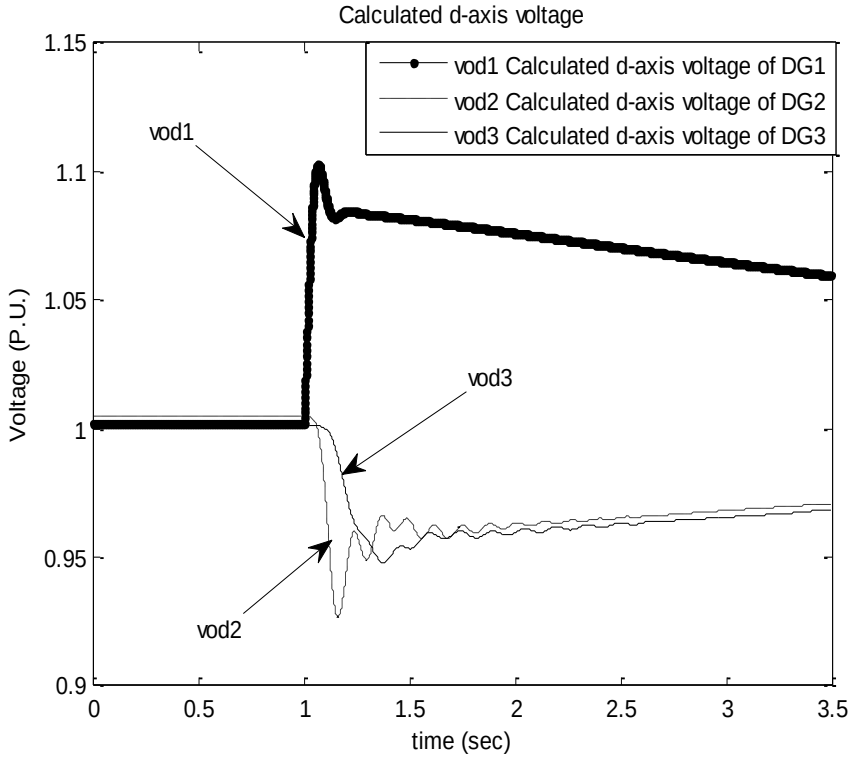

Fig. 6.76 D-axis output voltage response of the three DGs when the DG1 has been lost

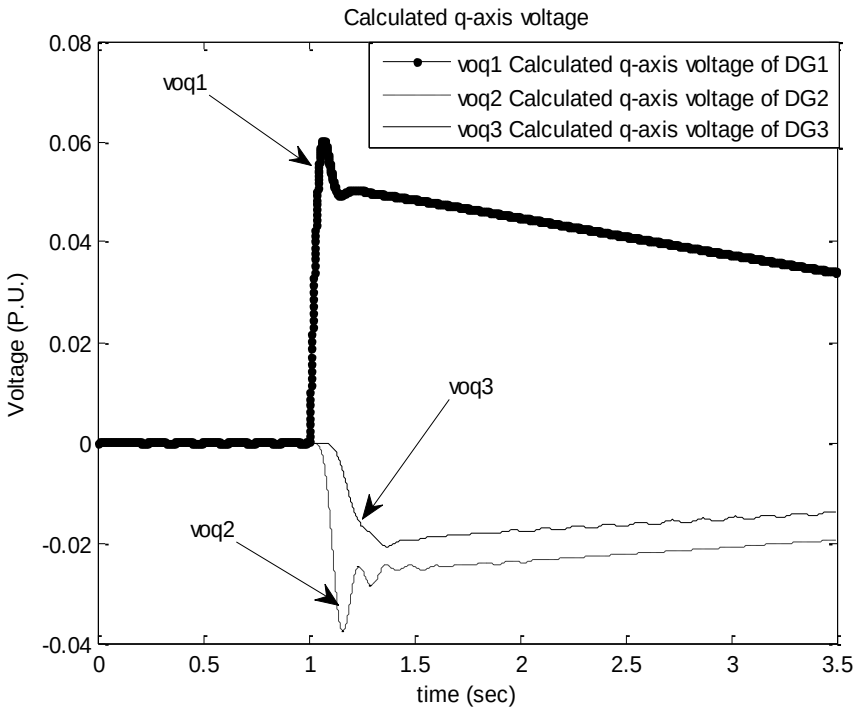

Fig. 6.77 Q-axis output voltage response of the three DGs when the DG1 has been lost

6.4 DISCUSSION AND CONCLUSION

The design of different controllers and power sharing coefficients has been formulated as an optimization problem. Two different objective functions to enhance the autonomous microgrid stability have been proposed. PSO technique is employed to search for the optimal settings of the optimized controller and power sharing parameters. System stability has been analyzed using both nonlinear time domain simulations and eigenvalue analysis. Step change and fault disturbances have been applied to demonstrate the effectiveness of the proposed design approach. The results confirm the effectiveness of the proposed PSO based approach for optimizing the parameters of PI controllers, and power sharing coefficients which achieve satisfactory system performance under different disturbances. The robustness of the proposed PSO technique with respect to its initial guess has been also confirmed.

CHAPTER 7

RESULTS AND DISCUSSIONS OF GRID-CONNECTED MODE

The complete layout of an inverter-based DG connected in the grid-connected mode presented in chapter two is analyzed. The parameters are given in Table 7.1. The DG unit is represented by a dc voltage source, a VSI, a series *LC* filter, and coupling inductance L_c. A single inverter was simulated in order to observe its steady-state and transient performance in its grid-connected mode of operation. The inverter is controlled to inject the real and reactive powers required by the utility. Nonlinear and linear models were developed using a MATLAB code to study the stability of an inverter-based microgrid in the grid-connected mode. The optimal parameters obtained using PSO have been used to check out the response of the power exported to the grid under disturbance. Different injected cases have also been taken to check the effectiveness of the controller and the ability of the inverter-based DG to inject the required powers.

Table 7.1 Grid-connected microgrid parameters

Parameter	Value
Nominal phase voltage	240 V
Grid frequency	50 Hz
Reference active power	10kW
Reference reactive power	5kVar
Filter Inductance (L_f)	1.35mH
Filter Capacitance (C_f)	50μF
Coupling impedance	(0.131 + j 0.30144)
Current Controller proportional gain in d-branch (K_p)	1.0
Current Controller integral gain in q-branch (K_i)	460
PLL proportional gain	2.1
PLL Integral gain	500

7.1 OPTIMAL PARAMETERS OBTAINED

The stability of the microgrids operating in the grid-connected mode is quite essential and it is affected by controller parameters and filter parameters. Generally, careful selection of the controller and filter maintains power quality within the regulated range and enhance the system performance against load changes and disturbances [73]. PSO has been employed to obtain the controller parameters and filter parameters. The optimal values obtained are given in Table 7.2.

7.2 EFFECTIVNESS AND ROBUSTNESS OF THE PROPOSED CONTROLLER

To demonstrate the effectiveness and to study the robustness of the proposed controller under different conditions, several runs have been carried out with different initial populations. The objective function convergence of grid-connected mode is shown in Fig. 7.1. The objective function reaches the same value in all runs as shown in Fig. 7.1. This

confirms the robustness of the proposed design approach with respect to its initial guess and its capability to avoid trapping in local minima.

Table 7.2 Optimized parameters of the grid-connected microgrid mode

Parameter	Value
Filter Inductance (L_f)	*0.324mH*
Filter Capacitance (C_f)	*36.979μF*
Damping Resistance (R_d)	*10 Ω*
P Controller of the current controller (K_p)	*0.8148*
I Controller of the current controller (K_i)	*36.156*

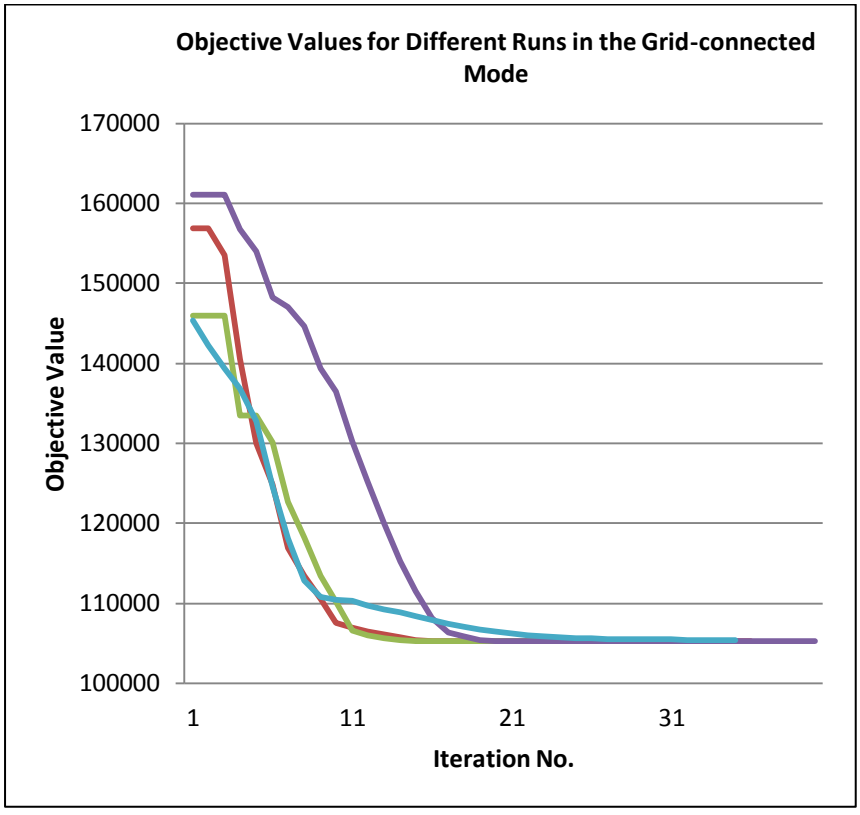

Fig. 7.1 Objective function convergence in the grid-connected mode

7.3 SIMULATION AND RESULTS

7.3.1 Nonlinear Time Domain Simulation

A nonlinear time domain simulation has been carried out. A step change in the injected active power has been done to assess the response of the exported power to the grid using the optimal parameters obtained using PSO. The injected power is stepped down from 10 KW to 5 KW at t=0.1sec. The system response and performance under this disturbance are given in Figs. 7.2 - 7.6. The results illustrate the stability of the system performance with the proposed controllers. Figs. 7.2 - 7.5 show how the optimal parameters make the proposed controllers capable of tracking the reference. It is also seen that the response to the change in reference values is fast and without significant overshoot.

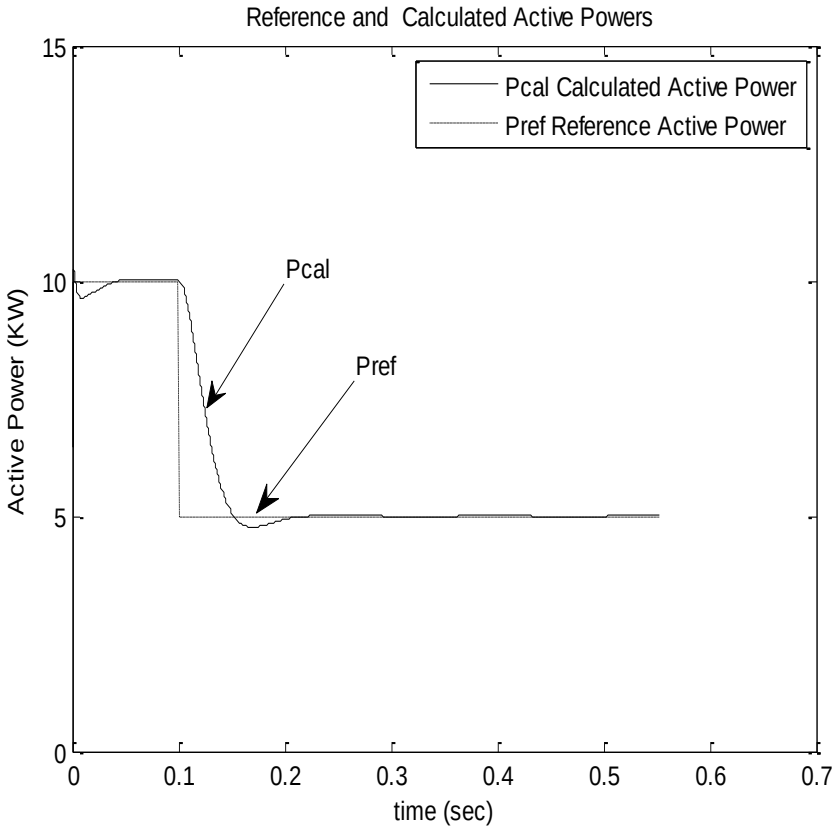

Fig. 7.2 Reference and calculated active powers

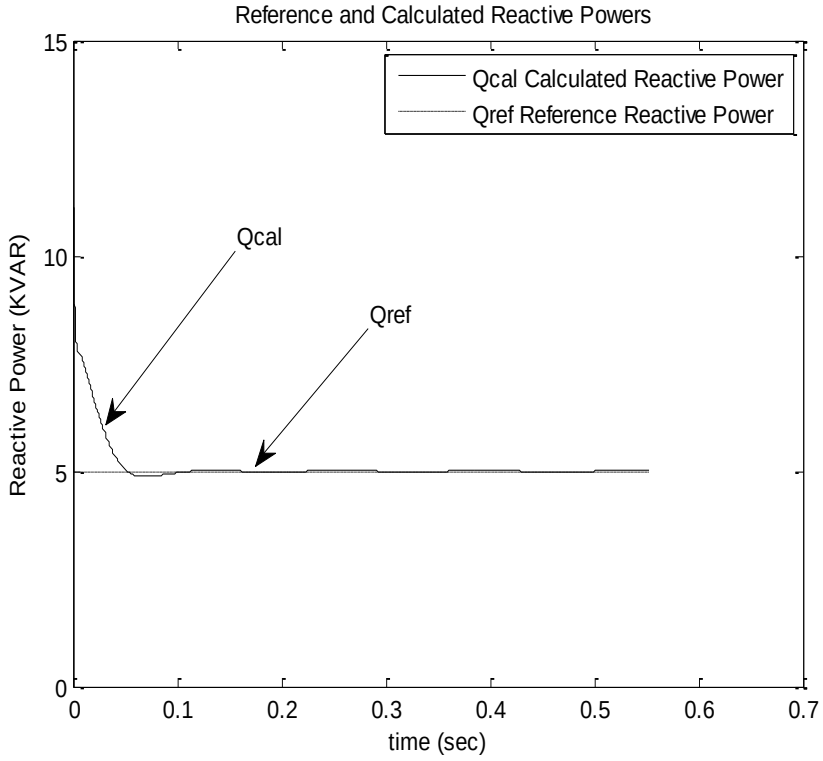

Fig. 7.3 Reference and calculated reactive powers

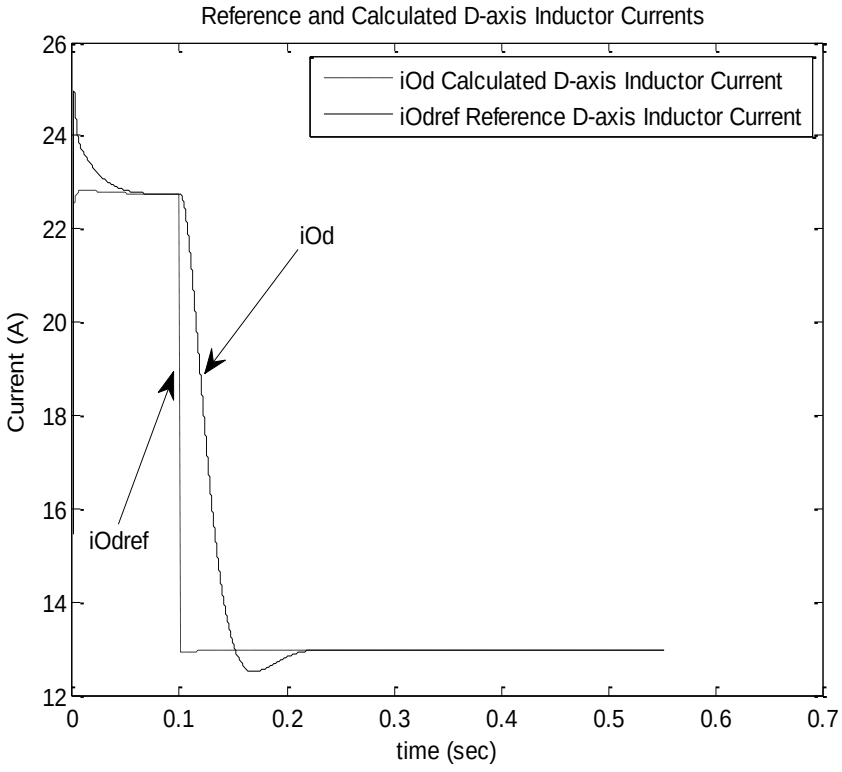

Fig. 7.4 Reference and calculated d-axis inductor currents

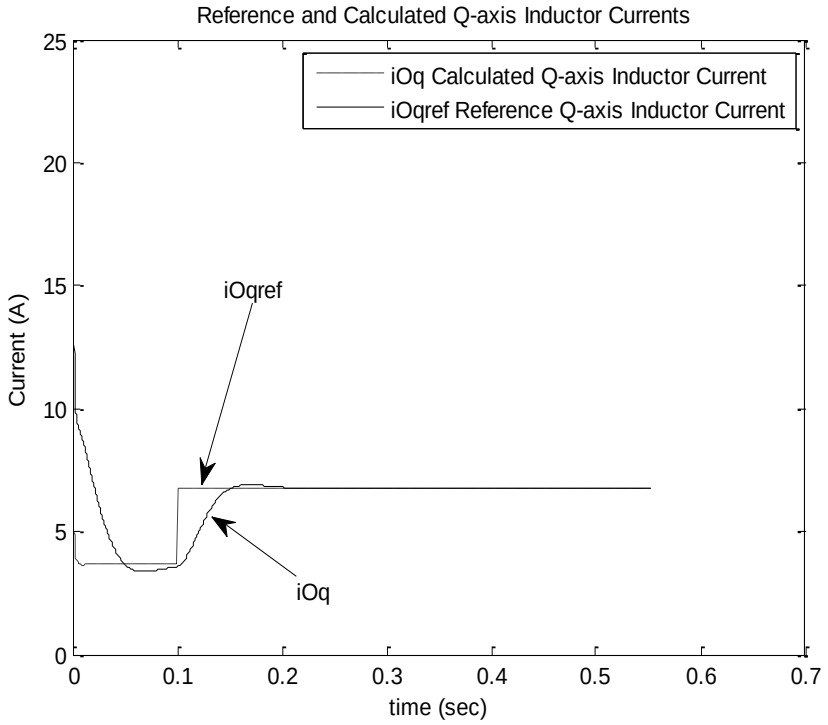

Fig. 7.5 Reference and calculated q-axis inductor currents

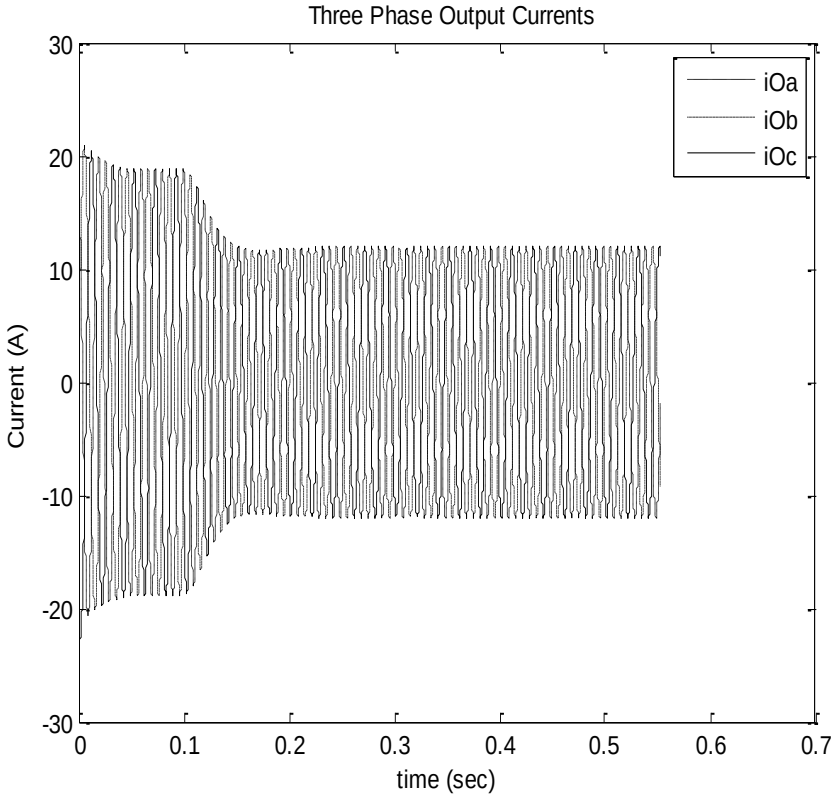

Fig. 7.6 Three phase output currents

Now, a big stepped change in the injected power (from 20 KW to 5 KW) is done at t=0.1sec. The system step response is shown in Figs. 7.7 - 7.11. The calculated power is tracking the reference power fast and without significant overshoot as illustrated in Fig. 7.7 and Fig. 7.8. Fig. 7.9 and Fig.7.10 present the reference and calculated dq inductor currents. Changing in three phase inductor currents at t=0.1sec is shown in Fig. 7.11.

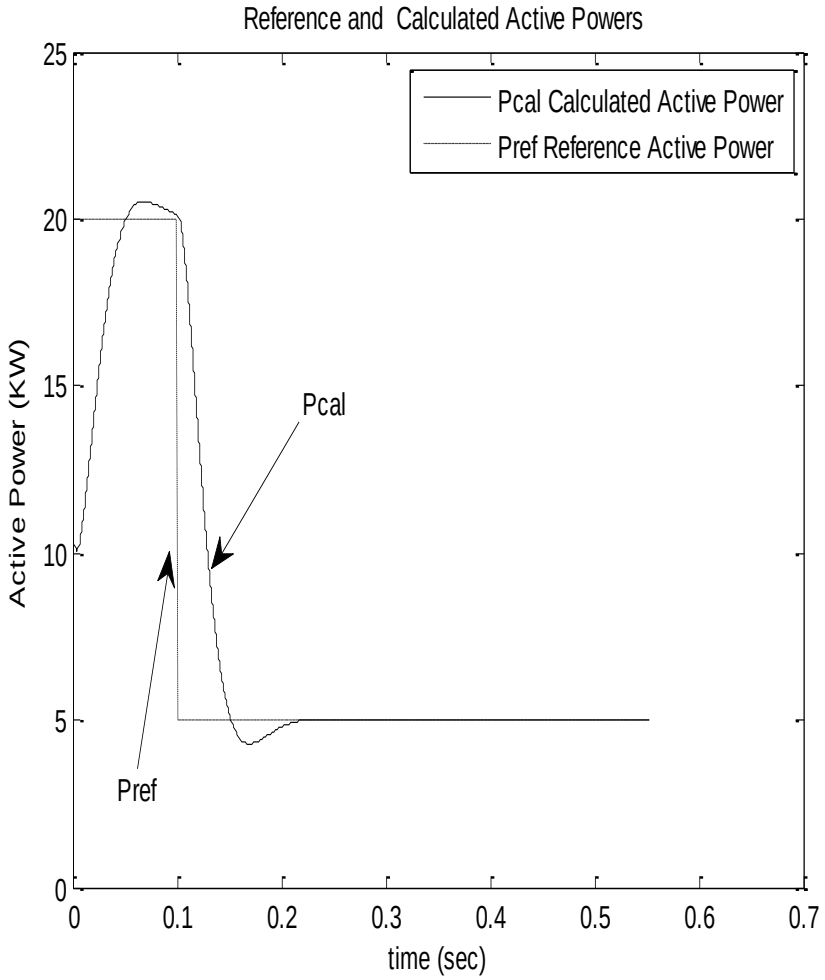

Fig. 7.7 Reference and calculated active powers

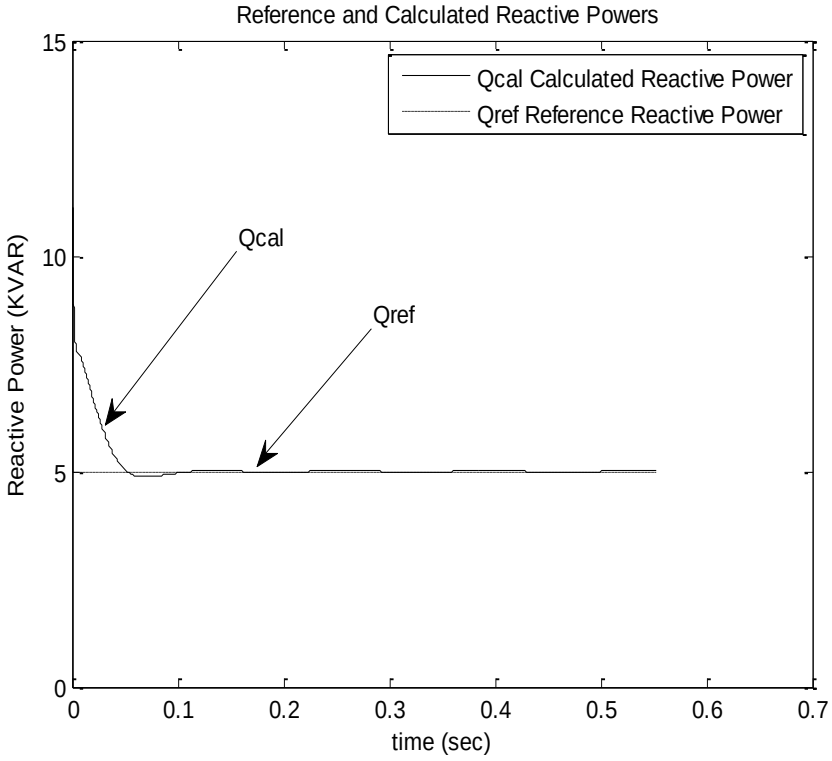

Fig. 7.8 Reference and calculated reactive powers

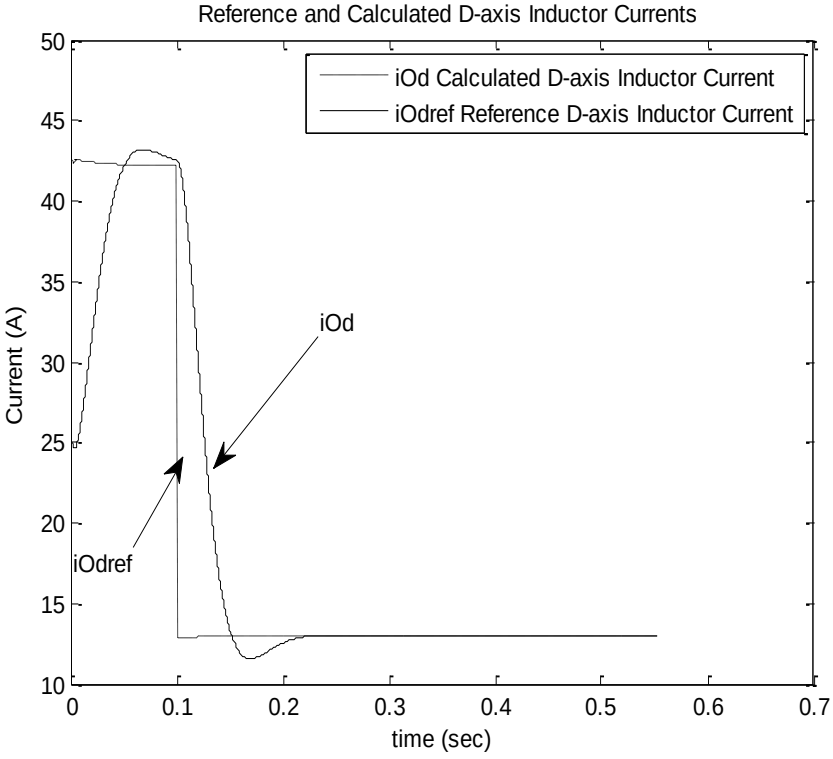

Fig. 7.9 Reference and calculated d-axis inductor currents

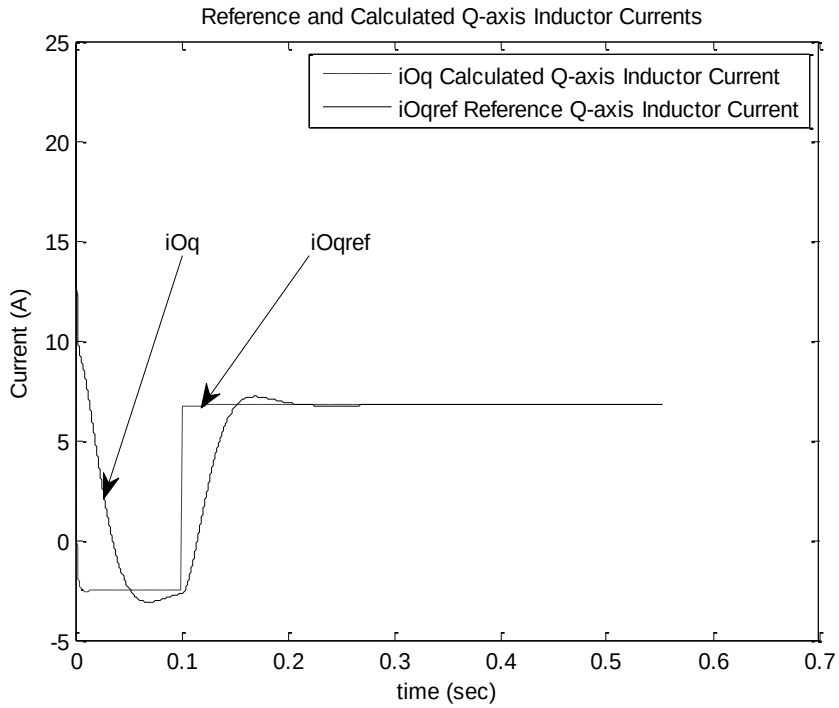

Fig. 7.10 Reference and calculated q-axis inductor currents

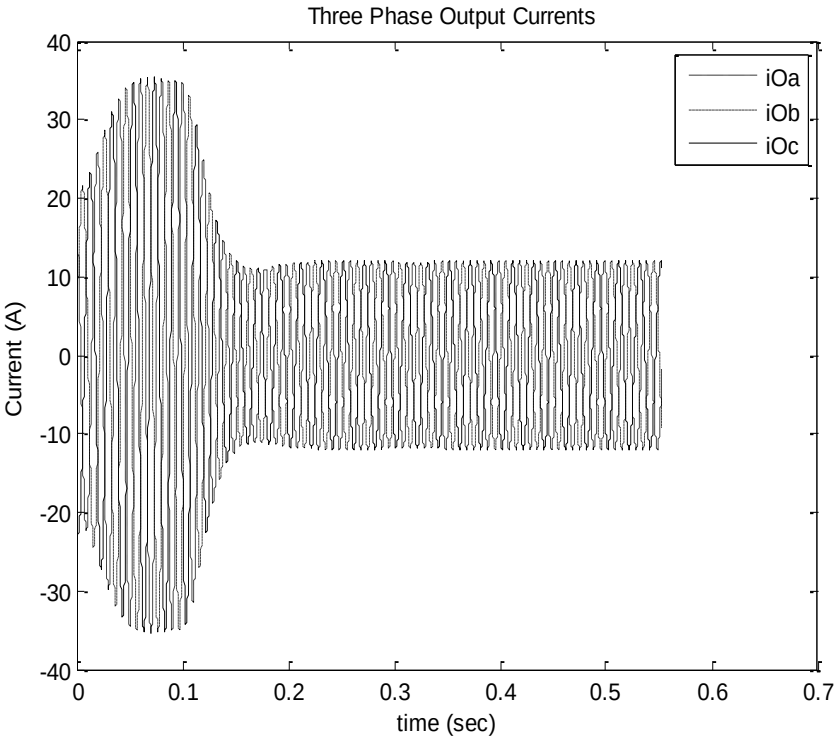

Fig. 7.11 Three phase output currents

The system response with the optimal controller has been investigated when the injected active power has been stepped up from 5 KW to 10 KW at t=0.1sec. The system response and performance are given in Figs. 7.12 - 7.16. The fast tracking of the calculated power to the reference power without significant overshoot is illustrated in Fig. 7.12 and Fig. 7.13. The reference and calculated dq inductor currents are shown in Fig. 7.14 and Fig.7.15. Three phase inductor currents is shown in Fig. 7.16. The results illustrate the stability of the system performance with the proposed controllers.

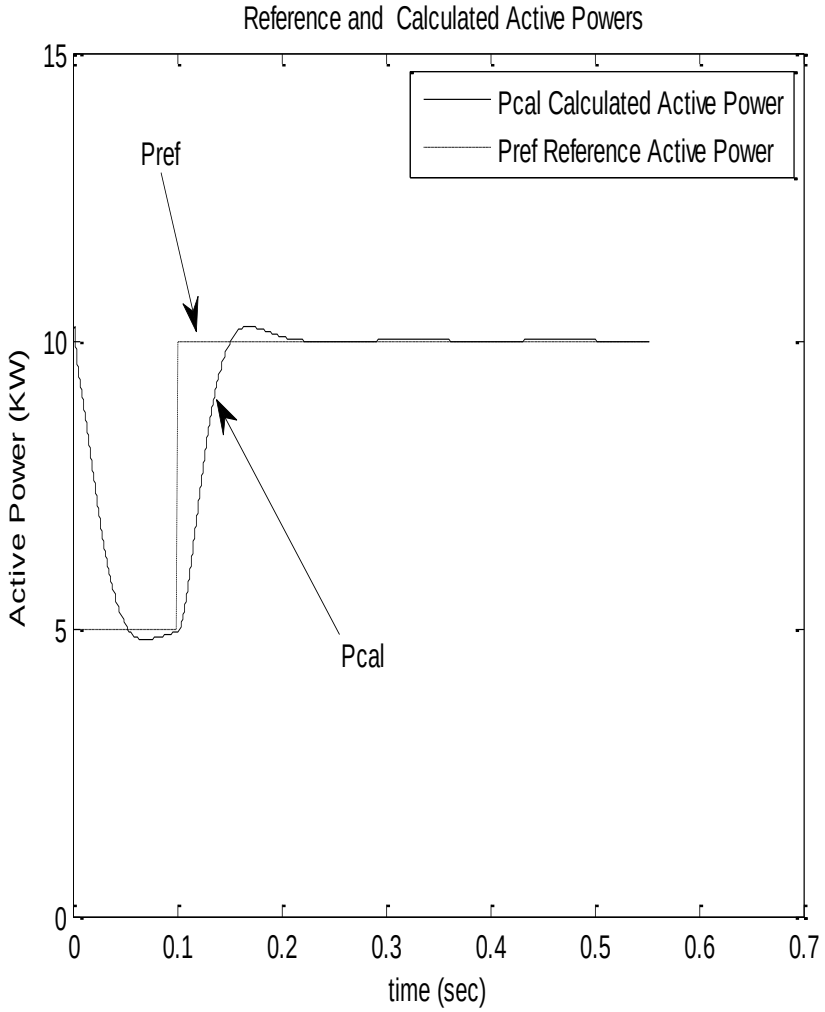

Fig. 7.12 Reference and calculated active powers

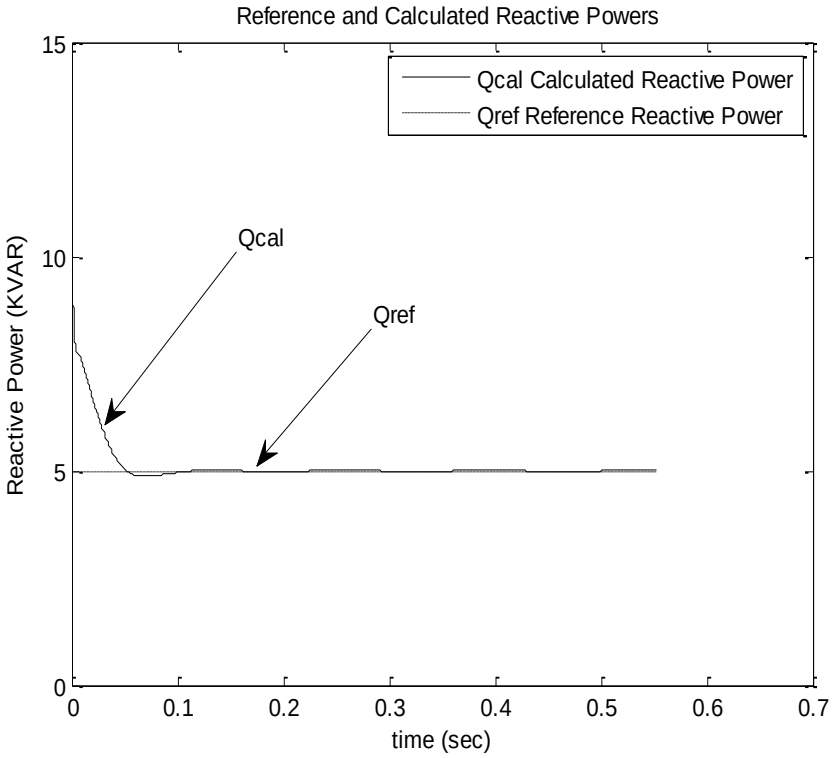

Fig. 7.13 Reference and calculated reactive powers

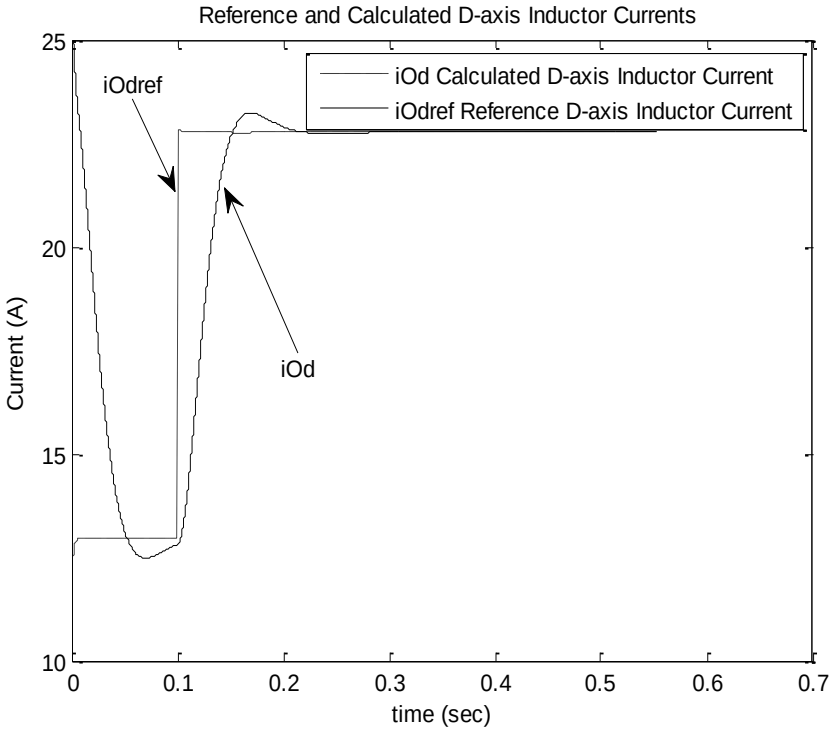

Fig. 7.14 Reference and calculated d-axis inductor currents

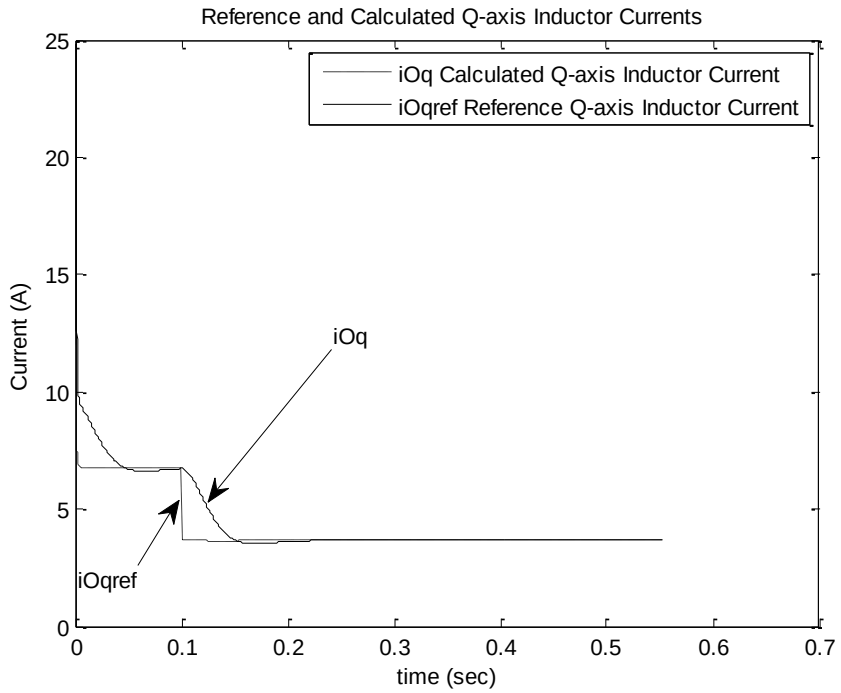

Fig. 7.15 Reference and calculated q-axis inductor currents

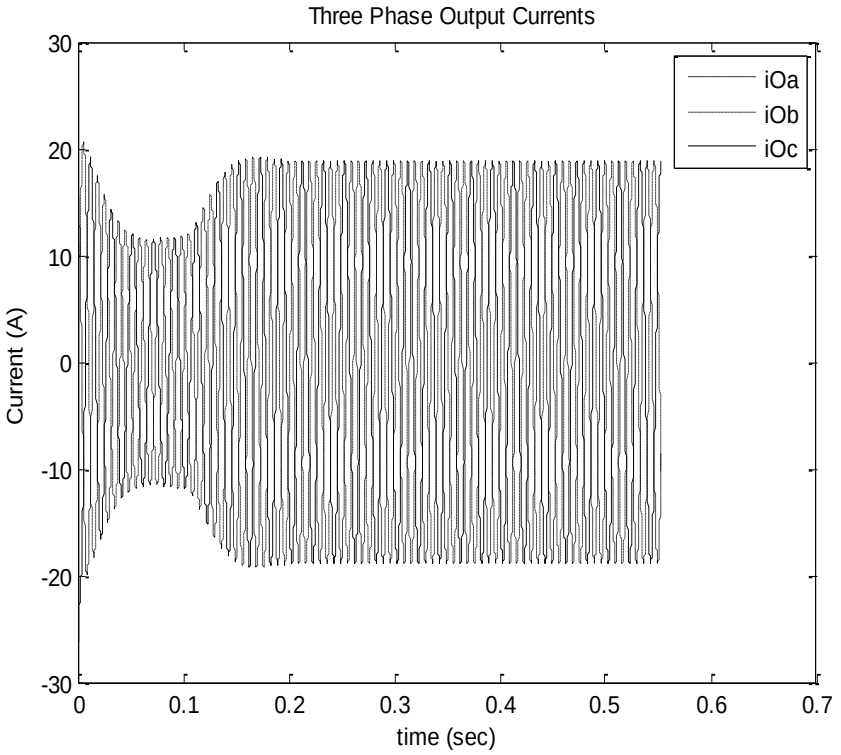

Fig. 7.16 Three phase output currents

Instead of using the inverter-based DG to inject active power, the inverter-based DG is used to inject reactive power. The injected reactive power is stepped down from 10 KVAR to 5 KVAR. Figs. 7.17 - 7.21 show the system response due to this step change. Fig. 7.17 shows the reference and calculated active powers while Fig. 7.18 illustrate how the calculated reactive power is fast following the reference reactive power without significant overshoot. Fig. 7.19 and Fig. 7.20 present the reference and calculated dq inductor currents. Three phase inductor currents is shown in Fig. 7.21.

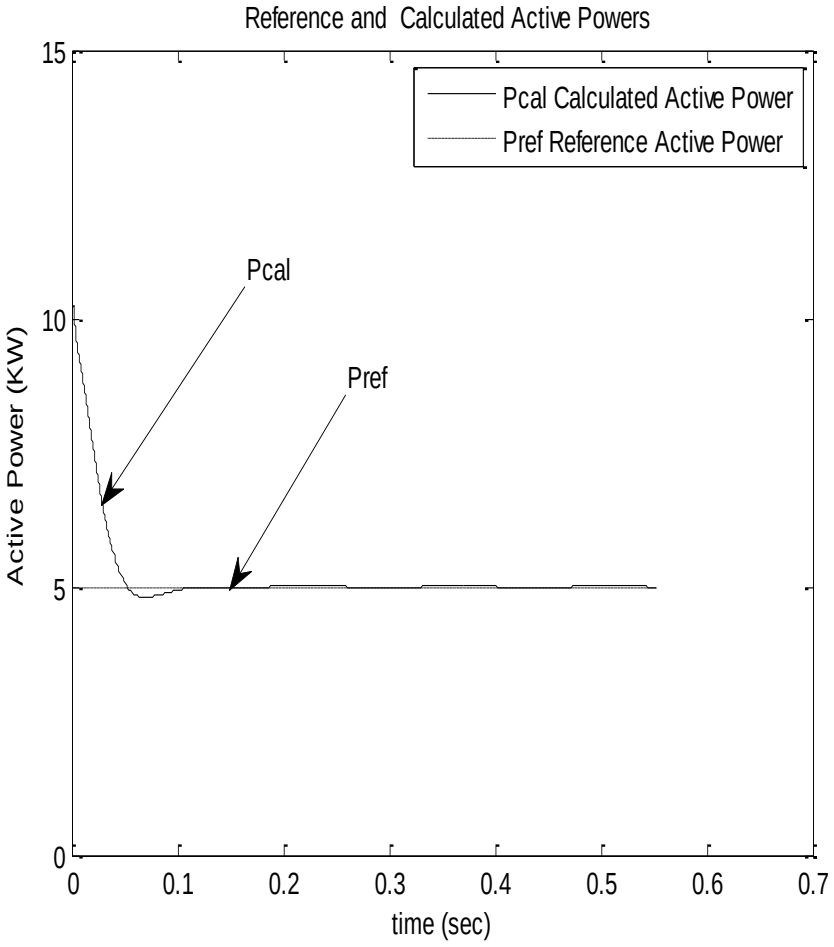

Fig. 7.17 Reference and calculated active powers

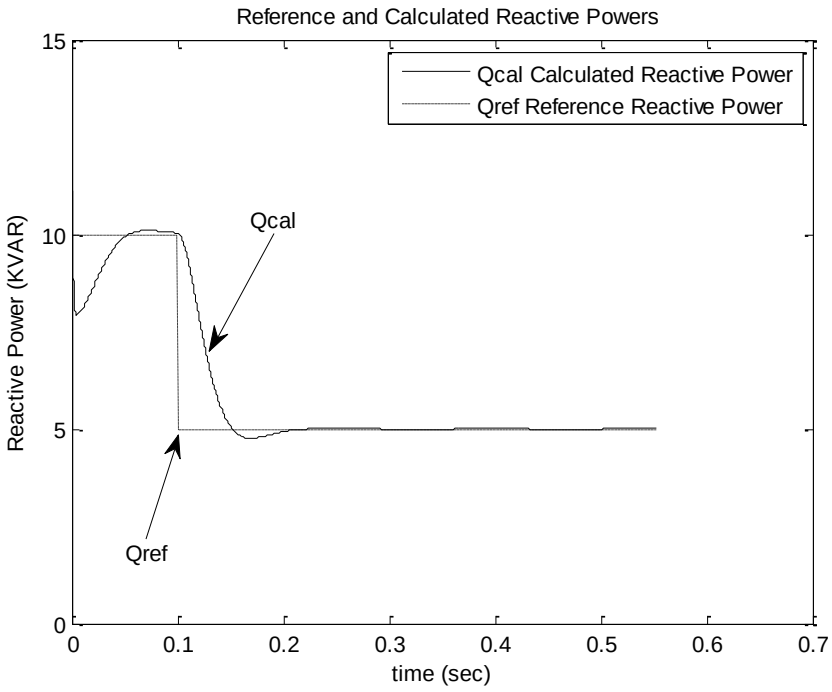

Fig. 7.18 Reference and calculated reactive powers

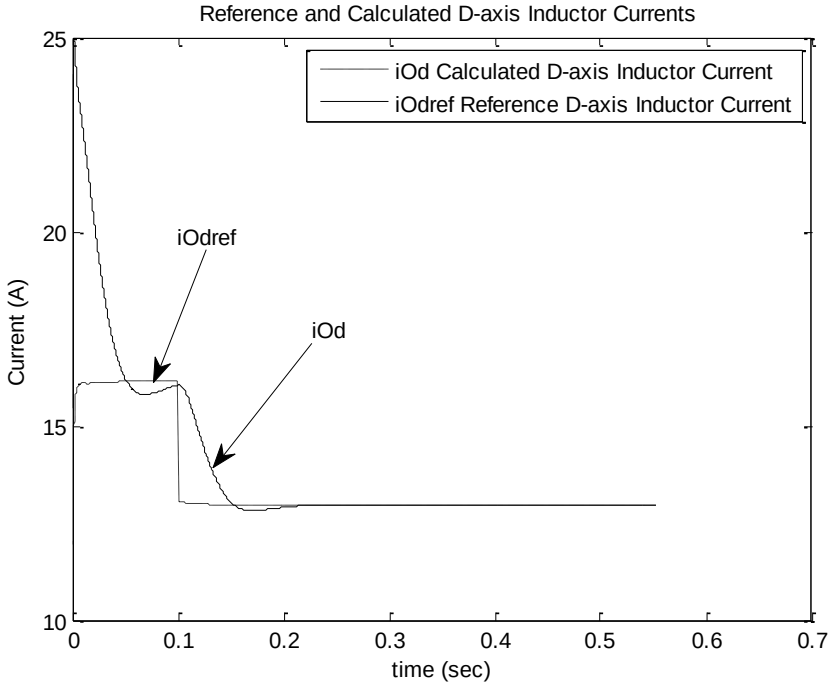

Fig. 7.19 Reference and calculated d-axis inductor currents

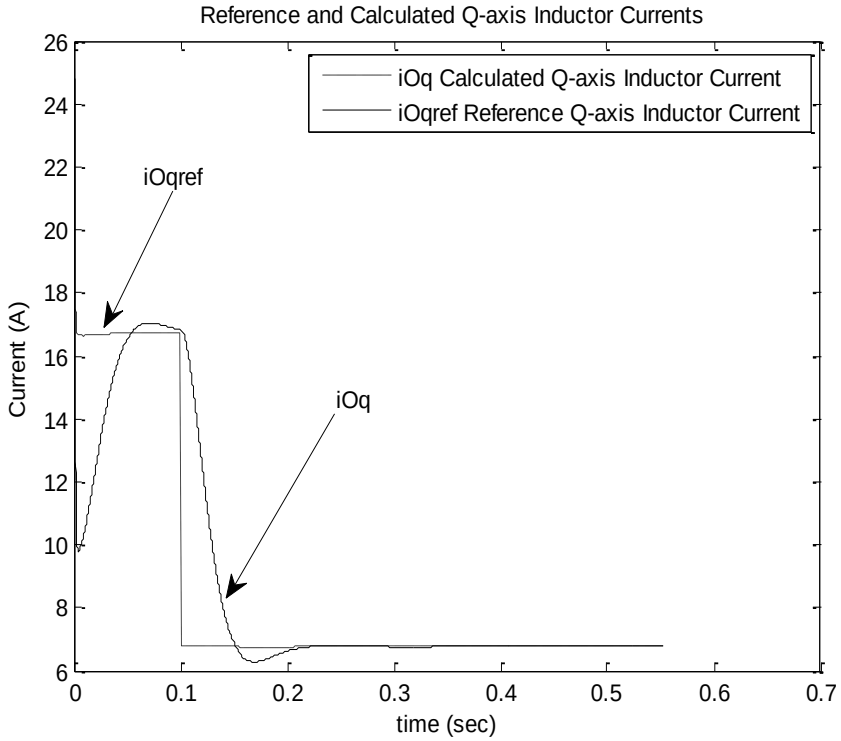

Fig. 7.20 Reference and calculated q-axis inductor currents

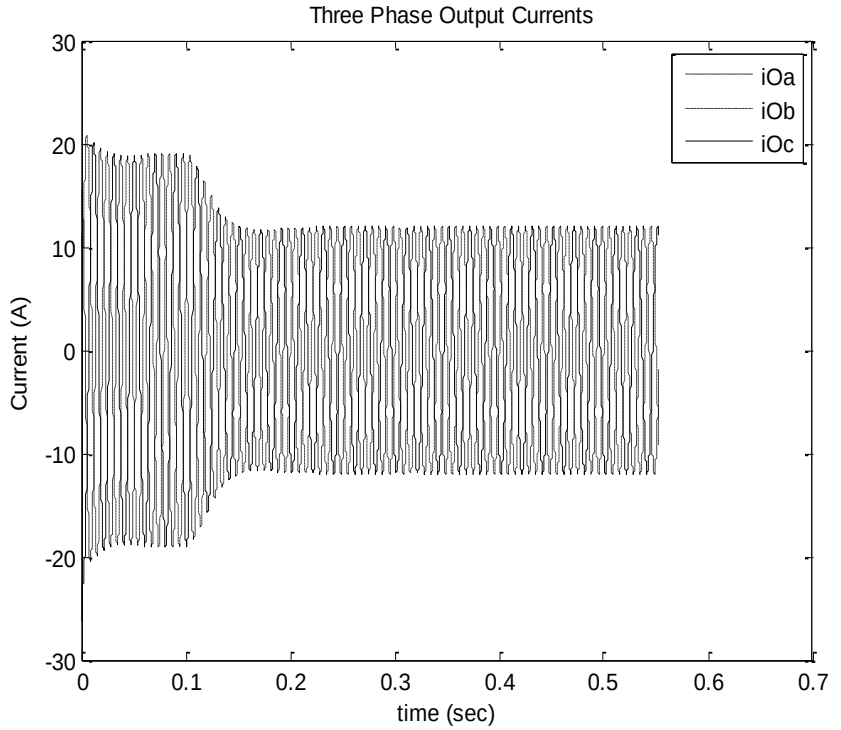

Fig. 7.21 Three phase output currents

Now, the injected reactive power is stepped up from 5 KVAR to 10 KVAR. The system response due to this step change is shown in Figs. 7.22 - 7.26. The reference and calculated active powers are presented in Fig. 7.22 while the following of calculated reactive power to the reference reactive power without significant overshoot is shown in Fig. 7.23. Fig. 7.24 and Fig. 7.25 give the reference and calculated dq inductor currents. Three phase inductor currents is shown in Fig. 7.26.

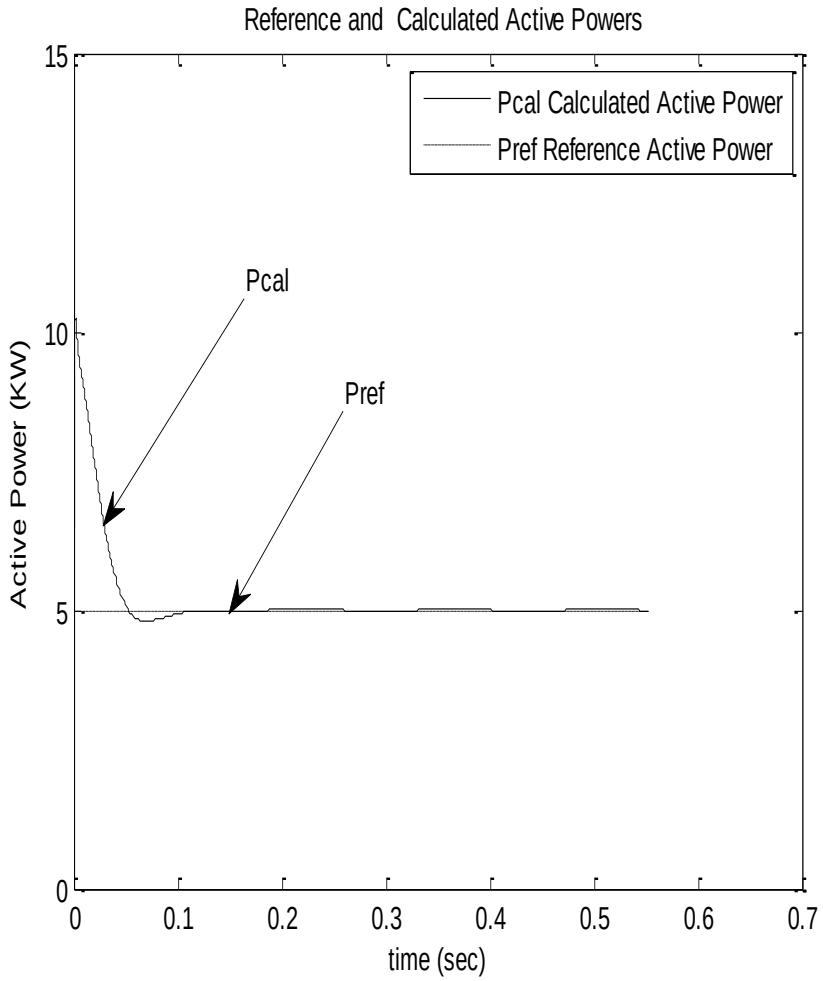

Fig. 7.22 Reference and calculated active powers

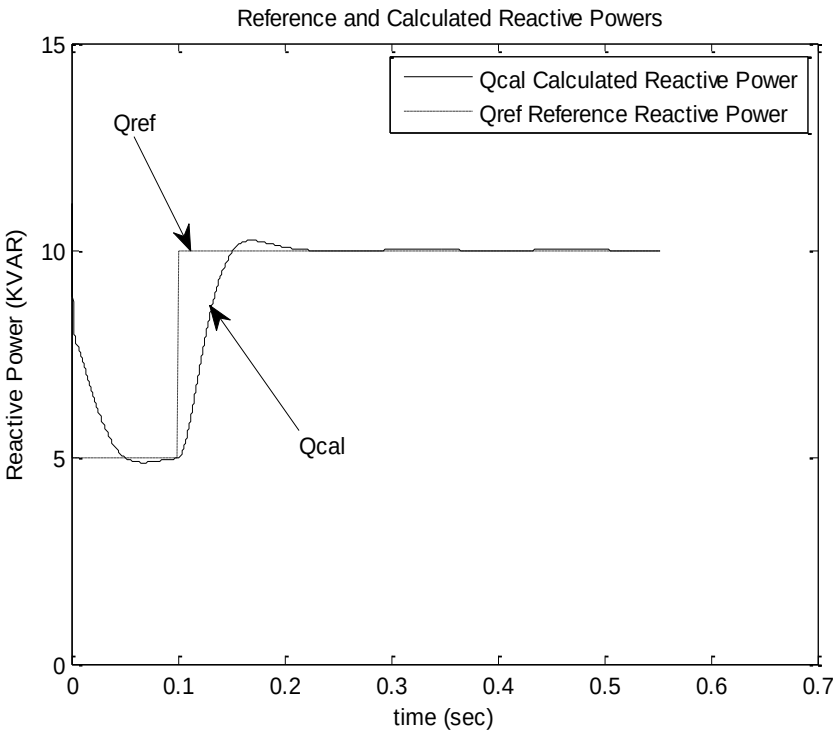

Fig. 7.23 Reference and calculated reactive powers

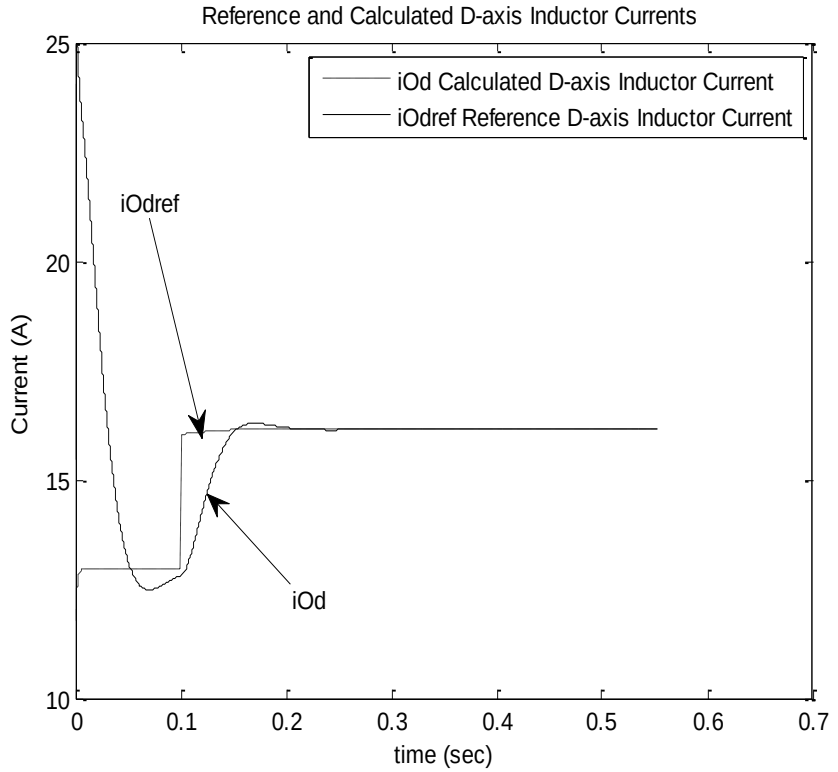

Fig. 7.24 Reference and calculated d-axis inductor currents

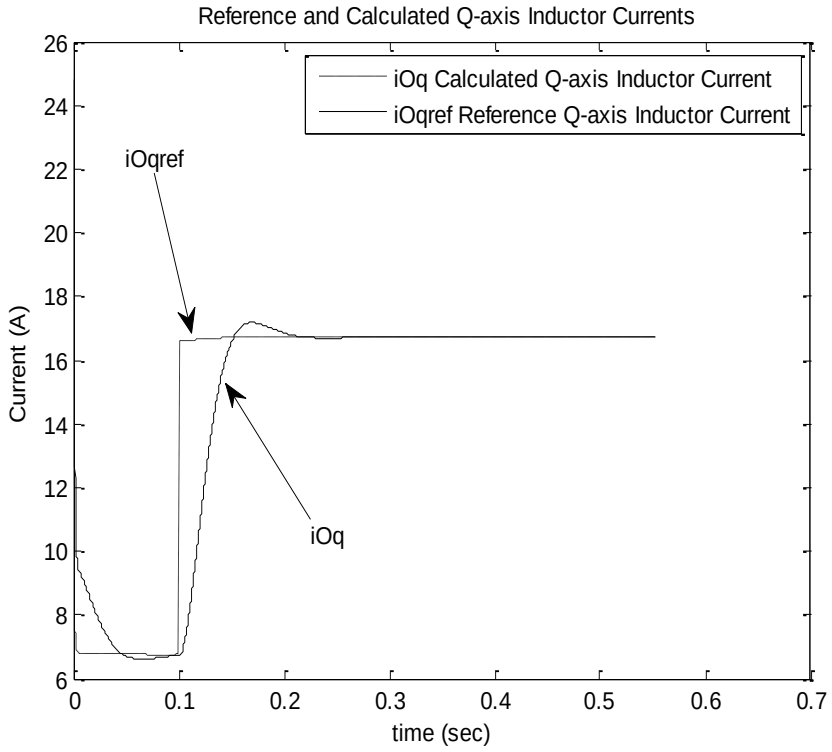

Fig. 7.25 Reference and calculated q-axis inductor currents

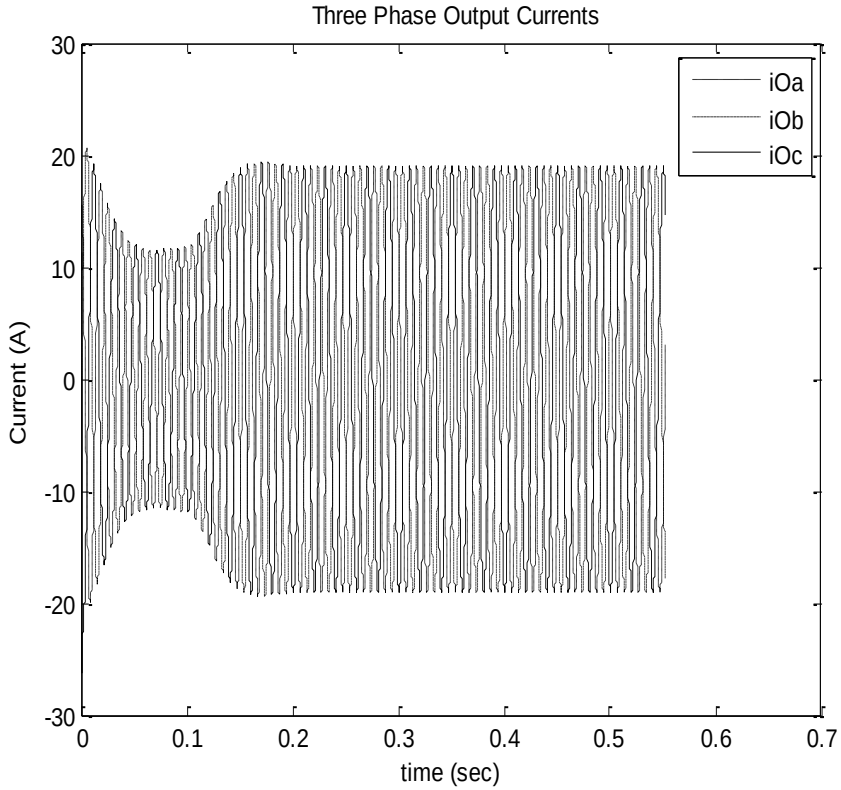

Fig. 7.26 Three phase output currents

7.3.2 Controller Capability for Step Changes

A series of further tests were conducted to illustrate the effectiveness of the controller and the ability of the inverter-based DG to inject the required powers. The response of the inverter to power reference changes is an important performance criterion. The initial reference values of the active and reactive powers were 10 KW and 5 KVAR. The active power is stepped up to 15 KW and the reactive power is stepped up to 7.5 KVAR for a time of 0.1sec then return back again to initial values. Figs.7.27 -7.31 illustrate the system response and performance under this disturbance. Fig. 7.27 and Fig. 7.28 show that how the calculated power exactly tracks the reference power. The system goes to stable mode after getting step change. The capability of the proposed controller to inject active and reactive powers to the grid can be investigated from these results especially when the inverter is used to inject both active and reactive powers to the grid. The step change response of the *dq* calculated and reference inductor current is depicted in Figs. 7.29 -7.30. Three phase output currents are shown in Fig. 7.31. The effectiveness of the controller and the ability of the inverter-based DG to inject the required powers have been assessed under heavy injected powers. The active power is stepped up to 20 KW and the reactive power is stepped up to 10 KVAR for a time of 0.1sec then return back again to initial values. The results given in Figs 7.32-7.36 investigate the controller capability of the inverter-based DG to inject heavy loads such as this load (20 KW and 10 KVAR). Figs. 7.32 -7.33 show that how the tracking of the reference current to the d-axis current is significant with acceptable overshoot and delay time.

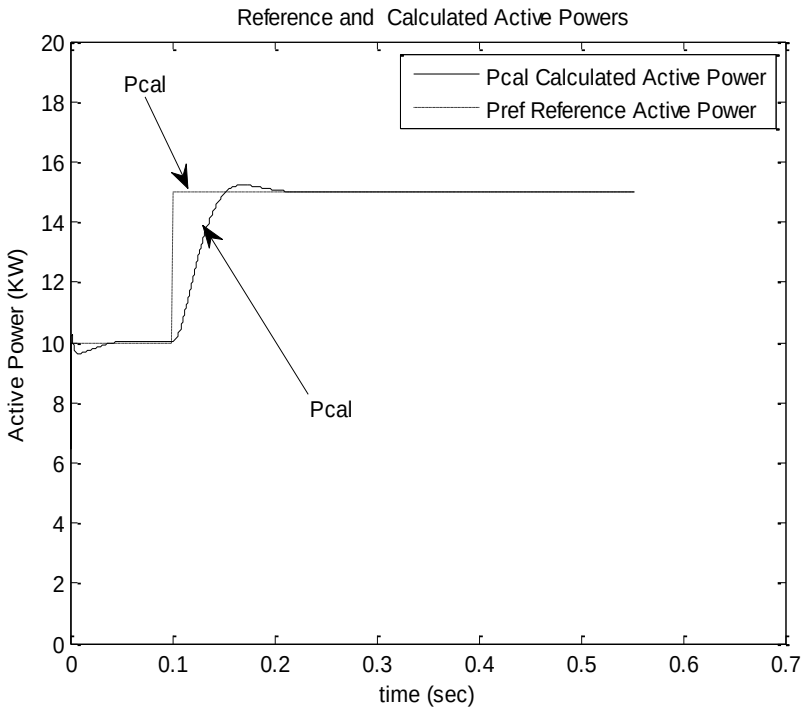

Fig. 7.27 Reference and calculated active powers

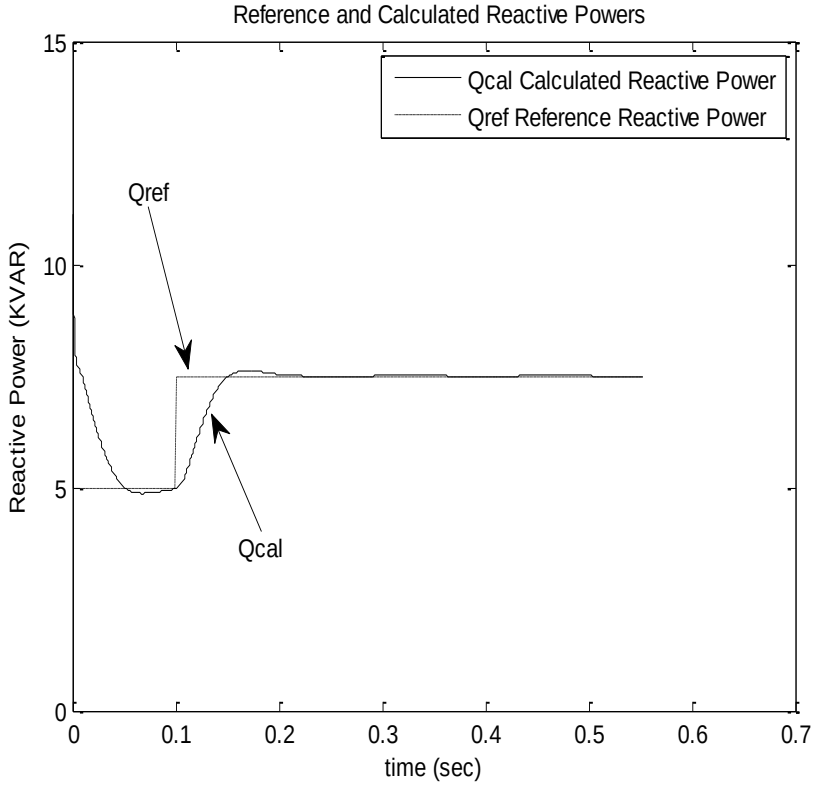

Fig. 7.28 Reference and calculated reactive powers

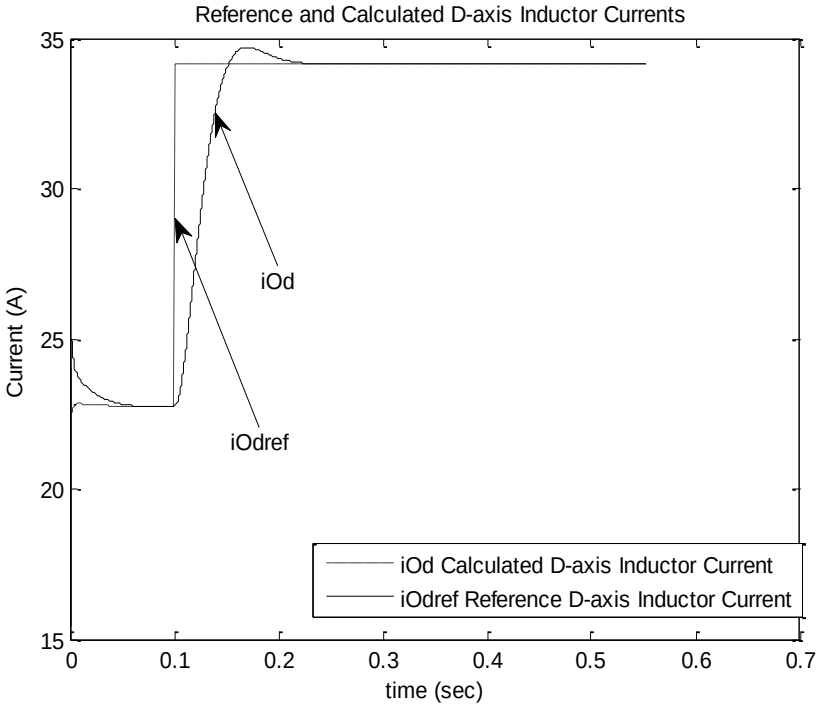

Fig. 7.29 Reference and calculated d-axis inductor currents

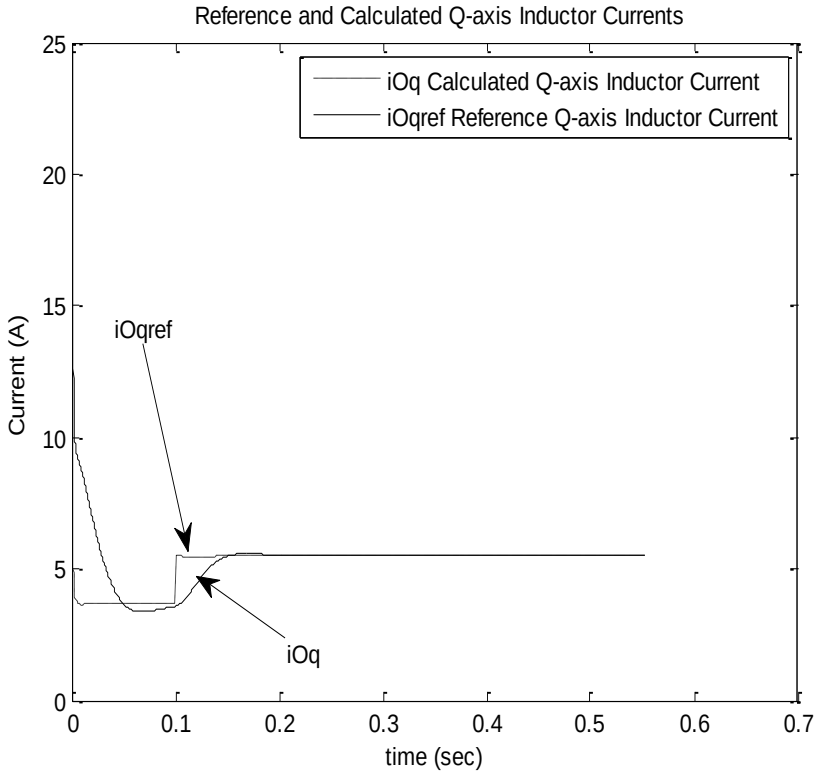

Fig. 7.30 Reference and calculated q-axis inductor currents

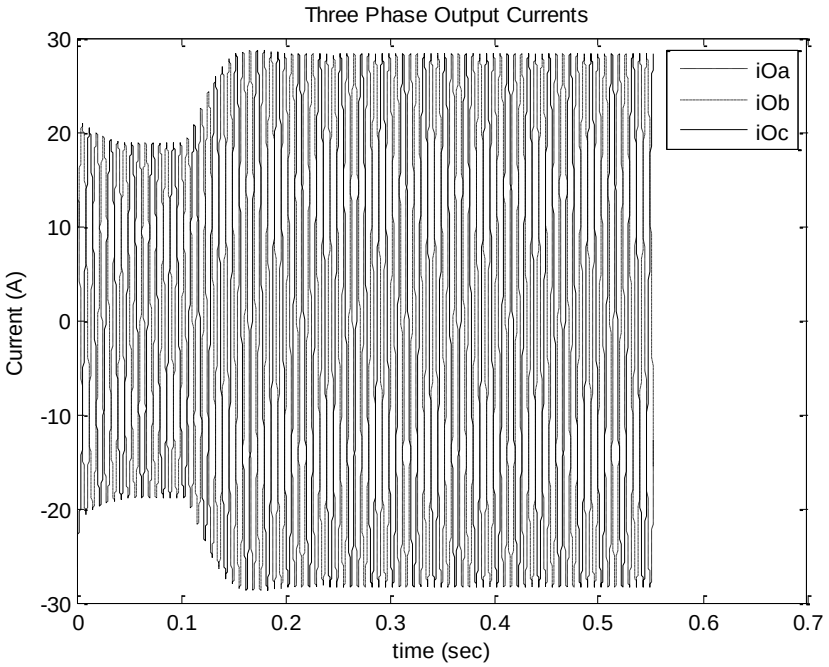

Fig. 7.31Three phase output currents

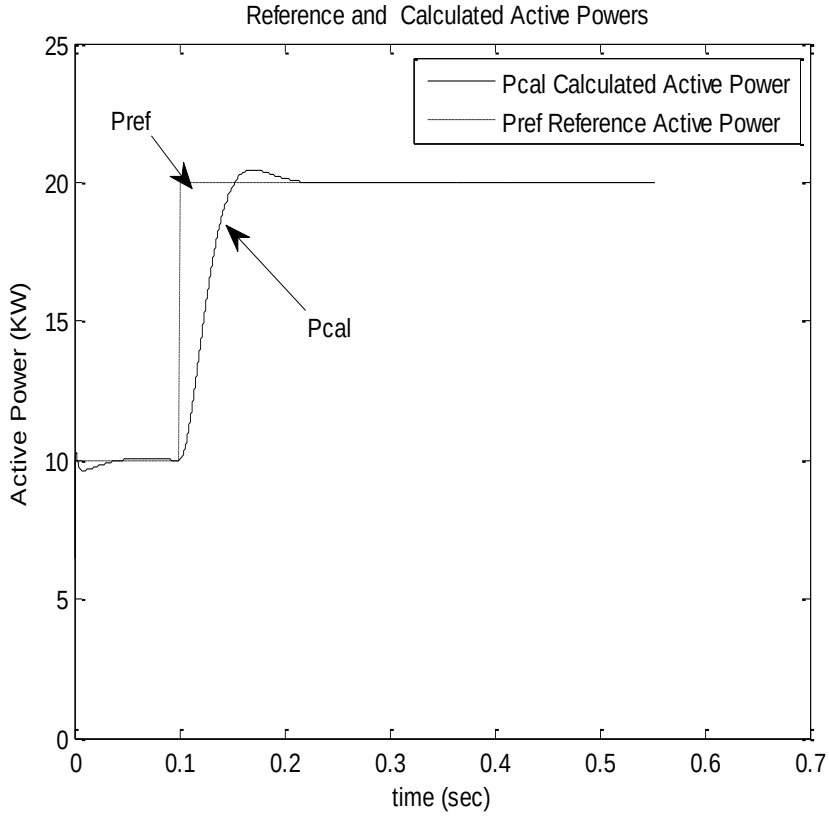

Fig. 7.32 Reference and calculated active powers

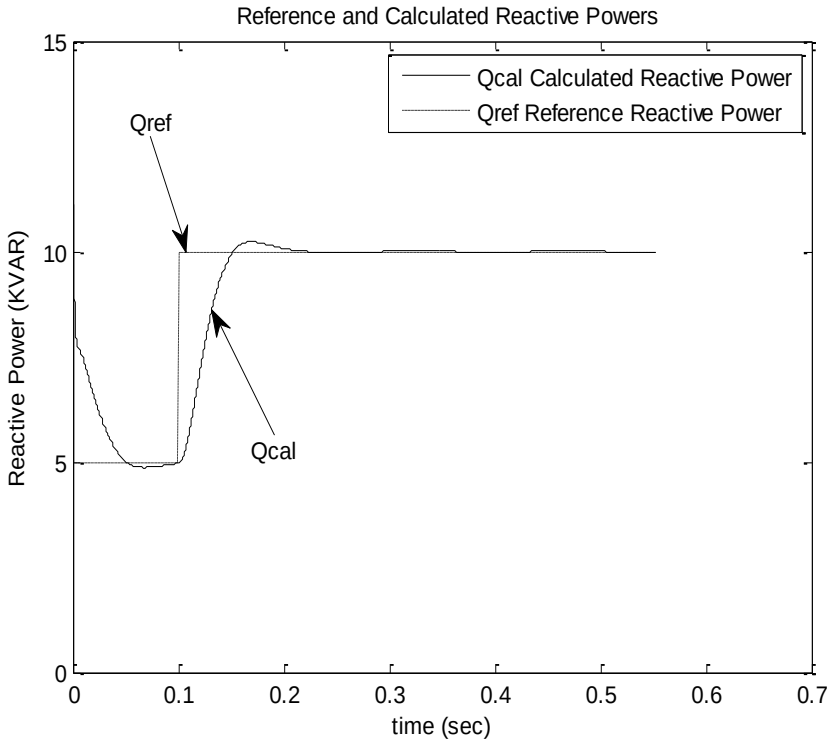

Fig. 7.33 Reference and calculated reactive powers

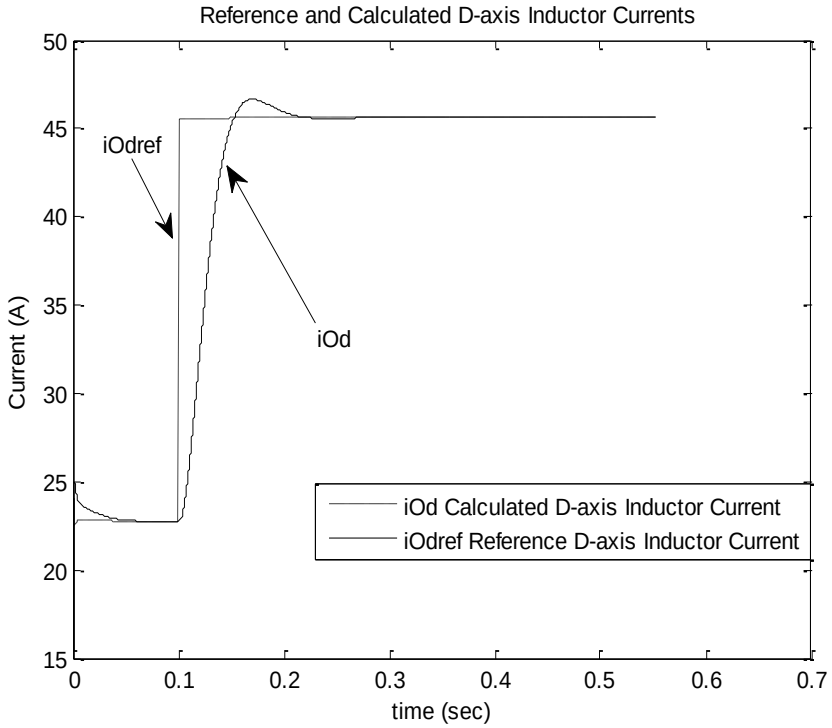

Fig. 7.34 Reference and calculated d-axis inductor currents

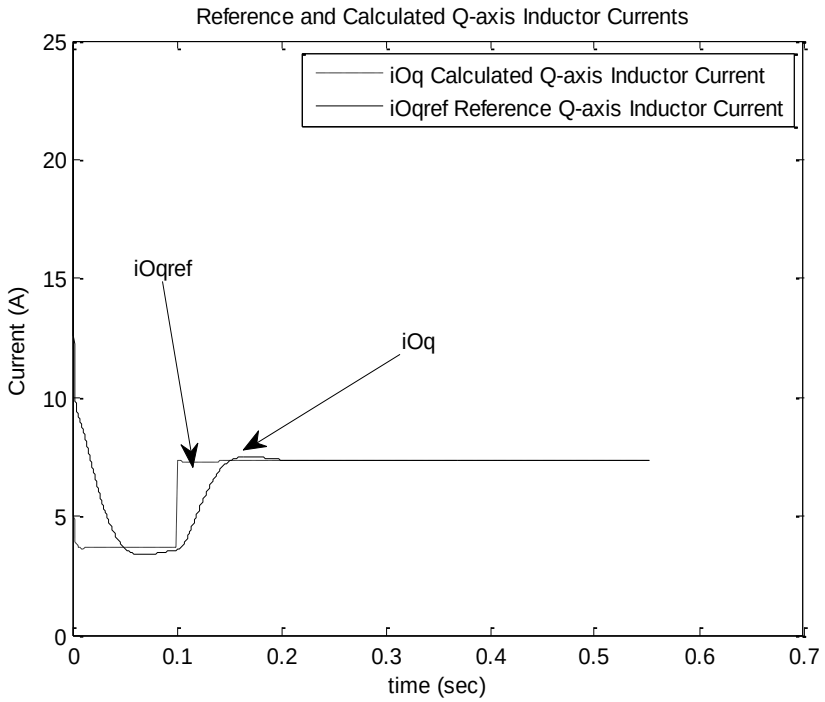

Fig. 7.35 Reference and calculated q-axis inductor currents

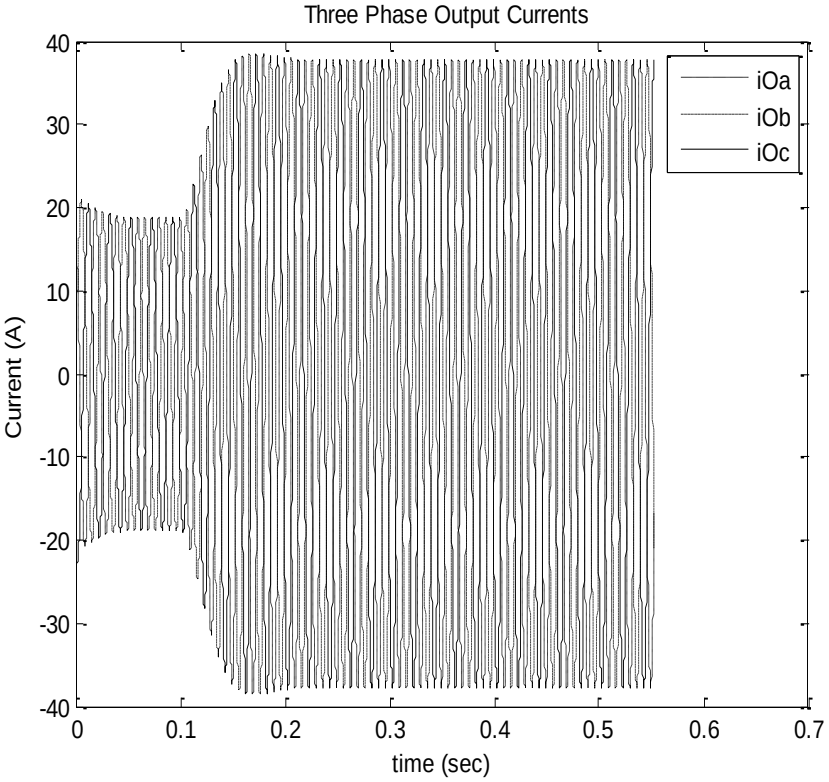

Fig. 7.36 Three phase inductor currents

7.3.3 Eigenvalues Analysis

Eigenvalues analysis has been carried out to demonstrate the effectiveness of the proposed controllers and design approach. Without optimization, the eigenvalues of the system given in Table 7.1 are shown in Fig. 7.37. It is clear that the system has positive eigenvalues which means that the system is unstable. The proposed PSO based design approach has been implemented to shift the eigenvalues to the left in s-plane. Fig. 7.38 shows that all unstable eigenvalues have been shifted to the left in s-plane. Comparing the result obtained using optimized parameters with the parameters given in Table 7.1 indicates the effectiveness of the proposed controller with the optimized settings obtained.

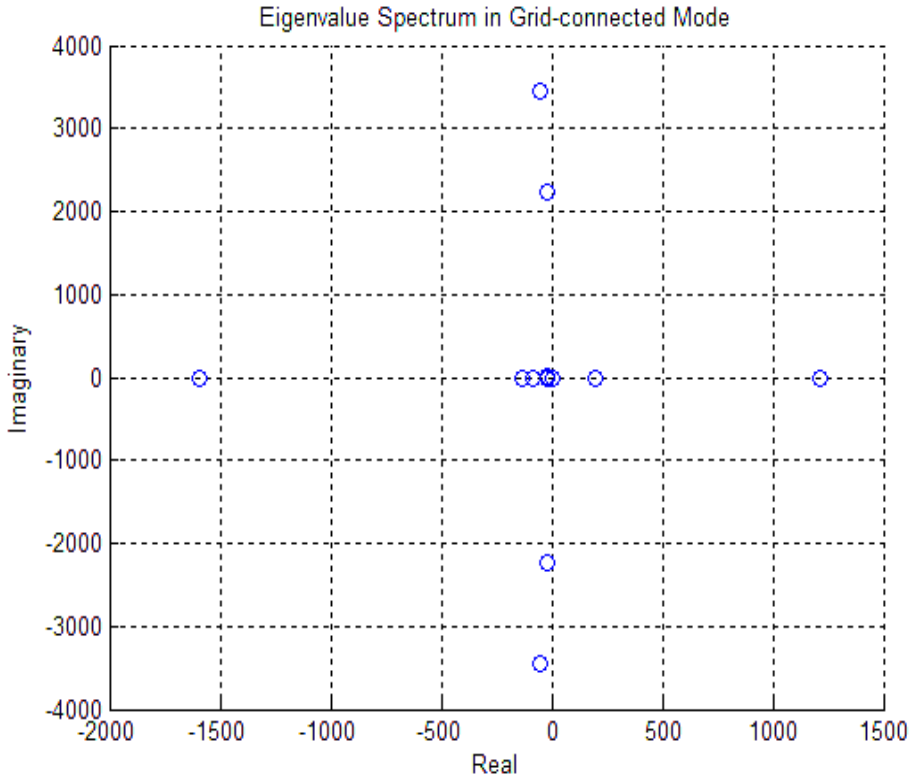

Fig. 7.37 The eigenvalues spectrum of the system without optimization

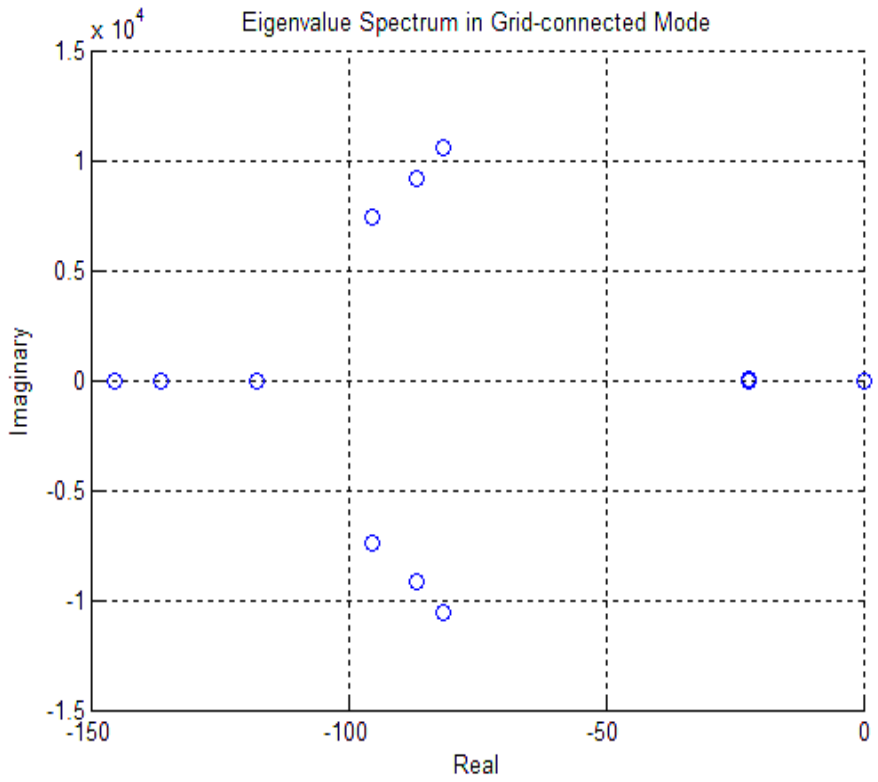

Fig. 7.38 The eigenvalues spectrum of the system with optimization

7.4 DISCUSSION AND CONCLUSION

In this chapter, two different objective functions to enhance the system stability have been proposed. PSO technique is employed to search for the optimal settings of the optimized parameters. Step change in the reference power has been applied to demonstrate the effectiveness of the proposed design approach. It has been used to test the system capability to follow this reference power. System stability has been analyzed using both nonlinear time domain simulations and eigenvalues analysis. The results confirm the effectiveness of the proposed PSO based approach for optimizing the parameters of PI controllers and filter. The robustness of the proposed PSO technique with respect to its initial guess has been also confirmed.

CHAPTER 8

MICROGRID IMPLEMENTATION OF RTDS

8.1 INTRODUCTION

DIGITAL technique is believed to be the one of the most important techniques which stimulates the development of modern power systems since later 1960s, especially for power system simulation [80], protection [81] and power electronics [82]. In the past, modern technology has gone through tremendous development in the area of power system and digital simulation. The microprocessor progresses, communication and transducer technologies have provided new means for the development in power system protection and relay testing.

The Real Time Digital Simulator (RTDS) is a fully digital electromagnetic transient power system simulator. It can be used to conduct close-loop testing of physical devices such as protection equipment and control equipment; to perform analytical system studies

and to educate operators, engineers and students [83]. It is a cost-effective replacement for transient network analyzers and analogue/hybrid simulators. RTDS allows the user to investigate the effects of disturbances on power system equipment and networks to prevent outages or complete failure. Moreover, RTDS added the capability to improve the simulation accuracy and better capture the switching events [84].

8.2 RTDS CAPABILITY

RTDS is generally designed to simulate power systems in real time with time step-sizes on the order of 50s. The system uses a number of digital signal processors (DSPs) which operated in parallel. It provides a number of digital and analog I/O ports for interfacing hardware to the simulation. It features a more powerful processor combined with FPGAs which allow the simulation of a limited number of power electronics devices with time step as small as 1.4-2.5s embedded in the 50s time-step environment. Therefore, it allows the simulation of power electronics converter operating at higher switching frequency with sufficient accuracy. In addition, its real time capability allows the user to incorporate real devices into the simulation in a closed loop environment.

The beauty of the RTDS is that it works in continuous, sustained real time. This means that it can solve the power system equations fast enough to continuously produce output conditions that realistically represent conditions in the real network. Because the solution is real time, the simulator can be connected directly to power system control and protective relay equipment and adjust its calculations based on their operation [83].

The studies were carried out using system developed by RTDS Technologies, the RTDS™ [85]. RTDS is a combination of advanced computer hardware and

comprehensive software. The custom parallel processing hardware architecture was assembled in modular units called racks. Each rack contains slot and rail-mounted cards. The specific composition of an RTDS™ depends on the processing and I/O requirements of the intended application. A common communications backplane links all rack mounted cards facilitating information exchange.

Any network such as microgrid can be created on the computer screen of the RTDS. This can be done by selecting the components from a number of customized component model libraries then arranging them to build the network. The RTDS™ employs an advanced and easy to use graphical user interface - the RSCAD Software Suite. The software is comprised of several modules designed to allow the user to perform the simulation and result analysis. The Software is used to interface with the RTDS hardware. It is designed to allow the user to perform all the steps necessary to prepare and run the simulation then analyze its output.

All loading, running and controlling of the simulation are done entirely from the host workstation through the RSCAD/RunTime module. The Power and Control System Software is an integral part of RSCAD for RTDS™. RSCAD allows the user to select a pictorial representation of the power system or control system components from the library in order to build the desired circuit. Once the system has been drawn and the parameters entered, the appropriate compiler automatically generates the low-level code necessary to perform the simulation using the RTDS™ Simulator. Therefore, this software determines the function of each processor card for each simulation in real time; the simulator can be connected directly to power system control and protective relay

equipment. It has now become one of the most important product test and development tools throughout the world [85].

8.3 LABORATY SETUP FOR REAL TIME DIGITAL SIMULATION

This section describes the autonomous and grid-connected modes in the RTDS environment by outlining the major components used. The models in RTDS environment have been developed for ideal voltage source inverters, their control schemes, filter models, coupling inductance model, lines models as well as a model for loads. Details of the models developed for implementation of grid-connected mode and its control scheme can be observed in Figs. 8.1- 8.6. The grid-connected microgrid circuit shown in Fig.4.1 is implemented in RTDS as shown in Fig 8.1. The RTDS model of the grid-connected mode of the microgrid includes the models of the inverter, LC filter, the coupling impedance and the grid. The firing pulse generator and triangle wave generator blocks are shown in Fig. 8.2. The PLL block in RTDS is shown in Fig. 8.3. It represents the PLL block diagram shown in Fig. 4.3. The power controller shown in Fig. 4.4 is presented in RTDS as shown in Fig. 8.4. The RTDS current controller model is shown in Fig. 8.5. It is similar to the current controller shown in Fig. 4.5. Fig. 8.6 shows the RTDS blocks of transforming the three-phase stationary (*ABC*) to *DQ* rotating coordinate system.

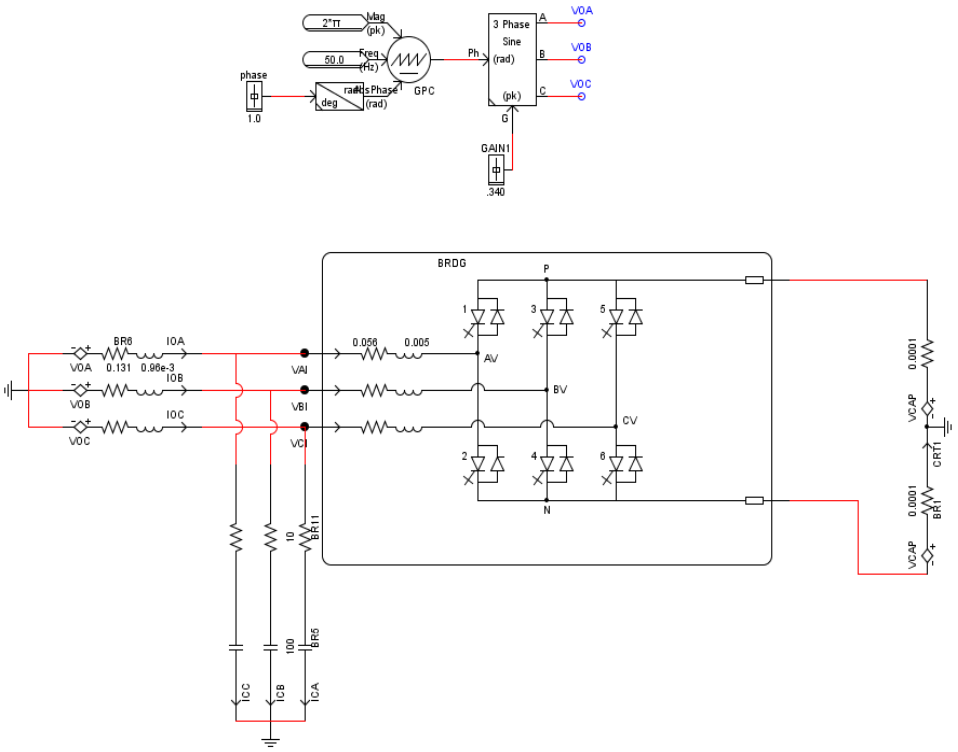

Figs. 8.1 Grid-connected mode in RTDS

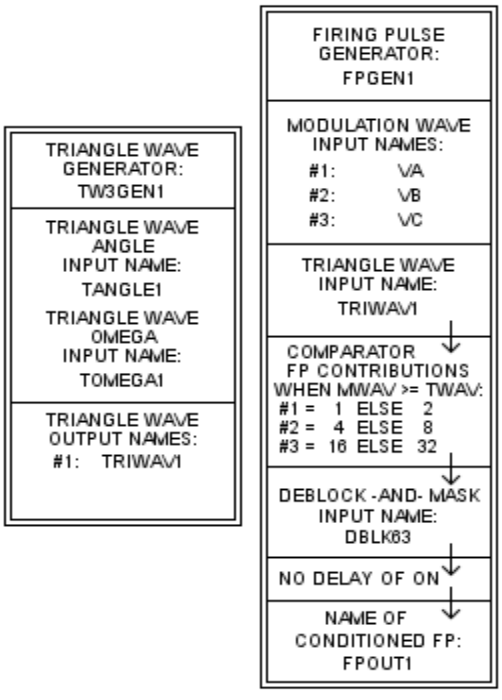

Figs. 8.2 VSC pulse and triangle wave generators in grid-connected mode

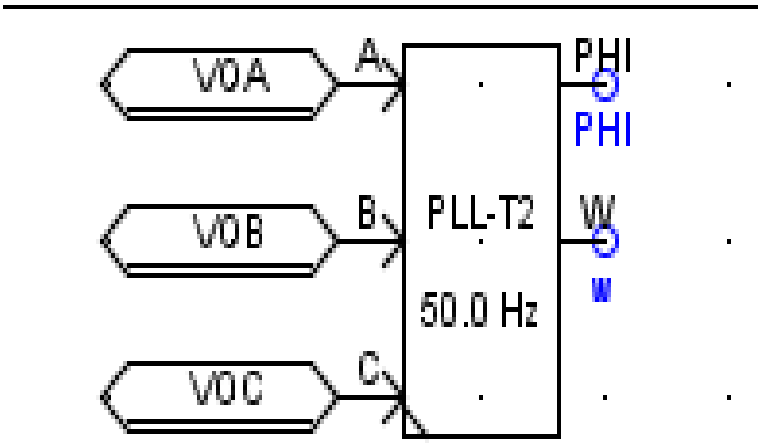

Fig. 8.3 PLL model

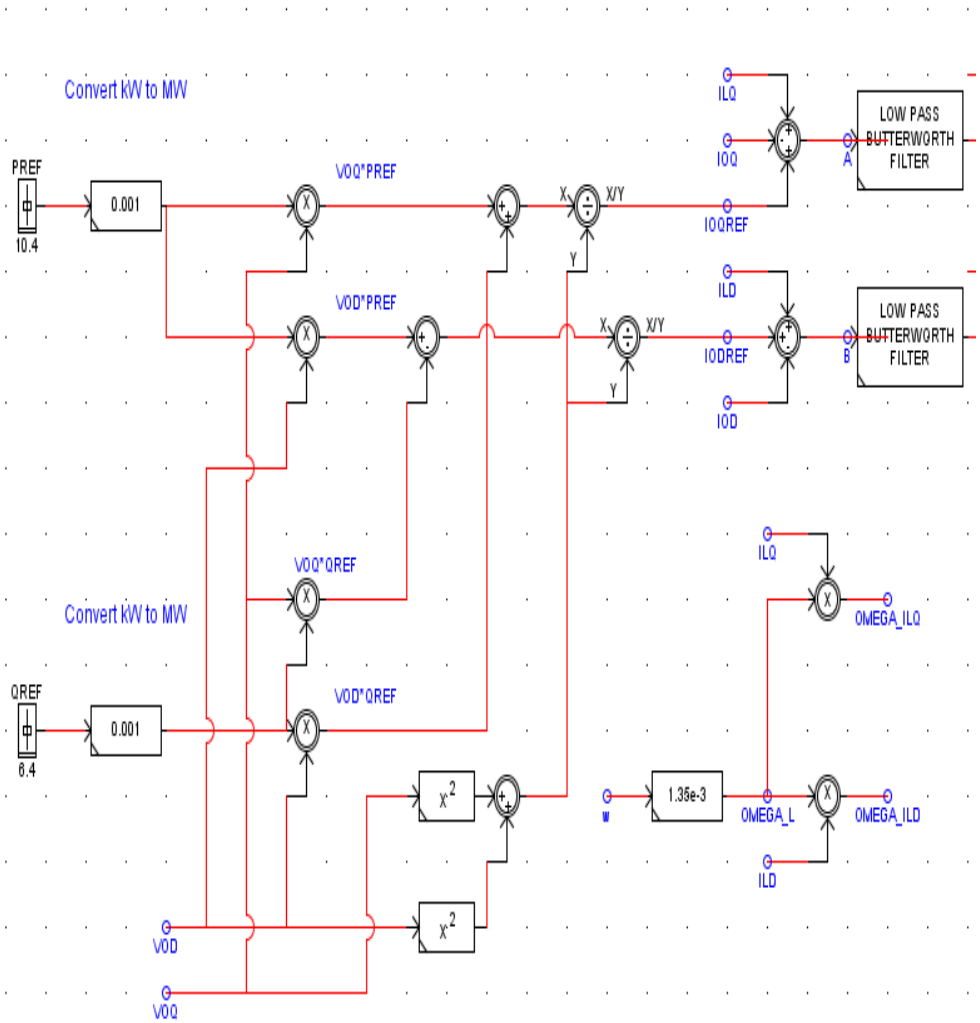

Figs. 8.4 Power controller of grid-connected mode

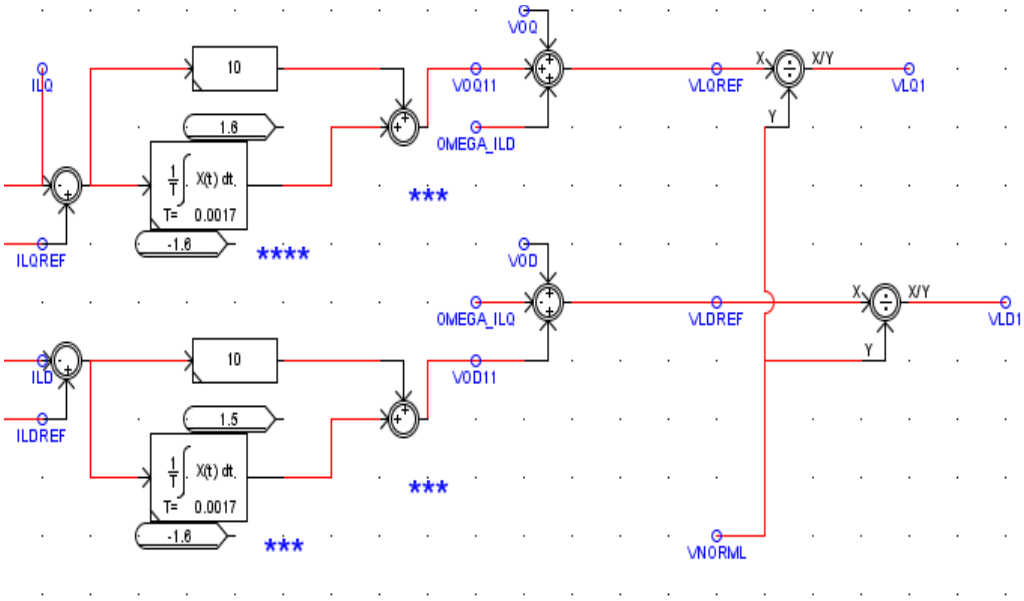

Figs. 8.5 Current controller of grid-connected mode

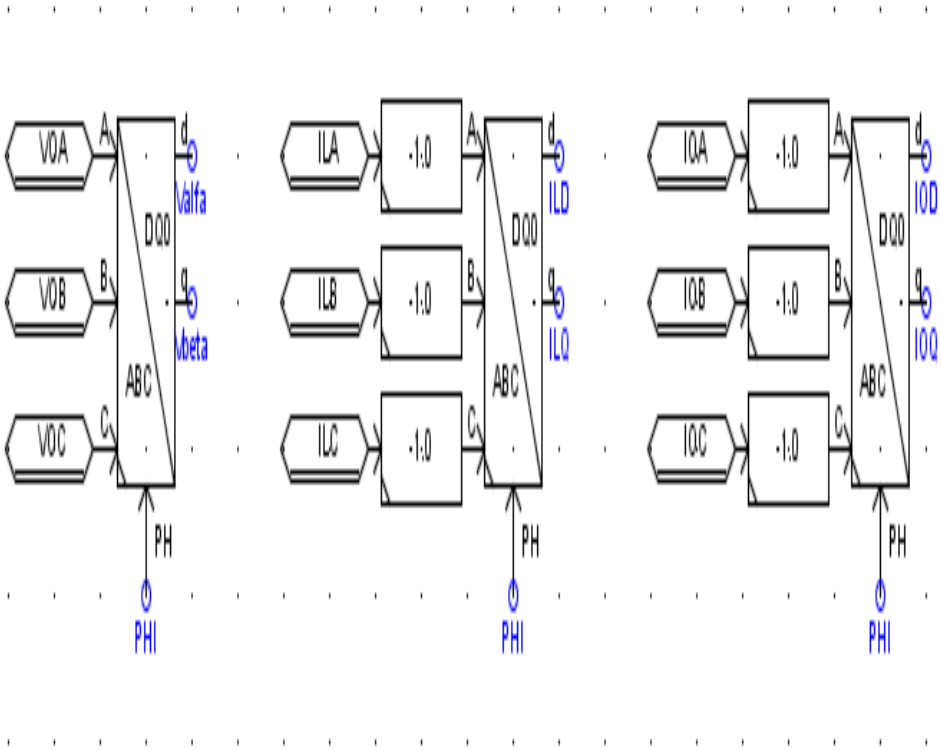

Figs. 8.6 ABC to DQ transformation of voltage and current signals of the grid-connected mode in RTDS

Details of the models developed for implementation of autonomous mode and its control scheme can be observed in Figs. 8.7 and 8.14. The equivalent model of the autonomous microgrid shown in Fig.3.1 is implemented in RTDS as shown in Fig. 8.7. The model includes the three-inverter based DGs, LC filter, coupling impedance, lines and loads. It is to the autonomous microgrid mode. The firing pulse generator and triangle wave generator blocks of the three inverters are shown in Fig. 8.8. The RTDS power controller model of the autonomous mode presented in Fig. 3.2 is shown in Fig. 8.9. The RTDS model of the voltage controller given in Fig. 3.5 is shown in Fig. 8.10. Using RTDS, the current controller model shown in Fig. 3.6 is implemented. The RTDS model of the current controller is shown in Fig. 8.11. Figs. 8.12-8.14 show the RTDS blocks of transforming the three-phase stationary (ABC) to DQ rotating coordinate system in the three DGs. The performance and accuracy of the developed models have been investigated through different scenarios and case studies in the next two chapters.

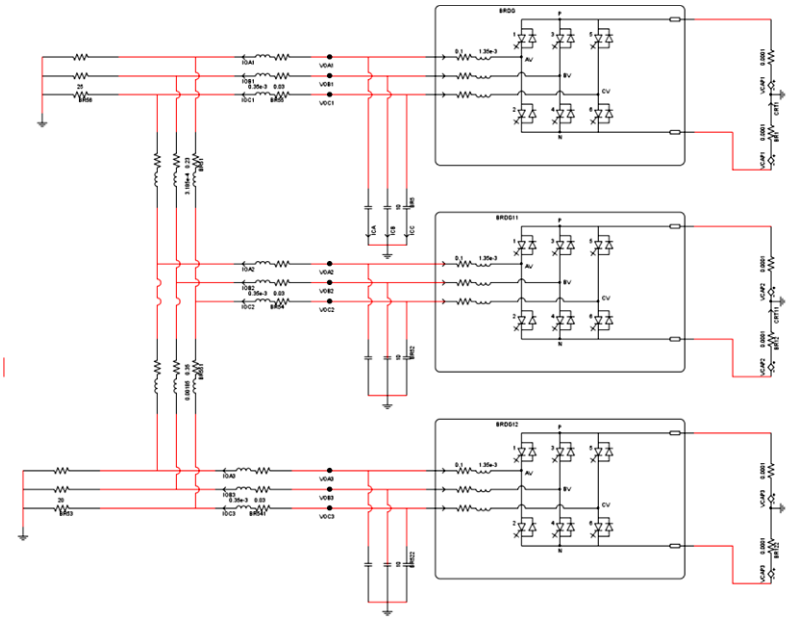

Figs. 8.7 Autonomous mode microgrid circuit in RTDS

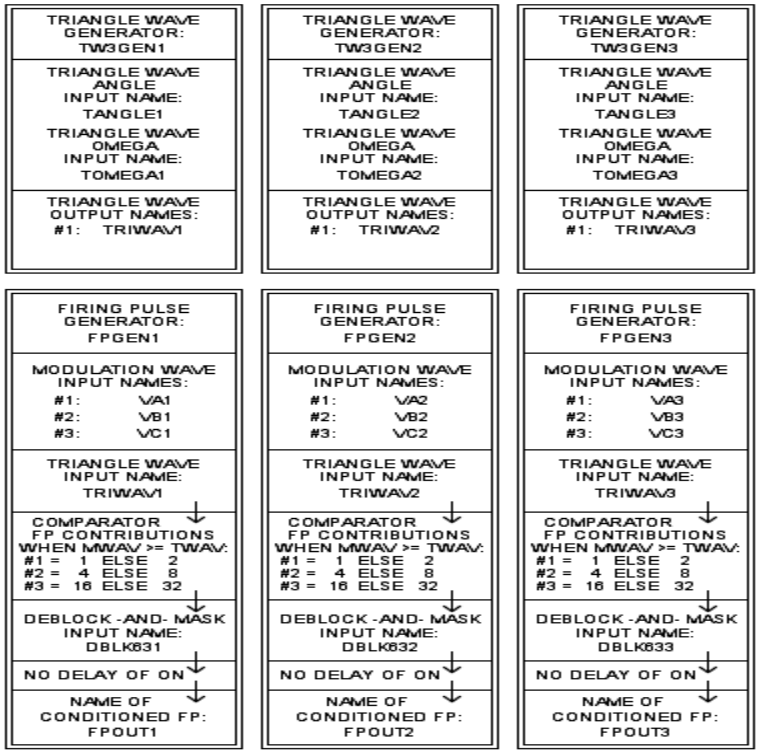

Figs. 8.8 VSC pulse and triangle wave generators in autonomous mode

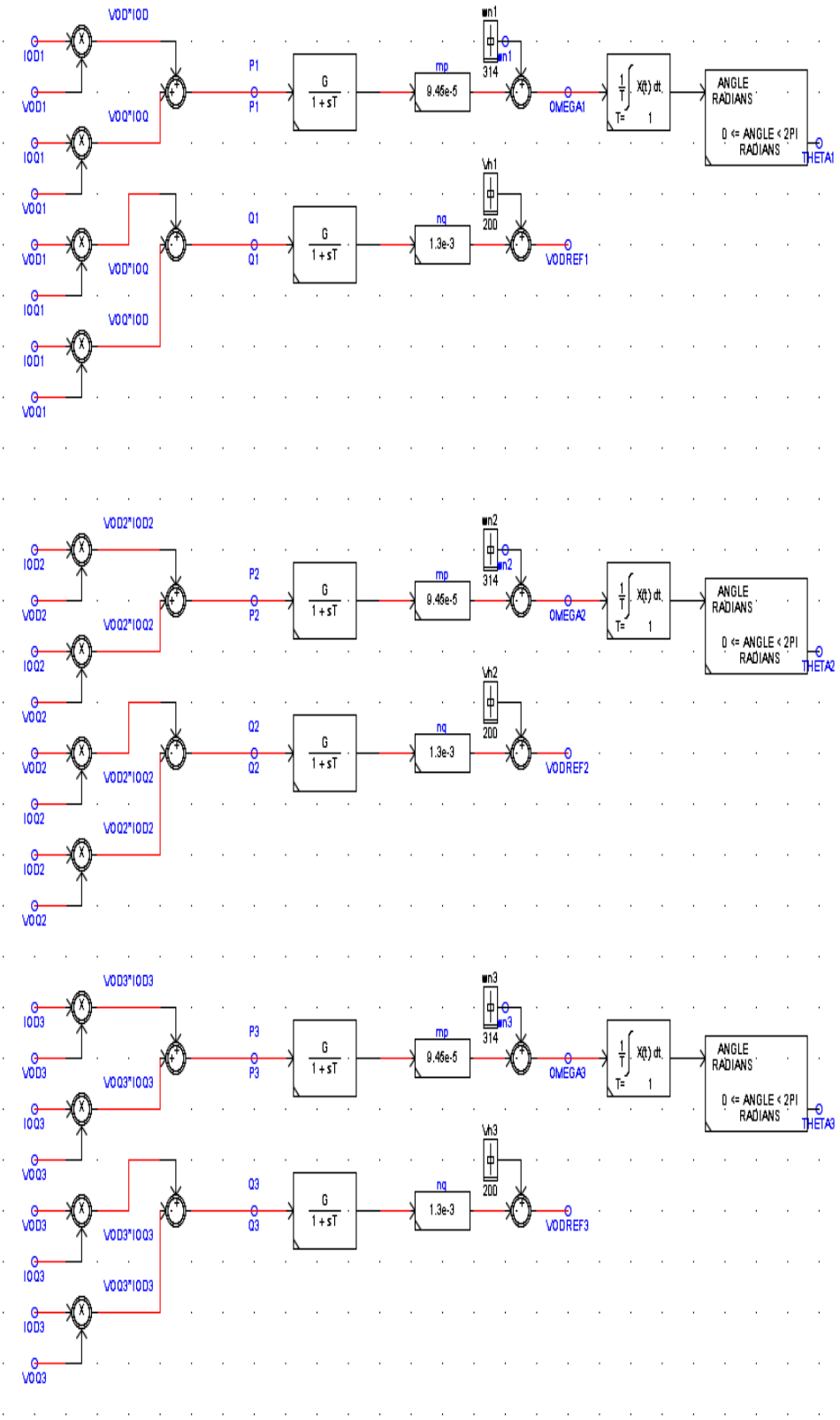

Figs. 8.9 Power controller of autonomous mode

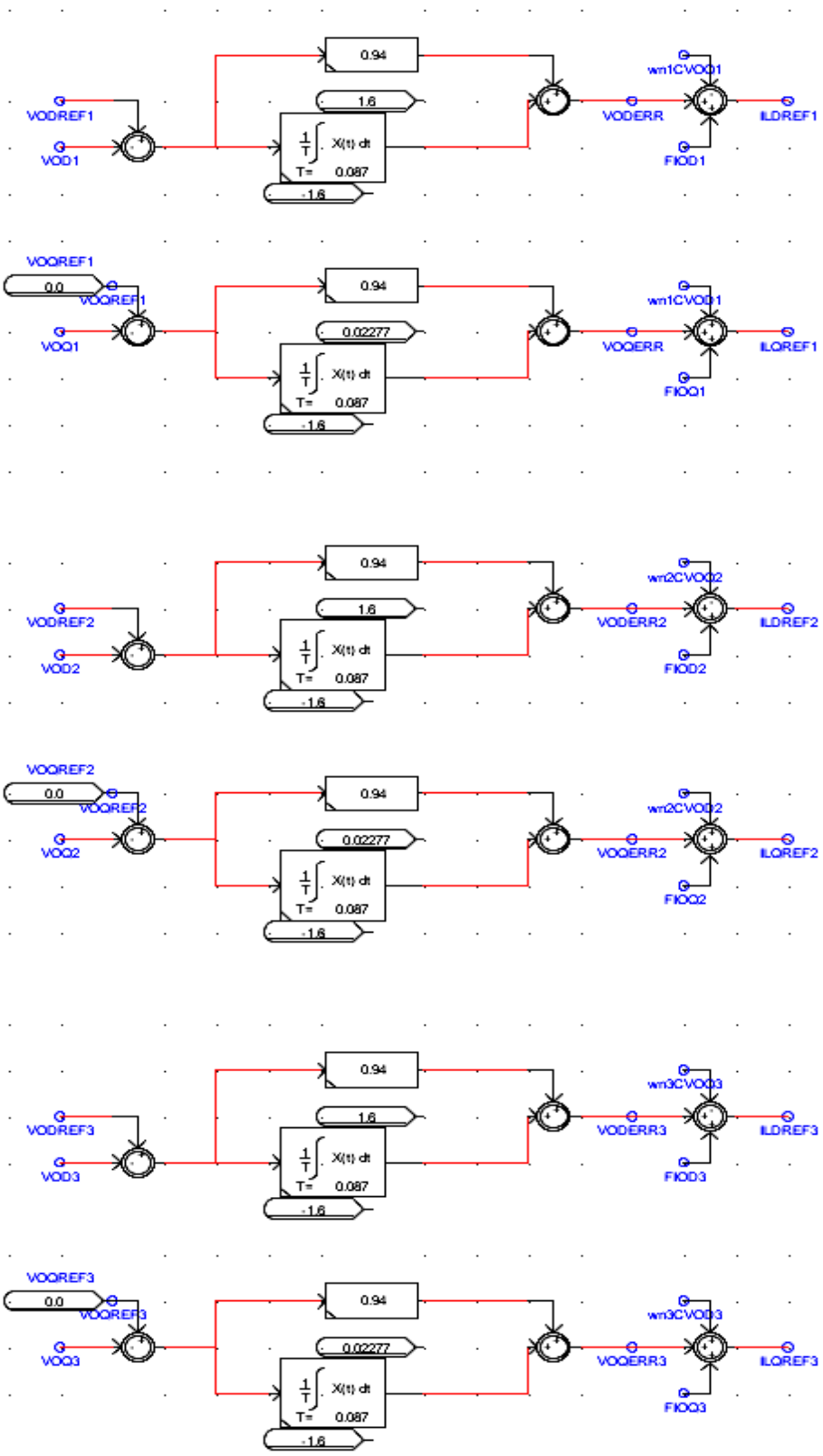

Figs. 8.10 Voltage controller of autonomous mode

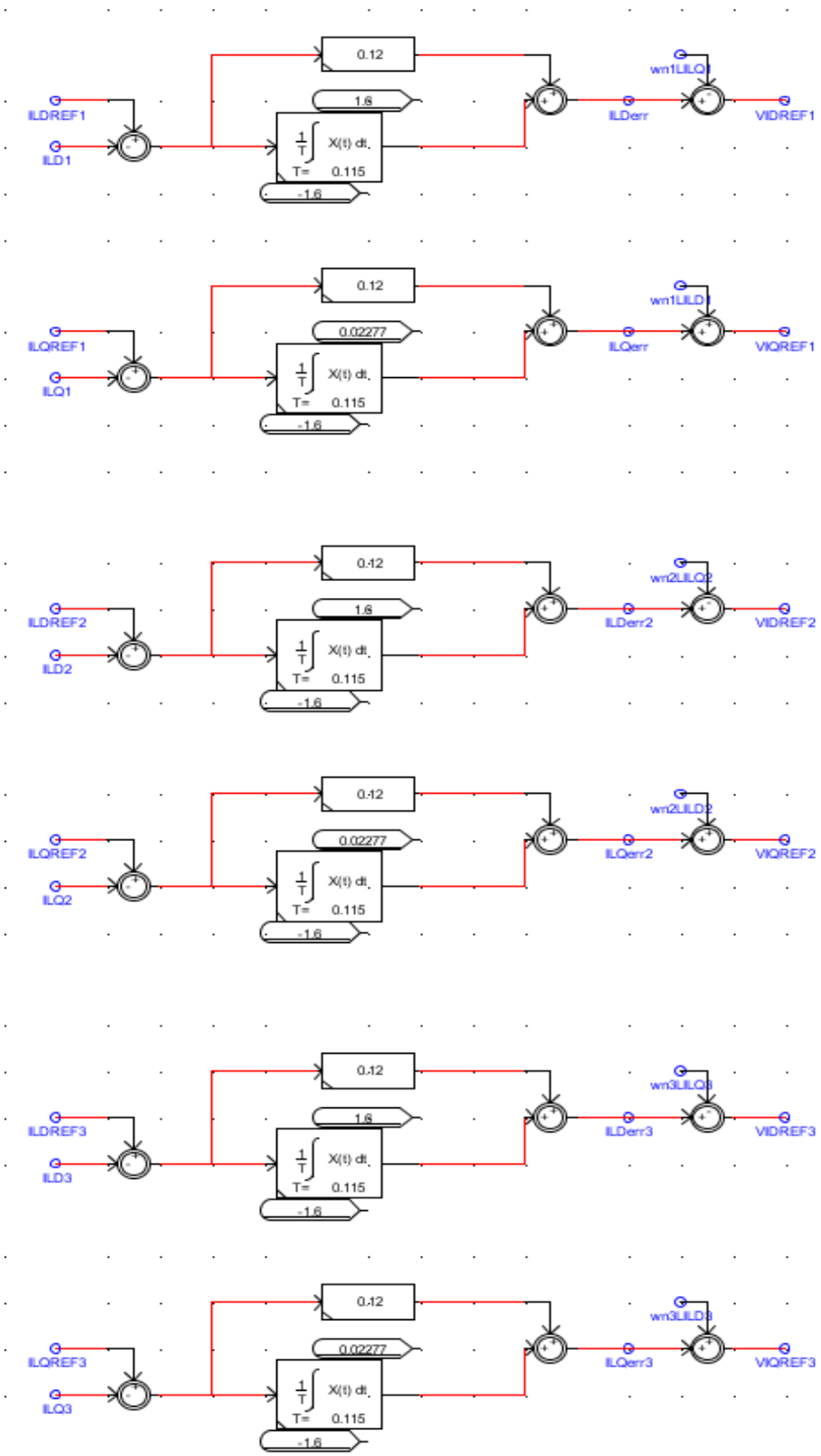

Figs. 8.11 Current controller of autonomous mode

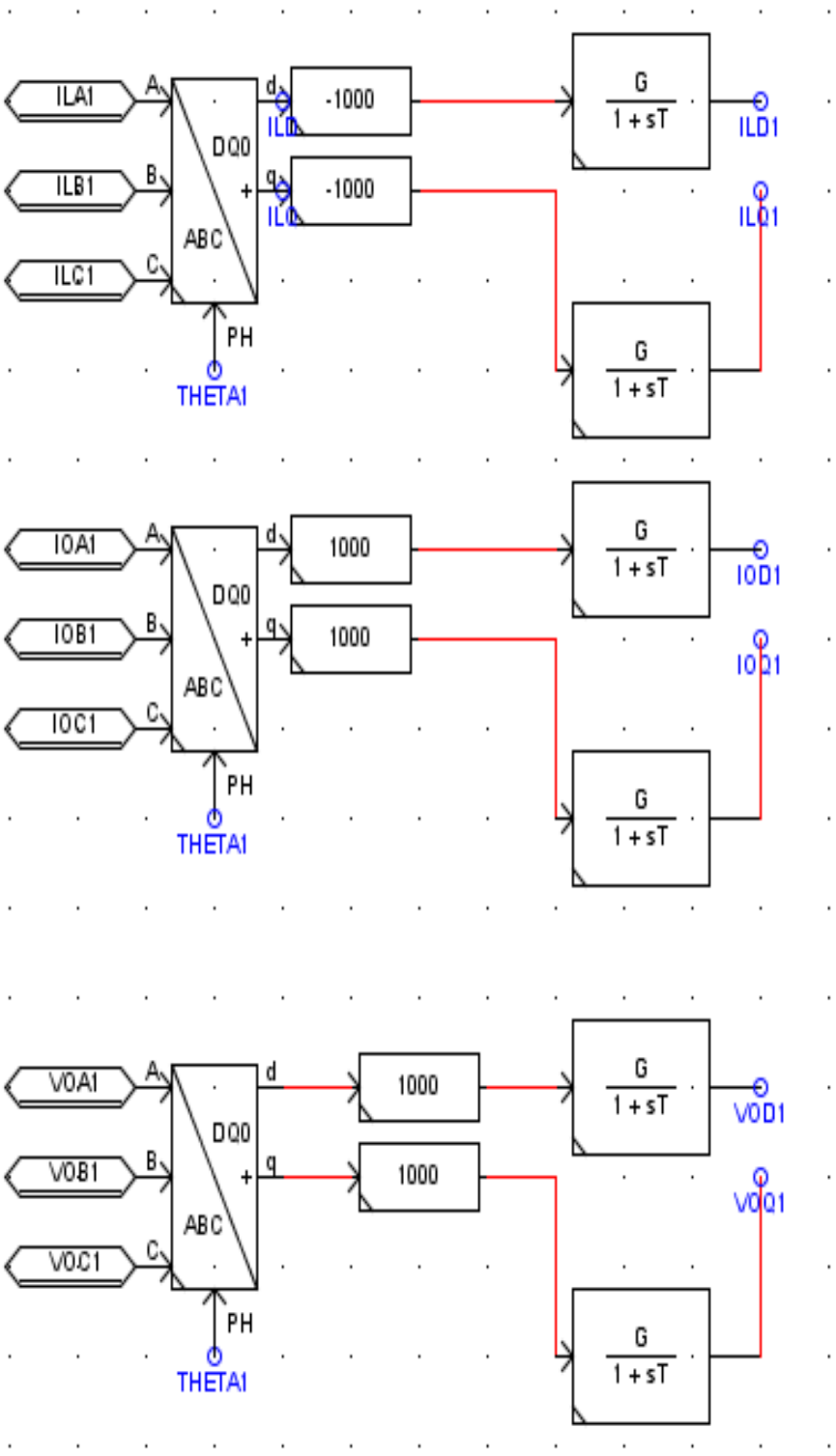

Figs. 8.12 ABC to DQ transformation of current and voltage signals of the autonomous mode (DG1) in RTDS

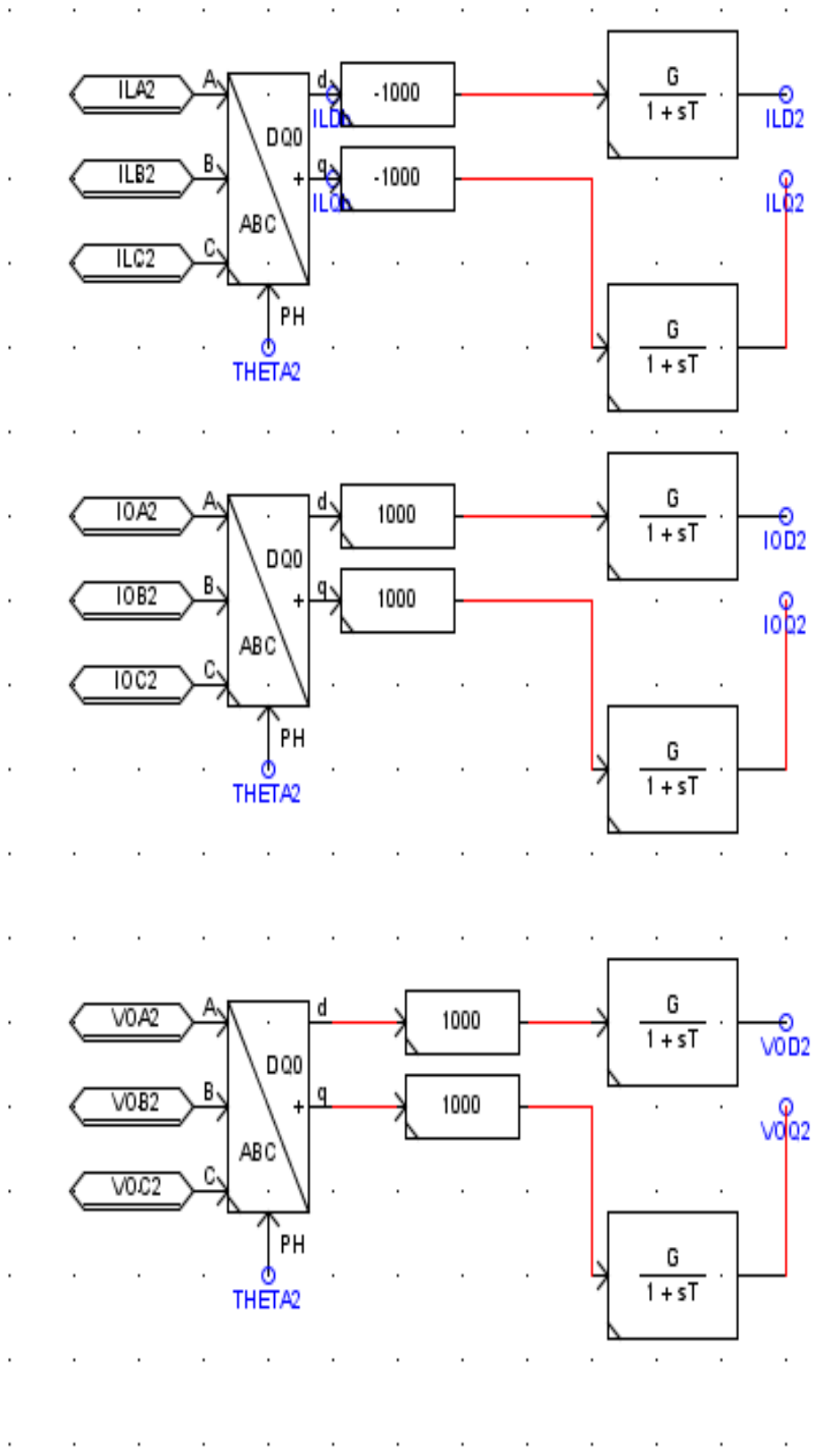

Figs. 8.13 ABC to DQ transformation of current and voltage signals of the autonomous mode (DG2) in RTDS

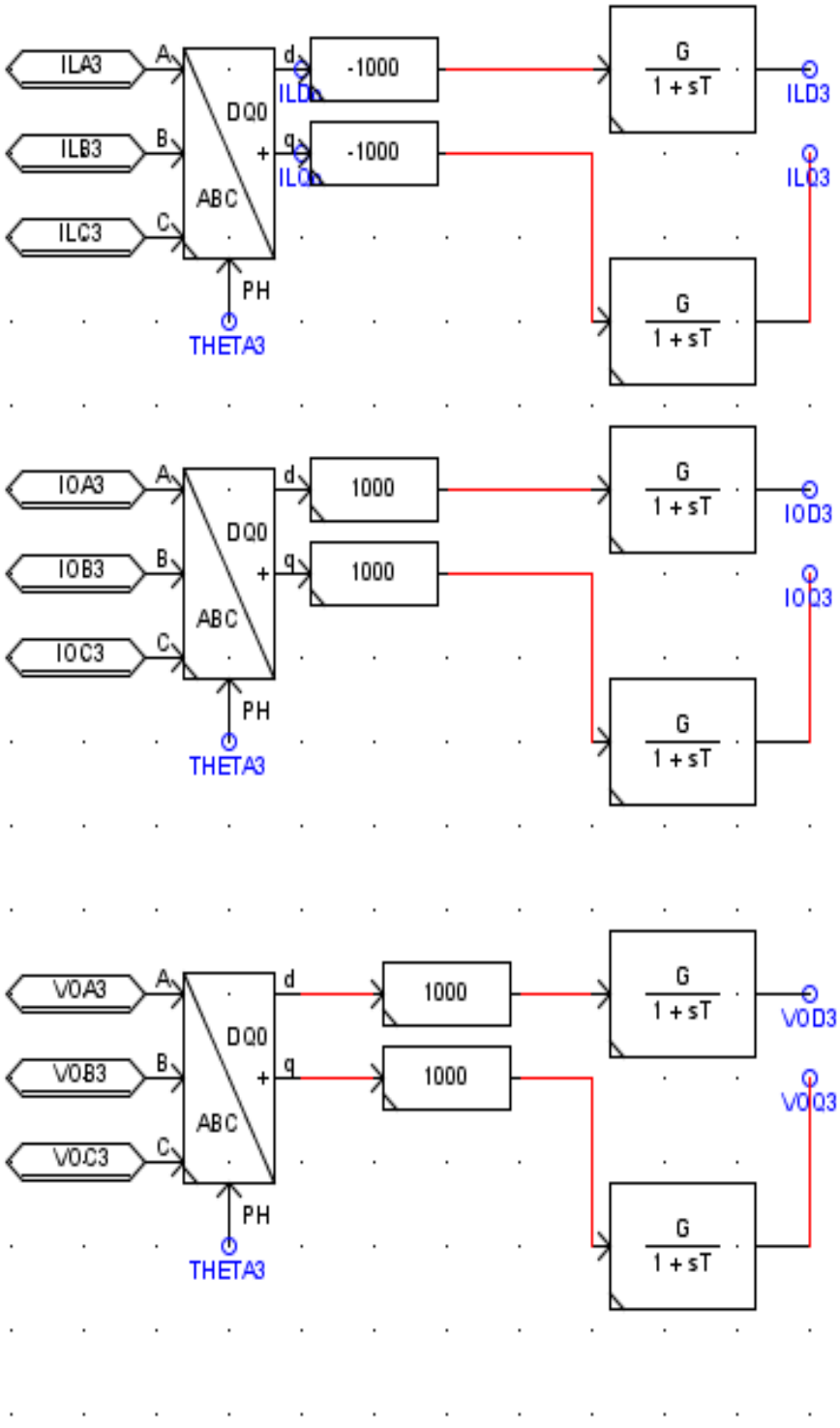

Figs. 8.14 ABC to DQ transformation of current and voltage signals of the autonomous mode (DG3) in RTDS

CHAPTER 9

RESULTS AND DISCUSSION OF GRID-CONNECTED MICROGRID IN RTDS

In this chapter, the performance of the proposed controller has been tested extensively using a real-time digital simulator (RTDS). The microgrid presented in chapter four operating in grid-connected mode is analyzed using the RTDS as well. The setup of the microgrid including the interfacing inverters is simulated using the RTDS. The optimal parameters of the controller obtained by PSO are used to assess the controller performance in the real time. The results of the system obtained using the RTDS have been compared with those obtained from MATLAB simulation to prove the validity and accuracy of the proposed controller model.

The stability of an inverter-based microgrid in the grid-connected mode has been investigated in the RTDS environment. The step response for different cases of heavy and light injected active and reactive power exported to the grid using RTDS has been investigated to explore the effectiveness of the controller and the ability of the inverter-based DG.

9.1 STEADY STATE RESPONSE

The steady state performance of the grid-connected microgrid, using the optimal parameters obtained by PSO has been first investigated before applying any disturbance. The results of the steady state performance are presented in Figs. 9.1- 9.7. The steady state performance of PCC voltage is depicted in Fig. 9.1. The measured as well as the reference values of both active and reactive powers are given in Fig. 9.2 and Fig. 9.3 respectively. From the results, it is obvious that the measured power tracks the reference power closely. The simulated results of both three phase inductor and output currents are shown in Figs. 9.4-9.5 respectively. Fig. 9.6 presents the waveforms of the grid voltage while its d and q components are shown in Fig. 9.7.

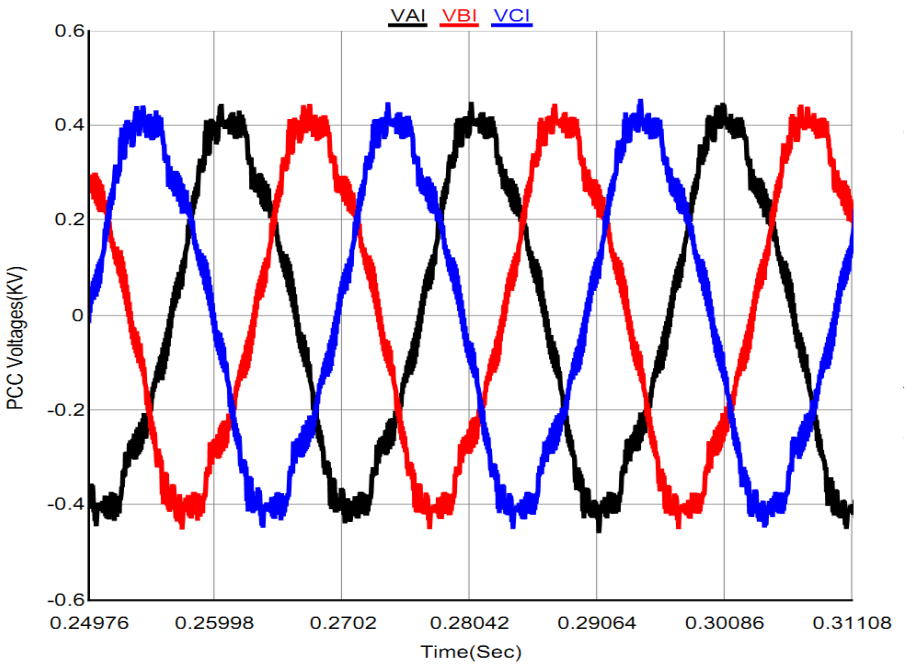

Fig. 9.1 PCC voltage

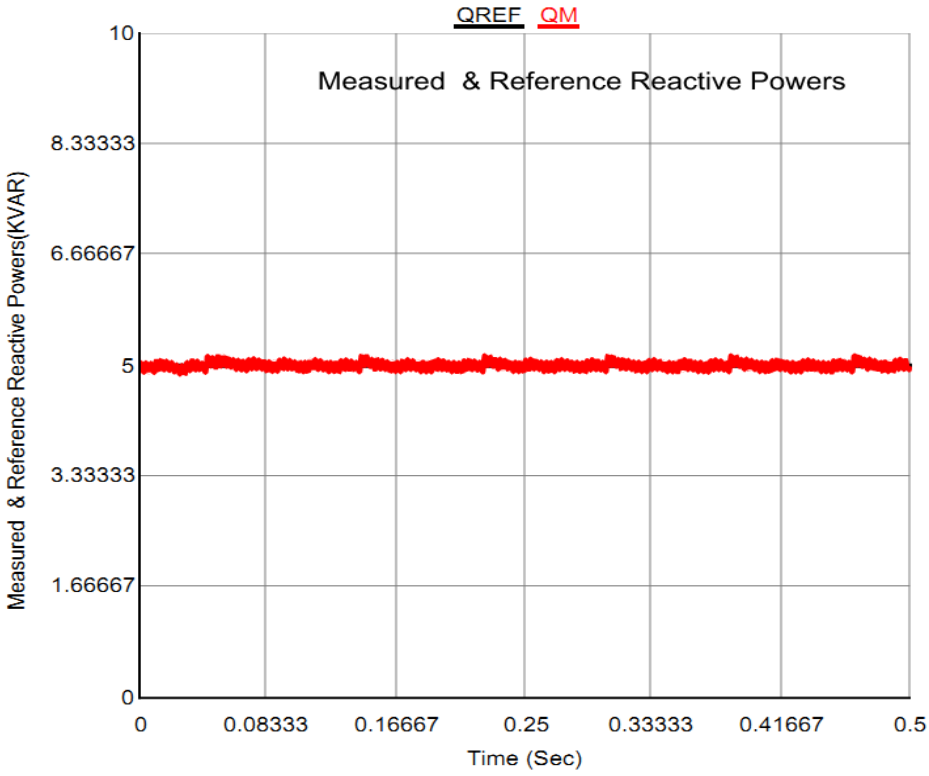

Fig. 9.2 Measured and reference reactive power

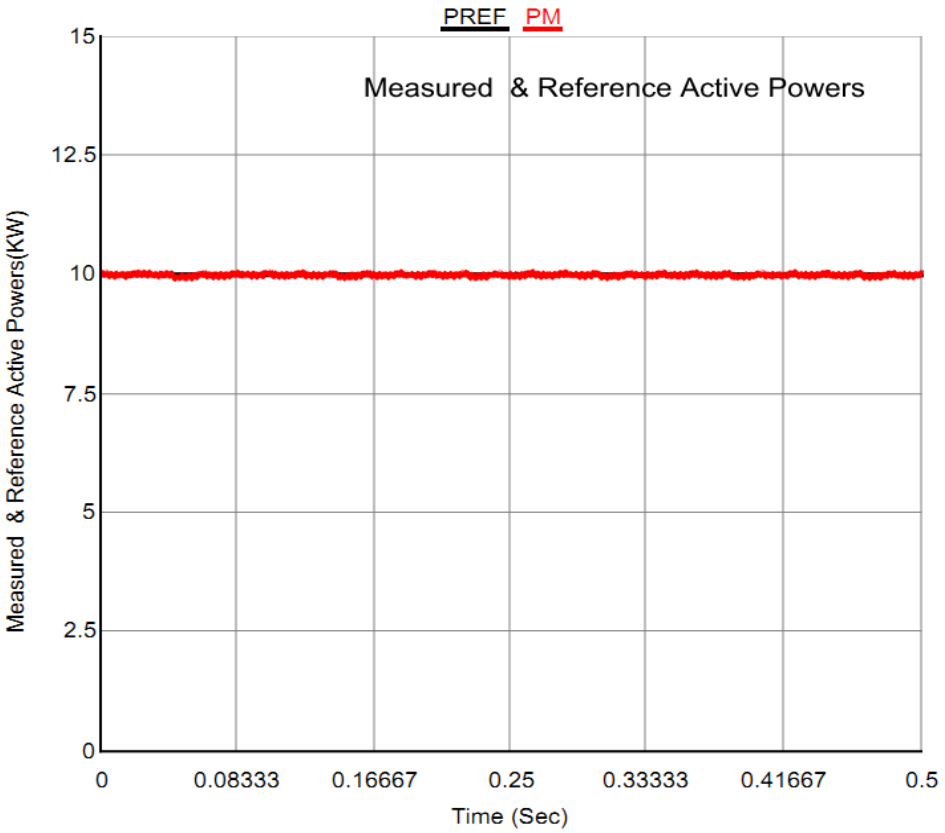

Fig. 9.3 Measured and reference active power

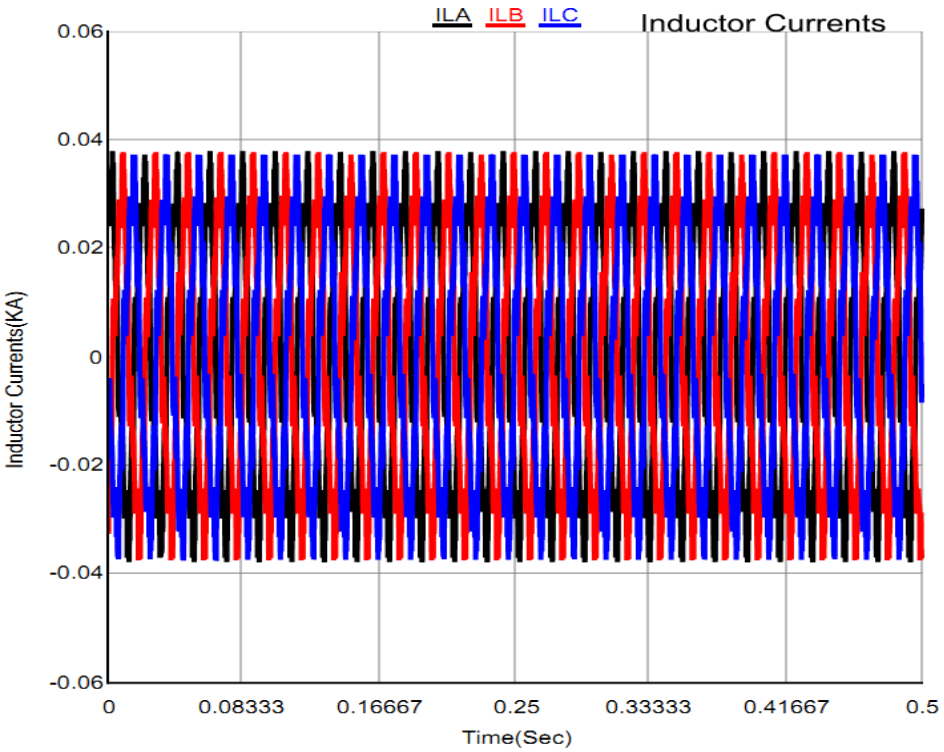

Fig. 9.4 Three phase inductor currents

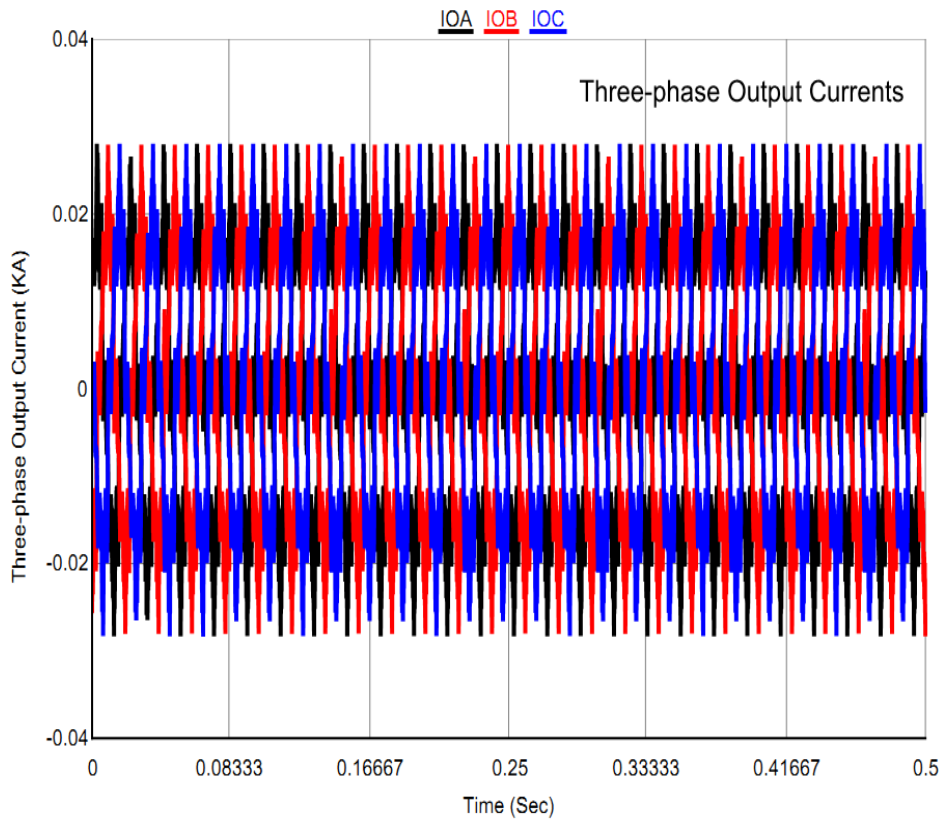

Fig. 9.5 Three phase output currents

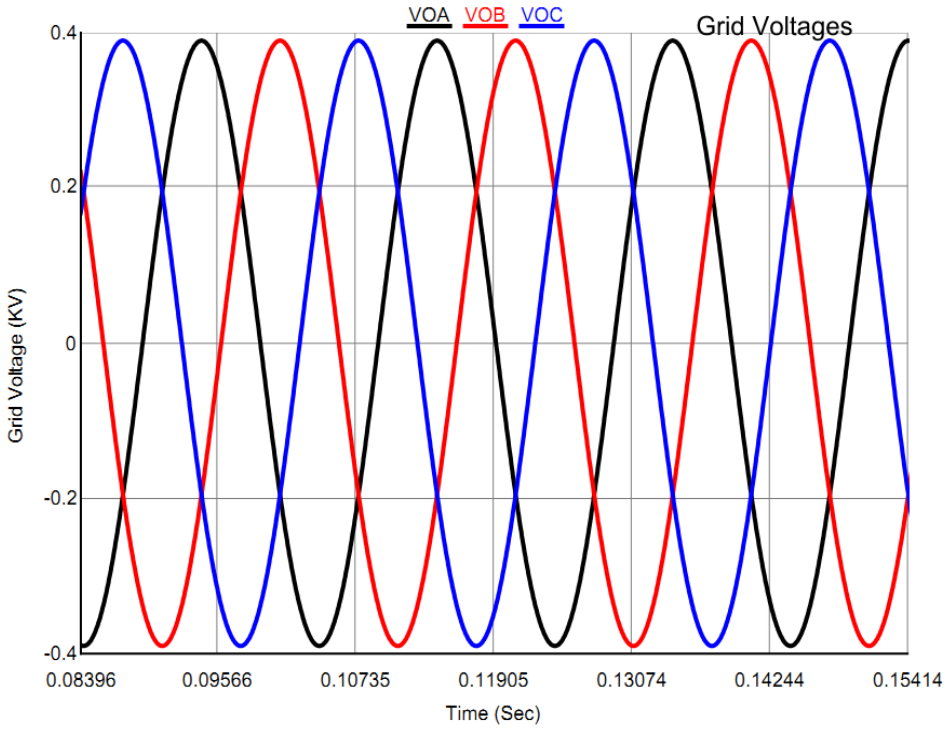

Fig. 9.6 Grid voltage

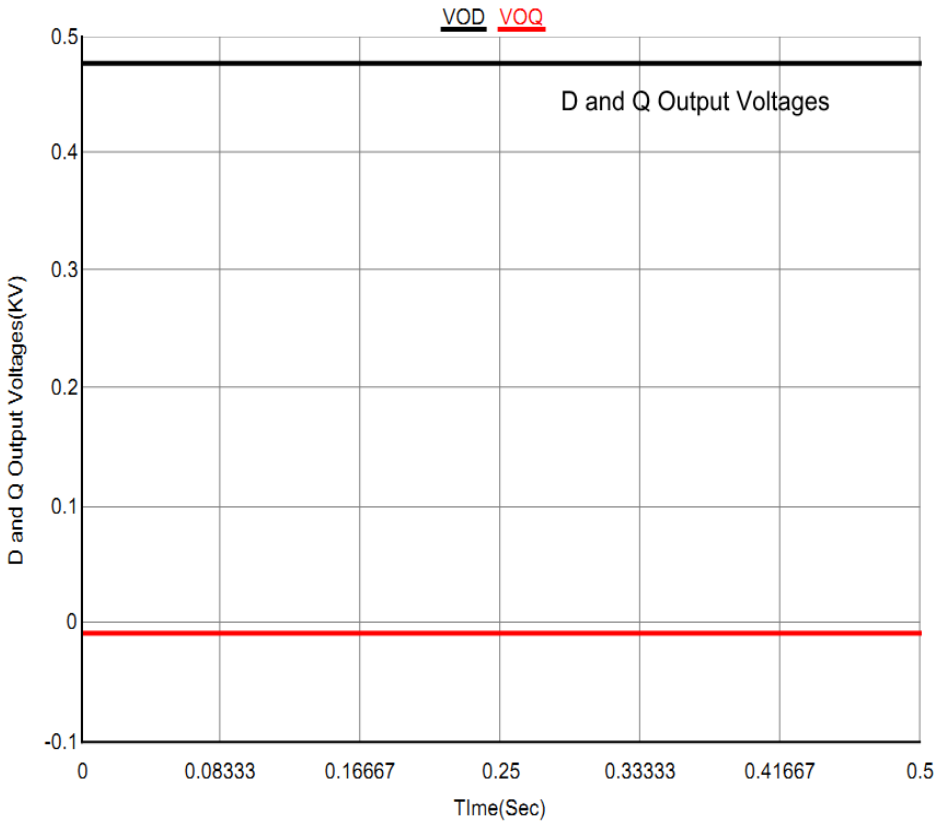

Fig. 9.7 D and Q components of the grid voltage

9.2 SYSTEM STEP RESPOSNE

A series of tests are conducted in the RTDS environment to examine the effectiveness of the proposed controller for different step changes in active and reactive powers as well as the ability of the inverter to inject the required powers. Some of the results obtained using the RTDS are compared with those obtained from MATLAB simulation to explore the validity of the proposed controller. The results show that the use of the optimization technique reflected noticeable improvements on the system response and system stability.

9.2.1 Active Power Step Change

The initial reference active and reactive powers are set to 10 KW and 5 KVAR respectively. Then a disturbance is applied to the system by stepping down the active

power to 5 KW to check out the system response. The system response and performance under such disturbance are shown in Figs. 9.8 - 9.14. The results obtained from the step response for the PCC voltage is shown in Fig. 9.8. As could be seen from Fig. 9.9, the controller capability during the step change is reasonable so that the active power is tracking the reference power without significant overshoot and delay time. The measured as well as the reference values of the reactive power is given in Fig. 9.10. The simulated results of both three phase inductor and output currents are presented in Figs. 9.11-9.12 respectively. Fig. 9.13 shows the waveforms of the grid voltage while its d and q components are depicted in Fig. 9.14.

The waveforms of the three phase output currents conducted in the RTDS shown in Fig. 9.12 is compared with the MATLAB simulation results of the three output currents presented in Fig. 7.8 to verify the MATLAB results. The results given by both figure prove the validity and accuracy of the proposed controller model. Using the optimal parameters allowed the proposed controllers to be capable of tracking the reference power perfectly without significant overshoot. On the other hand, the use of optimal parameters of the proposed controllers has enhanced the system performance and stability.

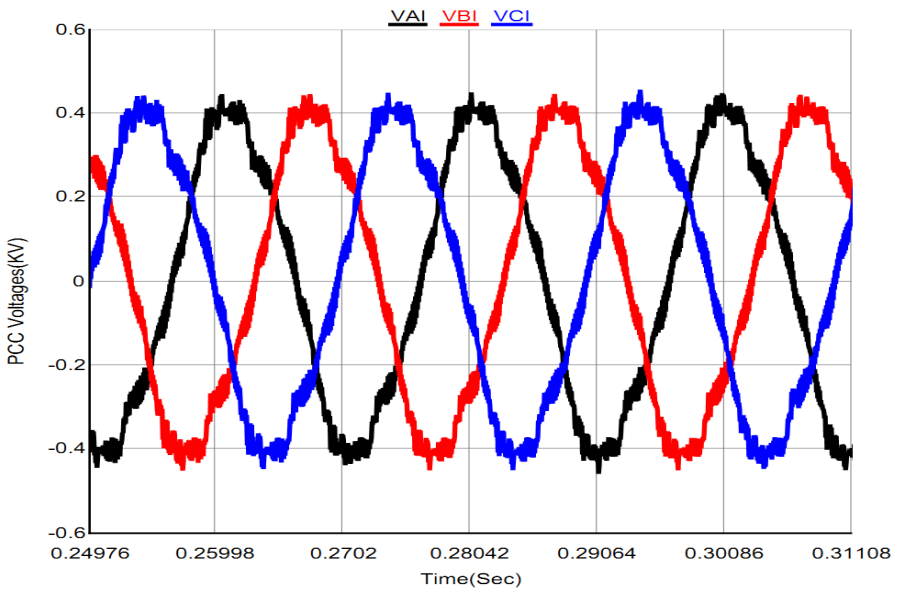

Fig. 9.8 PCC voltage

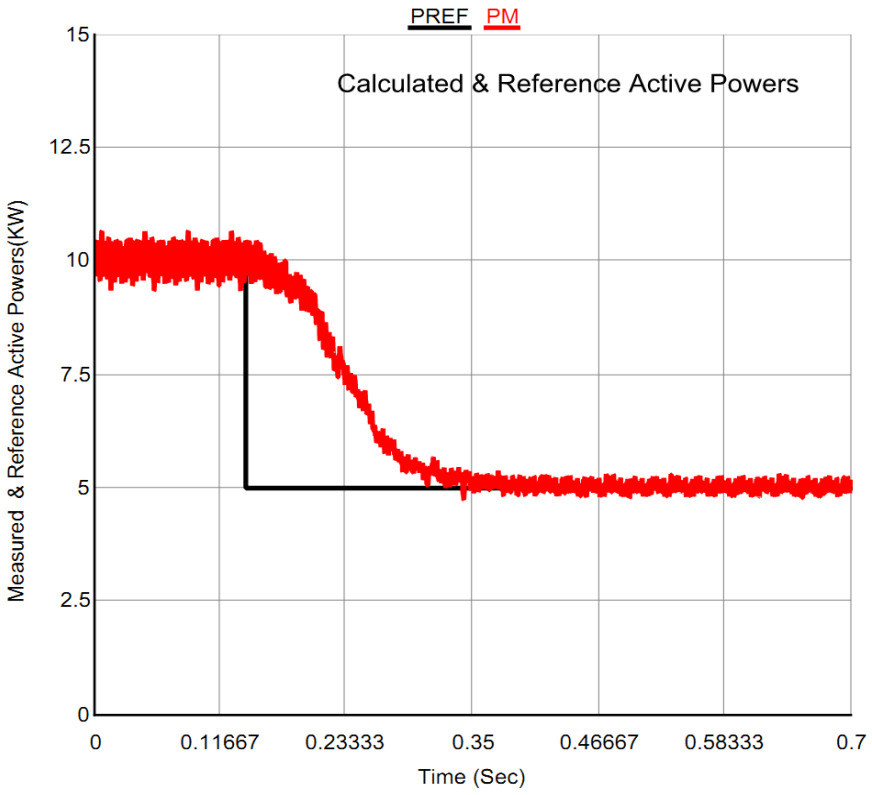

Fig. 9.9 Measured and reference active power

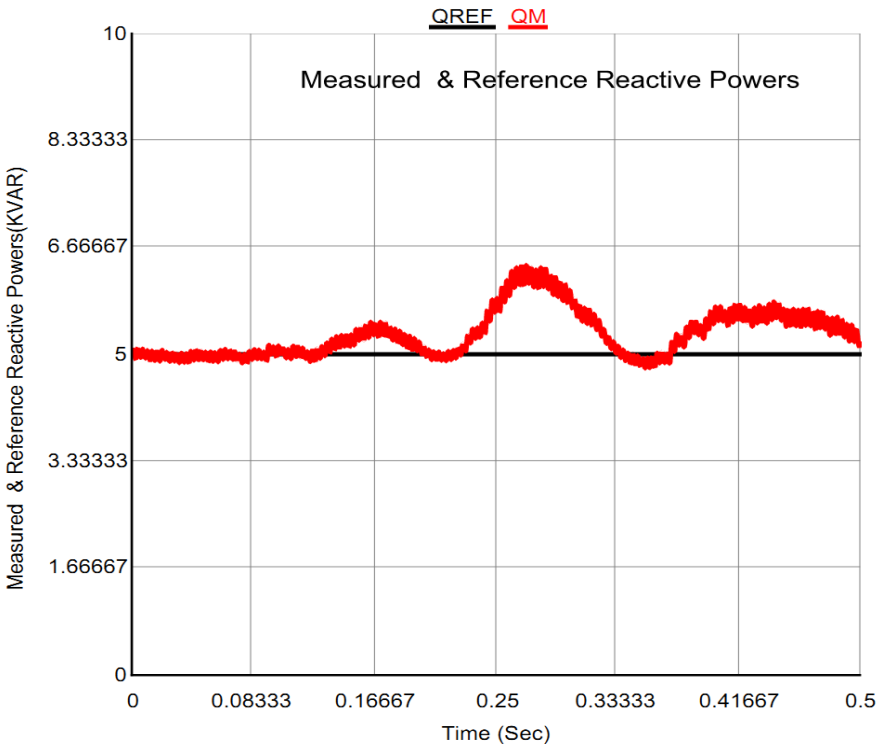

Fig. 9.10 Measured and reference reactive power

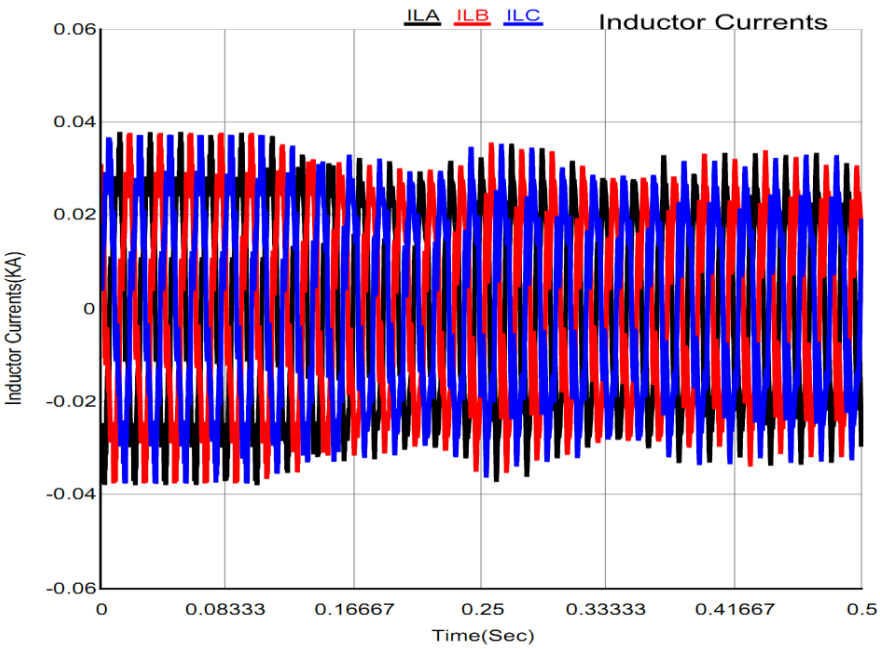

Fig. 9.11 Three phase inductor currents

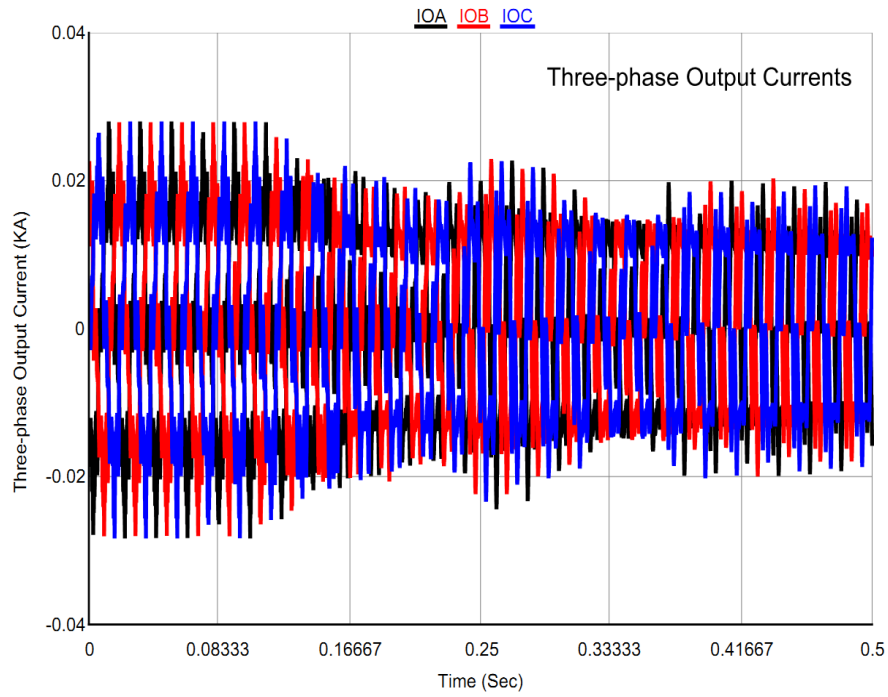

Fig. 9.12 Three phase output currents

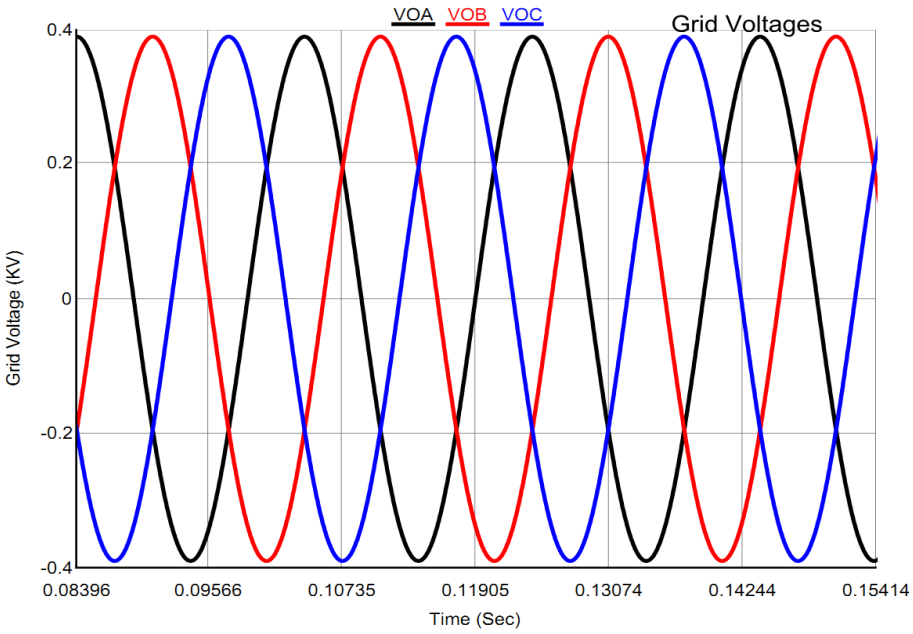

Fig. 9.13 Grid voltage

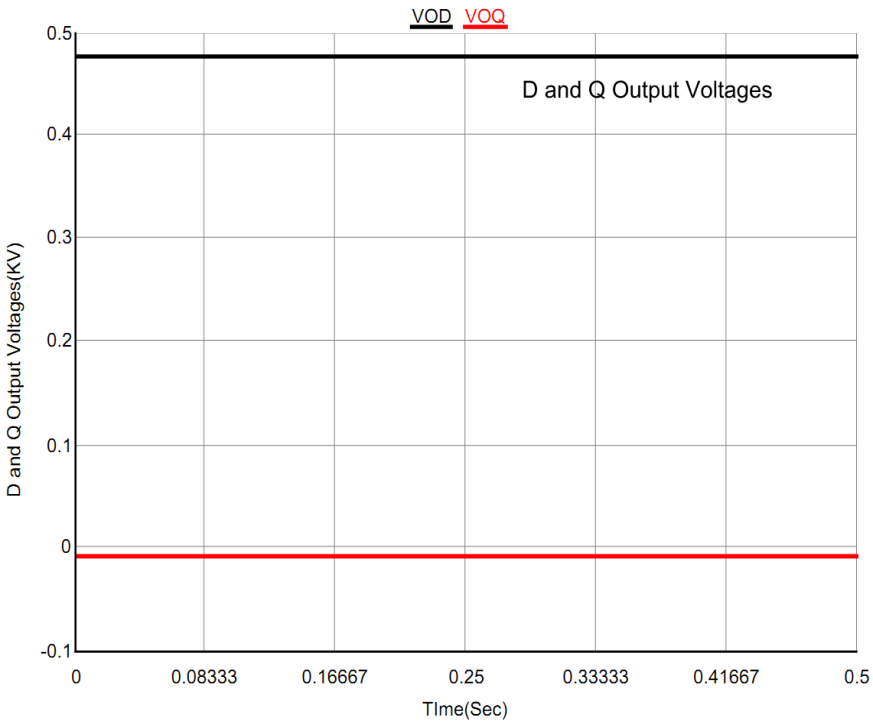

Fig. 9.14 D and Q components of the grid voltage

Instead of using step down disturbance, a step up disturbance has been applied to the system to investigate the system response. The reference active power is stepped up from 5 KW to 10 KW. Figs. 9.15- 9.19 present the system response and performance under this disturbance. Fig. 9.15 shows the PCC voltage under this step change. Fig. 9.16 illustrates how the tracking of the reference power to the active power is significant with acceptable overshoot and delay time. The measured and reference reactive power is depicted in Fig. 9.17. The three phase inductor currents and the three phase output currents are given in Fig. 9.18 and Fig. 9.19 respectively. It is observed that using the optimal parameters helped the proposed controllers to track the reference in the step up changes as well as step down changes.

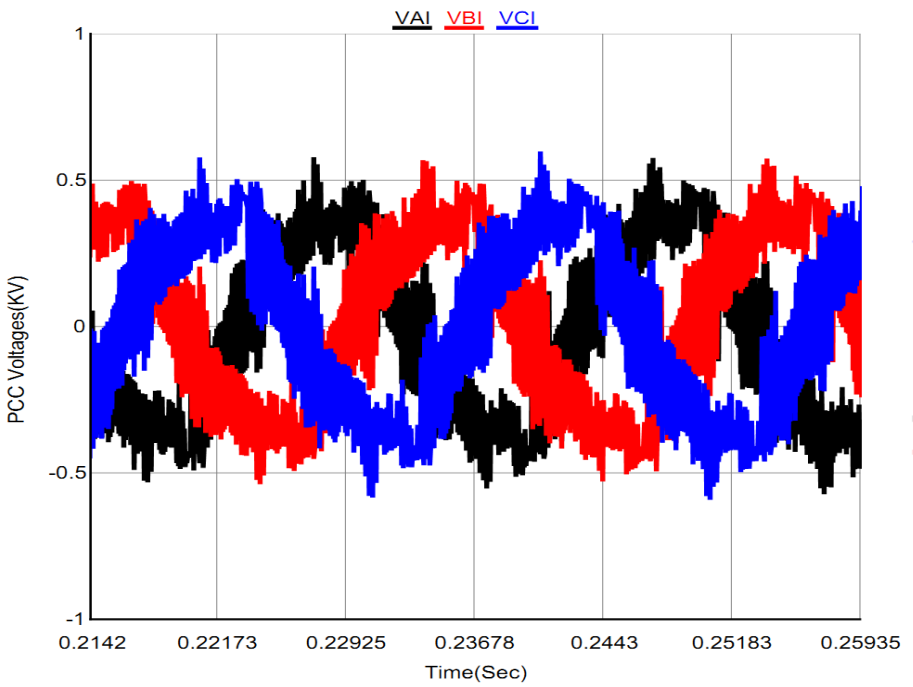

Fig. 9.15 PCC voltage

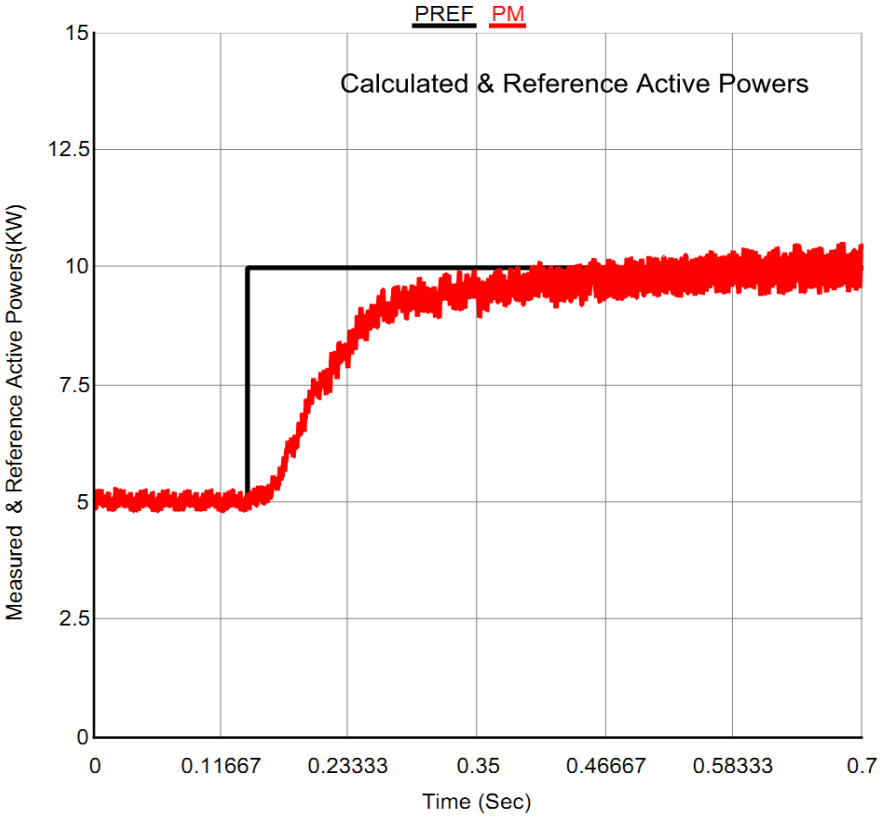

Fig. 9.16 Measured and reference active power

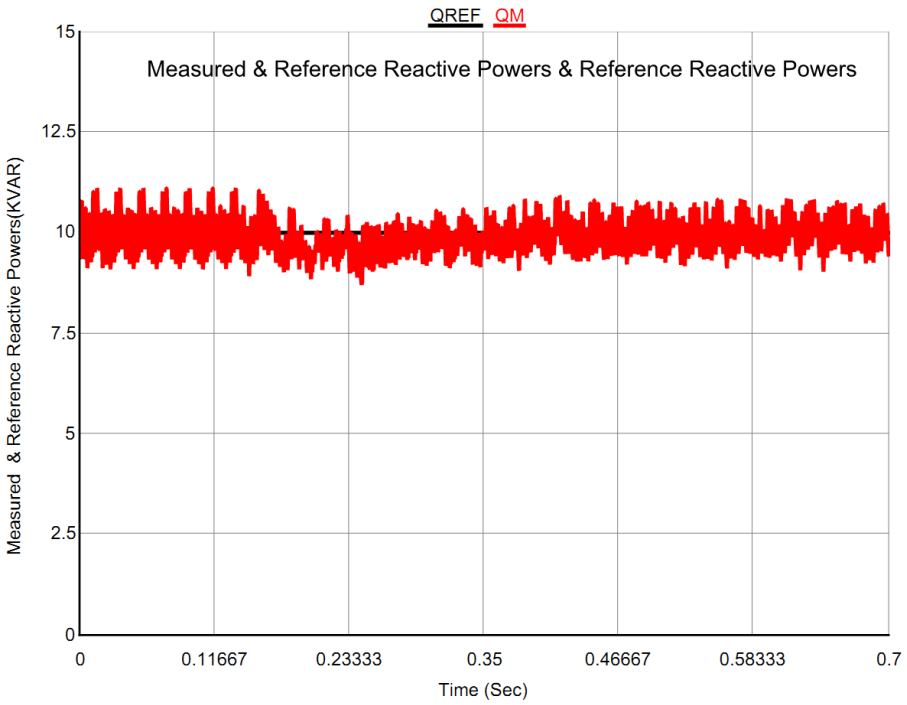

Fig. 9.17 Measured and reference reactive power

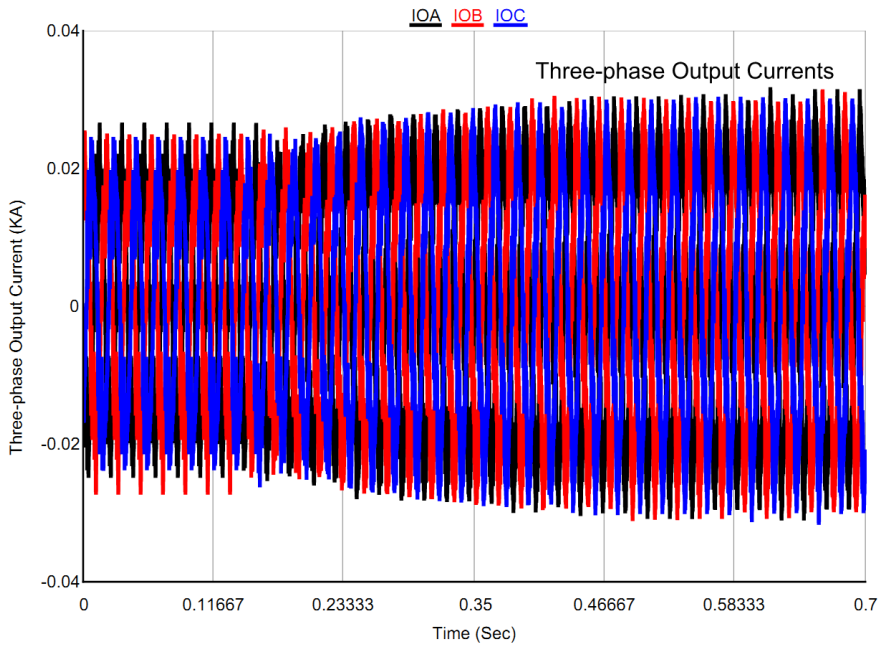

Fig. 9.18 Three phase output currents

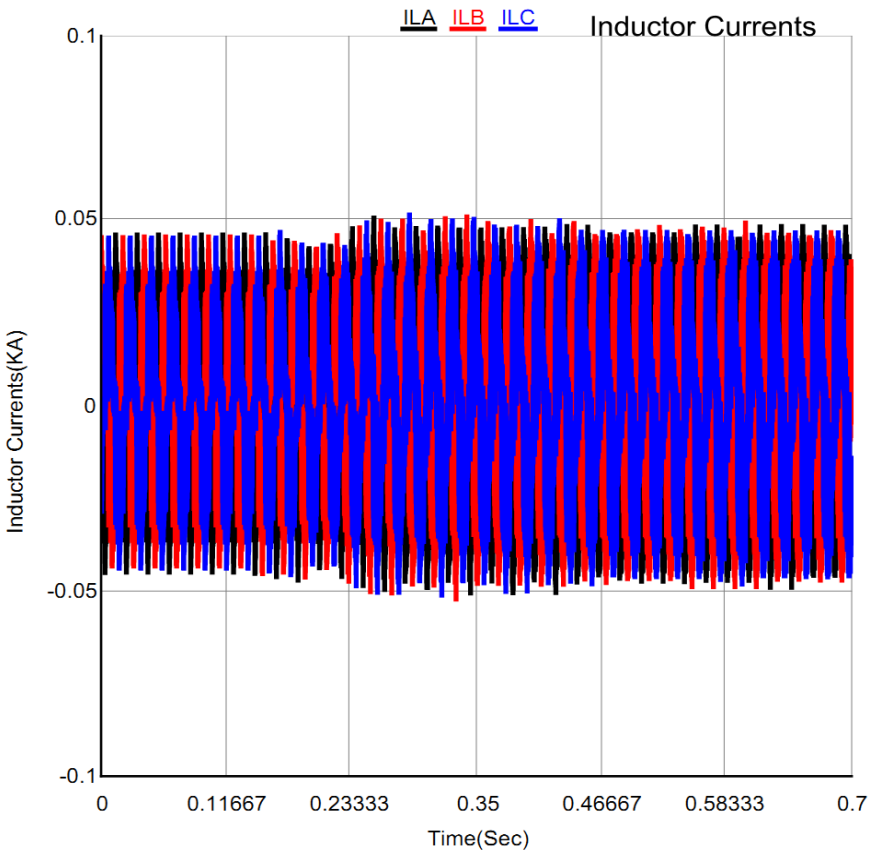

Fig. 9.19 Three phase inductor currents

Now a further step up change in the injected active power is conducted to examine the capability of the proposed controller and inverter to inject sever active power. The injected power has been stepped up from 5 KW to 20 KW. The system response and performance under this disturbance are depicted in Figs. 9.20 - 9.24. PCC voltage is shown in Fig. 9.20. The examination of tracking the reference active power is illustrated in Fig. 9.21 while Fig. 9.22 shows the reactive power following. Figs. 9.23 and 9.24 present the waveforms of the three phase inductor and output currents respectively.

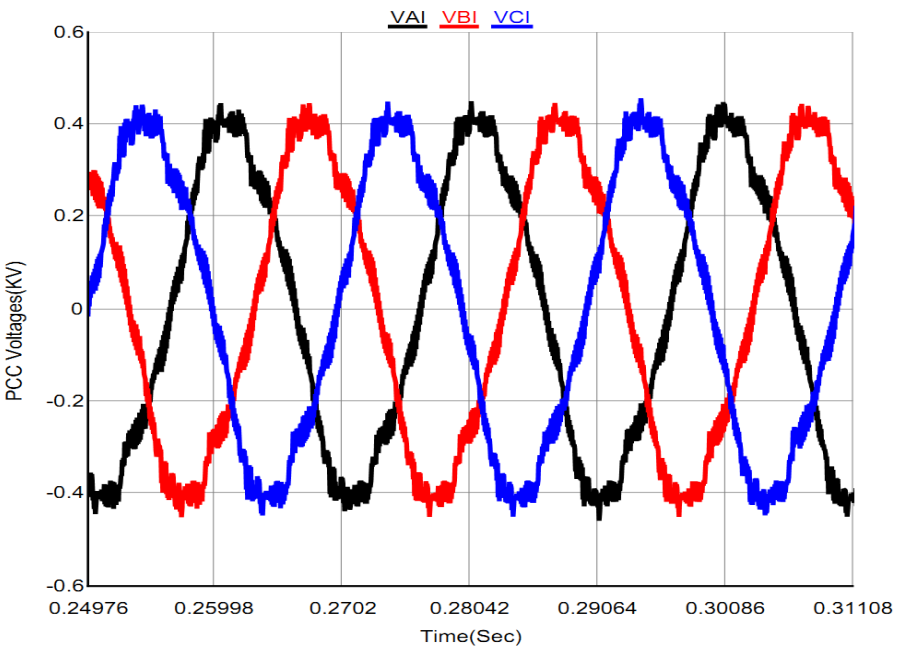

Fig. 9.20 PCC voltage

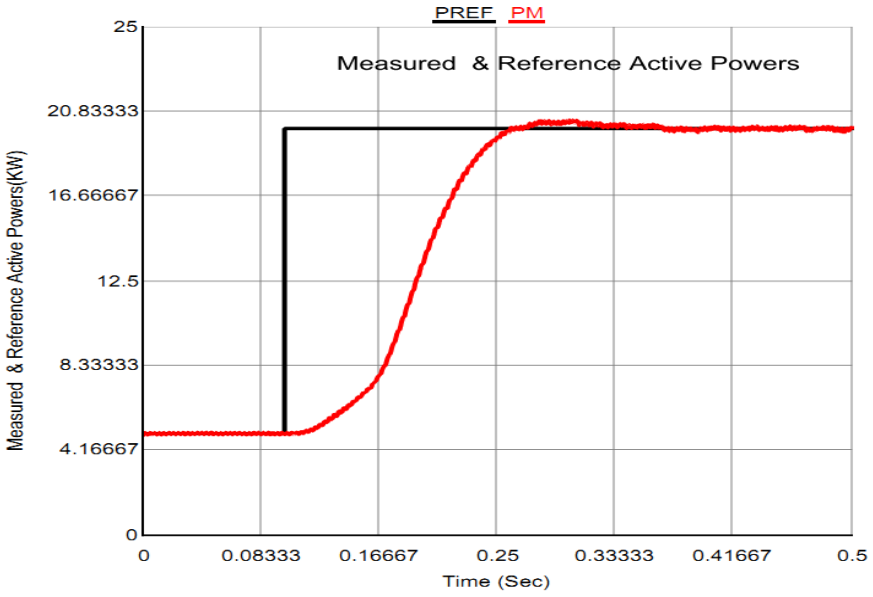

Fig. 9.21 Measured and reference active power

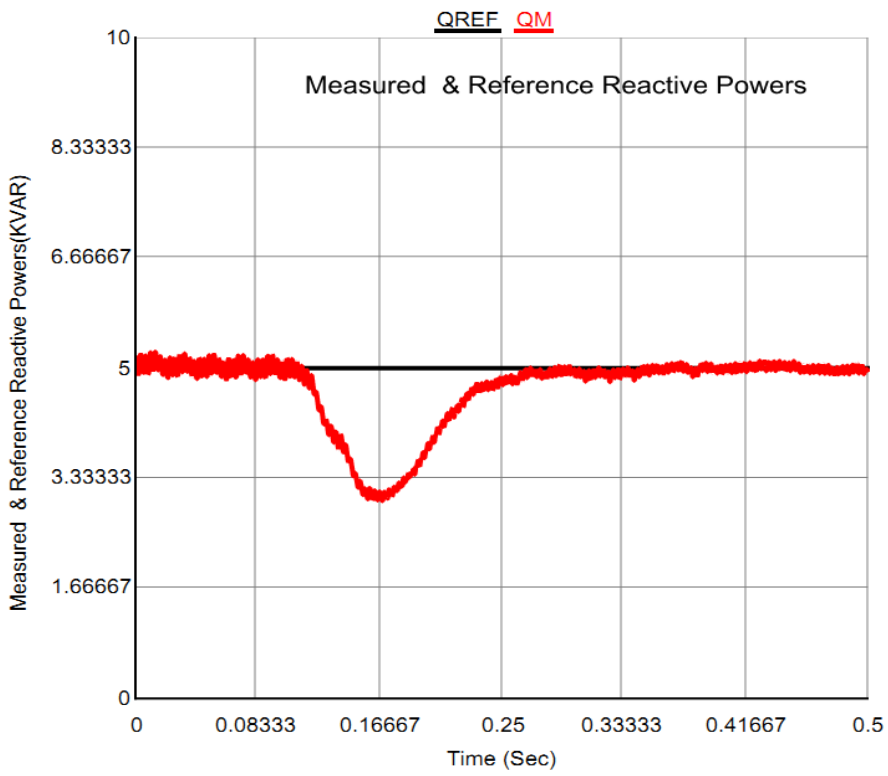

Fig. 9.22 Measured and reference reactive power

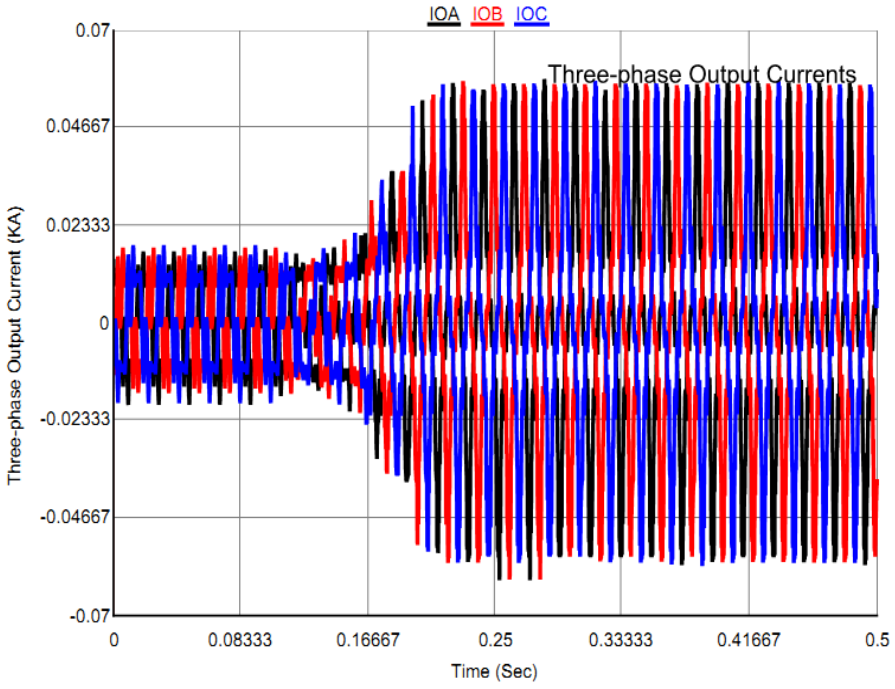

Fig. 9.23 Three phase output currents

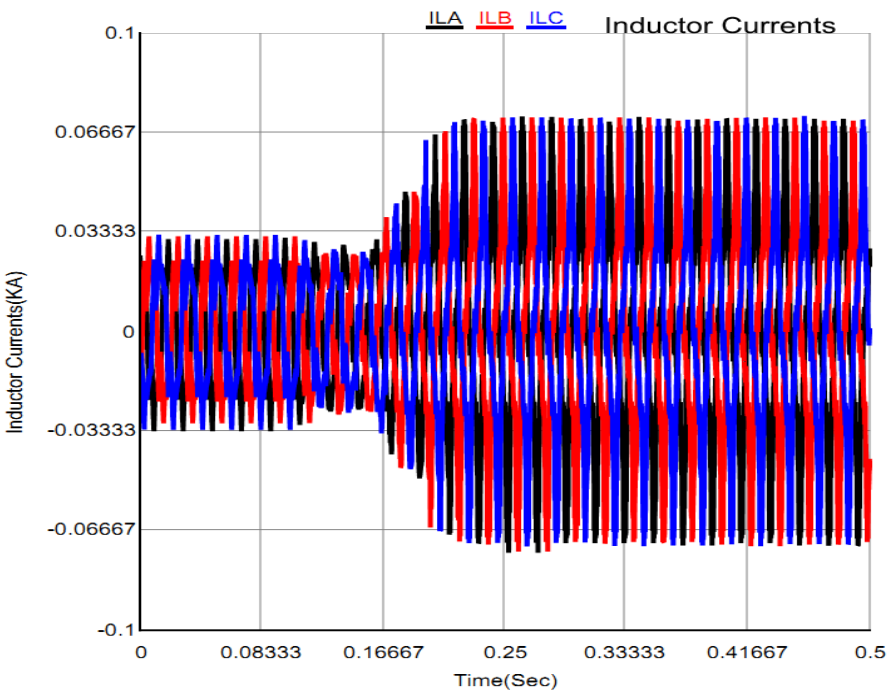

Fig. 9.24 Three phase inductor currents

9.2.2 Reactive Power Step Change

The effectiveness of the controller and the ability of the inverter are investigated when the inverter-based DG has been used to inject different values of reactive powers. A series of step reactive power changes were conducted in the RTDS to explore the use of optimal parameters obtained by PSO in the proposed controller. Firstly, the reactive power has been stepped up from 5 KVAR to 10 KVAR. The system response and performance under this disturbance are presented in Figs. 9.25- 9.29. Fig. 9.25 shows the PCC voltage. The optimal controller design allows the measured reactive power to track the reference reactive power closely with permissible time delay as illustrated in Fig. 9.26. Fig. 9.27 shows the waveforms of the measured and reference active power. The step response of the three phase output and inductor currents is given in Fig. 9.28 and Fig. 9.29 respectively. It is obvious from the given results that the inverter with the

optimal proposed controller is capable of tracking the reference reactive power as well as reference active power.

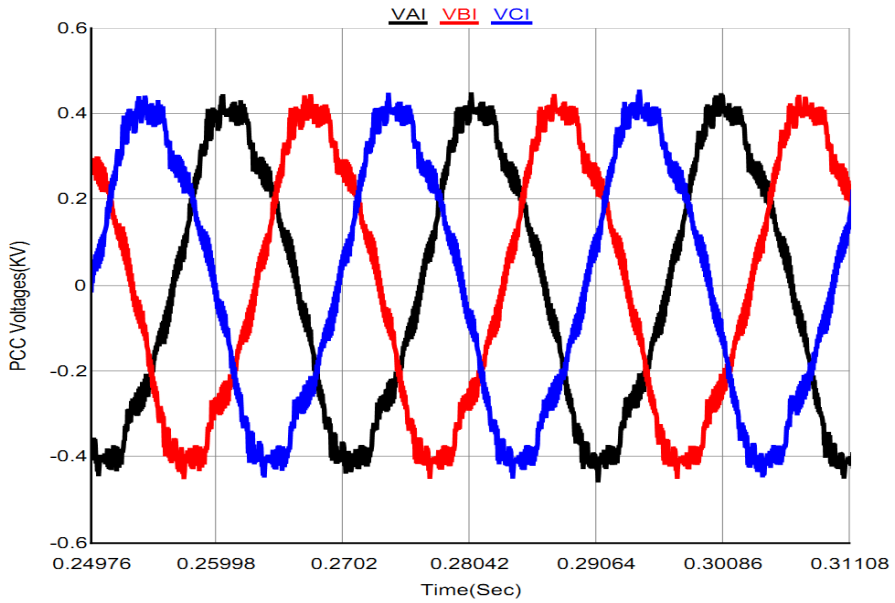

Fig. 9.25 PCC voltage

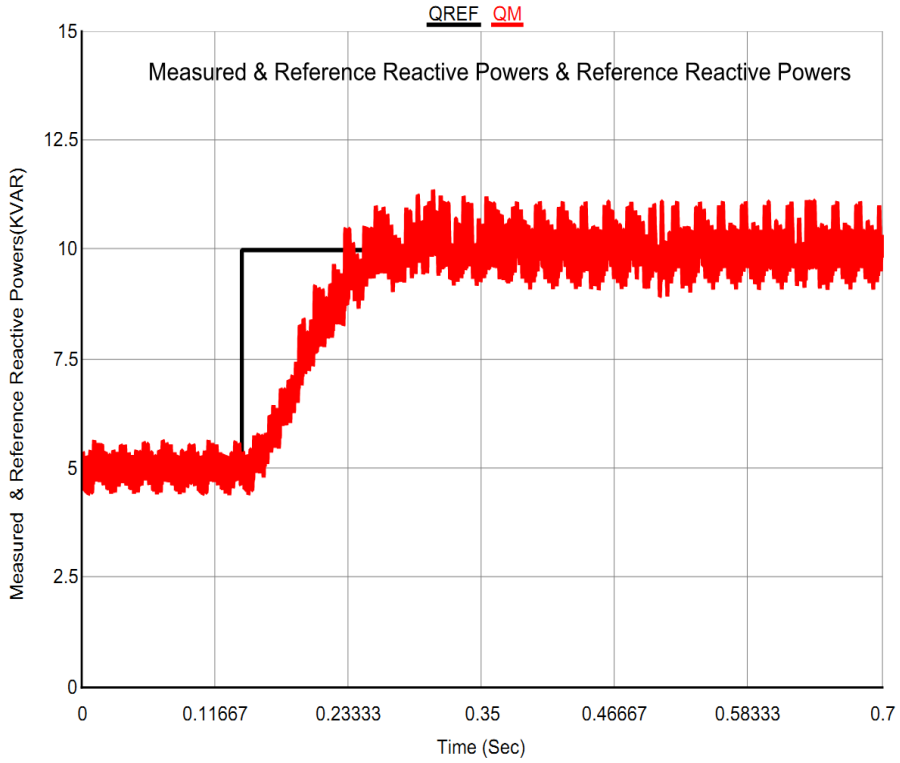

Fig. 9.26 Measured and reference injected reactive power

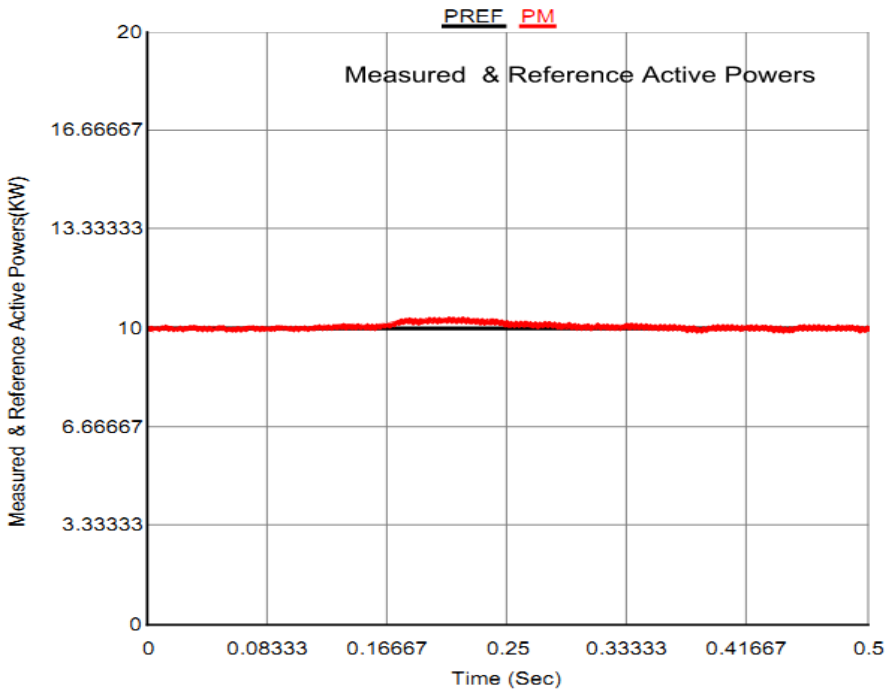

Fig. 9.27 Measured and reference injected active power

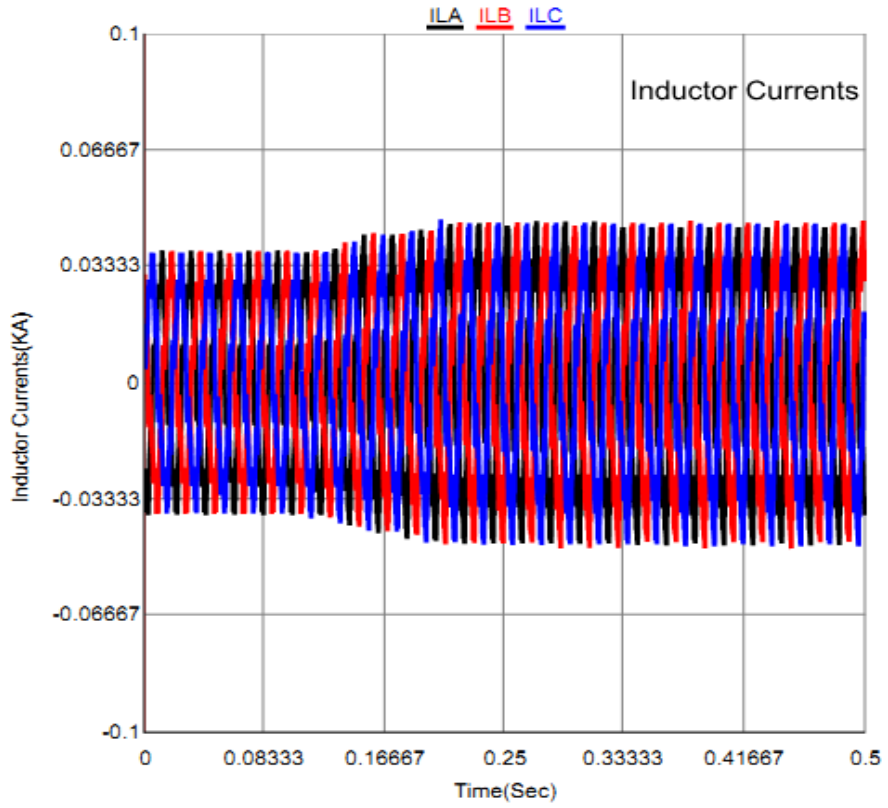

Fig. 9.28 Three phase inductor currents

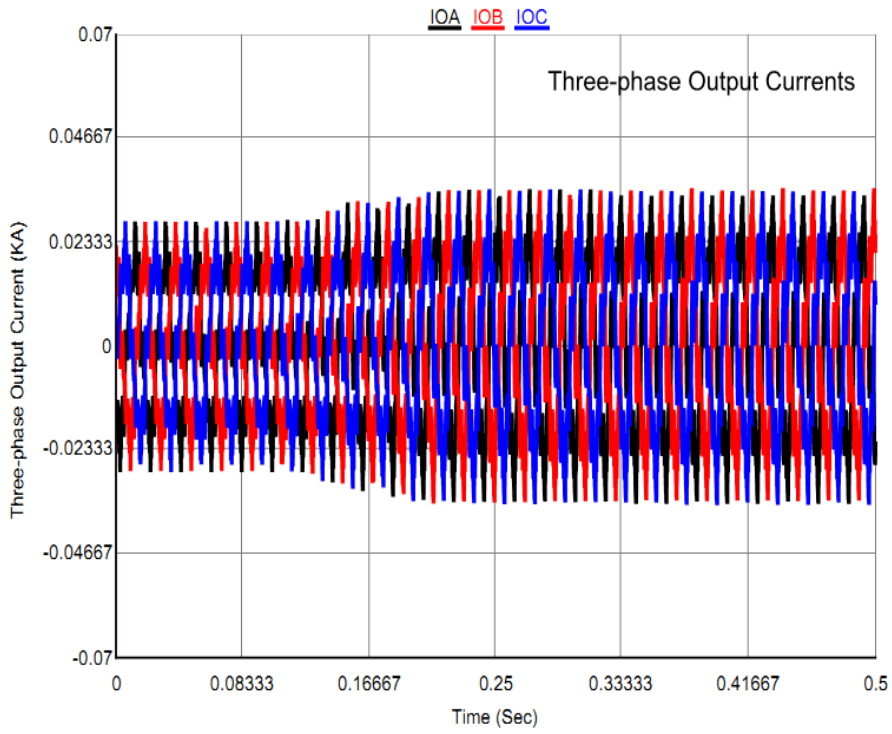

Fig. 9.29 Three phase output currents

Secondly, the reactive power has been stepped down from 10 KVAR to 5 KVAR. The system response of the PCC voltage is shown in Fig. 9.30. Fig. 9.31 and Fig. 9.32 depicted that the measured and the reference powers are so close to each other. The waveforms of the three phase inductor and output currents presented in Figs. 9.33 and 9.34 illustrate that the optimal proposed controller is working fine to follow the step change. It is clearly concluded from the previous results that the proposed controllers have good response to step down and step up changes of the reactive power as well as active power step changes without significant overshoot.

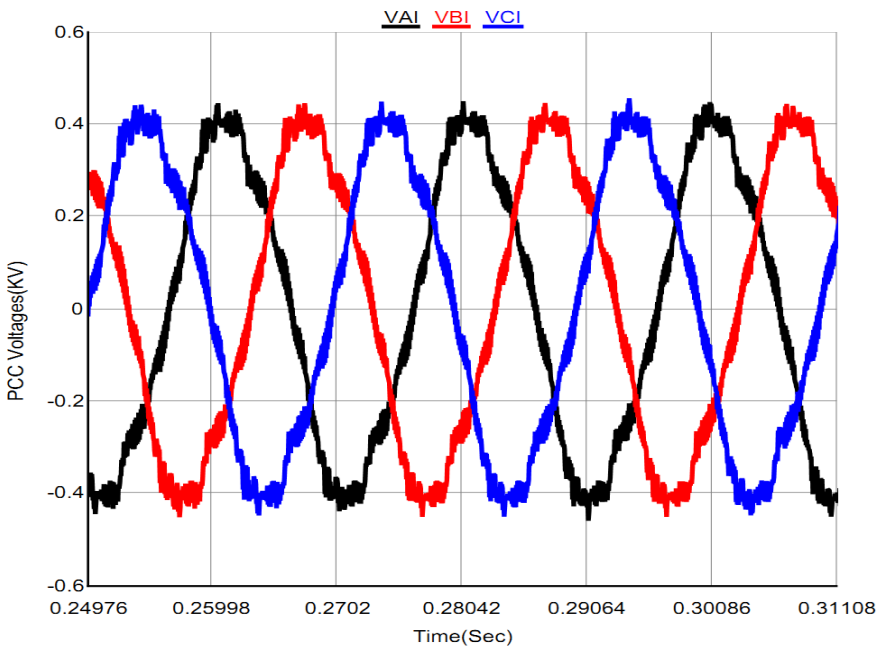

Fig. 9.30 PCC voltage

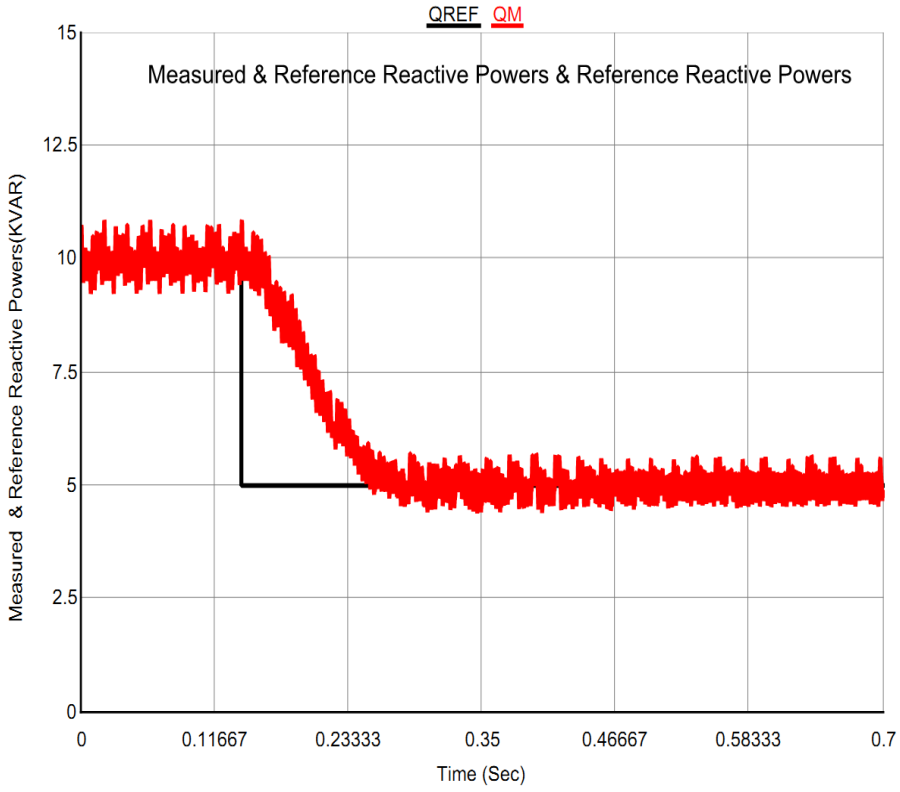

Fig. 9.31 Measured and reference reactive power

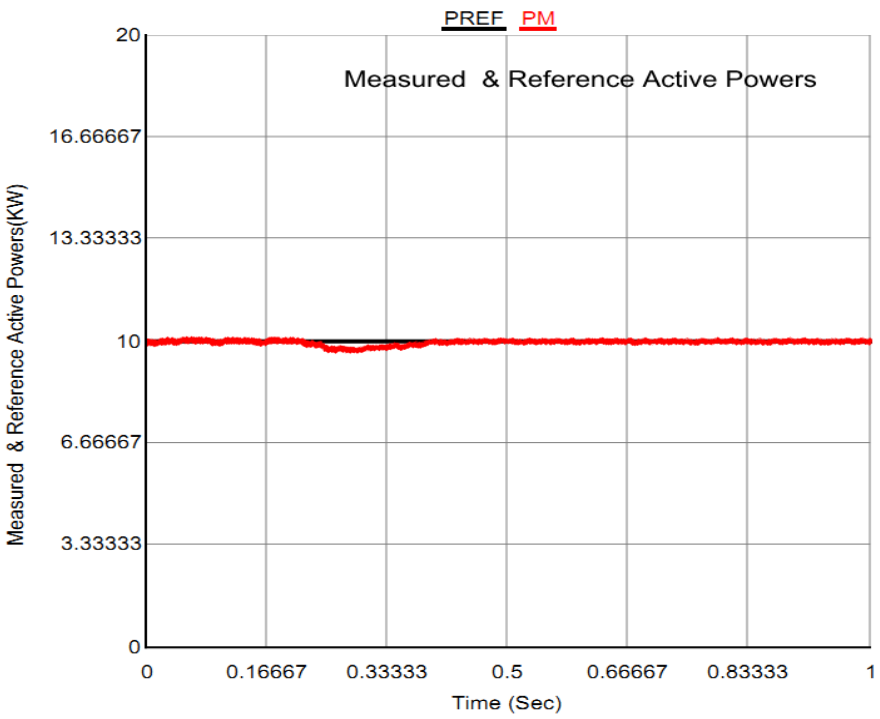

Fig. 9.32 Measured and reference active power

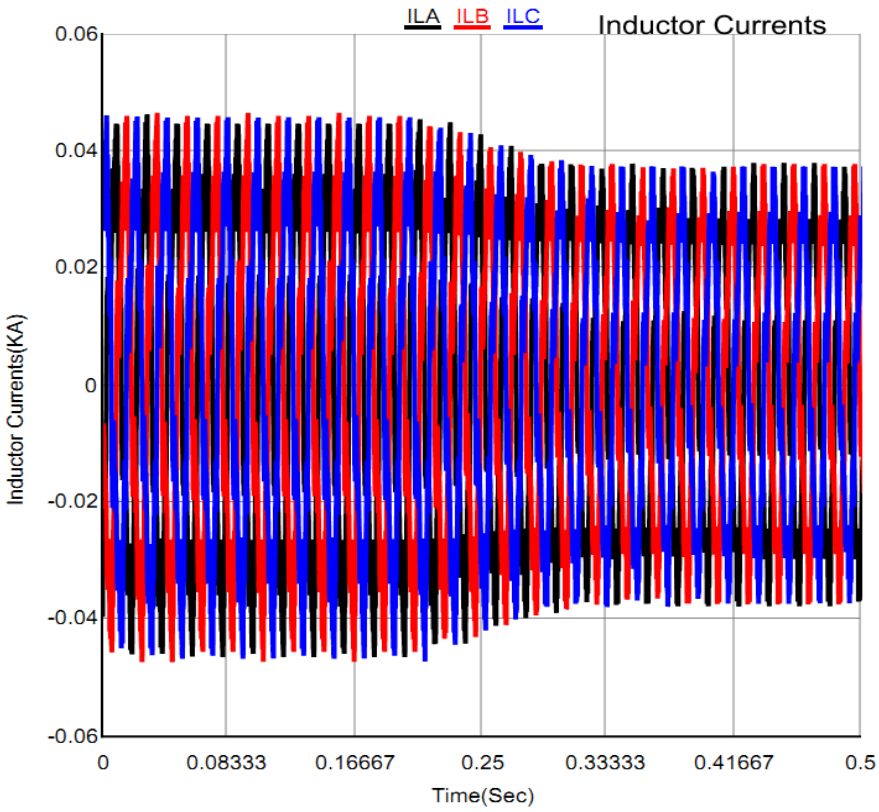

Fig. 9.33 Three phase inductor currents

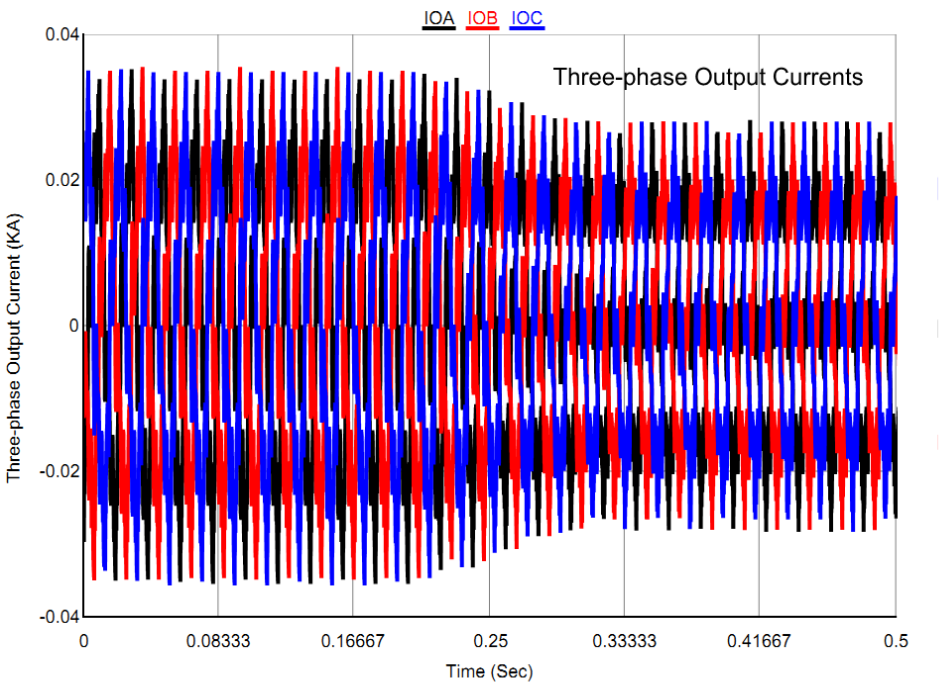

Fig. 9.34 Three phase output currents

Finally, the extreme reactive power has been stepped up from 5 KVAR to 20 KVAR. This step reactive power change has been done to test and evaluate the system response of the reactive power exported to the grid. Also, this will clarify the capability of the optimal proposed controller to track the extremes changes. The system response and performance under this disturbance are shown in Figs. 9.35 - 9.39. The PCC voltage waveform is shown in Fig. 9.35. The tracking of the reference reactive power is clearly presented in Fig. 9.36 while Fig. 9.37 shows the measured and reference active power. Fig. 9.38 and Fig. 9.39 illustrate the three phase inductor and output currents respectively. It can be concluded from the simulated results that the inverter can be used to inject heavy reactive powers as well as heavy active powers without significant overshoot. The optimal proposed controllers are capable of tracking the reference waveform.

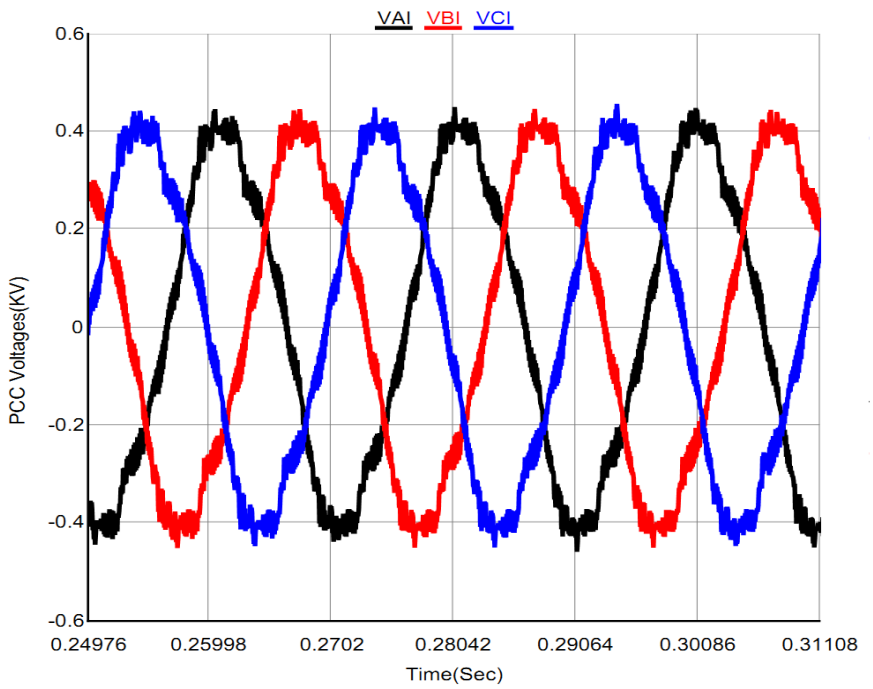

Fig. 9.35 PCC voltage

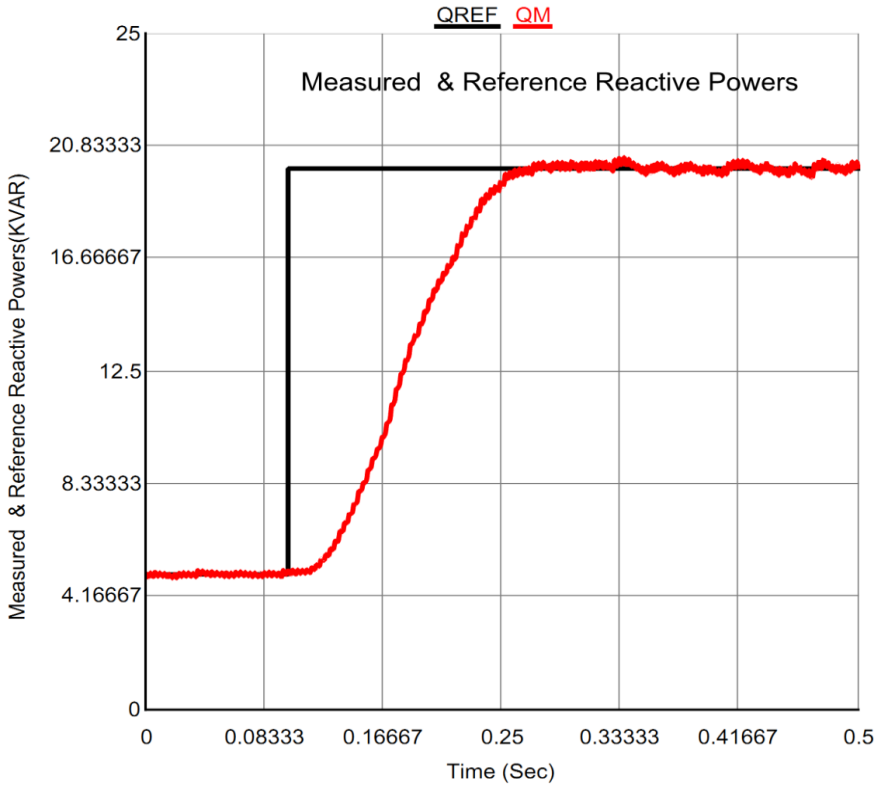

Fig. 9.36 Measured and reference reactive power

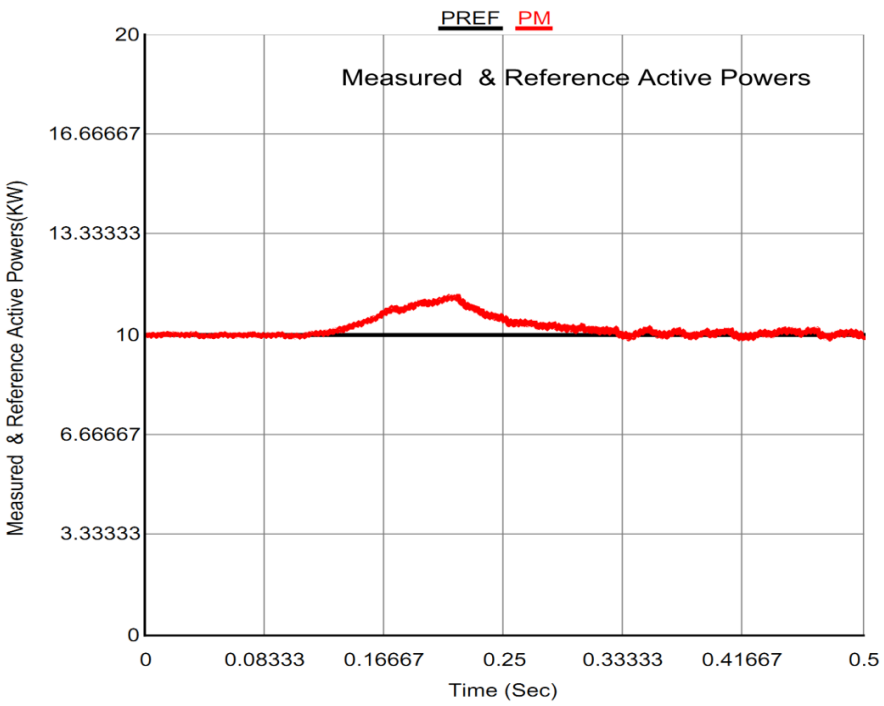

Fig. 9.37 Measured and reference active power

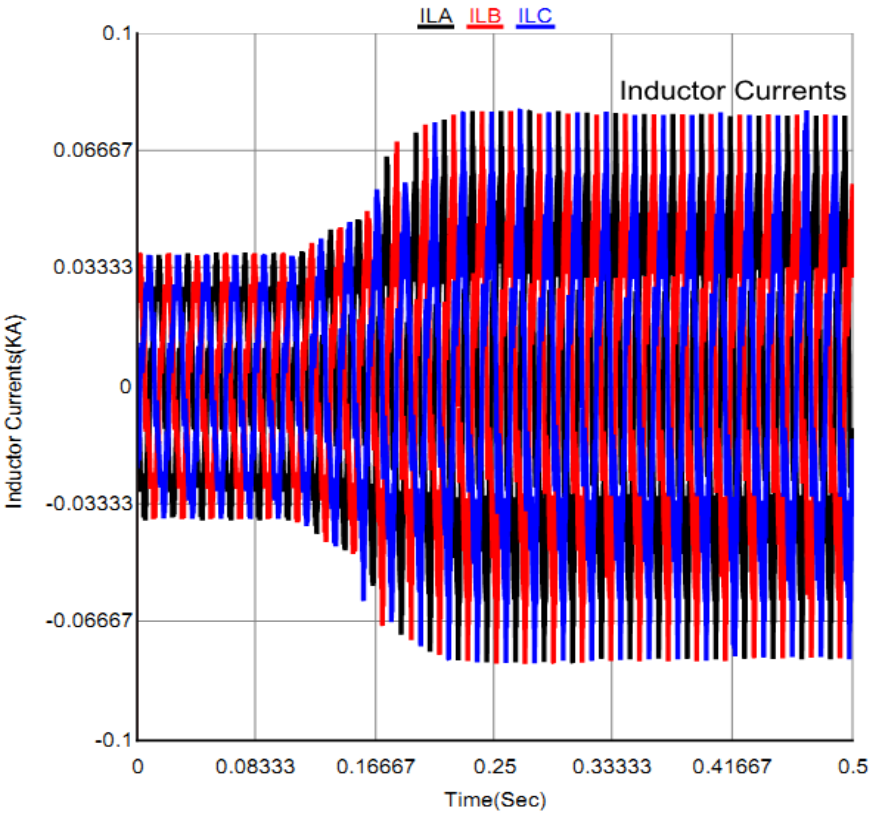

Fig. 9.38 Three phase inductor currents

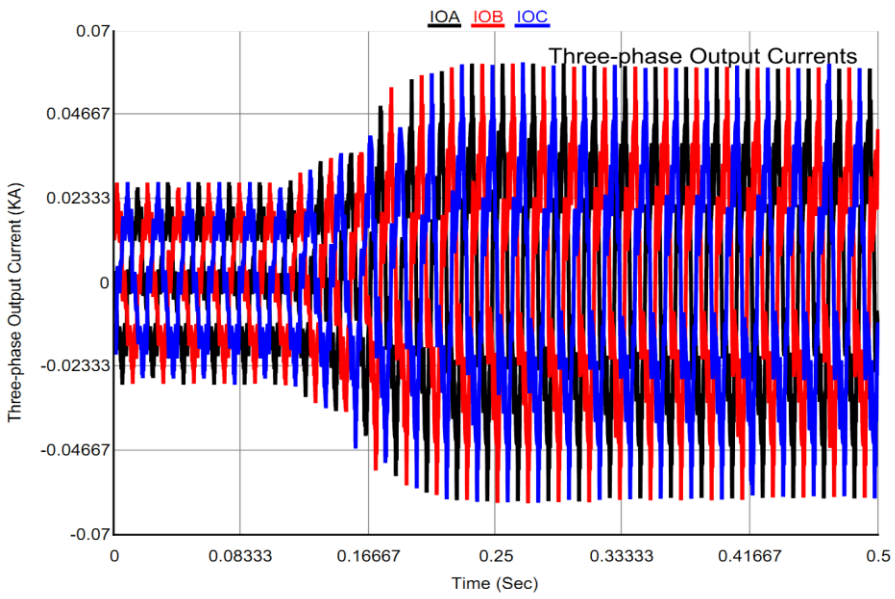

Fig. 9.39 Three phase output currents

9.3 COMPARISION BETWEEN MATLAB AND RTDS RESULTS

The results coming from MATLAB are compared with RTDS results to explore the validity of the proposed controller. The results show that the use of the optimization technique reflected noticeable improvements on the system response and system stability. Real-time simulated and MATALB results have confirmed the effectiveness of the PSO and robustness of the proposed controller in the grid-connected. Fig. 9.40 and Fig. 9.41 show how the calculated reactive powers in both MATALB and RTDS are tracking the reference reactive power when the injected reactive power has been stepped up from 5 KVAR to 10 KVAR and stepped down from 10 KVAR to 5 KVAR respectively. Fig. 9.42 and Fig. 9.43 present the calculated active power in MATALB, the calculated active power in RTDS, and the reference active power when the injected active power has been stepped up from 5 KW to 10 KW and stepped down from 10 KW to 5 KW respectively. The results given by both MATLAB and RTDS prove the validity and accuracy of the proposed controller model.

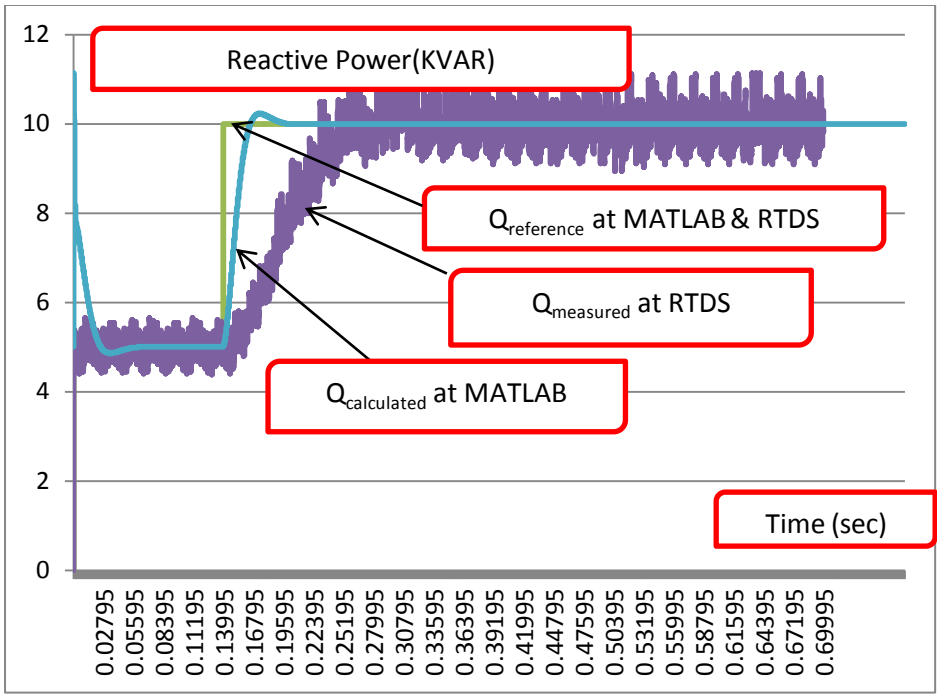

Fig. 9.40 Comparison between MALAB AND RTDS results when injected reactive power stepped up from 5KVAR to 10KVAR

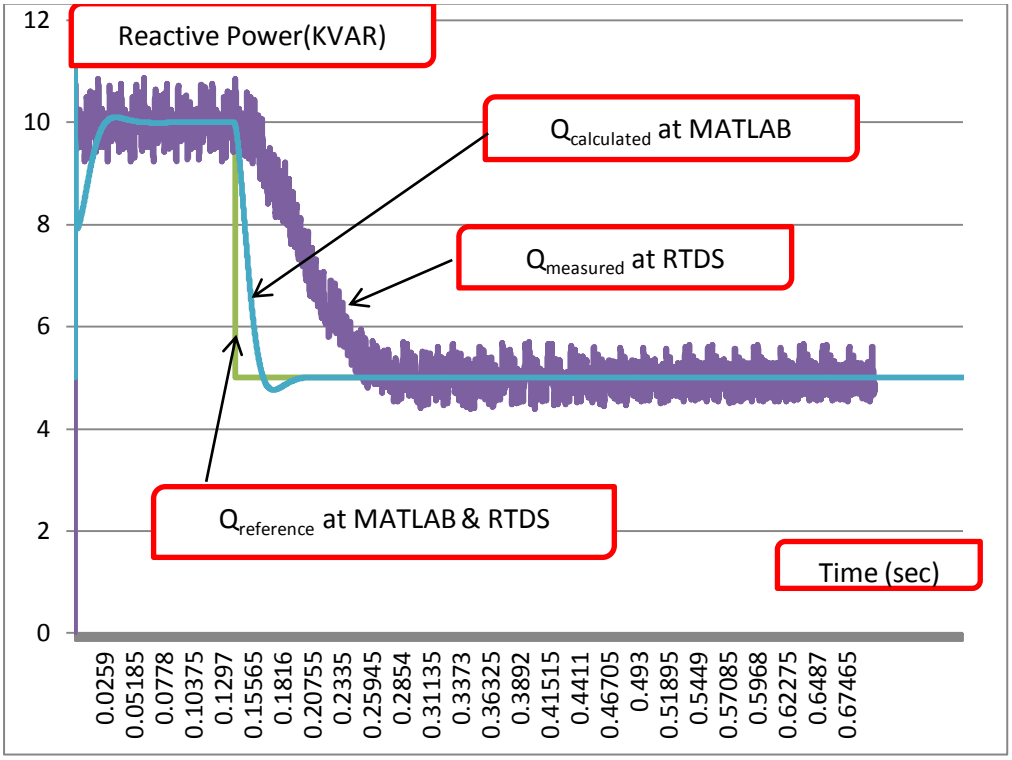

Fig. 9.41 Comparison between MALAB AND RTDS results when injected reactive power stepped up from 5KVAR to 10KVAR

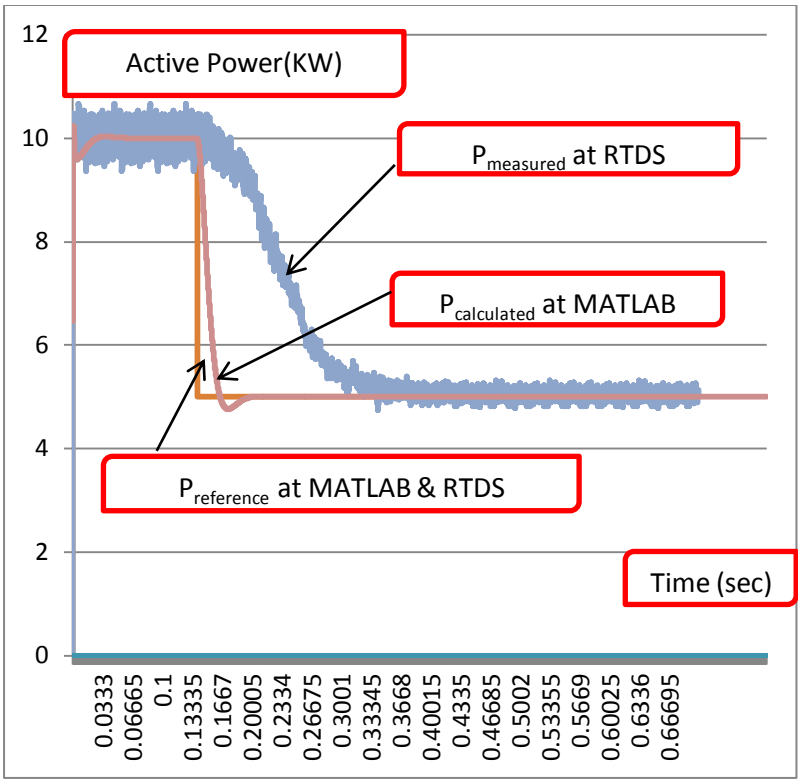

Fig. 9.42 Comparison between MALAB AND RTDS results when injected active power stepped down from 10KW to 5KW

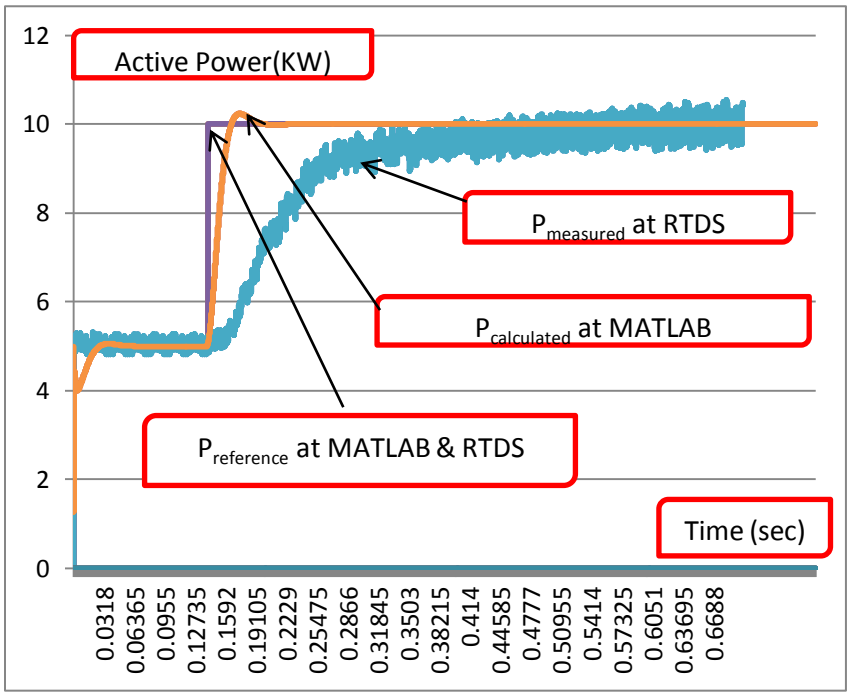

Fig. 9.43 Comparison between MALAB AND RTDS results when injected active power stepped up from 5KW to 10KW

9.4 DISCUSSION AND CONCLUSION

The stability of grid-connected microgrid under step change disturbance in the grid-connected mode has been checked in the RTDS environment. The response of the microgrid under these disturbances is checked out in the RTDS. Different active and reactive power step change cases show the effectiveness of the controller and the ability of the inverter to inject these required powers. The results obtained using the RTDS which compared with the MATLAB simulation results are used to explore the validity of the proposed controller. The results show that the use of the optimization technique reflected noticeable improvements on the system response and system stability. Real-time simulated and MATALB results have confirmed the effectiveness of the PSO and robustness of the proposed controller in the grid-connected.

CHAPTER 10

CONCLUSION & FUTURE WORK

10.1 CONCLUSIONS

A new technique for stability enhancement of a microgrid operating in both autonomous and grid-connected modes is proposed in this thesis. In this way, the linear and nonlinear models of both modes are using to investigate the parameters which affect the system stability on those modes. The control problem formulated as an optimization problem where PSO is employed efficiently to search for optimal settings of the optimized parameters.

In the Autonomous Microgrid Mode;

VSI, *LC* filter, coupling inductance, *PLL*, lines, loads, and power, current, and voltage controllers were modeled. The model analyzed in terms of the system eigenvalues gives view of the relation between stability of the system and the system parameters. The linear

model of the autonomous microgrid mode presented in this thesis helps in investigating the parameters that affect greatly the system stability. It is observed that the system stability has affected by the voltage and current controller parameters and the power sharing coefficients.

Using the optimized controller parameters, the poorly damped eigenvalues can be shifted to the LHS by minimizing the cost function. The optimized PI voltage and current controller gains are designed efficiently to reject the high frequency disturbances, to avoid the resonance between the output filter and the external network, and to enhance the autonomous microgrid stability illustrate the efficient of PSO in determining the optimal parameters which affect the system stability.

The nonlinear model of the autonomous microgrid mode verified that the stability of the system has also affected by controller parameters as well as power sharing coefficients.

Through the eigenvalue analysis and nonlinear time domain simulations, the performance of the microgrid with the proposed controllers has been improved using the optimal parameters under different disturbances. The results show the effectiveness of the proposed approach to enhance the stability of the microgrid considered.

In the Grid-connected Microgrid Mode;

Eigenvalue-based and nonlinear time domain simulation-based objective functions are considered with the aim of microgrid stability enhancement in the grid-connected mode where the controller parameters, LC filter components and damping resistance are optimized. An efficient controller of the inverter-based DG is required to inject the required active and reactive powers in effective way.

The linear model of the grid connected microgrid mode presented in this thesis helps in investigating the parameters that affect the system stability when it uses to inject the required active and reactive powers. Eigenvalue based objective functions are quite important to enhance the damping characteristics.

The nonlinear time domain simulation has been carried out to assess the effectiveness of the proposed controllers under different disturbances and loading conditions. In addition, nonlinear time-domain based objective function is quite important to minimize the error in the measured power.

The design problem of different microgrid components and controllers parameters was formulated as an optimization problem where PSO is employed to solve this design problem. Optimal design of LC filter, controller parameters, and damping resistance is essential to maintain power quality within the regulated range and to enhance the system performance against step change disturbances. Results show that using PSO as an optimization technique to solve the design problem is very efficient and robust. They show satisfactory performance with efficient damping characteristics of the microgrid considered in this study. The optimized parameters obtained by PSO illustrate that the system performance with the proposed controllers is stable. It can be observed that the optimal parameters make the proposed controllers capable of tracking the reference. It is also seen that the response to the change in reference values is fast and without significant overshoot.

Additionally, the effectiveness of proposed approach for optimizing different parameters and its robustness have been confirmed through the eigenvalue analysis and nonlinear time domain simulations.

The performance of this controller has been verified in simulation using RTDS. The RTDS gives results that correspond with experimental values. Real-time simulated results have confirmed the effectiveness and robustness of the proposed controller in grid-connected mode during operational mode transitions. Finally, comparison between MATALB and RTDS results has investigated the optimal controller effectiveness.

10.2 FUTURE WORK

The following subjects are suggested for future studies:

1. Different optimization techniques can be used instead of using PSO to study the difference between these optimization methods and which one is more effective.
2. Connecting more than one DG to the utility in the grid-connected mode. So we can study many things such as sharing the power between those DGs in the grid connected mode, losing one of them and stability of the system at this time and the PSO effectiveness in this case.
3. Different control techniques such as sliding control method can be used instead of PI controllers. Then we can compare these controller techniques with the proposed technique and study is these techniques are better than ours or not.
4. Different cost functions can be used to check the effectiveness of the optimization technique.
5. In our model, we assumed that dc voltage of the inverter in the DC side is constant dc. Of course, the dc coming from the energy source will not be constant dc voltage and it may contain fluctuations. So dc voltage dynamics can be

studied. Also, in this case, the optimal problem will include the controller parameters of the DC side.

6. Different loads can be used to study the dynamics of the system regarding different load changes and dynamics.
7. Study other different forms of power sharing such as modified droop function schemes and check the efficient of the PSO to this new power sharing control.
8. Study the harmonics effects on the DG operation on the autonomous mode as well as on the utility in grid-connected mode is also a great challenge.

Appendix A

A.1 RTDS CAPABILITY

RTDS works in real-time to provide solutions to power system equations quickly enough to accurately represent conditions in the real world. RTDS offers superior accuracy over analogue systems. It allows for comprehensive product and/or configuration tests. RTDS provides a variety of transient study possibilities. It is capable of testing three-terminal line protection applications including actual communications equipment.

1. *RTDS Applications*
    - Protective relaying schemes.
    - Integrated protection and control systems.
    - Control system for HVDC, SVC, FACTS devices and Synchronous machines.
    - General AC and DC system operations and behavior.
    - Interaction of AC and DC systems.
    - Interaction of various electrical installations (e.g. between two HVDC systems).
2. *RTDS Benefits*
    - Increase system reliability, security, dependability, stability and efficiency of equipment and networks.
    - Improve system understanding, knowledge and insight.
    - Maximize quality and quantity of studies.

- Minimize equipment or system failure.
- Decrease equipment commissioning time.
- Reduce R&D cycle time.

3. RTDS Technical Capabilities

- Database of simulation models.
- Generators.
- Transformers.
- Multi-Conductor Transmission Lines.
- Measurement Transducers (CT, CVT).
- AC Machines (Synchronous and Induction).
- Series Capacitors.
- Circuit Breakers.
- Fault Switches.
- Metal Oxide Varistor (MOV) protected Series Compensation.
- 6-pulse HVDC Valve Group.
- Faulted line model.
- Source of impedance.
- Passive Branches (1, 2, dual element).
- User Defined Models.
- Real-Time Communications Connection.
- The simulator is connected to equipment via fiber optic, I/O equipment and amplifiers.
- Output from Simulator to Equipment (Current, Voltage and Logic Signals).

- Feedback from tested equipment (Current, Voltage and Logic Signals).
- Test Types Available
- Open Loop (Playback)
- Closed Loop (Real-Time Feedback)
- Automatic Batch Tests
- Record/replay facility
- Script file facility
- Pre-processor components

4. *On-Hand Application Experts*

- Applications engineers are available to offer their knowledge and experience in protective relaying and communications architecture.
- Application review including specific product recommendations.
- Analysis of power system or network requirements.
- Configuration or modification of existing protection and control schemes.
- Design protection scheme according to customer requirements.
- Design and testing of telecommunications networks.
- Analysis of data files, test results and report creation.

5. *Detailed Test Reports and Case Documentation*

Applications engineers provide detailed analysis and documentation of the testing, including:

- Input data files (network configurations, parameters).
- Load-flow data.
- Result data files (comtrade files, setting files).

- Printed report of results with tables and graphs (also available in electronic format).

A.2 RTDS Euipments Used

1. *RTDS Simulator Software*

RTDS Simulation has two main software elements:

1.2 RSCAD Software Suite

RSCAD provides the ability to set up simulations, control, and modify system parameters during a simulation, data acquisition, and result analysis. The modules of the RSCAD Software Suite include FileManager, Draft, Tline, Cable, RunTime, MultiPlot and ComponentBuilder.

RSCAD includes several modules that allow all facets of the real time simulations to be created, executed, controlled and analyzed without the use of third party products.

RSCAD is a user-friendly interface used to create a working environment familiar to the power system engineer. This software is the main interface with the RTDS hardware. It is designed to allow the user to perform all of the necessary steps to prepare and run simulations, and to analyze simulation results.

- FileManager organizes simulation files and launch other modules.
- Draft is a graphical assembly and data input for simulation circuit.
- Cable is used to calculate the cable characteristics based on physical data.
- TLine is used to calculate the transmission line characteristics based on physical data or positive and zero sequence impedances.

- RunTime is used to run, to control and to acquire results from real time simulation.
- MultiPlot is used to post analysis and annotation of results.
- ComponentBuilder is used to create user defined components including graphical representation, data menus and real time code.

1.3 Component Model Libraries

The RTDS software also includes a multitude of power system, control system protection and automation component models, which can be used to create simulation cases. These models have been designed and tested by research team at RTDS Technologies and have been validated and refined by clients during their daily work with the Simulator. The component libraries are provided as an integral part of RSCAD. RSCAD allows the user to select the component icons from the library in order to build the desired circuit. Once the system has been drawn and the parameters entered the compiler automatically generates the low-level code necessary to perform the simulation. Therefore, it is the software that determines the function of each processor card during a simulation.

The Power System Component Library is included as an integral part of RSCAD and contains all the fundamental elements of an electrical power system. Each component model has been tested to ensure the accuracy and stability for long term real time simulation. Numerous features have been added to the components based on experience and customer feedback, refining their operation and increasing flexibility.

RTDS Technologies' simulation experts are continually expanding the component library based on customer requirements and in-house research. Models are developed to expand the application and the efficiency of the simulator. RTDS Technologies continues to work hard to accommodate more components on less hardware. However, if a component model is not available in the standard component libraries, the user can create them using ComponentBuilder.

(a) Power System Component Library - Component Types

The descriptions below provide an overview of the base components.

- Real Time Network Solution - solves nodal equations for simulation circuits including passive elements, breakers and faults. The network solution performs real time decomposition of the admittance matrix which allows continually varying conductance elements to be represented in the circuit. The current dimensioning of the network solution allows 66 single phase nodes per rack (i.e. per subsystem) and 56 switches.
- Sources - both voltage and current sources are available. Voltage sources provide several impedance options to act as network equivalent models and allow the positive and zero sequence impedance to be specified independently.
- Transmission Lines and Cables - traveling wave (Bergeron) and PI section components can represent full coupling between as many as 12 conductors. Frequency dependent model or phase domain components allow a maximum of 6 conductors.

- Machines - synchronous and induction machines, multi-mass model (maximum 7 masses). Optionally the synchronous machine model can also represent the unit transformer and the generator terminal bus, therefore reducing the load on the network solution and freeing up more nodes.
- HVDC - converter models for point-to-point and back-to-back schemes. The converter models can be easily configured to represent UHVDC (i.e with several series groups) and allow faults to points both internal and external to the converter. The improved firing algorithm is used to allow the converters to represent a continually variable firing instant with an accuracy of 1μs.
- SVC - including TCR (with improved firing) and TSC.
- Switched Filter - provides as many as 12 individually switched filters without requiring the use of any additional nodes. The entire component is embedded in the main network solution as variable conductance elements. Various filter configurations including single, double and triple tumed options are available.
- FACTS - VSC based devices such as STATCOM, SSSC, UPFC, VSC based HVDC, etc. are represented using small timestep VSC subnetworks.
- Series Compensation - either fixed or variable (TCSC) compensation components are available with MOV, bypass breaker, spark gap, capacitor bank unbalance, etc.
- Transformers - 2 and 3 winding transformers with on-load tap changers, saturation and hysteresis, internal faults.
- Instrument Transformers - CT, CVT with ferroresonance damping cct., and PT all with saturation and hysteresis representation.

- Distributed Generation - wind turbines, photo voltaic, fuel cell and various other power sources can be represented by library components while the corresponding VSC converters can be freely configured in small timestep subnetworks.

(b) Control System Component Model Library - Component Types

The Control System Component Library allows customized control systems to be created that can interact with the model power system and/or the outside world. In addition to individual control blocks, some complex controllers have been assembled as composite controls and they are included in the library (e.g. generator controls).

The descriptions provide an overview of the base components.

- User-Input - Slider, switch, button, dial
- Constants - integer, floating point, utility
- Data conversion - deg -> rad, int -> float, etc.
- Math functions - exp, log, gain, sqrt, inverse, abs, sum, multiply, divide, fourier transform, integrator, lead-lag, wash-out, etc.
- Trigonometric functions - sin, cos, tan, arcsin, arcos, 3 phase sin, etc.
- Standard control blocks - deadband, pulse generator, edge detector, time, counter, ramp, limiters, meters, phase-locked loop, flip-flops, etc.
- Logic functions - and, or, nor, bit shift functions, bit -> word, etc.
- Sequencer functions - wait, apply fault, close breaker, etc.
- Generator controls - exciters (IEEE Type 1, AC1, ST1, X1, SCRX, IVO, etc.), governors (IEEE Type 1, European BBGOV1, Gas turbine, steam turbine, hydro turbine, etc.), power system stabilizers (PT1ST1, PSS2A, IEEEST, IEE2ST).

(c) Small Timestep VSC Subnetworks

VSC based schemes require small timesteps to properly represent high frequency switching and circuit dynamics. To efficiently include such schemes in larger scale simulations, RTDS Technologies has developed the small timestep VSC subnetwork technique. The VSC subnetworks operate with timesteps in the range of 1-4µs. It can be interfaced to large scale simulations operating with timesteps in the order of 50µs. A key feature of VSC subnetworks is that the circuit and valve topology is user configurable. Two- and three-level converters can be freely configured to provide crow-bar circuits, etc. for PWM switching < 2kHz. A fixed topology two-level converter is also available for operation at PWM switching frequencies in the range of 10kHz. Multiple VSC subnetworks can be linked together by traveling wave transmission lines or cables to create entire systems running with timesteps <4µs.

APPENDIX B

LIST OF PUBLICATIONS

The following papers are published from the work described in this thesis.

Journal paper:

 M. A. Hassan and M. A. Abido, "Optimal Design of Microgrids in Autonomous and Grid-Connected Modes Using Particle Swarm Optimization," IEEE Transactions on Power Electronics, vol. 26, no. 3, pp. 755- 769, March 2011

Conference paper:

 M. A. Hassan and M. A. Abido, "Optimal autonomous control of an inverter-based microgrid using particle swarm optimization," ISIE 2010 - IEEE International Symposium on Industrial Electronics - Bari (Italy) 4-7 July 2010 IEEE.

NOMENCLATURE

ABBREVIATIONS AND SYMBOLS

P_m Instantaneous Active Power (W)

Q_m Instantaneous Reactive power (VAR)

v_{od} d- component of the output voltage on individual reference frame (V)

v_{oq} q- component of the output voltage on individual reference frame (V)

i_{od} d- component of the output current on individual reference frame (A)

i_{oq} q- component of the output current on individual reference frame (A)

P_c Real power corresponding to the fundamental components (W)

Q_c Reactive powers corresponding to the fundamental components (VAR)

m_p Real power droop gain of the power controller ($W^{-1}s^{-1}$)

n_q Reactive power droop gain of the power controller (V/VAR)

V_n Nominal output voltage reference of the inverter (V)

θ Phase angle reference of the inverter output voltage (rad)

v^*_{oq} q- component of the output voltage reference on individual reference frame (V)

v^*_{od} d- component of the output voltage reference on individual reference frame (V)

ω_n Nominal frequency of the inverter (rad/sec)

ω_{com} Frequency of the common reference frame (rad/sec)

V_n Nominal output voltage reference of the inverter (V)

V_{grid} Grid voltage (V)

P_i Output active power of each inverter (W)

Q_i Output reactive power of each inverter (VAR)

δ_i Angle between the inverter (i) and the common reference frames (rad)

ω_i Frequency of each inverter (rad/sec)

φ_d d-axis state variable of the voltage controller

φ_q q-axis state variable of the voltage controller

F Feed forward voltage controller gain

K_{pv} Proportion gain of the PI voltage controller parameters

K_{iv} Integral gain of the PI voltage controller parameters

C_f Capacitance of the filter capacitor (F)

i^*_{ld} Reference (d-axis) inductor current (A)

i^*_{lq} Reference (q-axis) inductor current (A)

γ_d d-axis state variable of the current controller

γ_q q-axis state variable of the current controller

i_{ld} d- component of the inductor current on individual reference frame (A)

i_{lq} q- component of the inductor current on individual reference frame (A)

K_{pc} Proportion gain of the *PI* current controller parameters.

K_{ic} Integral gain of the *PI* current controller parameters

L_f Inductance of the filter inductor (H)

v^*_{ld} d- component of the reference voltage on individual reference frame (V)

v^*_{lq} q- component of the reference voltage on individual reference frame (V)

L_c Inductance of the coupling inductor (H)

R_c Coupling resistance (Ω)

v_{ld} d- component of the inverter bridge voltage on individual reference frame (V)

v_{lq} q- component of the inverter bridge voltage on individual reference frame (V)

v_{od} d-axis output voltage (V)

v_{oq} q-axis output voltage (V)

v_{bd} d-axis load voltage (V)

v_{bq} q-axis load voltage (V)

$\Delta\omega_{com}$ Deviation in the frequency of the common reference inverter

v_o Supply voltage at the point of common coupling (PCC)

K_P^{PLL} Proportion gain of the PI controller of the PLL

K_c^{PLL} Integral gain of the PI controller of the PLL

i^*_{od} d- component output reference current

i^*_{oq} q- component output reference current

P^* Injected (reference) active power

Q^* Injected (reference) reactive power

i^{Σ}_d d-component reference coupling inductance currents

i^{Σ}_q q-component reference coupling inductance currents

i^*_{Ld} d-component reference current controller

i^*_{Lq} q-component reference current controller

ω_c Cut-off frequency of the low-pass filter

K_P^{d} d-axis P controller of the current controller in the grid connecting mode

K_I^{d} d-axis I controller of the current controller in the grid connecting mode

K_P^{q} q-axis P controller of the current controller in the grid connecting mode

K_I^{q} q-axis I controller of the current controller in the grid connecting mode

v^*_{ld} d-axis reference voltage (V)

v^*_{lq} q-axis reference voltage (V)

v_{od} d-axis output voltage (V)

v_{oq} Output voltage (V)

i_{Ld} d- component of the inductor current (A)

i_{Lq} q- component of the inductor current (A)

i^{err}_{Ld} d-axis difference between the reference and calculated currents (A)

i^{err}_{Lq} q-axis difference between the reference and calculated currents (A)

v_{la} Phase-a output voltage of the inverter (V)

v_{ba} Phase-a grid voltage of the inverter (V)

R_d Resistance of the damping resistor (Ω)

i_{La} Phase-a output current of the inverter (A)

i_{oa} Phase-a current of the coupling inductor (A)

v_{Ca} Phase-a voltage at the capacitor (V)

i_{Ca} Phase-a current of the capacitor (A)

i_{Ld} d- component of the inductor current (A)

i_{Lq} q- component of the inductor current (A)

i_{od} d- component of the coupling inductor current (A)

i_{oq} q- component of the coupling inductor current (A)

i_{cd} d- component of the capacitor current (A)

i_{cq} q- component of the capacitor current (A)

v_{ld} d- component of the inverter voltage (V)

v_{lq} q- component of the inverter voltage (V)

v_{bq} q- component of the grid voltage (V)

v_{bd} d- component of the grid voltage (V)

v_{cd} d- component of the capacitor voltage (V)

v_{cq} q- component of the capacitor voltage (V)

J_{best} Global best function

x_{best} Global best particle

w Inertia weight

J_{linear_model} Cost function of the linear model

$J_{nonlinear\_model}$ Cost function of the nonlinear model

Acronyms

PSO	Particle Swarm Optimization
RES	Renewable Energy Sources
VSI	Voltage Source Inverter
DG	Distributed Generation
DER	Distributed Energy Resources
PCC	Point of Common Coupling
RTDS	Real Time Digital Simulation
DE	Distributed Energy
UPS	Uninterruptible Power Supply
VPD	Voltage-Power Droop
FQB	Frequency-reactive Power Boost
VSC	Voltage Source Converters
EMS	Energy Management System
FFC	Feeder Flow Control
MTG	Microturbine Generation
GA	Genetic Algorithm
RHS	Right Hand Side
LHS	Left Hand Side
CERTS	Consortium for Electric Reliability Technology Solutions

BIBLIOGRAPHY

[1] J. Carrasco et al., “Power-electronic systems for the grid integration of renewable energy sources: a survey,” IEEE Trans. on Industrial Electronics, vol. 53, pp. 1002-1016, August 2006.

[2] F. Blaabjerg, Z. Chen, and S. Kjaer, “Power electronics as efficient interface in dispersed power generation systems," IEEE Trans. on Power Electronics, vol. 19, pp. 1184-1194, Sep. 2004.

[3] A. Keyhani, “Control of power converters for distributed generation applications,” Ph.D. Thesis, Electrical Engineering, Ohio State University, 2005.

[4] A. Arulampalam, M. Barnes, A. Engler, A. Goodwin and N. Jenkins, "Control of power electronic interfaces in distributed generation microgrids", International Journal of Electronics, pp. 503-523, 2004.

[5] Z. Chen and Y. Hu, “Control of power electronic converters for distributed generation units,” Industrial Electronics Society, IECON, 31th Annual Conference of IEEE, pp. 1-6, Nov. 2005

[6] B. Kroposki, R. DeBlasio, M. Simoes, and P. Sen, “Benefits of power electronic interfaces for distributed energy systems,” IEEE Trans. on Energy Conversion, vol. 25, no. 3, pp. 901- 908, Sep. 2010.

[7] F. Peng, Y. Li, and L. Tolbert, “Control and protection of power electronics interfaced distributed generation systems in a customer-driven microgrid,” Power & Energy Society General Meeting, PES, IEEE, pp.1-8, 2009.

[8] Y.A.I. Mohamed, “New control algorithms for the distributed generation interface in grid-connected and micro-grid systems,” Ph.D. Thesis, Department of Electrical and Computer Engineering, University of Waterloo, 2008.

[9] F. Katiraei, “Dynamic analysis and control of distributed energy resources in a microgrid,” Ph.D. Thesis, Department of Electrical and Computer Engineering, University of Toronto, 2005.

[10] T. Green and M. Prodanovic, "Control of inverter-based micro-grids," Electric Power Systems Research, vol. 77, pp. 1204–1213, 2007.

[11] I. Vechiu, A. Llaria, O. Curea and H. Camblong, “Control of power converters for microgrids,” EVER'09, pp. 1-6, Monaco, March 2009.

[12] D. Jayaweera, S. Galloway, G. Burt, and J. Mcdonald, “A sampling approach for intentional islanding of distributed generation,” IEEE Trans. on Power Systems, vol. 22, pp. 514-521, May 2007.

[13] P. Arboleya , D. Diaz, J. Guerrero, P. Garcia, F. Briz, C. Gonzalez-Moran, and J. Gomez Aleixandre, “An improved control scheme based in droop characteristic for microgrid converters,” Electric Power Systems Research, vol. 80, pp.1215–1221, 2010.

[14] Y. Mohamed and E. El-Saadany, “Adaptive decentralized droop controller to preserve power sharing stability of paralleled inverters in distributed generation microgrids,” IEEE Trans. on Power Electronics, vol. 23, no. 6, pp. 2806-2816, Nov. 2008.

[15] W. El-Khattam, and M. Salama, “Distributed generation technologies, definitions and benefits,” Electric Power Systems Research, vol. 71, pp.119-128, 2004.

[16] H. Jiayi, J. Chuanwen, and X. Rong, “A review on distributed energy resources and Microgrid,” Renewable and Sustainable Energy Reviews, vol. 12, pp. 2472–2483, 2008.

[17] CIGRE WG C6.01, “Development of dispersed generation and consequences for power systems”, July 2003.

[18] H. Zareipour, K. Bhattacharya and C. Canizares, "Distributed generation: Current status and challenges," presented at the 36th Annual North American Power Symposium (NAPS), University of Idaho, Moscow, Idaho, USA, 2004.

[19] K. Purchala et al., “Distributed generation and the grid integration issues”, Imperial College London, UK, EUSUSTEL, Work Package-3, Belgium.

[20] P. Dondi, D. Bayoumi, C. Haederli, D. Julian, and M. Suter, “Network integration of distributed power generation,” Journal of Power Sources, vol.106, no.1, pp.1–9, April 2002.

[21] A. Chambers, B. Schnoor and S. Hamilton, “Distributed generation: a nontechnical guide,” Tulsa, OK, USA: PennWell, 2001.

[22] G. Pepermans, J. Driesen, D. Haeseldonckx, R. Belmans and W. D’haeseleer, "Distributed generation: definition, benefits and issues", Energy Policy, vol. 33, pp. 787–798, 2005.

[23] T. Ackermann, G. Andersson, and L. Söder, “Distributed generation: a definition,” Electric Power Systems Research, vol. 57, no. 3, pp. 195-204, April 2001.

[24] S. Abusharkh, R. Arnold, J. Kohler, R. Li, T. Markvart, J. Ross, K. Steemers, P. Wilson and R. Yao, “Can microgrids make a major contribution to UK energy

supply?," Renewable and Sustainable Energy Reviews, vol. 10, pp. 78-127, April 2006.

[25] "MICROGRIDS – Large scale integration of micro-generation to low voltage grids", EU Contract ENK5-CT-2002-00610, Technical Annex, May 2002, also http://microgrids.power.ece.ntua.gr

[26] S. Amin and B. Wollenberg, "Toward a smart grid: Power Delivery for the 21st century," IEEE Power Energy Mag., vol. 3, pp. 34-41, September/October 2005.

[27] R. Lasseter, A. Akhil, C. Marnay, J. Stephens, J. Dagle, R. Guttromson, A. Meliopoulos, R. Yinger and J. Eto, "White thesis on integration of distributed energy resources—the CERTS Microgrid concept," Office of Power Technologies of the US Department of Energy, 2002, Contract DE-AC03-76SF00098.

[28] B. Lasseter, "Microgrids distributed power generation," IEEE Power Engineering Society Winter Meeting Conference Proceeding, Columbus, OH, USA, vol.1, pp. 146-149, 2001.

[29] F. Zerihun, "Power electronic interfaces in microgrid," M.Sc. Thesis, Department of Electrical Engineering, University of Stockholm, 2007.

[30] S. Chakraborty, B. Kramer and B. Kroposki, "A review of power electronics interfaces for distributed energy systems towards achieving low-cost modular design," Renewable and Sustainable Energy Reviews, vol. 13, pp. 2323–2335, 2009.

[31] H. Nikkhajoei and R. H. Lasseter, “Distributed Generation Interface to the CERTS Microgrid,” IEEE Transactions on Power Delivery vol. 24, no. 3, pp.1598–1608, 2009.

[32] M. Pedrasa and T. Spooner, “A survey of techniques used to control microgrid generation and storage during island operation," in Proceedings of the Australasian Universities Power Engineering Conference (AUPEC), 2006.

[33] J. Lopes, et al, “Defining control strategies for microgrids islanded operation,” IEEE Transactions on Power Systems, vol. 21, pp. 616-924, 2006.

[34] S. Arsali, M. Ceraolo, P. Pelacchi and D. Poli, “Control techniques of dispersed generators to improve the continuity of electricity supply,” Proceedings of IEEE, PES Winter Meeting 2002.

[35] A. Mehrizi-Sani, and R. Iravani, “Potential-function based control of a microgrid in islanded and grid-connected modes,” IEEE Trans. on Power Systems, vol. 25, no. 4, pp. 1883-1891, Nov. 2010.

[36] K. De Brabandere, K. Vanthournout, J. Driesen, G. Deconinck and R. Belmans, “Control of microgrids,” Power Engineering Society general Meeting, IEEE, pp.1-7, June 2007.

[37] I. Balaguer, U. Supatti, Q. Choi and F. Peng, “Intelligent control for intentional islanding operation of microgrids,” Sustainable Energy Technologies, ICSET. IEEE International Conference, pp. 898-903, Nov. 2008.

[38] S. Barsali, M. Ceraolo, P. Pelacchi and D. Poli “Control techniques of dispersed generators to improve the continuity of electricity supply”, in Proceedings of IEEE PES Winter Meeting, New York, NY, USA, vol. 2, pp. 789-794, Jan. 2002.

[39] H. Karimi, H. Nikkhajoei, and R. Iravani, "Control of an electronically-coupled distributed resource unit subsequent to an islanding event," IEEE Trans. on Power Delivery, vol. 23, pp. 493-501, Jan. 2008.

[40] B. Awad, J. Wu and N. Jenkins, "Control of distributed generation," International Journal of Distributed Energy Resources, vol. 4, pp. 409-414, 2008.

[41] F. Gakis, and S. Papathanassiou, "Simple control schemes for grid-connected three-phase voltage-source inverters of DG units". Proc. ICEM, Hania, Crete, Sept. 2006

[42] C. Dobariya and S. Khaparde, "Decoupled power controller for inverter-interfaced distributed generation system," Power Engineering Society General Meeting, IEEE, pp 1- 6, June 2007.

[43] W. Sinsukthavor, E. Ortjohann, M. Lingemann, S. Jaloudi, and D. Morton, "A control hierarchy of interconnected mini-grids," Developments in Power System Protection (DPSP). Managing the Change, 10th IET International Conference, pp. 1-5, April 2010.

[44] C. Lee, C. Chuang, C. Chu, and P. Cheng, "Control strategies for distributed energy resources interface converters in the low voltage microgrid," Proc. IEEE ECCE, pp. 2022-2029, 2009.

[45] W. Weaver, and P. Krein, "Game-Theoretic control of small-scale power systems," IEEE Trans. on Power delivery, vol. 24, no. 3, pp. 1560 - 1567, July 2009.

[46] M. Popov, H. Karimi, H. Nikkhajoei and V. Terzija, “Dynamic model and control of a microgrid with passive loads,” In s.n. (Ed.), IPST Conference Theses, pp. 1-6, 2009.

[47] J. Guerrero, J. Vásquez, J. Matas, M. Castilla, and L. García de Vicuña, “Control strategy for flexible microgrid based on parallel line-interactive UPS systems,” IEEE Trans. on Industrial Electronics, vol. 56, no. 3, pp. 726 – 736, March 2009.

[48] A. Molderink, V. Bakker, M. Bosman, J. Hurink, and G. Smit, “Management and control of domestic smart grid technology,” IEEE Trans. on Smart Grid, vol. 1, no. 2, pp. 109-118, Sep. 2010.

[49] H. Karimi, E. Davison, and R. Iravani, “Multivariable servomechanism controller for autonomous operation of a distributed generation unit: design and performance evaluation,” IEEE Trans. on Power Systems, vol. 25, no. 2, pp. 853-865, May 2010.

[50] A. Engler, "Applicability of droops in low voltage grids." DER Journal. no. 1, Jan. 2005.

[51] K. De Brabandere, B. Bolsens, J. Van den Keybus, A. Woyte, J. Driesen, and R. Belmans, “A voltage and frequency droop control method for parallel inverters,” IEEE Trans. on Power Electronics, vol. 22, no.4, July 2008.

[52] K. Sao and P. Lehn, “Control and power management of converter fed microgrids,” IEEE Trans. on Power Systems, vol. 23, no.3, pp.1088 – 1098, Aug. 2008.

[53] F. Katiraei, and M. Iravani, "Power management strategies for microgrid with multiple distributed generation units," IEEE Trans. on Power System, vol. 21, no. 4, pp. 1821–1831, Nov. 2006.

[54] E. Barklund, N. Pogaku, M. Prodanovic´, C. Hernandez-Aramburo and T. Green, "Energy management in autonomous microgrid using stability-constrained droop control of inverters," IEEE Trans. on Power Electronics, vol. 23, no.5, pp. 2346 – 2352, Sep. 2008.

[55] Y. Li, "Power Management of Power Electronics Interfaced Low-Voltage Microgrid in Islanding Operation," Master thesis, Department of Electrical and Computer Engineering, University of Alberta, Spring 2010, Edmonton, Alberta.

[56] S. Ahn, J. Park, I. Chung, S. Moon, S. Kang, and S. Nam, "Power-sharing method of multiple distributed generators considering control modes and configurations of a microgrid," IEEE Trans. on Power delivery, vol. 25, no. 3, pp. 2007-2016, July 2010.

[57] G. Díaz, C. González-Morán, J. Gómez-Aleixandre, and A. Diez, "Scheduling of droop coefficients for frequency and voltage regulation in isolated microgrids," IEEE Trans. on Power Systems, vol. 25, no. 1, pp. 489-496, Feb. 2010.

[58] Z. Zhanga, X. Huanga, J. Jianga, and B. Wub, "A load-sharing control scheme for a microgrid with a fixed frequency inverter," Electric Power Systems Research, vol.80, pp. 311–317, 2010.

[59] D. Reigosa, P. Arboleya, C. González-Morán, and J. Gómez-Aleixandre, "An improved control scheme based in droop characteristic control for microgrid

converters," International Conference of Electrical Machines and Systems, ICEMS, pp. 1-6, 2009.

[60] R. Majumder, A. Ghosh, and G. Ledwich, and F. Zare, "Angle droop versus frequency droop in a voltage source converter based autonomous microgrid," IEEE Power Engineering Society General Meeting, 26-30 July 2009, Calgary Telus Conventional Centre, Calgary.

[61] S. Rosado "Voltage Stability and Control in Autonomous Electric Power Systems with Variable Frequency," Ph.D. Thesis, Department of Electrical and Computer Engineering, Virginia Polytechnic Institute and State University, 2007.

[62] D. Ariyasinghe and D. Vilathgamuwa , "Stability analysis of microgrids with constant power loads", Sustainable Energy Technologies, ICSET, IEEE International Conference, pp. 279-284, 2008.

[63] R. Majumder, A. Ghosh, G. Ledwich and F. Zare, "Stability analysis and control of multiple converter based autonomous microgrid," 7th IEEE International Conference on Control and Automation (ICCA), New Zealand, Christchurch, pp. 1663-1668, 2009.

[64] S. Iyer, M. Belur, and M. Chandorkar, "A generalized computational method to determine stability of a multi-inverter microgrid," IEEE Transactions on Power Electronics, vol. 25, no. 9, pp. 2420 – 2432, 2010.

[65] R. Majumder, B. Chaudhuri, A. Ghosh, R. Majumder, G. Ledwich, and F. Zare, "Improvement of stability and load sharing in an autonomous microgrid using supplementary droop control loop," IEEE Trans. on Power Systems, vol. 25, no. 2, pp. 796- 808, May 2010.

[66] G. Venkataramanan, M. Illindala, "Small signal dynamics of inverter interfaced in a chain-microgrid." In Proceedings of the IEEE Power Engineering Society General Meeting, pp.1-6, 2007.

[67] F. Katiraei, R. Iravani and P. Lehn, "Small-signal dynamic model of a microgrid including conventional and electronically interfaced distributed resources," IET Proc. Generation Transmission Distribution, vol. 1, no. 3, pp. 369-378, 2007.

[68] D. Gaonkar, R. Patel and G. Pillai, "Dynamic model of microturbine generation system for grid connected/islanding operation," International Conference on Industrial Technology (ICIT), IEEE, pp. 305-310, 2006.

[69] Y. Xu, F. Li, J. Kueck and D. Rizy, "Experiment and simulation of dynamic voltage regulation with multiple distributed energy resources," Bulk Power System Dynamics and Control - VII. Revitalizing Operational Reliability, iREP Symposium, pp. 1-7, 19-24 Aug. 2007.

[70] G. Mine, R. Borer, F. Kupzog, and H. Nishi, "Construction method of dynamic microgrid by using optimized grouping method," Proceedings of the 8th IEEE International Conference on Industrial Informatics (INDIN 2010), pp. 780-785, 2010.

[71] N. Pogaku, M. Prodanovic and T. Green, "Modeling, analysis and testing of autonomous operation of an inverter-based microgrid," IEEE Trans. Power Electronics, vol. 22, pp. 613-624, March 2007.

[72] Il-Yop Chung, W. Liu, D. A. Cartes, and K. Schoder, “Control parameter optimization for a microgrid system using particle swarm optimization,” ICSET 2008, IEEE, pp. 837–842, 2008.

[73] M. Prodanovic´, and T. Green, “Control and filter design of three-phase inverters for high power quality grid connection,” IEEE Trans. on Power Electronics, vol. 18, no. 1, pp. 373- 380, Jan. 2003.

[74] E. Twining and D. Holmes, “Grid current regulation of a three-phase voltage source inverter with an LCL input filter,” IEEE Trans. on Power Electronics, vol. 18, no. 3, pp. 888–895, May 2003.

[75] T. Wang, Z. Ye, G. Sinha, and X. Yuan, “Output filter design for a grid interconnected three-phase inverter,” PESC, IEEE 34th Annual, vol. 2, pp. 779-784, June 2003.

[76] B. Panigrahi,A. Abraham, and S. Das (Eds.), Computational intelligence in power engineering, Springer-Verlag Berlin Heidelberg, 2010.

[77] A. Abido, “Optimal design of power–system stabilizers using particle swarm optimization,” IEEE Trans. on Energy Conversion, vol. 17, no. 3, pp. 406-413, Sept. 2002.

[78] Il-Yop Chung, W. Liu, D. Cartes, E. Collins and S. Moon, “Control methods of inverter-interfaced distributed generators in a microgrid system,” IEEE Trans. on Industry Applications, vol. 46, no. 3, pp. 1078- 1088, May/June 2010.

[79] J. Kennedy, and R. Eberhart, "Particle swarm optimization," in Proc. IEEE International Conference on Neural Networks, 4ed, pp. 1942-1948, 1995.

[80] H. Dommel, “Digital Computer Solution of Electromagnetic Transient in Single and Multiphase Networks,” IEEE Trans. on Power Apparatus and Systems, vol. PAS-88, no.4, pp388-399, April 1969.

[81] G. Rockerfeller, "Fault Protection with Digital Computer", IEEE Trans. on PAS, vol. 88, no.4, pp.438-461, April 1969.

[82] Q. Li, S. Woodruff and M. Steurer, “Study of Power Loss of Small Time-Step VSC Model in RTDS,” Power Engineering Society General Meeting, IEEE, pp. 1 – 7, 2007.

[83] Z. Bo, A. Klimek, Y. Ren and J. He, “Real Time Digital Simulation System for Testing of Integrated Protection Schemes,” Power System Technology and IEEE Power India Conference, POWERCON, pp. 1-5, 2008.

[84] Y. Deng, S. Foo and H. Li, “Real Time Simulation of Power Flow Control Strategies for Fuel Cell Vehicle with Energy Storage by Using Real Time Digital Simulator (RTDS),” IEEE IPEMC, pp. 2323 – 2327, May 2009.

[85] P. McLaren, R. Wierckx, J. Giesbrecht and L. Arendt, “A real time digital simulator for testing relays,” IEEE. Trans. on Power Delivery, vo1.7, pp.207-213, Jan 1992.

Vitae

- Mohamed Ali Ali Hassan
- Born in Mansoura, Egypt on May 21, 1973.
- Egyptian.
- Receive Bachelor of Science (B.S.) and Master of Science (M.Sc.) degrees in Electrical Engineering from Mansoura University, Mansoura, Egypt in 1995 and 1999 respectively.
- Joined King Fahd University of Petroleum & Minerals in Feb. 2006.
- KFUPM, Dhahran 31261, Building 1925, Saudi Arabia,

  Tel:+96638607332 and+966559121315
- 50 Hekmat Abu El-Naga Str. From Galaa Str, Mansoura, 35516, Egypt,

  Tel:+20502366999 and +20122660770
- E-mail: mhassan@kfupm.edu.sa and moh_ali_ali@yahoo.com